

Site characterization mapping in New England using fundamental frequency (f_0)

A dissertation submitted by
Marshall A. Pontrelli

In partial fulfillment of the requirements for the degree of

Doctor of Philosophy
in
Civil and Environmental Engineering

TUFTS UNIVERSITY

August 2023

© 2023, Marshall A. Pontrelli

Advisor: Dr. Laurie Baise

Committee Members: Dr. John Ebel, Dr. Juan Pestana, Dr. Jon Lamontagne, Dr. Jack Ridge

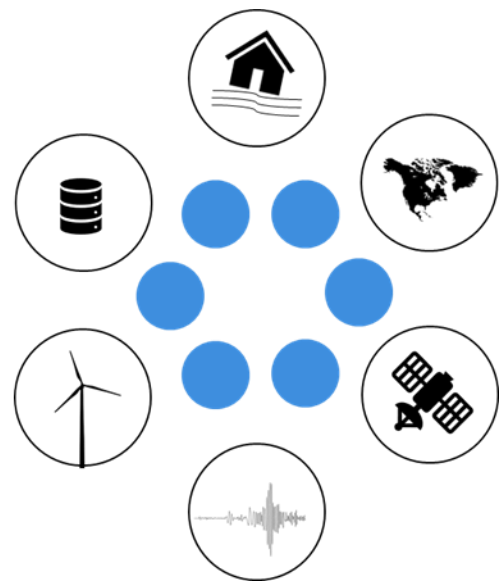
Abstract

Site response is a phenomenon where seismic energy is altered by near surface geologic structures. These structures' geometric and material properties cause the amplification of seismic waves which can lead to infrastructure damage and loss of life. Site characterization maps are a way to quantify site response on a regional scale and are essential for regional planning and seismic hazard analyses. They are often represented using the time-averaged shear-wave velocity of the top 30 meters of a geotechnical profile ($Vs30$) a measurement on which seismic design is primarily based. Though $Vs30$ is a useful and broadly available measurement, it has two important limitations: 1) it does not incorporate information from layers deeper than 30 meters and 2) using $Vs30$ to assign site classes ignores the frequency of maximum site amplification of the sediment transfer function and therefore performs poorly for highly resonant sediment. This dissertation explores the use of site fundamental frequency (f_0) as a mapping parameter for seismic site response and its applicability to estimating site response in New England, USA, a region with few earthquake recordings. f_0 has gained traction in the earthquake engineering community for its physical relationship to depth-to-bedrock and overburden shear-wave velocity, and the ability to measure it using easily attainable seismic noise rather than earthquake records. In Chapter 1, a database of 1577 f_0 measurements are compiled from the literature and a field campaign. Using a national 1:5,000,000 scale surficial geologic map of the US, the f_0 stations are grouped by their geologic unit and distributions are computed for each unit. $Vs30$ distributions are then estimated for each of the surficial geologic units based on the f_0 distributions by assuming a layer-over-halfspace overburden model and establishing estimates of sediment average shear-wave velocity (Vs_{avg}) for each of the units based on a limited number of shear-wave velocity profiles from the region. Chapter 2 uses a similar framework to that of Chapter 1 but incorporates higher resolution surficial geologic maps and a local sedimentary deposit subregion map to improve the map resolution and reduce residuals between measured f_0 values and f_0 distribution medians. Additionally in Chapter 2, Vs_{avg} is estimated as a random variable, rather than a single number, improving the estimates of $Vs30$ distribution compared to the estimates in Chapter 1. Chapter 3 uses a depth-to-bedrock (z) model

to make predictions of f_0 distributions by propagating distributions of z through developed $f_0 - z$ relationships. The $f_0 - z$ relationships themselves contain well characterized uncertainty representing shear-wave velocity variability which is incorporated in the analysis, and which had not been as well characterized in Chapters 1 and 2 due to a lack of shear-wave velocity measurements. In each chapter of this dissertation, higher resolution information is incorporated into the development of regional f_0 maps providing improved quantification of central tendency and dispersion of f_0 distribution estimates across New England and in Massachusetts specifically in Chapter 3. The two techniques developed in this dissertation exist within a framework that uses estimates of depth-to-bedrock and overburden shear-wave velocity. The combination of these parameters and the measurement of their uncertainty provides a holistic understanding of overburden mechanical properties and geometry on a regional scale and thus the improved quantification of important site response characteristics and their uncertainties.



Tufts Geohazards



Natural disasters strike us down together, and it is together that we will get back on our feet.

-Dr. Lucy Jones “Big Ones”

*To my mother, Heather; father, Mike; sister, Eva; brother, Bobby; and partner, Laura. Thank
you for your everlasting love and support.*

Acknowledgments

I would like to thank Dr. Laurie Baise for her continuing support of this research, insightful comments, attention to detail, and weekly meetings. She backed me through high and low periods in the process of developing this dissertation with a steady hand and an eye towards the future. Laurie is an amazing mix of administrator, scientist, engineer, technician, teacher, and good person who makes everyone around her better. She is the best advisor a PhD student could ask for. Dr. John Ebel was an instrumental voice during my PhD who calmly and consistently identified what was right with the work I was doing and then clearly suggested what he believed still needed to be done. This clarity and confidence he showed was essential during difficult episodes of data processing and decision-making about methodological paths forward. A quote that will always stick with me that he said repeatedly is “The science is fine, you need to stop worrying about it. What you need to do is write more clearly and present your work so the audience can understand it”. Dr. Jon Lamontagne began at the same time as I did at Tufts and has been there for me to talk about statistics and academic life for my entire time here. He has guided me in statistical analysis and optimization as well as communicated with me in informal meetings that are small, yet over time, powerful. Dr. Juan Pestana was my Earthquake Engineering professor and introduced me to time-domain analyses of site response and provided a historic and holistic setting for the practice. Dr. Jack Ridge helped me grow as a professional and a person with his kind guidance and constant support - we had a great time in Death Valley too.

Thank you to my family. My Mom, Heather, has been an inspiration to me as she has to many. She has driven me to always strive for excellence in my work and in my life and, most importantly, has steered me to continually try to be a good person. It was also nice having someone to commiserate with about bad reviewers. My Dad, Mike, had breakfast with me practically every week in graduate school. He supported me constantly, and his weekly wisdom helped me find my way forward in tricky situations. We talked about everything under the sun which was fun and insightful – I have loved having someone to share ideas with. My partner, Laura, has been a rock in my life during my time in graduate school. She is inspirational, caring,

and insightful and spent hours listening to me when I had issues, providing support and guidance. My sister, Eva, is herself a PhD student and has been a source of excellent wisdom and witty insight on graduate school life. She has been so insightful about the PhD process because of her own success in one, something that inspires me. My brother, Bobby, provided me with consultation over the years, offering guidance and helpful support through new situations I found myself in. To all these loved-ones and the many more who directly and indirectly supported me, thank you and I love you.

Thank you to the faculty of the CEE department, especially Drs. Rob Viesca, Jack Germaine, Lucy Jen, Chris Swan, Luis Dorfmann and others who provided the intellectual and personal support in the office to make this dissertation possible. Thank you to the administrative staff on whom I constantly rely for aid: Laura Sacco and Debra Mcknight. There are several people outside of Tufts who were extremely technically influential on my work and my skillset. Dr. Steve Mabee of the Massachusetts Geological Survey at UMASS Amherst let me participate in the depth-to-bedrock project which turned into the third chapter of this dissertation. This project had extraordinary ambition and a long-term mentality built on decades of meticulous data collection that was eye-opening to me. It was an honor to work on it and I am so grateful. Steve was amazing letting me be a part of the project and guiding me along the way. Both Chris Duncan and Bill Clement also worked on this project and met with me individually multiple times to discuss technical issues about the spatial model and geophysical models, respectively. Weiwei Zhan was a postdoc at Tufts during the second half of my PhD and had the technical skills I wanted to have and more. He could identify my issues exactly providing specific guidance to challenging problems having gone through the same issues himself. Finally, Jim Kaklamanos, was hugely inspirational to me. I read all his work and then spent time with him asking deeper technical questions. He shared his years of wisdom in these sessions graciously. Jim is extremely organized, practical, creative, nice, and relatable. He runs a tight ship that I and his students appreciate, and which makes everything easier, something that I try to emulate. Thank you to all these people for the time they put in mentoring me and guiding me on my research journey.

Thank you to my colleagues: Christina Sanon, Adel Asadi, Catherine Knox, Jeremy Salerno, Alex Chansky, Lekan Sodeinde, Lichen Wang, Parker Aubin, Stephen Lambert, Deniz Ranjpour, Vahid

Rashidian, Fatemeh Kazemiparkouhi, Illaria Cinelli, Avis Carrero, Mark Zobacki, Sofia Puerto, Caitlin Barber, Flannery Dolan, Ashkan Akhlaghi., Liz Fletcher, Amanda Parry, Justin Reyes, Azin Mehrjoo and many others all of whom have had enormous influence on me and become my friends. Finally, thank you to all the amazing students I have had the privilege of working with in all the classes I have taught and TA'd.

Table of contents

Title page.....	<i>i</i>
Abstract.....	<i>ii</i>
Front matter.....	<i>iv</i>
Dedication.....	<i>vi</i>
Acknowledgments.....	<i>vii</i>
Table of contents.....	<i>x</i>
List of figures.....	<i>xiii</i>
List of tables.....	<i>xv</i>
List of equations.....	<i>xvi</i>

Chapter 1: Introduction

1.1 Introduction.....	2
1.2 Theoretical transfer functions.....	3
1.3 Empirical transfer functions.....	5
1.3.1 Standard spectral and borehole spectral ratio.....	7
1.3.2 Computing a spectral ratio.....	8
1.4 Horizontal-to-vertical spectral ratio.....	11
1.4.1 HVSR theory.....	11
1.4.2 Computing an HVSR.....	12
1.4.3 Importance of the HVSR to this dissertation.....	13
1.5 Motivation.....	14
1.5.1 Chapters 1 and 2 - Lack of existing site characterization maps of New England.....	14
1.5.2 Chapter 3 – Using the Massachusetts depth-to-bedrock map to make an f_0 map.....	16
1.5.3 Using f_0 as a mapping parameter.....	17
1.5.4 Incorporating uncertainty.....	18
1.6 Dissertation organization.....	18

Chapter 2: Regional-Scale Site Susceptibility Mapping in High Impedance Environments Using Soil Fundamental Resonance (f_0): New England, USA

Abstract.....	22
1.0 Introduction.....	23
2.0 Data.....	27
2.1 Conterminous US surficial geology map.....	27
2.2 HVSR database.....	29
2.3 V_s data.....	34
3.0 Methods.....	36
3.1 Wills and Clahan methodology for creating f_0 distributions by geologic polygons.....	37
3.2 Estimating V_{s30} from f_0 with the procedure of Hassani and Atkinson (2016)	38
4.0 Results.....	39
4.1 f_0 distributions.....	39
4.2 Mapping each unit f_0 distribution median and interquartile range.....	41
4.3 Estimating V_{savg}	43
4.4 Developing V_{s30} distributions by applying Equation 7 to the f_0 distributions.....	46
5.0 Discussion.....	49
6.0 Conclusion.....	54
Acknowledgements.....	55

Chapter 3: Mapping fundamental frequency (f_0) as a site response parameter using a multi-scale approach with state-level surficial geologic maps and local sedimentary deposit information

Abstract.....	57
1.0 Introduction.....	58
2.0 Data.....	61
2.1 State-scale surficial geologic maps.....	61
2.2 Local sedimentary deposit subregion map.....	63
2.3 f_0 data.....	67
2.4 V_s data.....	69
3.0 Methods.....	70
3.1 f_0 distributions.....	70
3.2 $V_{s_{avg}}$ distributions.....	72
3.3 V_{s30} distribution estimation.....	75
4.0 Results.....	77
4.1 f_0 distributions by surficial geologic unit.....	77
4.2 $V_{s_{avg}}$ μ_{ln} and σ_{ln} and Mdn maps.....	82
4.3 V_{s30} μ_{ln} and σ_{ln} and Mdn maps.....	83
5.0 Discussion.....	86
6.0 Conclusion.....	90
Data availability.....	92
Acknowledgements.....	92

Chapter 4: Maps of distributional parameters of f_0 for Massachusetts, USA derived from a high-resolution continuous depth-to-bedrock map

Abstract.....	94
1.0 Introduction.....	95
2.0 Data.....	99
2.1 Depth-to-bedrock map.....	99
2.2 Surficial geologic map.....	102
2.3 Subregion map.....	104
2.4 f_0 dataset.....	105
3.0 Methods.....	106
3.1 $f_0 - z$ relationships and the link to power-law velocity profiles.....	106
3.2 Developing the shear-wave velocity profiles from f_0 and z	107
3.3 Predicting f_0 distributions from the depth-to-bedrock model	110
3.4 Selecting an f_0 threshold to mask the f_0 map.....	112
4.0 Results.....	115
4.1 $f_0 - z$ relationships and corresponding α and β coefficients	115
4.2 Estimating shear-wave velocity profiles from the α and β coefficients using Equation 4.....	118
4.3 Maps of masked f_0 , μ_{ln} , and σ_{ln} and Mdn	121
5.0 Discussion.....	124
6.0 Conclusion.....	131

Chapter 5: Conclusion

Conclusion.....	133
-----------------	-----

Appendix A: Supplementary material for Chapter 2

1.0 Attached data files.....	137
2.0 The Conterminous US surficial geology map.....	138
2.1 Grouping the US Conterminous surficial geology map.....	141

Appendix B: Supplementary material for Chapter 3

1.0 Data sources.....	146
1.1 Attached data files.....	147

Appendix C: Supplementary material for Chapter 4

1.0 Data sources.....	150
1.1 Attached data files.....	150

References

References.....	151
-----------------	-----

List of figures

Chapter 1: Introduction

<i>Figure 1.</i> Site response damage.....	2
<i>Figure 2.</i> Theoretical transfer function demonstration.....	5
<i>Figure 3.</i> Site response cartoon.....	7
<i>Figure 4.</i> Array geometries cartoon.....	8
<i>Figure 5.</i> Computing an ETF.....	9
<i>Figure 6.</i> Computing an ETF with many recordings.....	10
<i>Figure 7.</i> Computing an <i>mHVSR</i>	13
<i>Figure 8.</i> Existing site characterization maps.....	15
<i>Figure 9.</i> <i>Vs30</i> site classification maps for Mass DOT.....	17

Chapter 2: Regional-Scale Site Susceptibility Mapping in High Impedance Environments Using Soil Fundamental Resonance (f_0): New England, USA

<i>Figure 1.</i> Existing site characterization maps.....	26
<i>Figure 2.</i> Soller et al. (2009) map.....	28
<i>Figure 3.</i> HVSR database.....	30
<i>Figure 4.</i> Computing an HVSR curve.....	32
<i>Figure 5.</i> HVSR curve examples.....	33
<i>Figure 6.</i> <i>Vs</i> data.....	34
<i>Figure 7.</i> MASW analysis.....	36
<i>Figure 8.</i> f_0 grouping.....	37
<i>Figure 9.</i> f_0 distribution box-and-whisker plot.....	40
<i>Figure 10.</i> Final f_0 median and IQR maps.....	41
<i>Figure 11.</i> f_0 median map in the major geologic units.....	43
<i>Figure 12.</i> Vs_{avg} estimation.....	45
<i>Figure 13.</i> f_0 – $Vs30$ relationship.....	46
<i>Figure 14.</i> $Vs30$ distribution box-and-whisker plot.....	47
<i>Figure 15.</i> Site class pie charts.....	48
<i>Figure 16.</i> Relationship to other studies.....	51
<i>Figure 17.</i> f_0 residuals map.....	53

Chapter 3: Mapping fundamental frequency (f_0) as a site response parameter using a multi-scale approach with state-level surficial geologic maps and local sedimentary deposit information

<i>Figure 1.</i> Resolution comparison of geologic maps.....	62
<i>Figure 2.</i> High resolution geologic map.....	63
<i>Figure 3.</i> Subregion development.....	67
<i>Figure 4.</i> f_0 data.....	68
<i>Figure 5.</i> <i>Vs</i> data.....	70
<i>Figure 6.</i> f_0 distribution example.....	71
<i>Figure 7.</i> Soft geology and till distributions.....	72
<i>Figure 8.</i> Vs_{avg} distributions.....	74
<i>Figure 9.</i> Uncertainty propagation.....	77
<i>Figure 10.</i> f_0 distributions by subregion.....	79
<i>Figure 11.</i> f_0 distributions	79
<i>Figure 12.</i> f_0 μ_{ln} . and <i>Mdn</i> maps.....	81

<i>Figure 13.</i> f_0 σ_{ln} , and station density maps.....	81
<i>Figure 14.</i> Vs_{avg} Mdn , μ_{ln} , and σ_{ln} maps.....	82
<i>Figure 15.</i> $Vs30$ Mdn , μ_{ln} , and σ_{ln} maps.....	84
<i>Figure 16.</i> Two-axis approach.....	88
<i>Figure 17.</i> Residual reduction.....	89

Chapter 4: Depth-to-bedrock based f_0 distribution map of Massachusetts, USA for seismic site response hazard using $f_0 - z$ relationships

<i>Figure 1.</i> Depth-to-bedrock points.....	100
<i>Figure 2.</i> Depth-to-bedrock prediction and uncertainty maps.....	101
<i>Figure 3.</i> Surficial geology.....	103
<i>Figure 4.</i> Subregions.....	104
<i>Figure 5.</i> f_0 data.....	105
<i>Figure 6.</i> Data cleaning.....	108
<i>Figure 7.</i> Boston Basin model demonstration.....	109
<i>Figure 8.</i> Boston Basin velocity profile.....	110
<i>Figure 9.</i> f_0 distribution computation demonstration.....	111
<i>Figure 10.</i> Peak flattening demonstration.....	112
<i>Figure 11.</i> f_0 threshold selection.....	114
<i>Figure 12.</i> Geologic grouping models.....	116
<i>Figure 13.</i> Subregion models.....	117
<i>Figure 14.</i> Geologic grouping Vs profiles.....	119
<i>Figure 15.</i> Subregion Vs profiles.....	120
<i>Figure 16.</i> f_0 μ_{ln} and σ_{ln} maps.....	122
<i>Figure 17.</i> f_0 Mdn maps.....	124
<i>Figure 18.</i> Power law Vs profiles compared to measured profiles.....	126
<i>Figure 19.</i> Residual reduction.....	127
<i>Figure 20.</i> Calculating $Vs30$ distributions.....	128
<i>Figure 21.</i> $Vs30$ μ_{ln} and σ_{ln} maps	129
<i>Figure 21.</i> Site Class from $Vs30$ Mdn	130

Appendix A: Supplementary material for Chapter 2

<i>Figure 1.</i> Soller et al. (2009) map.....	139
<i>Figure 2.</i> Grouped Soller et al. (2009) map.....	144

List of tables

Chapter 1: Introduction

<i>Table 1. Vs30 – based site classifications.....</i>	15
--	----

Chapter 2: Regional-Scale Site Susceptibility Mapping in High Impedance Environments Using Soil Fundamental Resonance (f_0): New England, USA

<i>Table 1. Vs30 – based site classifications.....</i>	26
<i>Table 2. Surficial geologic unit groupings.....</i>	28
<i>Table 3. f_0 distribution statistics.....</i>	40
<i>Table 4. Vs_{avg} distribution statistics.....</i>	44
<i>Table 5. Vs30 distribution statistics.....</i>	47
<i>Table 6. Comparison to other studies.....</i>	51

Chapter 3: Mapping fundamental frequency (f_0) as a site response parameter using a multi-scale approach with state-level surficial geologic maps and local sedimentary deposit information

<i>Table 1. State surficial geologic maps.....</i>	62
<i>Table 2. Elevation thresholds for subregions.....</i>	66
<i>Table 3. Vs_{avg} distribution statistics.....</i>	74
<i>Table 4. Final output table.....</i>	84
<i>Table 5. Residual reduction.....</i>	90

Chapter 4: Depth-to-bedrock based f_0 distribution map of Massachusetts, USA for seismic site response hazard using $f_0 - z$ relationships

<i>Table 1. Surficial geologic groupings.....</i>	102
<i>Table 2. Model results.....</i>	115
<i>Table 3. f_0 and z mask thresholds.....</i>	121

Appendix A: Supplementary material for Chapter 2

<i>Table 1. Information on attached table.....</i>	137
<i>Table 2. Information on attached shapefile.....</i>	137
<i>Table 3. Attributes of Soller et al. (2009) map.....</i>	140
<i>Table 4. f_0 statistics of ungrouped Soller et al. (2009) map.....</i>	142
<i>Table 5. Geologic groupings.....</i>	143

Appendix B: Supplementary material for Chapter 3

<i>Table 1. Information on attached table.....</i>	147
<i>Table 2. Information on attached shapefile.....</i>	147

Appendix C: Supplementary material for Chapter 4

<i>Table 1. Description of attached data.....</i>	150
---	-----

List of equations

Chapter 1: Introduction

<i>Equation 1.</i> Impedance contrast.....	3
<i>Equation 2.</i> Quarter wavelength.....	3
<i>Equation 3.</i> Amplification.....	3
<i>Equation 4.</i> Seismic wave convolution.....	6
<i>Equation 5.</i> Seismic wave Fourier spectra multiplication.....	6
<i>Equation 6.</i> ETF.....	6
<i>Equation 7.</i> ETF median.....	9
<i>Equation 8.</i> ETF confidence interval.....	9
<i>Equation 9.</i> ETF standard deviation.....	9
<i>Equation 10.</i> ETF in the HVSR derivation.....	11
<i>Equation 11.</i> Influence of the Rayleigh wave.....	12
<i>Equation 12.</i> Removing influence of the Rayleigh wave.....	12
<i>Equation 13.</i> HVSR.....	12
<i>Equation 14.</i> Vs30.....	14

Chapter 2: Regional-Scale Site Susceptibility Mapping in High Impedance Environments Using Soil Fundamental Resonance (f_0): New England, USA

<i>Equation 1.</i> HVSR median.....	31
<i>Equation 2.</i> HVSR standard deviation.....	31
<i>Equation 3.</i> Significant peak criteria.....	31
<i>Equation 4.</i> Quarter wavelength.....	38
<i>Equation 5.</i> Vs_{avg}	38
<i>Equation 6.</i> Vs30.....	38
<i>Equation 7.</i> Vs30 as a function of f_0	39

Chapter 3: Mapping fundamental frequency (f_0) as a site response parameter using a multi-scale approach with state-level surficial geologic maps and local sedimentary deposit information

<i>Equation 1.</i> Mdn calculation.....	71
<i>Equation 2.</i> Quarter wavelength.....	75
<i>Equation 3.</i> Vs_{avg}	75
<i>Equation 4.</i> Vs30.....	75
<i>Equation 5.</i> Vs30 as a function of f_0	75

Chapter 4: Depth-to-bedrock based f_0 distribution map of Massachusetts, USA for seismic site response hazard using $f_0 - z$ relationships

<i>Equation 1.</i> Power-law velocity profile.....	106
<i>Equation 2.</i> $f_0 - z$ relationship computing f_0	106
<i>Equation 3.</i> $f_0 - z$ relationship computing z	106
<i>Equation 4.</i> Vs profile from α and β coefficients.....	107
<i>Equation 5.</i> Linearizing equation 2.....	107

<i>Equation 6. Linearizing equation 2</i>	107
<i>Equation 7. Linearized $f_0 - z$ relationship</i>	107
<i>Equation 8. Lognormal u_{ln} parameter estimation</i>	110
<i>Equation 9. Lognormal σ_{ln} parameter estimation</i>	110

CHAPTER 1

Introduction

1.1 Introduction

Seismic site response is a phenomenon where seismic waves are altered by near surface geologic structures. The typical structure that causes these alterations is a sedimentary basin with low velocity and low-density sediments overlying higher velocity and density basement rock. Given these conditions, seismic energy amplifies and de-amplifies at differing frequencies depending on the basin's geometry and mechanical properties, posing risk for civil infrastructure and the people who depend on it. Many cities are built on sedimentary basins including San Francisco, California; Mexico City, Mexico; Seattle, Washington; Boston, Massachusetts; Kobe, Japan, and many others. The study and quantification of site response is therefore imperative for the construction of earthquake resilient infrastructure and the security of these city's citizens.

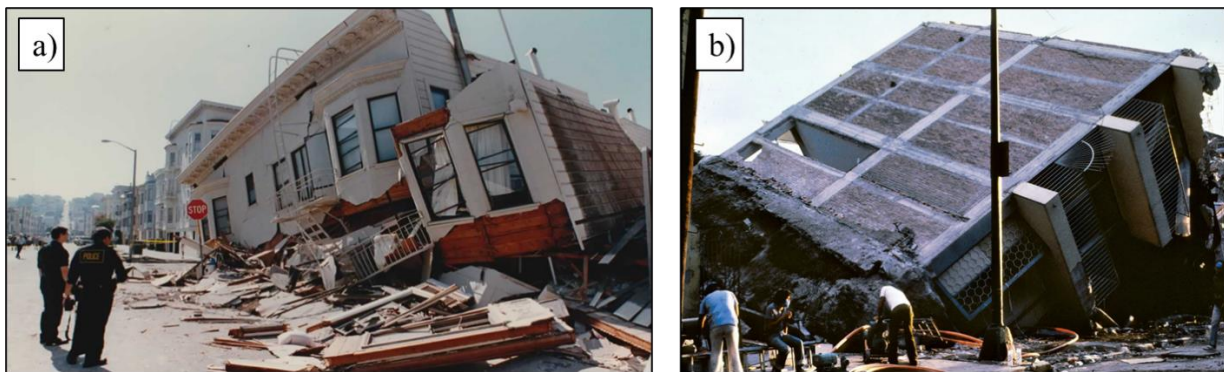


Figure 1. Examples of collapsed buildings from earthquakes with widely documented site response effects. a) The Loma Prieta earthquake in San Francisco, 1989. b) The Michoacán earthquake in Mexico City, 1985

The first qualitative site response assessment was performed following the 1906 San Francisco Earthquake by Dr. Andrew C. Lawson of the University of Berkley. He noted that intensity of shaking during the event was larger in areas underlain by soft geologic material (Lawson, 1908). In its simplest form, the quantification of this phenomenon assumes linearly propagating shear waves through horizontally stratified media with frequency independent damping and a strain independent shear modulus overlying high velocity bedrock, known as the SH1D assumptions. Given these conditions, the interface between the sediments and bedrock is known as the impedance contrast (*IC*). Impedance contrasts and the mechanical

and geometric properties of the sediment layers in a geotechnical profile yield several essential relationships to understanding site response.

The impedance contrast is equal to the ratio of the velocity (β_s) times the density (ρ_s) of the sediment layer to the velocity (β_r) times the density (ρ_r) of the bedrock layer:

$$IC = \frac{\beta_s \rho_s}{\beta_r \rho_r} \quad (1)$$

The maximum amplification of seismic energy takes place at frequencies

$$f_n = (2n + 1) \frac{\beta_s}{4z} \quad (2)$$

where z is the depth to the impedance contrast. The amplitude at those frequencies is

$$\frac{v_A}{v_{B_{max}}} = \frac{1}{IC} \quad (3)$$

where v_A is the amplitude of shaking at the free surface and v_B is the amplitude of shaking at the impedance contrast. These equations provide several key general insights into the behavior of seismic energy in sedimentary basins. Firstly, from Equation 1, as the shear-wave velocity of the overburden decreases, the frequencies of the modes decrease. Secondly, from Equation 1, as the depth to the impedance contrast increases, the frequencies of the modes decrease. Lastly, from Equation 3, as the impedance contrast (Equation 1) decreases, the ratio of the amplitudes of the modes of maximum shaking increase equal to the inverse of the impedance contrast. These relationships show how the mechanical properties and geometry of a basin affect the frequency and shaking of seismic energy (Thomson, 1950; Haskell, 1953; Haskell, 1960; Borcherdt, 1970; Kramer, 1996; Le Pense, 2011).

1.2 Theoretical transfer functions

A transfer function is a plot of the ratio of amplitude of shaking at the free surface to that of a reference location as a function of frequency. Transfer functions define the “site response” of a site. Transfer functions can be calculated using constitutive sediment models and using data. The reference location is often selected to be at the impedance contrast. A transfer function shows how much seismic energy is

amplified by near-surface geologic structures and at what frequencies. In their simplest form, which assumes linearly propagating shear-waves through horizontally stratified media with frequency independent damping and a strain independent shear modulus, theoretical transfer functions (TTF) are a function of six parameters: a shear-wave velocity profile (β_s), a layer thickness profile (z), a density profile (ρ_s), a quality factor profile (Q), a bedrock shear-wave velocity (β_r), and a bedrock density (ρ_r). This model of site response is known as the “SH1D” model. The quality factor, Q , represents generalized seismic attenuation which includes attenuation by wave scattering and intrinsic attenuation due to particle friction. In general, the lower the quality factor, the more seismic energy is attenuated and the less amplification there is in the near surface. Q is related to the common structural engineering parameter the damping ratio (ζ) by $\zeta = 0.5*1/Q$. Figure 2 shows a transfer function from the simplest overburden geologic structure: a single, homogeneous layer over bedrock. In Figure 2c, with an infinite Q value and thus no attenuation through the overburden, the amplification of the maximum frequencies is equal to the inverse of the impedance contrast (Equations 1 and 3). The frequencies of maximum amplification are at the values described in Equation 2. The first mode in the transfer function, and a major subject of this dissertation, is the fundamental frequency (f_0) which is highlighted in Figure 2c. Figure 2d shows the influence of Q : as Q decreases, more seismic energy is attenuated in the overburden which results in lower amplification overall with greater attenuation in the higher frequencies. This simplified layer-over-halfspace model and its corresponding transfer function are essential to understand how the geometric and mechanical properties of the overburden affect amplification of seismic waves through the near surface.

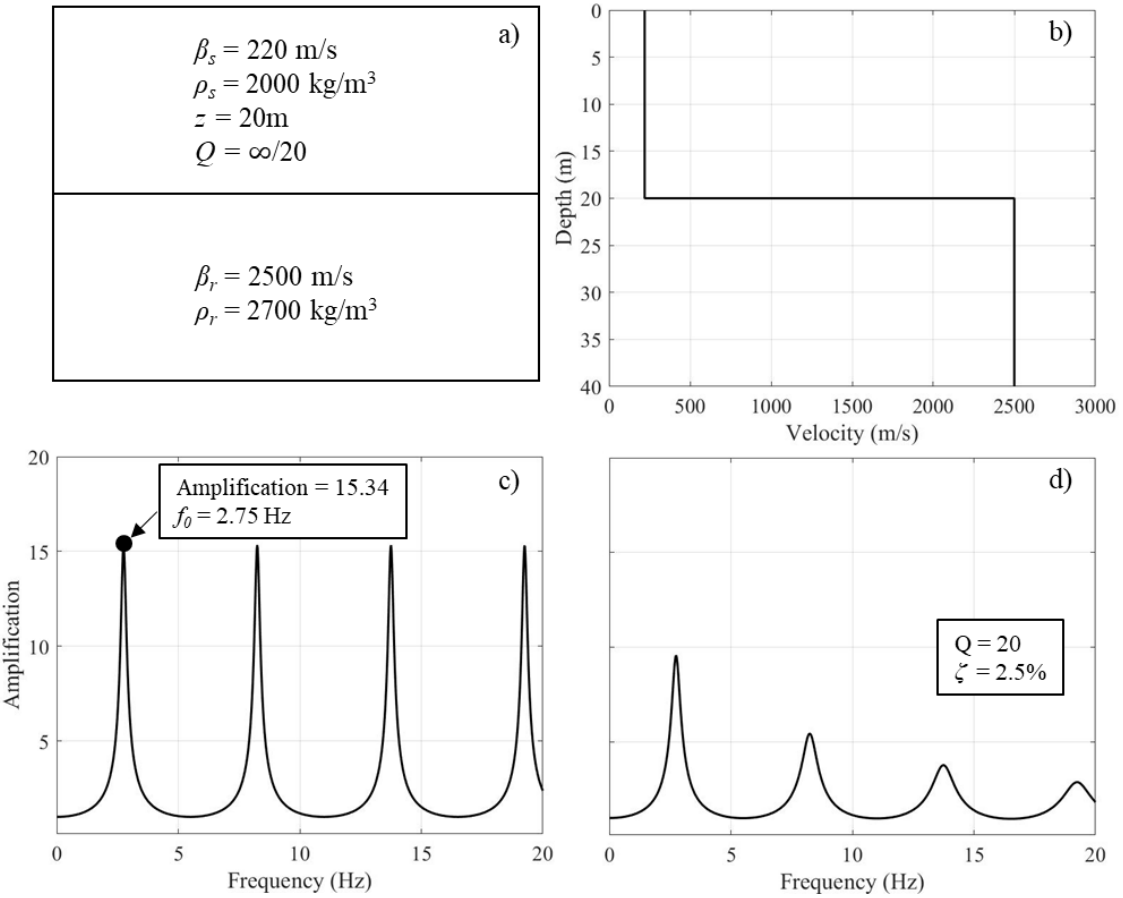


Figure 2. Demonstration of the basic geometric and mechanical property relationships with sediment transfer functions. a) A cartoon of a layer-over halfspace model with the sediment properties used in the demonstration. b) The shear-wave velocity profile of the model in Figure 2a. c) The sediment transfer function given the properties in Figure 2a with an infinite Q value. d) The sediment transfer function given the properties in Figure 2a with a Q value of 20. The theoretical transfer functions are computed using the routine from Boore (2005).

1.3 Empirical transfer functions

Theoretical transfer functions are obtained by measuring the required sediment properties, choosing a constitutive model, which could be more complex than the SH1D model presented in section 1.2, and predicting the transfer function by inputting the estimated properties into the constitutive model. It is also possible to obtain transfer functions empirically (ETF) by deconvolving earthquake waveforms at a sediment site and a rock site. The theory behind this method simplifies the earth through which seismic energy passes as a source $i(t)$, a path $h_e(t)$, a site geology $h_g(t)$ (Figure 3). Assuming the earth is a causal

linear, time-invariant system, the recorded ground motion at a sediment site $s(t)$ is a convolution of these three terms and an instrument response $h_r(t)$ term (Equation 4).

$$s(t) = i(t) * h_e(t) * h_g(t) * h_r(t) \quad (4)$$

(Borchert, 1970; Sheriff and Geldart, 1995) Since the multiplication of Fourier response spectra in the frequency domain is equivalent to convolution of the corresponding time domain signals, Equation 4 can also be written as

$$S(f) = I(f) H_e(f) H_g(f) H_r(f) \quad (5)$$

where each term is the Fourier spectra of the corresponding term in Equation 4. Given an earthquake with a large hypocentral distance from a sedimentary basin, it is assumed that seismic recordings with the same instrument (and therefore same instrument response $H_r(f)$) that are close to one another have equal source $I(f)$, and path $H_e(f)$ terms. The empirical transfer function, therefore, can be computed if the site instrument is located on soft sediments and the reference instrument is located on bedrock. This computation is the deconvolution of the horizontal component of the site instrument recording $S_a(f)$ and the reference instrument $S_b(f)$. It is common to use the Fourier amplitude spectra rather than the whole spectrum or phase spectrum to analyze how much the amplitude of seismic energy is affected and at which frequencies by the overburden properties which is represented in Equation 6 by the absolute value symbols represent the Fourier amplitude spectra (FAS).

$$ETF = \frac{|S_a(f)|}{|S_b(f)|} \quad (6)$$

Equation 6 is an empirical transfer function which is also often referred to as a spectral ratio (SR).

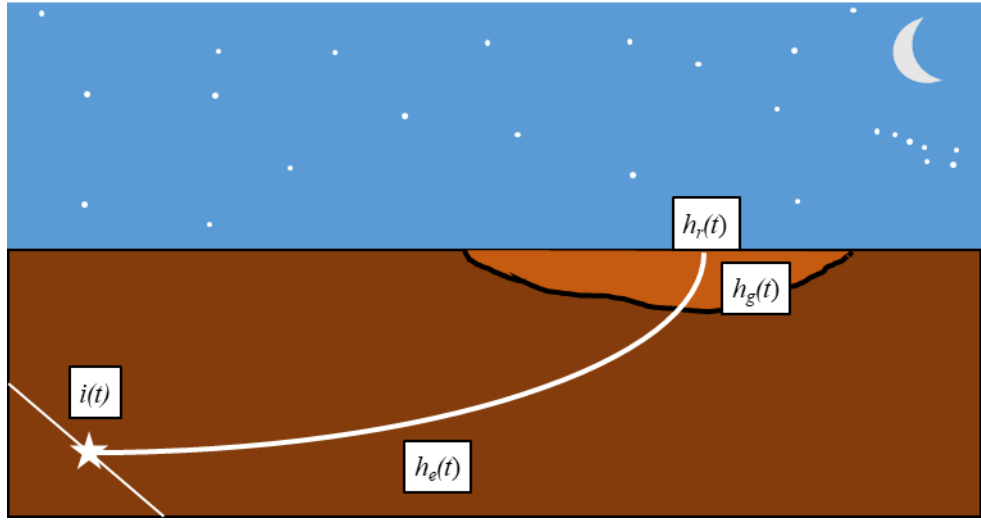


Figure 3. Cartoon of the theory behind the development of an empirical transfer function. The source term $i(t)$, path term $h_e(t)$, site term $h_g(t)$, and instrument response term $h_r(t)$ are convolved together into the instrument record $s(t)$. To compute an empirical transfer function, two seismic recordings in a basin, one located at the sedimentary site, and one located on bedrock are deconvolved using Equation 6.

1.3.1 Standard spectral and borehole spectral ratio

To compute an empirical transfer function, two station geometries are typically used. A standard spectral ratio (SSR) uses a reference site which is a bedrock location somewhere outside of the soft sedimentary basin as the instrument recording for the denominator of Equation 6. This method assumes that the seismic shaking at this reference site is approximately equal to that of the seismic shaking at the sediment-bedrock interface below the site of interest. A borehole spectral ratio (BSR) uses a coupled surface-borehole seismometer pair where the borehole station is at the sediment-bedrock interface. It is much more expensive to set up. In Figure 4, the array geometries for both methods are presented with the station for the recording of the denominator in Equation 6 for the standard spectral ratio labeled “ b ” and for the borehole spectral ratio labeled “ c ”. The station for the recording of the numerator in Equation 6 for both methods is station “ a ”.

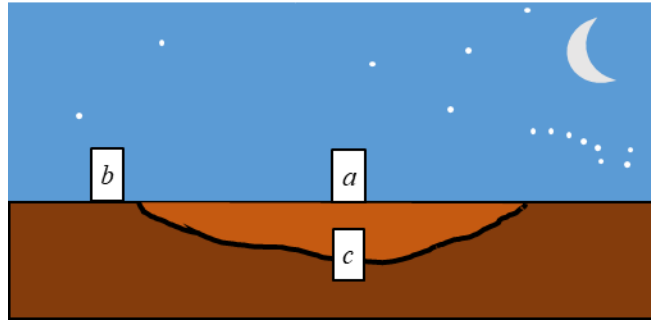


Figure 4. Array geometries for an *SSR* and a *BSR*. Station *a* is the sediment site station at which each method is computing the empirical transfer function. The recording at station *a* is the numerator in Equation 6 for both methods. Station *b* is the reference station for the *SSR* method whose recording is the denominator of Equation 6. Station *c* is the reference station for the *BSR* method whose recording is the denominator of Equation 6.

1.3.2 Computing a spectral ratio

Computing a standard and a borehole spectral ratio requires instrument recordings of earthquakes at a sediment site and a reference site or borehole site, respectively. Given these pieces of information, an *ETF* is computed from the horizontal components of the two recordings using Equation 6. Figure 5 shows the basic procedure of computing a standard spectral ratio using a single event. A borehole spectral ratio is computed the same way, but the reference site recording is a downhole instrument coupled with the surface instrument rather than an instrument located on bedrock outside of the basin. In this procedure, the Fourier amplitude spectra of both recordings is computed, and the ratio is taken to obtain the *ETF*.

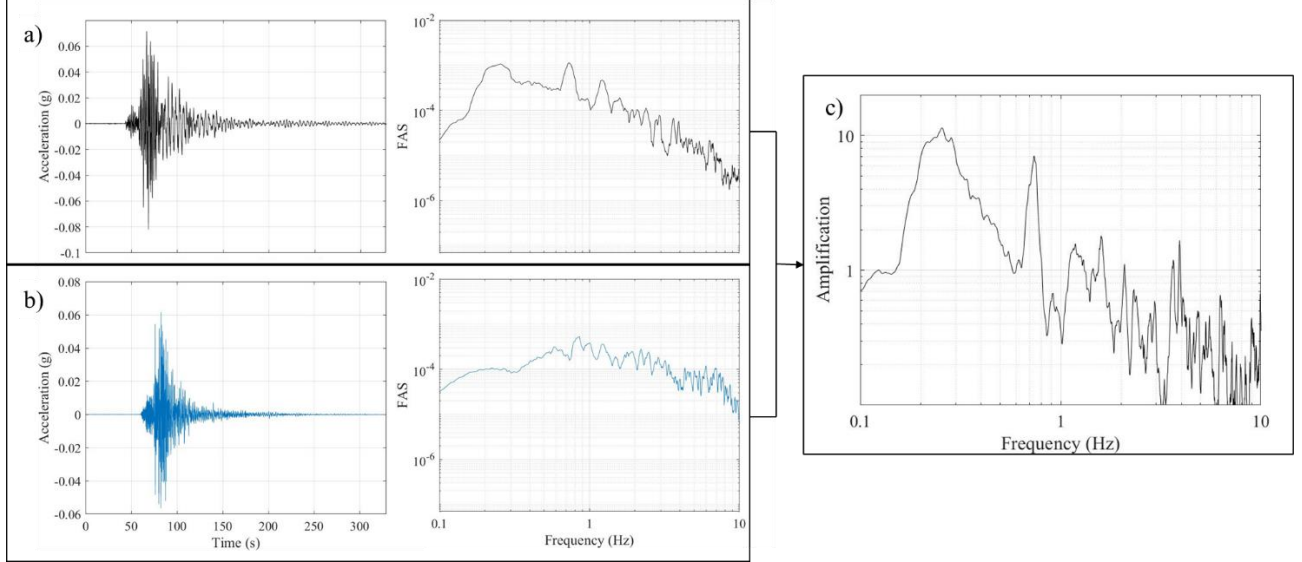


Figure 5. The procedure for computing an empirical transfer function for a standard or borehole spectral ratio with a single earthquake recording. This is the numerator in Equation 6. a) The time series and Fourier amplitude spectrum for the sediment site. b) The time series and amplitude spectrum for the reference site. This is the denominator in Equation 6. For a standard spectral ratio, this is the recording at station *b* in Figure 4. For a borehole spectral ratio, this is the recording at station *c* in Figure 4. c) The *ETF* for the event which is the ratio of the two Fourier amplitude spectra.

It is common to compute a median *ETF* given several earthquakes recorded at both site and reference stations. The median *ETF* of several events recorded at two stations is computed using the maximum likelihood estimator:

$$ETF_{mdn}(f) = \exp\left(\frac{1}{n} \sum_{i=1}^n \ln[ETF_i(f)]\right) \quad (7)$$

where $ETF_i(f)$ is the $ETF(f)$ for $i = 1, \dots, n$ ground motions. In Figure 6, ETF_{mdn} is plotted with a large sample $100(1-\alpha)$ confidence interval:

$$\exp\left(\ln[ETF_{mdn}(f)] \pm z_{1-\alpha/2} \times \sigma_{ln}(f)\right) \quad (8)$$

with standard deviation:

$$\sigma_{ln}(f) = \sqrt{\frac{1}{n} \sum_{i=1}^n (\ln[ETF_i(f)] - \ln[ETF(f)])^2} \quad (9)$$

(Thompson et al. 2012). In the example in Figure 6, many earthquakes are recorded at both site and reference stations. For each event in Figure 6a, the procedure in Figure 5 is performed and then averaged together using Equations 7-9 (Figure 6b and c).

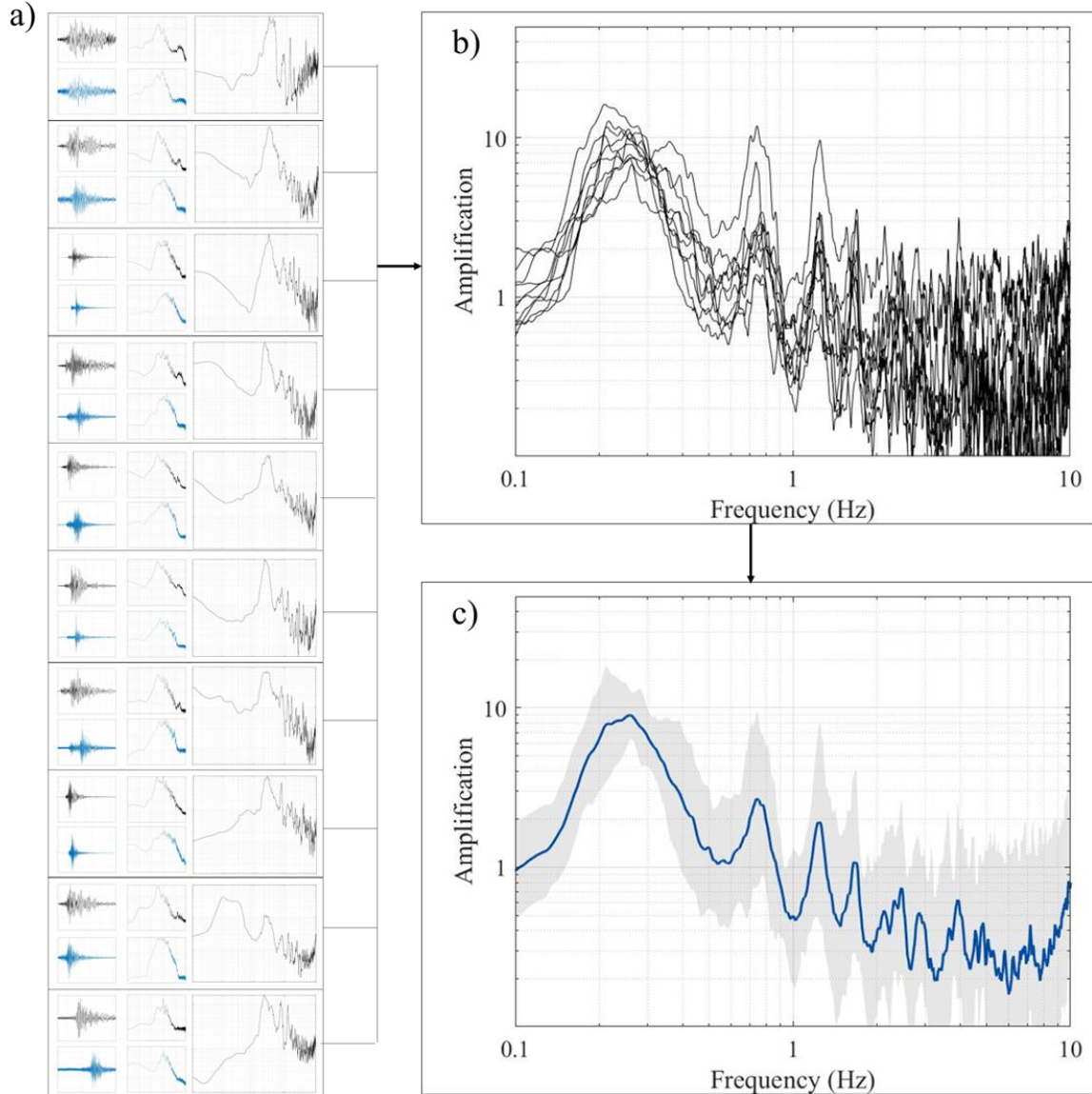


Figure 6. The procedure for computing an empirical transfer function for a standard or borehole spectral ratio with many earthquake recordings. a) The left two columns show the time series and Fourier amplitude spectra of the sediment site recordings (in black and station *a* in Figure 4) and reference site recordings (in blue and station *b* for an *SSR* and station *c* for a *BSR* in Figure 4) for 10 events recorded at both sediment site and reference site instruments. The right column is the ETF for the individual earthquake record. b) The 10 ETFs on one plot. c) The averaged ETFs computed using Equations 7-9. The blue line is the median line, and the grey fill is the 95% confidence interval computed using Equation 8.

1.4 Horizontal-to-vertical spectral ratio

Theoretical and empirical transfer functions are both ways to estimate seismic site response, but both require significant effort to measure and have uncertainties. Theoretical transfer functions require the collection of data to estimate the sediment properties necessary for the parameters of the chosen constitutive model which introduces aleatoric uncertainty to the transfer function estimation. Additionally, the physical model chosen is itself uncertain. This uncertainty in the constitutive model introduces epistemic uncertainty to the site response estimation. Empirical transfer functions require a seismic network with multiple stations and quality seismic recordings. Borehole seismometers are very expensive with reference station seismometers less so, but still costly. Given these uncertainties and costs, the estimation of a sediment transfer function is challenging and so researchers have devised other ways of making the estimation. The Horizontal-to-Vertical Spectral Ratio (*HVSR*) is a methodology that allows for the approximation of the fundamental peak of the sediment transfer function using earthquake recordings or seismic noise recorded at a single station (Nakamura, 1989) which significantly reduces complexity and cost of estimating site response.

1.4.1 HVSR theory

An *HVSR* is defined as the ratio of the *FAS* of the horizontal component of a recording (earthquake or noise) divided by the vertical component of the same recording. The theory states that the surface ground motion is composed of shear-waves (*S*-waves), compressional wave (*P*-waves) and surface-waves at different amplitudes and frequencies. Since a surface record is composed of all these motions, a simple *FAS* is insufficient to characterize the shear-wave content of the record. The *HVSR* works by reducing the Rayleigh and *P*-wave influences on the surface record to enhance the imaging of the shear-wave resonance. The derivation starts with a sediment empirical transfer function (the same as Equation 6 which has been simplified in this demonstration):

$$a(f) = H_a/H_c \quad (10)$$

where H_a is the horizontal FAS at location a on the ground surface, and H_c is the horizontal FAS at location c at depth (Figure 4). The surface site, H_a , is influenced by Rayleigh waves, the amount of which relative to the bedrock site is

$$\text{Influence of Rayleigh wave} = V_a/V_c \quad (11)$$

where V_a is the vertical magnitude response at location a , and V_c is the vertical magnitude response at location c . This assumes that the Rayleigh wave particle ellipse dimensions are uniform and scaled throughout the material. Dividing the shear-wave amplification by the influence of the Rayleigh wave, therefore, removes the influence of the Rayleigh wave.

$$a(f)/\text{Influence of Rayleigh wave} = \frac{H_a}{H_c} \times \frac{V_c}{V_a} \quad (12)$$

There is little amplification of multiple reflecting P -waves propagating from location c to location a at the shear-wave resonant fundamental frequency (f_0) because the P -wave has a higher velocity than the S -wave, thus the P -wave f_0 will be higher than the S -wave f_0 . Similarly, Rayleigh waves influence the record at higher frequencies than the S -wave f_0 . The ratio of the vertical motions at the S -wave f_0 is therefore approximately 1, while at higher frequencies, the correction normalizes out the Rayleigh wave and P -wave influences. The Rayleigh and P -wave resonance peaks beyond the S -wave f_0 are therefore diminished without significantly affecting the amplitude or shape of the fundamental peak. The S -wave f_0 frequency and amplification at location a can therefore be approximated by the *HVSR* at the fundamental frequency (f_0) defined as

$$\text{HVSR}(f_0) = \frac{H_a}{V_a} \quad (13)$$

because $V_c/H_c = 1$. Equation 13 defines the Horizontal-to-Vertical Spectral Ratio.

1.4.2 Computing an HVSR

HVSR curves can be computed using earthquake records (*eHVSR*) and seismic microtremors (*mHVSR*). To compute an *eHVSR*, the same procedure as demonstrated in Equations 7-9 and Figure 6 is

used except instead of the *FAS* of the horizontal component of the reference site as the denominator, the *FAS* of the vertical component of the surface record is used as the denominator. For an *HVSR*, the black time series' and *FAS'* of Figure 6a are the vertical component of the site recording rather than the horizontal component of a reference site. To compute an *mHVSR*, seismic noise is collected (Figure 7a). The noise is windowed and the *FAS* of each component in each window is computed. The horizontal component *FAS* are combined by their geometric mean and then the *HVSR* of each window is computed by dividing the geometric mean of the horizontal component *FAS* by the vertical component *FAS*. This creates an *HVSR* curve for each window (Figure 7b). Finally, these windows are combined using Equations 7-9 to compute median *HVSR* curves, a standard deviation at each frequency and, if needed, confidence intervals (Figure 7c). The fundamental frequency (f_0) is selected from the median *HVSR* curve using the process described in Chapter 1.

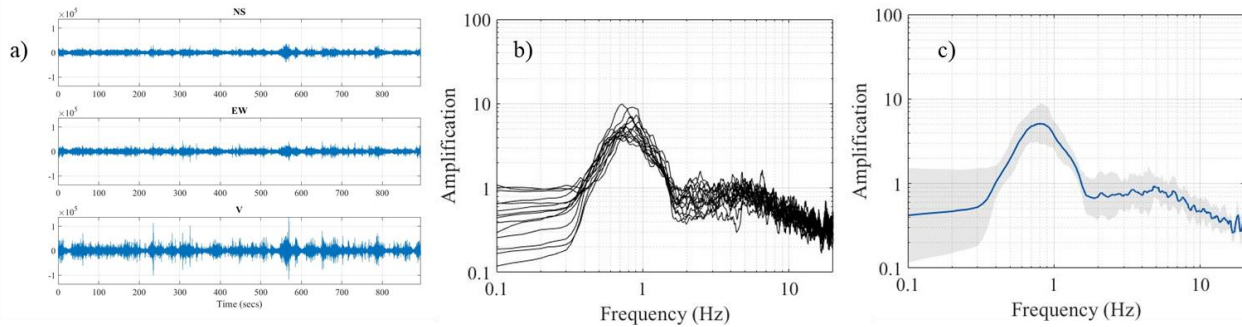


Figure 7. Steps for computing an *mHVSR*. a) A time series of three components (north-south, east-west, and vertical) of seismic noise. b) The *HVSR* of each individual noise window. c) the median *HVSR* curve and 95% confidence interval (grey) computed from all the windowed *HVSR* curves in Figure 7c using Equations 7-9.

1.4.3 Importance of the HVSR to this dissertation

This dissertation is a study of seismic site response in New England, USA, which involves understanding the geometric and mechanical properties of the major surficial geologic units in the region. New England is a low seismicity region and therefore has little data with which to compute earthquake *ETFs* and calibrate sediment models to those *ETFs*. The *HVSR* is therefore an essential tool to studying site response in New England because it approximates the fundamental peak of the sediment transfer function

using seismic noise, and therefore doesn't require earthquake recordings. It is inexpensive to collect and relatively simple to compute and therefore can be collected widely to study many of the region's major geologic units. The f_0 value picked from an *HVSR* curve is a function of the depth to the impedance contrast and shear-wave velocity of the overburden and therefore provides insight into these values which are necessary for understanding site response. Site response is a known phenomenon well studied in earthquake prone areas. By using *HVSR* curves and the sediment fundamental frequency picked from those curves in a region with few seismic recordings, it is possible to model potential site response in future seismic events in a region without a robust historical record. The work of this dissertation was done operating under the philosophy that significant, costly earthquake will happen in New England in the future and therefore that potential site effects should be studied with the tools available to better anticipate and quantify this risk.

1.5 Motivation

1.5.1 Chapters 1 and 2 - Lack of existing site characterization maps of New England

Prior to the work of this dissertation, two regional site characterization maps existed for New England: Becker et al. (2011) and Wald and Allen (2007). Both studies map $Vs30$ which is the time-averaged shear-wave velocity of the top 30 meters from the free surface:

$$Vs30 = \frac{\sum_{i=1}^{30} h_i}{\sum_{i=1}^{30} V_{s_i}} \quad (14)$$

where h_i is the thickness of a layer and V_{s_i} is the shear-wave velocity of that layer. $Vs30$ is typically converted to seismic site classes (A-E) using the ranges in Table 1 (Federal Emergency Management Agency, 1994; Borcherdt, 1994). Becker et al. (2011) use surficial geologic maps to convert geologic units directly into seismic site classes. Their conversions are based off shear-wave velocity profiles and local geologist knowledge for typical velocity ranges of the different units (Figure 8b). Wald and Allen (2007) develop a global database of $Vs30$ measurements and relate it to slope from the global Shuttle Radar Topography (SRTM, Farr and Kobrick, 2000) digital elevation model (Figure 8a). This map makes a $Vs30$ prediction at each 30 arc second (approximately 1km resolution) pixel based on the global slope vs. $Vs30$

relationship. Both projects were important steps to towards developing quality site characterization maps for the region, however, both studies are general and can be improved with better local information and new methodologies. The first two chapters of this dissertation develop site characterization maps for New England and Massachusetts by compiling a database of local site characterization measurements and processing them in a framework that is conducive to the New England region.

Table 1. Vs30-based seismic site classifications defined by NEHRP (1994).

Site Class	Generic Description	Range of Vs30
A	Hard Rock	> 1500 m/s
B	Rock	760-1500 m/s
C	Very dense sediment and soft rock (firm horizon)	360 < 760 m/s
D	Stiff sediment	180 < 360 m/s
E	Sediment profile with soft clay	< 180 m/s

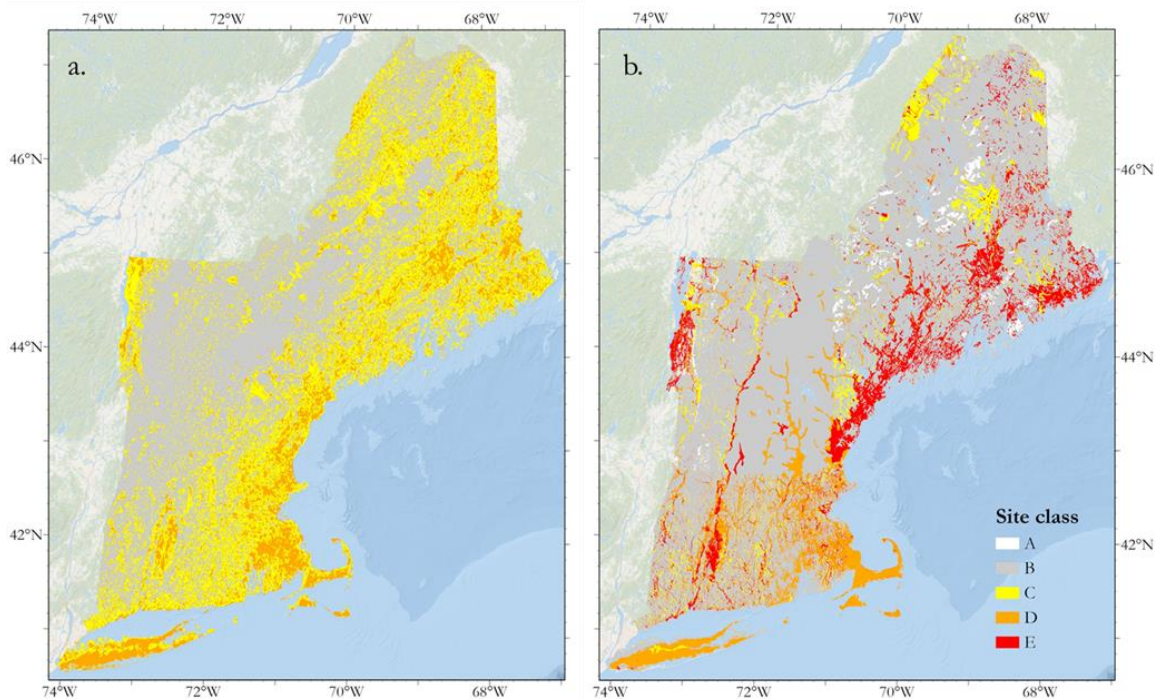


Figure 8. New England seismic site class from a) the Vs30 model of Wald and Allen (2007) and b) the geology-based site class methodology of Becker et al. (2011). The range of Vs30 values for each site class are provided in Table 1.

1.5.2 Chapter 3 – Using the Massachusetts depth-to-bedrock map to make an f_0 map

Chapter 3 was motivated by a project that the Massachusetts Geological Survey undertook on a contract through the Department of Transportation (DOT). The Survey was contracted to compile depth-to-bedrock borings into a depth-to-bedrock model of the State. One of the byproducts of this model specified by the contract was a NEHRP seismic site classification map to use in a HAZUS seismic risk assessment for the state (Mabee et al. 2023). The author helped on this part of the project, making the site classification map that was used in the HAZUS analysis in the DOT report using similar techniques to those developed in Chapters 1 and 2 of the dissertation (Figure 9). Though this project was a valuable study, particular for the improvement it made to the existing NEHRP site classification map in the state, it lacked uncertainty quantification and existed within the V_{s30} framework, which motivated the decision to use the Massachusetts depth-to-bedrock map to create an f_0 map with quantified uncertainty. This excellent dataset and the possibilities it presented to fit within the f_0 , overburden velocity, depth to the impedance contrast framework was a major motivation in the development of Chapter 3.

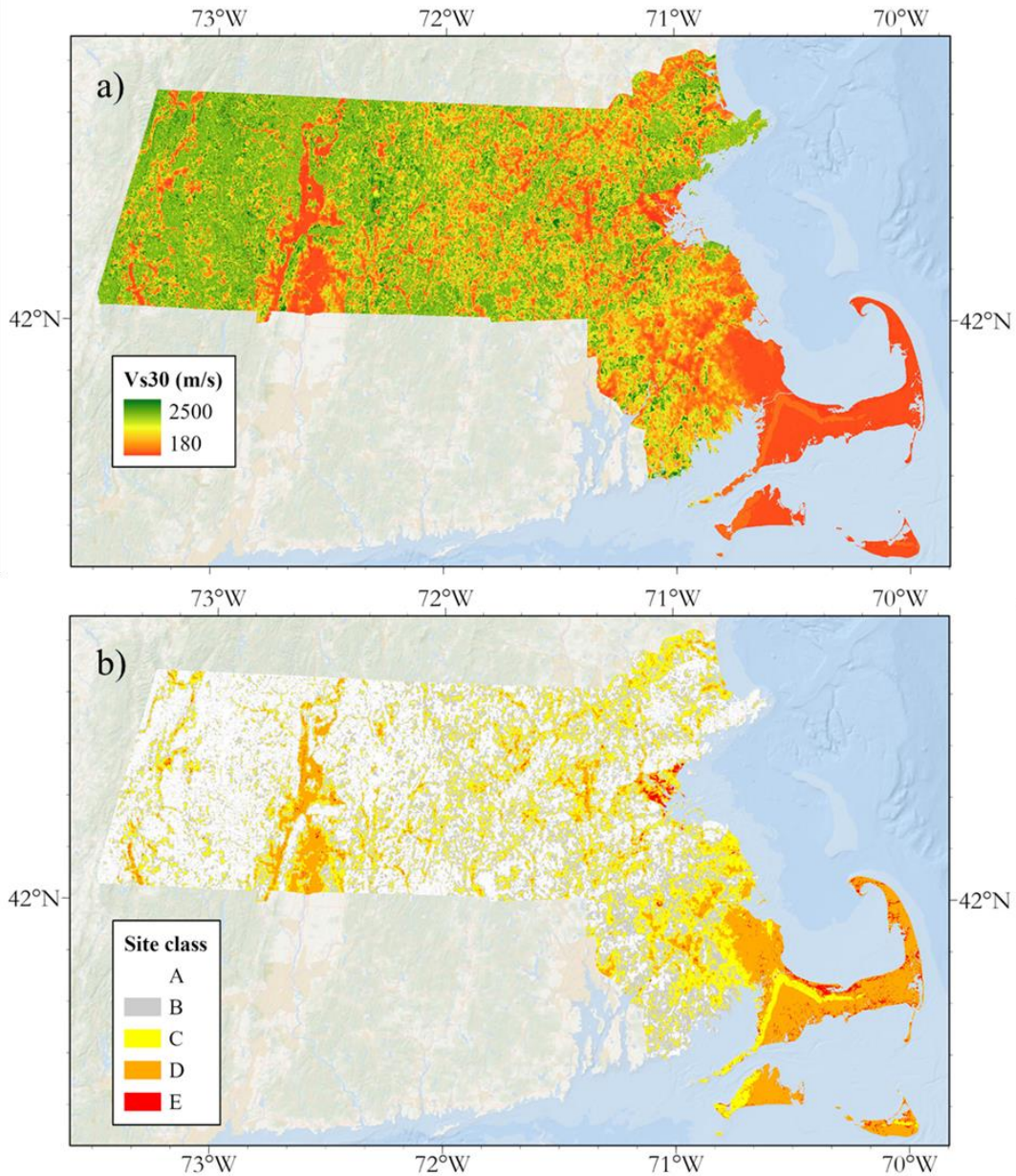


Figure 9) Vs30-based site classification maps developed by the author for the Massachusetts Geological Survey's depth-to-bedrock project for the Department of Transportation. a) The Vs30 map and b) the corresponding Vs30-based site classification map using the categories in Table 1.

1.5.3 Using f_0 as a mapping parameter

This dissertation uses site fundamental frequency (f_0) as a mapping parameter for seismic site response and provides two techniques to make f_0 maps. Many studies have mapped Vs30 to use as inputs into seismic hazard assessment routines like HAZUS and Ground Motion Models (GMMs) (Wills and

Clahan, 2006; Yong, 2016; Wald and Allen, 2007; Foster, 2019; Thompson et al. 2014; Parker et al. 2017; Mori et al. 2020b; Stewart et al. 2014; Heath et al. 2020). This dissertation proposes that f_0 , overburden shear-wave velocity and depth to the impedance contrast are a better framework to analyze site response than $Vs30$ and thus should have methodologies developed to map it. This dissertation is one of the first works that develops regional maps of f_0 (which is most often mapped on the city-scale in microzonation studies) as a site characterization parameter which is abundant, relatively inexpensive to collect, and has simple physical relationships to overburden velocity and depth to the impedance contrast.

1.5.4 Incorporating uncertainty

One of the motivations for this dissertation was to map site characterization where it hadn't been well-mapped and to develop new techniques to do this, proposing the use of f_0 as a new site characterization mapping parameter. Another motivation is more general which is to quantify uncertainty in site characterization estimation. This operating philosophy influenced the selection and development of the methodologies presented this dissertation. For example, the product for the Department of Transportation in Figure 9 does not incorporate uncertainty. This was expanded in Chapter 3 to output distributions of f_0 rather than single values of $Vs30$. This work is a part of a larger movement of researchers incorporating uncertainty into their estimates to quantify probabilities of possible outcomes on which to base decisions rather than single predictions.

1.6 Dissertation organization

This dissertation makes maps of site fundamental frequency (f_0) using increasingly refined methodologies and higher resolutions. Chapter 1 compiles all the f_0 data that exists in New England in the literature and collects 487 additional HVSR stations across the region where data is sparse and site amplification effects are likely. The f_0 database is aggregated using the classifications of the Soller et al. (2009) conterminous US surficial geologic map and distributions of f_0 in the major geologic units are developed. In this chapter, estimates of average overburden velocity (Vs_{avg}) are developed using existing shear-wave velocity profiles in the region and grouping them within the surficial geologic classifications.

The methodology of Hassani and Atkinson (2016) is then applied to estimate $Vs30$ distributions from f_0 and Vs_{avg} . This chapter establishes estimates of possible f_0 values in the major surficial geologic units in New England and develops the framework to integrate f_0 , shear-wave velocity, and surficial geologic datasets.

While Chapter 1 provides estimates of typical f_0 values in large geologic units and demonstrates a methodology to make those estimations, it does not parse the f_0 dataset in a way that addresses variations in depth between large, congruent deposits which are defined in this work as local sedimentary deposit subregions. This causes some of the distributions describing each geologic unit to have central tendencies that deviate from the f_0 central tendencies of some local deposits of the same geologic classification. For example, in Chapter 1, the fine-grained, proglacial sediments are the geologic classification that composes many of the sediments in both the Boston Basin and the Maine coast. The Maine coast, however, tends to have shallower deposits than the Boston Basin and therefore has f_0 values that are consistently higher than those in the Boston Basin. Chapter 2 addresses this issue by introducing a map of local sedimentary deposit subregions. These subregions are defined using a digital elevation model and state-scale local geologic maps. The extent of a local geologic subregion is the line of equal elevation at which the soft geologic units in a local congruent deposit meets the till classification. Using this additional spatial classification, the f_0 dataset is parsed to create f_0 distributions that better represent each local deposit. In addition to the inclusion of local deposit information, this Chapter uses a geologic map that is much higher resolution than the map used in Chapter 1, improving site characterization especially in higher resolution topographic features like tight river valleys. Finally, Chapter 2 models Vs_{avg} in different geologic units as a random variable rather than a single number better classifying $Vs30$ distribution estimates. Using a similar framework to that of Chapter 1, Chapter 2 shows that increased resolution of the geologic maps and the inclusion of local congruent deposit information significantly reduces the residuals between the f_0 distribution median and the values of the f_0 stations in local deposits.

Chapter 3 maps f_0 as a site characterization parameter in the state of Massachusetts using a depth-to-bedrock model as its primary input. Additionally, it develops velocity models of the overburden using a

different technique than that used in the first two chapters. In the first two chapters, shear-wave velocity central tendency and dispersion are estimated using shear-wave velocity profiles in the region. Though this works in principle, there are very few shear-wave profiles on which to base the estimates. As a result, the uncertainty estimates were not as well characterized in the first two chapters as they are in the third chapter. In Chapter 3, this issue is addressed by developing $f_0 - z$ relationships using the methodology of Ibs-von Seht and Wohlenberg, J. (1999). By developing these relationships using z values from the depth to bedrock map and assuming a velocity-depth power law relationship the shear-wave velocity of the overburden is modeled with significantly more data than the models using the few shear-wave velocity profiles to create the average profile. With depth-to-bedrock at 100m resolution and shear-wave velocity profile estimates, both with well-characterized uncertainty, f_0 distributions are computed across the state. This Chapter has the same output as that of the first two chapter (f_0 distributions) but is built on a foundation of significantly more data and robust processing with a different methodology.

CHAPTER 2

Regional-Scale Site Susceptibility Mapping in High Impedance Environments Using Soil Fundamental Resonance (f_0): New England, USA

Pontrelli, M.A., Basie, L.G., Ebel, J.E. (2023a) Regional-scale site characterization mapping in high impedance environments using soil fundamental resonance (f_0): New England USA. *Engineering Geology*, Vol. 315, doi: <https://doi.org/10.1016/j.enggeo.2023.107043>

Abstract

In this work, we develop regional-scale site susceptibility maps of New England, a glaciated region in the Eastern United States, using site fundamental frequency (f_0). Due to the strong impedance contrast that creates strongly resonant site response behavior in New England, f_0 is the preferred site response proxy for the region and best characterizes spatial variability in soil amplification. We first develop a database of 1577 f_0 values collected from the literature (1313) and picked from HVSR curves collected during an additional field campaign (487). Using the surficial geologic units from the conterminous US surficial geology map of Soller et al. (2009) and the methodology that Wills and Clahan (2006) used to create surficial geology based $Vs30$ maps, we compute distributions of f_0 for each of the surficial geologic units mapped in New England. We find that the thick glaciofluvial ice-contact sediments and thick proglacial sediments of Cape Cod and Long Island are characterized by f_0 distributions with the lowest medians (1.06 and 1.03 Hz respectively) and narrowest interquartile ranges (0.23 and 0.28 Hz respectively) in New England, which we interpret as being the thickest sediments in the region. The f_0 distribution of the thin, proglacial sediments, mostly fine-grained in the Boston Basin, the coast of Lake Champlain and the Maine coast has a relatively low median (2.70 Hz), however it has high variability (3.65 Hz interquartile range) since the sediment thickness varies widely in this geologic unit. The f_0 distribution of the thin alluvial sediments of the Connecticut River Valley also has a low f_0 median (1.83 Hz) however, it has less variability than the proglacial sediments, mostly fine-grained thin (1.59 Hz). We present maps of the median and interquartile range of the f_0 distributions and their corresponding $Vs30$ distribution approximations. $Vs30$ distributions are developed for each of the surficial geologic units by assuming a layer-over-halfspace model for site response and establishing estimates of sediment average shear-wave velocity (Vs_{avg}) for each of the units based on a limited number of shear-wave velocity profiles from the region. We compare our results against two existing site susceptibility maps for the region, Wald and Allen (2007) and Becker et al. (2011) and find that our updated maps result in median $Vs30$ values that tend to be higher than Becker et

al. (2011) except in geologies with consistently deep profiles, and lower than Wald and Allen (2007) median values, with the exception of coastal zone sediments.

1.0 Introduction

Regional-scale site susceptibility maps are useful for earthquake planning, seismic hazard assessment, loss estimation and many other applications. Several site amplification parameters have been developed by the earthquake engineering community, including $Vs30$ which is defined as the average shear wave velocity over the top 30 meters of the soil profile (Borcherdt, 1992, 1994) and site fundamental frequency, f_0 , which can be picked from the fundamental resonance peak of a Horizontal-to-Vertical Spectral-Ratio using the technique introduced by Nakamura (1989). $Vs30$ has been used extensively to map regional seismic site amplification hazard using a variety of techniques but in general assigns regional averages of site-specific properties to develop estimates of site susceptibility over large areas (Parker et al. 2017; Stewart et al. 2014; Wald and Allen, 2007; Borcherdt, 1991a). f_0 is gaining popularity in the ground motion modeling community (e.g. Braganza et al. 2016, Gallipoli and Mucciarelli 2009, Ptilakis et al. 2019, Stambouli et al. 2017), yet, similar regional-scale susceptibility maps for f_0 currently do not exist. Nakamura (1989) showed that the site fundamental frequency, f_0 , of the HVSR curve is empirically similar to the fundamental peak of the site empirical transfer function and thus can be used as a measure of the soil fundamental resonance. Site amplification resulting from high impedance contrasts yields strong resonance which is well characterized using the horizontal-to-vertical spectral ratio (HVSR, Nakamura, 1989) as shown by Yilar et al. (2017) for Boston, Massachusetts and, Braganza et al. (2016) in Eastern Canada. Impedance contrasts in the New England, USA region are consistently between 5-20 and the SESAME project recommends the HVSR method for impedance contrasts > 2 (SESAME, 2004 a and b). Researchers commonly use the HVSR to estimate site response in resonant sediments because it is inexpensive and requires relatively simple processing steps (Lermo and Chávez-Garcia, 1993; Carpenter et al. 2018; Zhu et al. 2020). Researchers have been interested in the use of f_0 as a predictor of site response and as a site term in ground motion models (Braganza et al. 2016, Gallipoli and Mucciarelli 2009, Ptilakis et al. 2019,

Stambouli et al. 2017). Researchers have also shown that f_0 can complement and sometimes outperform $Vs30$ as a site parameter in ground motion models as Hassani and Atkinson (2016) demonstrated in Eastern Canada.

New England, USA is a good region to develop f_0 regional-scale site susceptibility maps due to the high impedance contrast observed between sediments and bedrock. During the Wisconsin glaciation period, the Laurentide ice sheet covered the region and the glaciers cleared most of the existing sediment and weathered bedrock and began depositing glacial sediments on the clean bedrock surface creating high impedance contrasts. High near-surface impedance contrasts are common throughout New England due to the soft overburden layers found in the regional geologic environments, specifically outwash, glacial lake deposits, marine clays, and flood plain alluvium that overlie the crystalline bedrock. The NGA-East project established that bedrock seismic velocities range from 2000 to 3000 m/s in Central and Eastern North America whereas marine clays, alluvial sands, and other sediments often have seismic velocities ranging from 150-350 m/s setting up strong impedance contrasts (Stewart et al. 2020). Baise et al. (2016) demonstrated that the Boston Basin, a relatively small sedimentary basin underlying the greater Boston area in eastern New England, has a high impedance contrast between the sediments (marine clay, known as the Boston Blue Clay, sands, and artificial fill) and the underlying glacial till and bedrock which results in significant site amplification. Due to the fundamental relationship between f_0 and soil amplification in strongly resonant environments, the site susceptibility maps developed herein for New England use f_0 as the primary mapping parameter. Additionally, f_0 is a relatively rapid and inexpensive measurement to collect and is therefore a good measurement on which to base a regional-scale site susceptibility map since many stations can be collected over a broad area.

Two $Vs30$ -based site susceptibility maps currently exist for the region: the global Wald and Allen (2007) slope-based $Vs30$ map includes New England and the Becker et al. (2011) which was specifically developed for New England. The Wald and Allen (2007) model is a 1 km pixel resolution global model that uses a relationship derived between slope data from the Shuttle Radar Topography Mission 30-sec

(SRTM30) global digital elevation model and $Vs30$ data compiled in the US, Taiwan, Italy, and Australia (see Figure 1a for the New England region, shown as seismic site class for comparison to Becker et al. 2011). NEHRP seismic site classes are defined in Table 1 for reference. The relationship is applied across the globe to map $Vs30$. This method has been widely used globally and has been modified locally and regionally when data are available (Thompson et al. 2018; Wills and Clahan, 2006). The Becker et al. (2011) model is a geology-based site classification map of New England (see Figure 1b) which uses a relational table converting surficial geology into NEHRP seismic site class. The Becker et al. (2011) authors observed that the Wald and Allen (2007) based maps for New England tend to assign higher $Vs30$ to soft soils like clays and artificial fills than a geologist would using the surficial geology and depositional environment. The relational table that the authors of Becker et al. (2011) developed is based on a similar table from Cadwell (2003) which uses Vs measurements collected in four counties and eight surficial geologic units in New York state and provides ranges of Vs for the geologic units that were translated into site classes. In Becker et al. (2011), the authors created a similar table to that of Cadwell (2003) for all the surficial units in New England. Both the Wald and Allen (2007) and Becker et al. (2011) maps display areas in New England with site amplification potential; however, the Becker et al. (2011) map indicates significantly more site class E soils than Wald and Allen (2007). Of note are the large areas of site class E soils mapped along the Maine coast (the Presumpscot Formation), throughout the Connecticut River valley, and in northwestern New England (the Champlain Sea sediments).

In this paper, we develop a region-scale site susceptibility map that differs from the existing Wald and Allen (2007) and the Becker et al. (2011) maps, because we map f_0 as the primary site variable and we incorporate local f_0 data as we develop distributions by surficial geologic unit. For comparison to Wald and Allen (2007) and Becker et al. (2011), we show that an f_0 map can be coupled with Vs_{avg} (average velocity in the sediments) using the layer-over-halfspace framework for site response to provide estimates of regional $Vs30$ distributions by surficial geologic unit. Assuming a layer-over-halfspace site response model

results in the well-known relationship, $f_0 = Vs_{avg}/4d$, and provides a simple way of relating f_0 to Vs_{avg} and depth to the impedance contrast.

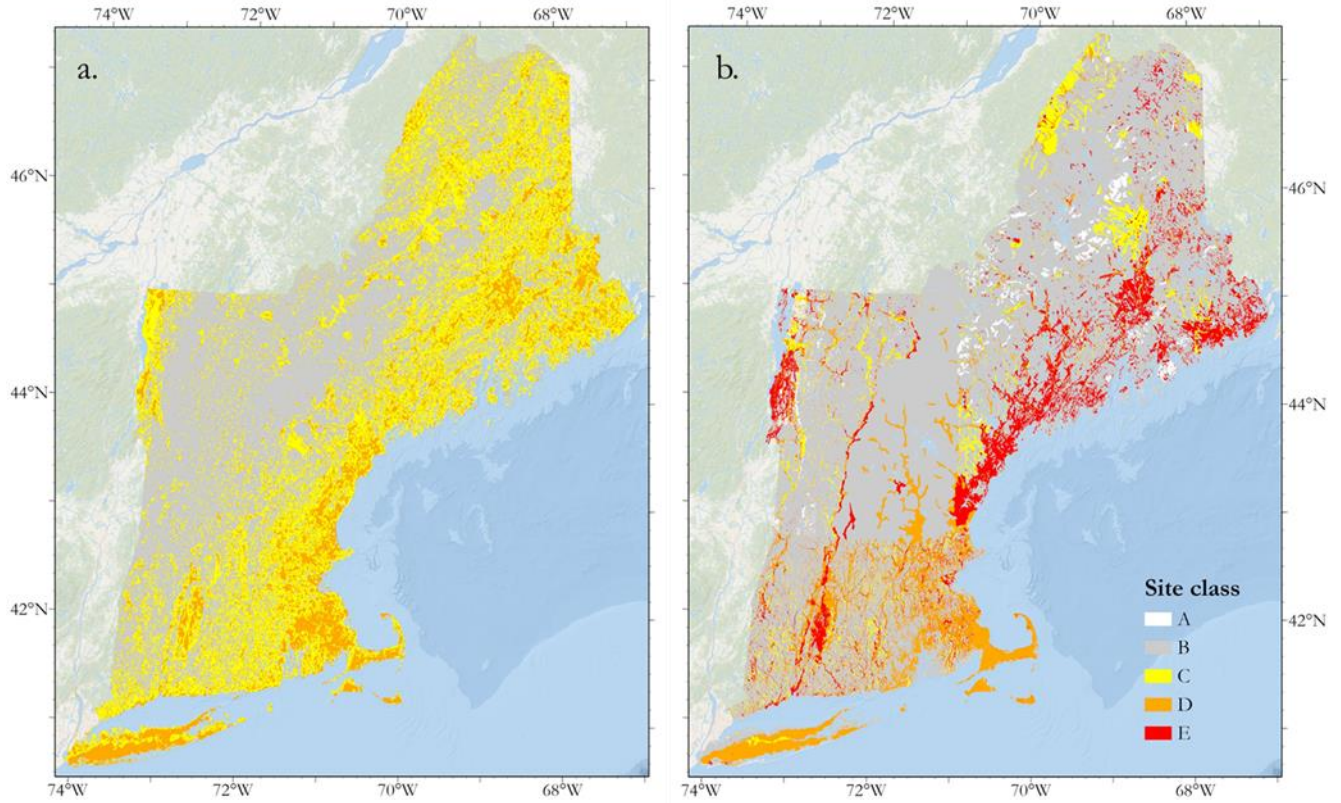


Figure 1. New England seismic site class from a) the $Vs30$ model of Wald and Allen (2007) and b) the geology-based site class methodology of Becker et al. (2011). The range of $Vs30$ values for each site class are provided in Table 1.

Table 1. $Vs30$ -based seismic site classifications defined by NEHRP (1994).

Site Class	Generic Description	Range of $Vs30$
A	Hard Rock	> 1500 m/s
B	Rock	760-1500 m/s
C	Very dense soil and soft rock (firm horizon)	$360 < 760$ m/s
D	Stiff Soil	$180 < 360$ m/s
E	Soil profile with soft clay	< 180 m/s

2.0 Data

This paper develops a site susceptibility map for New England using f_0 and the US conterminous surficial geologic map (Soller et al, 2009) as the mapping layer. We group all the surficial geologic units into a set of 8 combined units with similar depositional environments, sediment thicknesses, and grain size descriptions. We use 1577 f_0 values from HVSR analyses collected from Yilar et al. (2017), Fairchild et al. (2013), Mabee et al. (2022), and a field campaign of 487 additional HVSR tests from this study. We estimate Vs_{avg} values for each grouped geologic unit using 37 Vs profiles from Thompson et al. (2014), Hager Geoscience (2016), Lens and Springston (2013), and 5 profiles from this study. Each of these data sets are described below.

2.1 Conterminous US surficial geology map

The US conterminous surficial geology map is a 1:5,000,000 scale map compiled through a process of communication with state geological surveys identifying priority geologies and developing general overviews of each state's geology (Soller et al. 2009). The authors of Soller et al. (2009) are candid about the generalized nature of the map and acknowledge its simplification of the surficial geologic units. While higher resolution state-based surficial geology maps exist for Massachusetts (Stone et al. 2018), Vermont (Doll et al. 1970), Maine (Thompson and Borns, 1985) and Connecticut (Stone et al. 1992), they do not exist for all the New England states; therefore, we chose to use the consistent conterminous map of Soller et al. (2009) as the map layer for this project. When the conterminous map of Soller et al. (2009), is clipped to the New England region, the resulting map contains 20 surficial geologic units representing 3 different thicknesses, 8 depositional environments and 8 grain sizes. We grouped these 20 units into 8 combined units based on their sediment composition (Figure 2, Table 2).

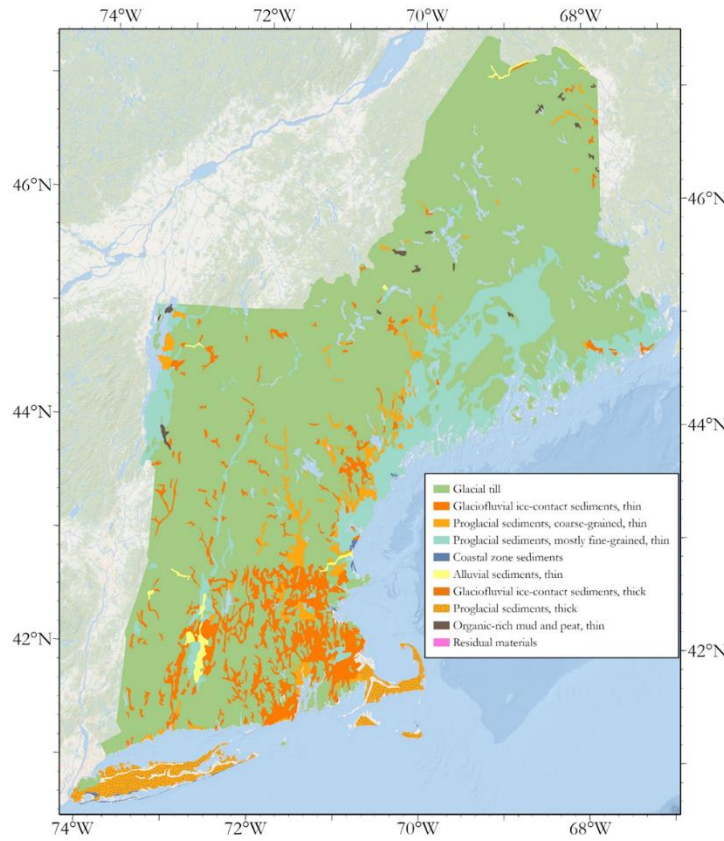


Figure 2. Grouped surficial geologies of the Soller et al. (2009) surficial geologic map of the Conterminous US using the groupings in Table 2.

Table 2. Surficial geologic unit grouping based depositional environment, sediment thickness, and grain size descriptions. Each of these new names is represented by its “Unit Code” in the rest of the figures and tables.

New surficial name	Surficial unit groups	Thickness
Glaciofluvial ice-contact sediments, thin	Glaciofluvial ice-contact sediments, mostly sand and gravel, thin; Glaciofluvial ice-contact sediments, mostly sand and gravel, discontinuous	Thin
Proglacial sediments, fine grained, thin	Proglacial sediments, mostly fine grained, thin; Proglacial sediments, mostly fine grained, discontinuous	Thin
Glacial till	Glacial till sediments, mostly sandy, thin; Glacial till sediments, mostly sandy, discontinuous; Glacial till sediments, mostly silty, thin; Glacial till sediments, mostly silty, discontinuous	Thin
Proglacial sediments, thick	Proglacial sediments, mostly coarse-grained, thick; Proglacial sediments, mostly fine grained, thick; Alluvial sediments, thick; Glacial till sediments, mostly silty, thick; Eolian sediments, mostly dune sand, thick	Thick

Proglacial sediments, coarse grained, thin	Proglacial sediments, mostly coarse-grained, thin	Thin
Alluvial sediments, thin	Alluvial sediments, thin	Thin
Glaciofluvial ice-contact sediments, thick	Glaciofluvial ice-contact sediments, mostly sand and gravel, thick	Thick
Coastal zone sediments	Coastal zone sediments, mostly fine-grained; Coastal zone sediments, mostly medium-grained	Thin
Organic-rich muck and peat, thin	Organic-rich muck and peat, thin	Thin
Residual materials	Residual materials developed in igneous and metamorphic rocks	Thin

2.2 HVSR database

To develop the regional f_0 database for this study, we compiled measurements from three prior projects: 570 measurements from the greater Boston area in Yilar et al. (2017), 198 measurements on Cape Cod from Fairchild et al. (2013), and 545 measurements across Massachusetts from Mabee (2022). Yilar et al. (2017) presented an f_0 microzonation study in the Boston basin and validated the ability of the HVSR method to perform well in regions underlain by artificial fill, marine clays, and glaciofluvial sediments. Fairchild et al. (2013) mapped bedrock topography in Western Cape Cod to predict the transport of groundwater contamination originating at the Massachusetts Military Reservation. Mabee (2022) compiled 27 depth-to-bedrock datasets in Massachusetts including boring logs and geophysical datasets to provide the public with the data necessary to develop top-of-rock maps for a variety of stakeholders. We extracted the f_0 data from these projects and did not process the raw data. To complement these data from the literature, we collected 487 additional HVSR measurements with a field campaign aimed to cover New England using major highways and targeting geologic deposits where we expected local amplification of seismic shaking. With these goals in mind, the field collection targeted Long Island, the southern (Connecticut-portion) of the Connecticut River Valley, the Presumpscot clays in coastal Maine and the Champlain Sea Sediments in northwestern Vermont. These targeted regions, illustrated in Figure 3b, were identified through our own local knowledge and discussions with the New England state geologists (Steve

Mabee, Mike Howley, personal communication). Additionally, we calculated f_0 values at all the permanent seismic stations in New England and included them in the study (Figure 3).

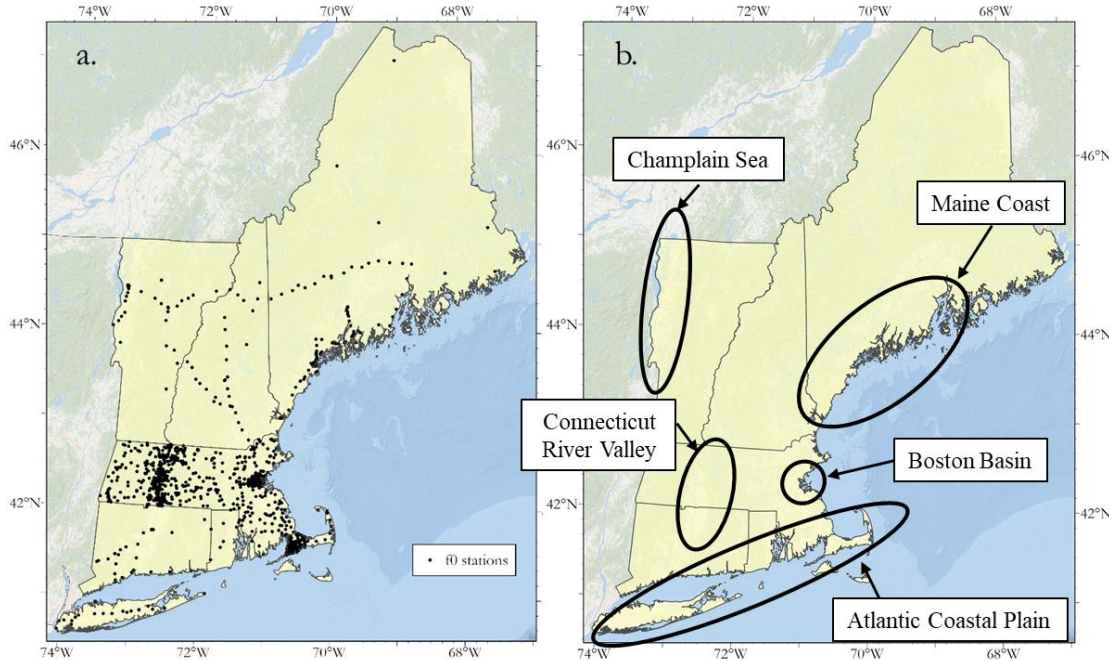


Figure 3. a) Spatial distribution of the HVSR database developed in this study. The north-south trending lines in the northern states are collection lines along interstate highways and the east-west transect across VT, NH and ME, is Route 2, running from the Berkshires through the Connecticut River Valley, the White Mountains and into Maine along the Androscoggin River. b) Major regions with amplifiable sedimentary units identified in this study.

We process the HVSR data using the Nakamura (1989) method and generally following the guidelines of the SESAME project (SESAME, 2004a and b), first collecting 15 minutes of ambient noise data sampled at 100 Hz using a CMG-40t broadband seismometer and a Reftek 130 digitizer. Our goal in processing of the microtremor data was to select the fundamental peak to characterize the resonant behavior of the site. We filter the noise using a four-pole Butterworth filter with a low corner frequency of 0.1 Hz and a high corner frequency of 49 Hz and then divide the resulting time series into twenty windows, each of forty seconds duration, and with one second window spacing. After windowing the data, we compute the Fourier amplitude spectra (FAS) of each window and each component and smooth the spectra with a 0.5 Hz wide moving average filter; however, we illustrate a Konno-Omachi filter for comparison in Figure 4b. We then combine the horizontal components using the geometric mean and divide the horizontal

component by the vertical component of each window to get 20 HVSR curves (Figure 4a). Finally, we compute the median and standard deviation HVSR curve (Figure 4b) from the 20 windows using the maximum likelihood estimator:

$$HVSR_{med}(f) = \exp\left(\frac{1}{n} \sum_{i=1}^n \ln[HVSR_i(f)]\right) \quad (1)$$

where $HVSR_i(f)$ is the $HVSR(f)$ for $i = 1, \dots, n$ windows with standard deviation:

$$\sigma_{ln}(f) = \sqrt{\frac{1}{n} \sum_{i=1}^n (\ln[HVSR_i(f)] - \ln[HVSR(f)])^2} \quad (2)$$

Following the development of the final median HVSR curve, we select f_0 from the curve by finding the first peak along the curve (the fundamental) that meets the criteria:

$$A - P < P/\sqrt{2} \quad (3)$$

Where A is the amplitude of the peak and P is the prominence of the peak where prominence is defined as the difference between A and the highest of the two interval minima on the signal on each side of the peak (MathWorks, 2022; Figure 4b). This definition ensures that the peak is at least $A/\sqrt{2}$ larger than the highest of the interval minima on each side of the peak. All the HVSR curves that were collected in the field campaign and their selected peaks are in the supplementary material

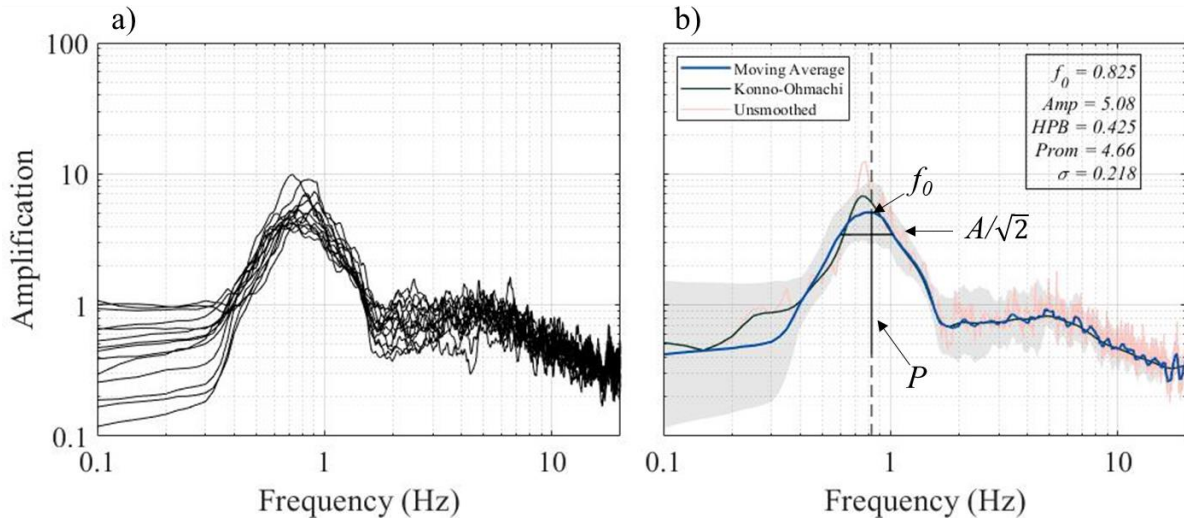


Figure 4. Processing steps for computing HVSR curves, a) individual HVSR curves of the 20 windows and b) final median HVSR curve (blue) with f_0 , P and $A/\sqrt{2}$ indicated along with the unsmeared median curve (pink) and the median curve smoothed with a Konno-Ohmachi smoothing filter (green) with a smoothing coefficient = 20.

In Figure 5, we have selected four HVSR curves to demonstrate typical resonance behavior in the high impedance New England region. Figure 5a is from a station in Orleans, MA on Cape Cod in the thick, glaciofluvial ice contact sediments. The sediments on Cape Cod and Long Island (the Atlantic Coastal Plain sediments) are all low frequency with distinct peaks indicating deep sediments with a large impedance contrast. Figure 5b is a station in Springfield, MA located in the thin, alluvial sediments adjacent to the Connecticut River. These sediments show consistently prominent single peaks with low frequencies and relatively low variability. Figure 5c is a station in Addison, VT in the Champlain Sea sediments which are classified as proglacial sediments fine-grained, thin. This station is in a large flat expanse adjacent to Lake Champlain which was the seabed of the Champlain Sea. Figure 5d is a station in Portland, ME adjacent to the Fore River located in proglacial sediments fine-grained, thin which are the Presumpscot formation. This is an instance where the Presumpscot formation is deep and low frequency, but many stations we collected in the formation show higher frequency peaks in less shallow profiles. Finally, Figure 5e is a station in the Boston Basin located on a shallow fill layer overlying Boston Blue Clay overlying high velocity argillite basement rock.

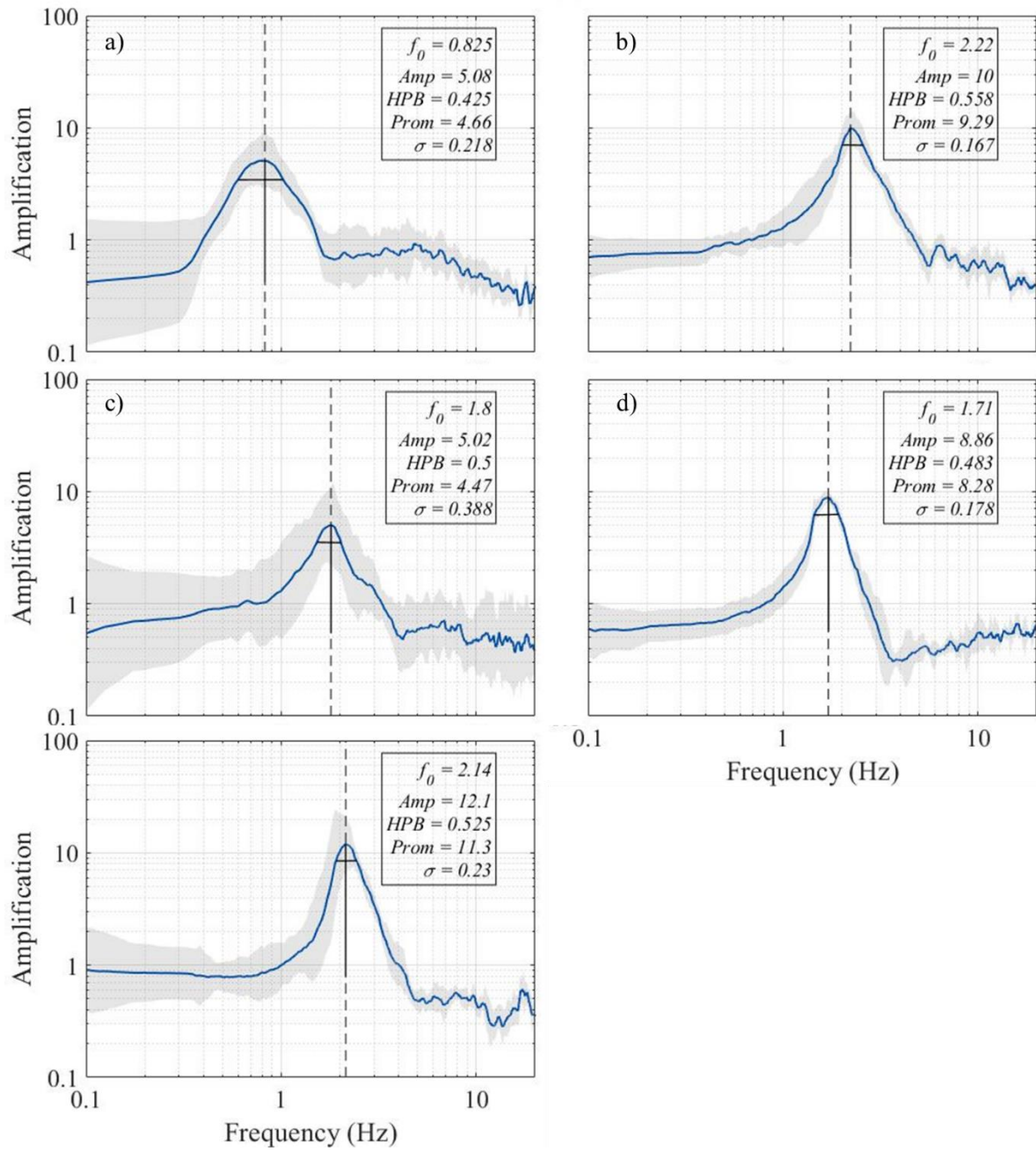


Figure 5. Examples of distinct HVSР fundamental peaks in a) Cape Cod, b) the Connecticut River Valley, c) the Champlain Sea, d) the Maine Coast, and e) the Boston Basin.

2.3 V_s data

To estimate $V_{s\text{avg}}$ for each surficial geologic unit, we assembled 42 shear-wave velocity profiles in the New England area. Twenty-two of the profiles were collected in the Boston area by Thompson et al. (2014) using SASW, 6 were collected in the Connecticut River Valley by Hager Geosciences (2016) using MASW, 3 were collected in Lens and Springston (2013) using MASW, and 5 were collected by us in this study using MASW (Figure 6). The majority of V_s profiles were found in three of the combined surficial geologic units used in this study: glacial till, glaciofluvial ice-contact sediments, thin, and proglacial sediments, mostly fine grained, though 7 of the 8 units have at least one profile (Figure 6).

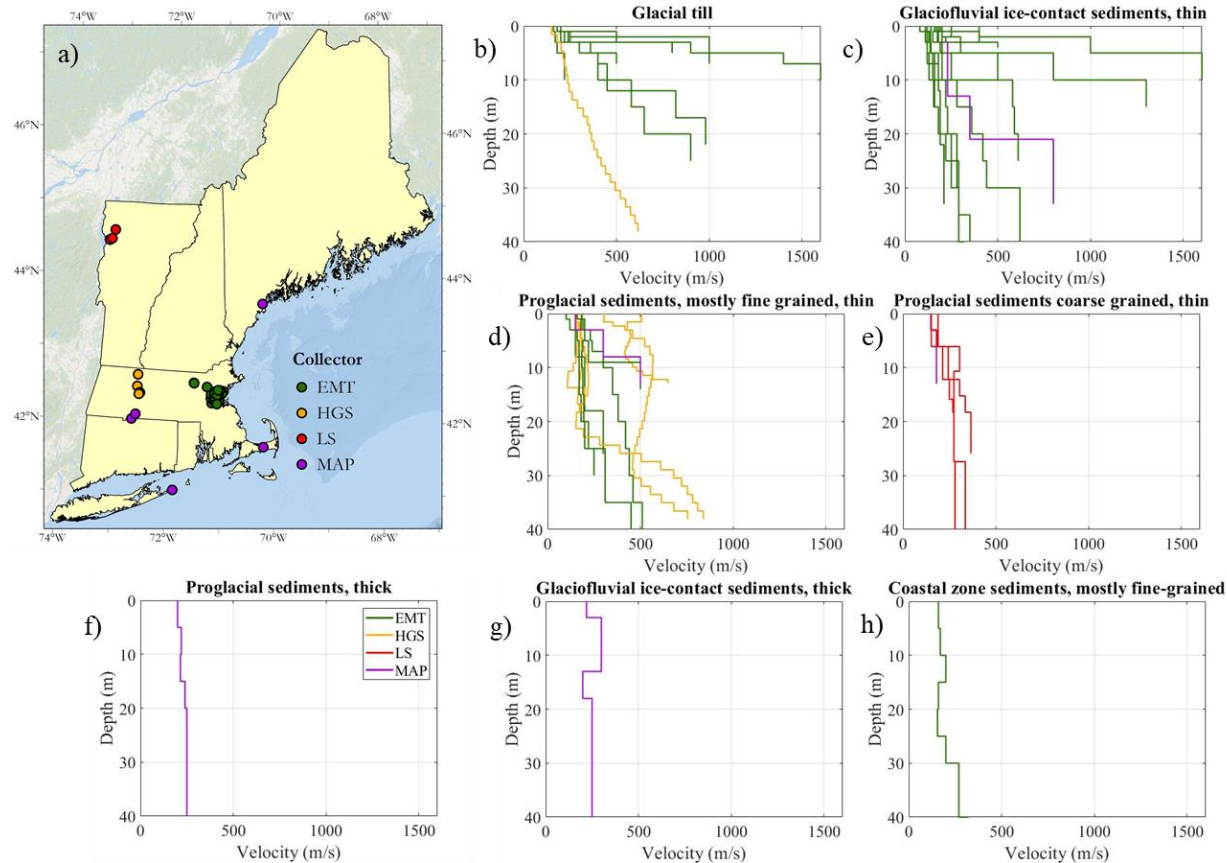


Figure 6. a) Locations of shear-wave velocity profiles in the study. Collector EMT is Thompson et al. (2014), HGS is Hager Geoscience (2016), LS is Lens and Springston (2013), and MAP is the data collected in this study. Profiles grouped by their geology for b) glacial till, c) glaciofluvial ice-contact sediments, thin, d) proglacial sediments, mostly fine-grained, thin, e) proglacial sediments coarse grained, thin, f) proglacial sediments, thick, g) glaciofluvial ice-contact sediments, thick, and h) coastal zone sediments, mostly fine-grained. The low velocity profile in Figure 6b is grouped as “glacial till” but may be misclassified geologically.

For the 5 shear-wave velocity profiles that we estimate in the region, we used a 24-channel Seistronix RAS-24 digitizer sampling at 500 Hz with 4.5 Hz geophones at 1-meter spacing with a 2-meter trigger offset with sledgehammer strikes as a trigger and a set of 5 stacked traces for the final trace. We then computed dispersion curves and inverted for shear-wave velocity profiles using the MASW tool from Olafsdóttir et al. (2017). At each station where we collected MASW data, we also collected an HVSR curve. The dispersion curve is used to identify the general overburden velocity and the HVSR curve is used to identify the fundamental site frequency. For each of the shear-wave profiles, we use f_0 to ensure that the inverted V_s profile meets the criteria $f_0 = V_s/4d$, where V_s is the $V_{s\text{avg}}$ for the site. For example, in Figure 7, the f_0 value at this station, L62A in the Connecticut River Valley, is 1.92 Hz (Figure 7e). The inversion assumes a basement rock V_s of 2500 m/s and assumes three layers of sediment based on the regional stratigraphy. The inversion results in an 8-meter thick 150 m/s layer overlying a 10-meter thick 200 m/s layer overlying an 8-meter thick 300 m/s layer over a 2500 m/s basement rock. We changed the thickness of the third layer until the velocity profile met the criteria $f_0 = V_s/4d$. After changing the thickness to conform to the criteria, the profile has a depth to the impedance contrast of 26 m and the time averaged shear-wave velocity of 200 m/s giving an f_0 estimate of 1.92 Hz, the same as was measured at the site from the HVSR analysis.

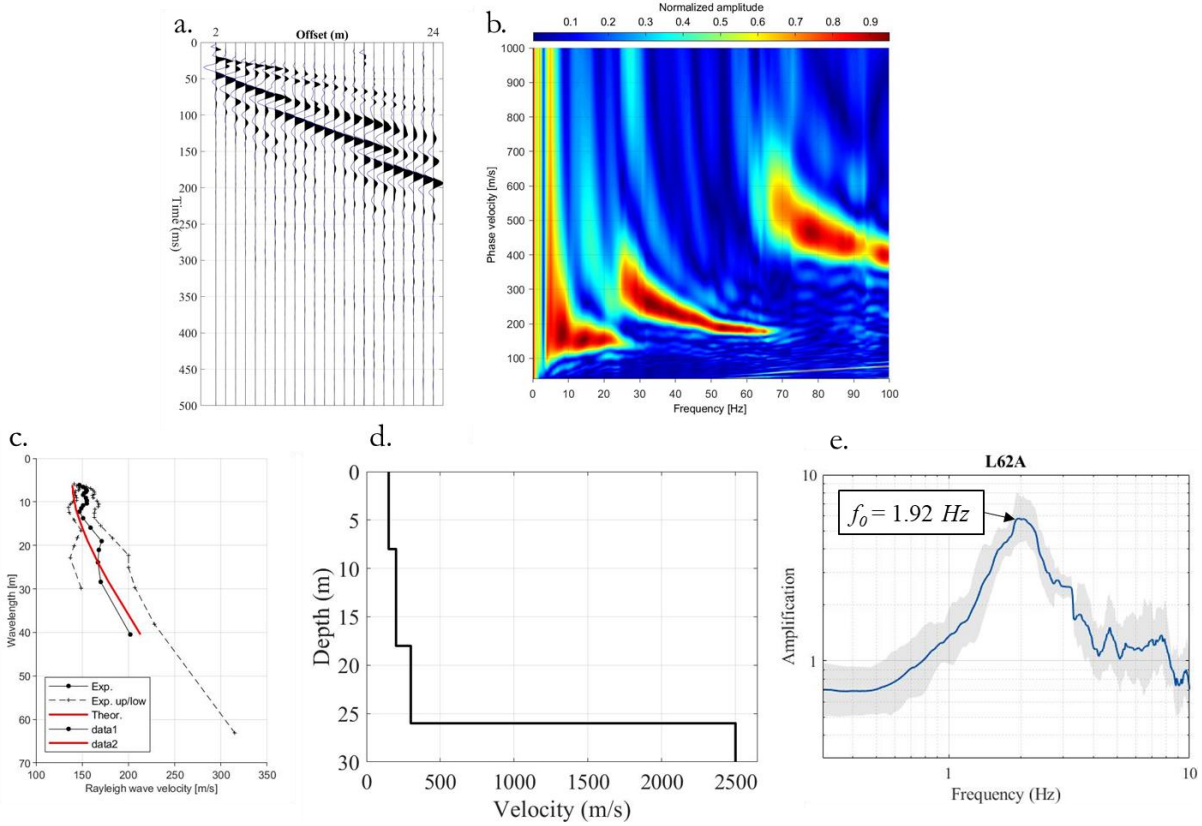


Figure 7. Process used to estimate the 5 shear-wave velocity profiles collected by the researchers in this study. a) traces, b) dispersion curve, c) model and dispersion curve, d) velocity profile, e) HVSR curve. This example is Transportable Array station L62A located in the Connecticut River Valley, the southernmost purple point in the Connecticut River Valley in Figure 6a.

3.0 Methods

We compute distributions of f_0 picked from HVSR curves by surficial geologic units to characterize site susceptibility across New England. The procedure is similar to the methodology used in Wills and Clahan (2006) where they grouped V_{s30} measurements in California by surficial geologic unit. We calculate the f_0 distribution using the eight combined surficial geologic units defined for the project (Table 2) and use the median and interquartile range to describe the central tendency and dispersion of the distribution. The interquartile range is defined as the distribution's 75th percentile minus its 25th percentile. We then use an average shear-wave velocity of the overburden ($V_{s\text{avg}}$), estimated by grouping the 42 shear-wave velocities across the same eight combined surficial geologic units. In order to draw comparisons with

prior region-scale site susceptibility maps by Wald and Allen (2007) and Becker et al. (2011), we use the layer-over-halfspace site response model with the f_0 distribution and Vs_{avg} estimates by surficial geologic unit, to estimate the $Vs30$ distribution for each surficial geologic unit following Hassani and Atkinson (2016).

3.1 Wills and Clahan methodology for creating f_0 distributions by geologic polygons

Wills and Clahan (2006) used a database of $Vs30$ stations and surficial geologic polygons to develop distributions of $Vs30$ within each surficial geologic unit in California. In our study, we apply the same technique to f_0 data. Using the eight combined surficial geologic units described in Table 2, we first group the f_0 data within each surficial geologic unit by performing a spatial join between the f_0 database and the surficial geologic unit. We then compute distributions of f_0 within each unit and calculate summary statistics of those distributions which are appended to the surficial geology attribute table (Figure 8).

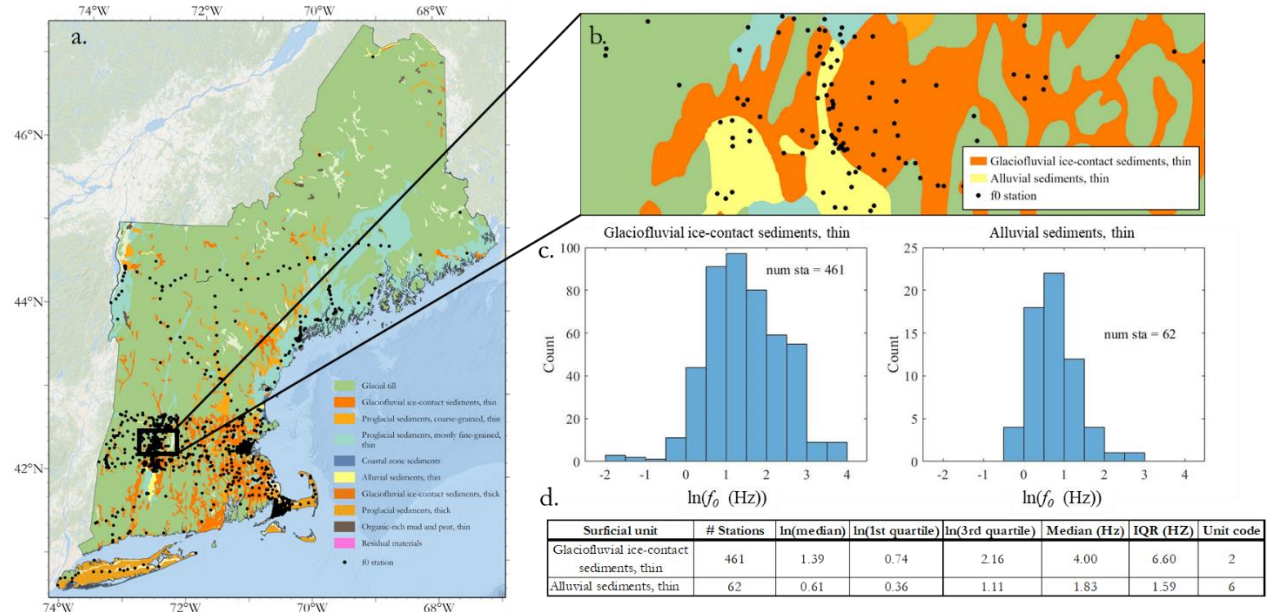


Figure 8. Example of the process used to group f_0 points by their respective geologic unit to compute spatial distributions of f_0 . a) Soller et al. (2009) map with f_0 stations overlain. b) A zoomed in section of the Connecticut River Valley and the f_0 points within that area. c) The actual f_0 distributions of two of the geologic units in this study, and d) the table developed from the distributions in Figure 8c.

3.2 Estimating $Vs30$ from f_0 with the procedure of Hassani and Atkinson (2016)

Starting with a map of f_0 distributions, we estimate $Vs30$ using the average shear-wave velocity of the overburden and the shear-wave velocity of the basement rock. We assume a layer-over-halfspace model where

$$f_0 = \frac{Vs_{avg}}{4d_s} \quad (4)$$

where Vs_{avg} is the average shear wave velocity of the overburden soil (Equation 5) and d_s is the depth of the overburden soil (Thomson, 1950; Haskell, 1953 and 1960; Kramer, 1996). Since we are modeling a high impedance environment, the layer-over-halfspace model is a decent approximation for performing large-scale generalized mapping. Vs_{avg} is equal to the average shear-wave velocity of the overburden and is computed using

$$Vs_{avg} = \sum_{i=1}^n \frac{h_i}{h_i/V_i} \quad (5)$$

where n is the layer number in the soil column, h is the thickness of that layer and V is the velocity of that layer (Kramer, 1996, Strambouli, 2017). By simplifying our model to a layer over halfspace and using Vs_{avg} assigned to surficial geologic units, we can use f_0 to approximate $Vs30$. $Vs30$, which is the time-averaged shear-wave velocity of the upper 30 meters, can be computed for the single layer over halfspace model using the equation

$$Vs30 = \frac{30}{\left(\frac{d_s}{Vs_{avg}} + \frac{d_R}{V_R} \right)} \quad (6)$$

where d_R is the depth of the basement rock and V_R is the shear-wave velocity of the basement rock. This relationship is valid for $d_s < 30$ m. In the single layer-over-halfspace model, $d_R = 30 - d_s$. By rearranging equation 4 and replacing d_s in Equation 6 with $d_s = Vs_{avg}/(4 * f_0)$ and d_R with $d_R = 30 - d_s$, we obtain the following equation relating f_0 to $Vs30$

$$Vs30 = \frac{30}{\frac{1}{4f_0} \left(1 - \frac{Vs_{avg}}{V_R} \right) + \frac{30}{V_R}} \quad (7)$$

Hassani and Atkinson (2016) outlined this derivation in a paper with similar goals and methods to this one applied in Eastern Canada. With $d_s > 30$ m, $Vs30 = Vs_{avg}$. We estimate $Vs30$ using this methodology for all the f_0 values in the database to estimate the $Vs30$ distribution within each surficial geologic unit. We then compare the results relate to the Wald and Allen (2007) and Becker et al. (2011) models.

4.0 Results

4.1 f_0 distributions

After performing the spatial join of the f_0 stations with the eight surficial geologic units, we compute f_0 distributions for each of the geologic units as summarized in Table 3 and Figure 9. Of these distributions, glacial till has the highest f_0 median (6.16 Hz) and thick, proglacial sediments has the lowest f_0 median (1.03 Hz) (Table 3, Figure 9). The high frequency glacial till unit is distributed throughout New England where there is a shallow, fast veneer of till. The low frequency thick proglacial sediments and thick glaciofluvial sediments are both contained entirely on Cape Cod and Long Island. There are two classifications with low to mid-range f_0 medians of 1.83 and 2.70 Hz: these are thin, alluvial sediments and the thin, fine grained proglacial sediments respectively. The alluvial sediments are predominantly deposited in the Connecticut River Valley and the thin, fine-grained proglacial sediments are contained on the seacoast in Maine and Massachusetts and the coast of Lake Champlain. These sediments are also in the Connecticut River Valley where the Glacial Lake Hitchcock lacustrine sediments are located. There are three classifications with mid to high-range frequencies of 3.31, 3.70 and 4.00 Hz: the coastal zone sediments, the thin, coarse-grained proglacial sediments and the thin glaciofluvial ice-contact sediments, respectively. The coastal zone sediments are located in pockets along the coast. The thin, coarse-grained proglacial sediments are deposited in large moraine areas. The thin glaciofluvial ice-contact sediments are deposited in the river valleys that are smaller than the Connecticut River Valley with less sediment build-up in their river beds (Figure 9).

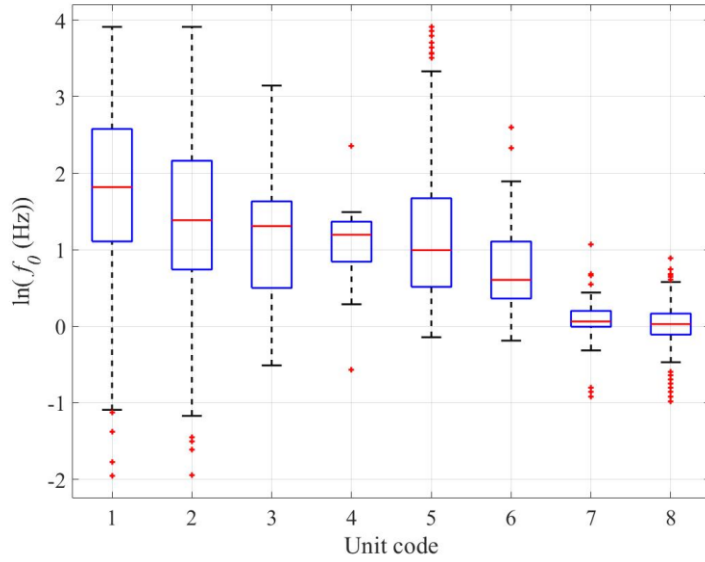


Figure 9. Box and whisker plots of the f_0 distributions within each surficial geologic unit. The median (red line) and IQR (the height of each blue box) is contained in Table 3 with the same values in their natural units. The top of each box represents the 75th percentile of the distribution and the bottom represents the 25th percentile. Each horizontal black line on the outside of the dashed lines (the whisker) represents the maximum value within 1.5 times the interquartile range from the bottom or top of the box. Any red crosses outside of the whisker are greater than 1.5 times the interquartile range from the bottom or top of the box. The x-axis is labeled with the unit code found in Table 3.

Table 3. Final output table for the f_0 distributions by combined surficial geologic units with calculated medians and IQRs.

Surficial unit	# Stations	ln(median)	ln(IQR)	Median (Hz)	IQR (HZ)	Unit code
Glacial till	359	1.82	1.47	6.16	10.15	1
Glaciofluvial ice-contact sediments, thin	461	1.39	1.42	4.00	6.60	2
Proglacial sediments, coarse-grained, thin	74	1.31	1.13	3.70	3.47	3
Coastal zone sediments, mostly fine-grained	26	1.20	0.52	3.31	1.60	4
Proglacial sediments, mostly fine grained, thin	381	0.99	1.16	2.70	3.65	5
Alluvial sediments, thin	62	0.61	0.74	1.83	1.59	6
Glaciofluvial ice-contact sediments, thick	32	0.06	0.21	1.06	0.23	7
Proglacial sediments, thick	182	0.03	0.27	1.03	0.28	8

4.2 Mapping each unit f_0 distribution median and interquartile range

With distributions of f_0 for each surficial geologic unit, we can observe the central tendency and dispersion of each distribution as a map. In Figure 10a, we plot the median f_0 value of each surficial geologic distribution and in Figure 10b, we plot the IQR of the distribution of each surficial geologic unit. The geologic units with low frequency f_0 distributions are entirely contained on Cape Cod and Long Island where sediments are deep. The low to mid ranged frequency units are on the Coast of Lake Champlain, the Coast of Maine, the Boston Basin, and the Connecticut River Valley. Cape Cod and Long Island also have the lowest IQR followed by the previously listed regions and units. The till across the entire region tends to have high f_0 values with high variability indicating shallow, laterally varying sediments (Figure 10b). In general, as the distribution central tendency decreases, the IQR also decreases, implying that deeper deposits have lower lateral fundamental frequency variation than shallower deposits.

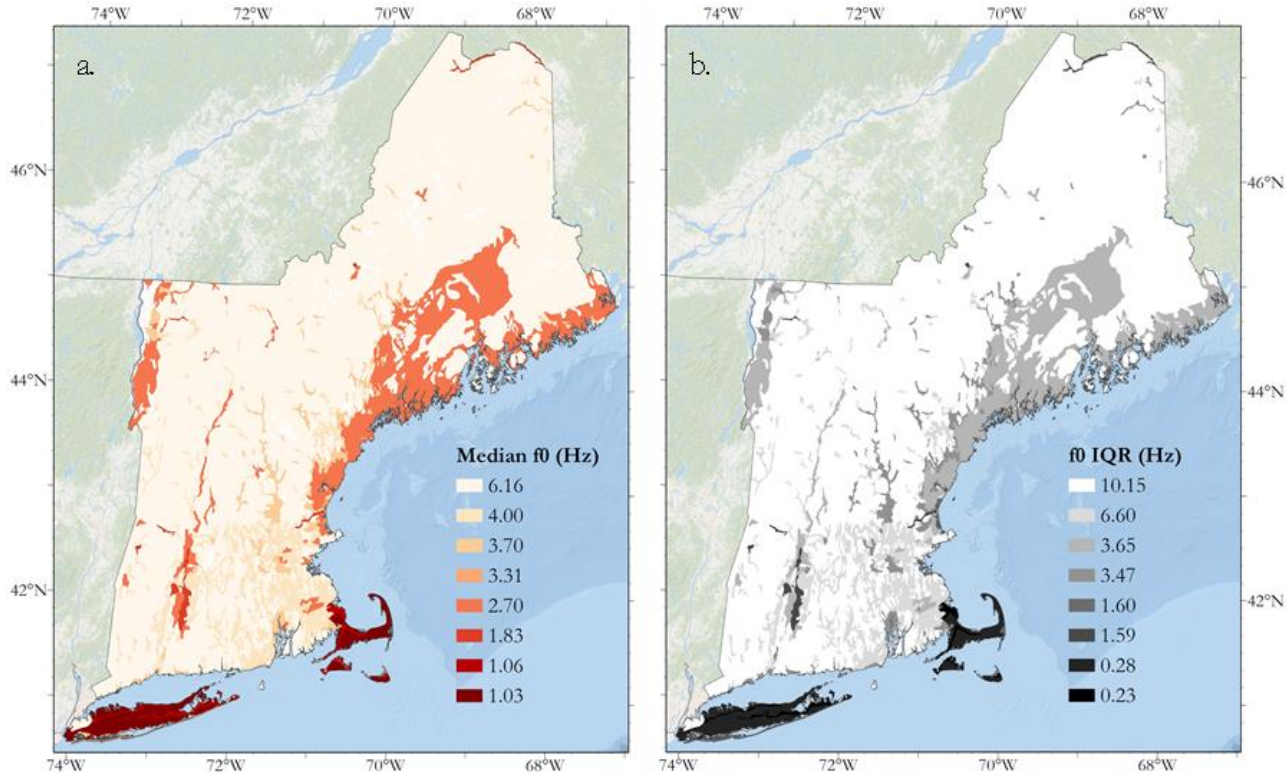


Figure 10. a) Map of the median f_0 of each surficial geologic unit's f_0 distribution. b) Map of the interquartile range of each surficial geologic unit's f_0 distribution. The median and IQR values are also in Table 3.

Within the New England f_0 median map, five subregions stand out for their potential site susceptibility: the Maine coast, the Lake Champlain coast (Champlain Sea), the Boston Basin, the Connecticut River Valley and Cape Cod and Long Island (Atlantic Coastal Plain). The Atlantic Coastal Plain sediments are made up of thick glaciofluvial ice contact sediments and thick proglacial sediments and have the f_0 spatial distribution with the lowest median (Figure 11e). The Connecticut River Valley has a band of low-frequency thin alluvial sediments (median 1.83 Hz) within a deposit of proglacial sediments, mostly fine-grained, thin (median 2.70 Hz). The alluvial sediments in this structure are composed of the flood-plain alluvium deposited by the Connecticut River, and they sit on fine grained clays of Glacial Lake Hitchcock (Figure 11d). Adjacent to Lake Champlain in Vermont is a large deposit of thin proglacial sediments, mostly fine-grained, (median 2.70 Hz) which is composed of the Champlain Sea sediments, a marine clay deposited when Lake Champlain existed during the Wisconsin glaciation (Figure 11b). Along the east coast of New England, particularly in the Boston Basin and Maine, there is a deposit of thin, mostly fine-grained proglacial sediments (median 2.70 Hz). These are the Boston Blue Clay and the Presumpscot formation and, like the Champlain Sea sediments, are marine clays deposited when relative sea level was higher than it is today (Figure 11 a and c).

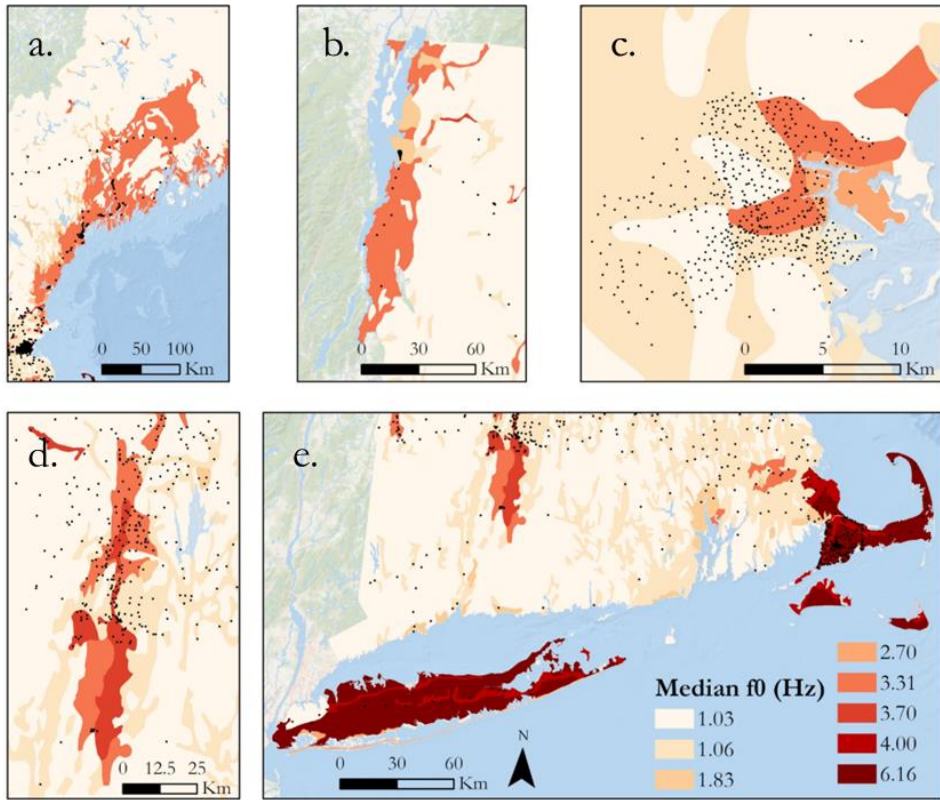


Figure 11. f_0 spatial distribution median map zoomed in on susceptible geologic units a) the Maine coast, b) the Lake Champlain coast, c) the Connecticut River Valley, d) Cape Cod and Long Island. The f_0 station locations are plotted in black.

4.3 Estimating Vs_{avg}

Our shear-wave velocity database for the region contains 42 profiles. We group these profiles by their surficial geologic unit and plot the Vs_{avg} measurements (Equation 5) for each geologic unit (Figure 12). In each of the combined geologic units, we calculate Vs_{avg} for each of the existing profiles and then calculate the mean, median, and standard deviation as summarized in Table 4. Since our Vs data for the region is limited, we requested input from two local state geologists (Steve Mabee, Mike Howley; Personal communication) who helped provided input on the final estimates for Vs_{avg} in Table 4. For glacial till, the mean value of the 9 profiles (Figure 6b) within the unit is 378 m/s and the median is 310 m/s (Table 4). We use a slightly higher Vs_{avg} estimate for this unit of 400 m/s because several of the low Vs_{avg} profiles in glacial till are areas abutting softer geologies like the Boston Basin. For thin glaciofluvial ice contact sediments,

the mean value of the 16 profiles (Figure 6c) within the unit is 335 m/s and the median is 245 m/s. The difference in median and mean of these values implies that there are several outliers skewing the distribution, which is apparent in Figure 12, so we use 250 m/s for this unit's Vs_{avg} estimate. The thin coarse grained proglacial sediments unit has a mean value of 236 m/s for the 4 profiles within the unit and a median of 250 m/s (Figure 6e). We use 250 m/s for this unit's Vs_{avg} estimate. We only have one profile for the coastal zone sediments unit with a Vs_{avg} of 206 m/s (Figure 6h). We use a conservative (lower than the data indicate) Vs_{avg} of 180 m/s for this unit. The thin mostly fine-grained proglacial sediments unit has a mean Vs_{avg} value of 282 m/s and a median of 253 m/s for the 10 profiles within the unit (Figure 6d). This unit contains the significant marine and lacustrine clay layers in the region and in the Becker et al. (2011) model is mapped as site class E. We therefore use a more conservative Vs_{avg} estimate than the data indicate of 220 m/s for this unit. There are no profiles within the alluvial sediments, but similar unconsolidated geologies have Vs_{avg} values near 220 m/s – we use this Vs_{avg} estimate for this unit. The thick glaciofluvial ice contact sediments have one profile with a Vs_{avg} value of 250 m/s which we use as the Vs_{avg} estimate for the unit (Figure 6g). Finally, the thick proglacial sediments unit has one profile with a Vs_{avg} value of 329 m/s (Figure 6h). We use 250 m/s for this unit since these deposits are located on Cape Cod and Long Island which we expect to have Vs_{avg} values of around 250 m/s (Table 4, Figure 12).

Table 4. Vs_{avg} distribution characteristics for the 42 shear-wave velocity profiles in the database grouped by surficial geologic unit. The number of profiles, mean, median, standard deviation and interquartile range of the profiles in each geologic unit are on the left of the table and the estimate we use in this study is in the Vs_{avg} estimate (m/s) column. This Vs_{avg} estimate was made in consultation with two local state geologists (Steve Mabee and Mike Howley; Personal communication)

Surficial unit	# stations	Mean Vs_{avg} (m/s)	Median Vs_{avg} (m/s)	STD Vs_{avg} (m/s)	IQR Vs_{avg} (m/s)	Vs_{avg} estimate (m/s)	Unit Code
Glacial till	9	378	310	160	173	400	1
Glaciofluvial ice-contact sediments, thin	16	335	245	236	107	250	2
Proglacial sediments, coarse-grained, thin	4	236	250	43	31	250	3
Coastal zone sediments, mostly fine-grained	1	206.22	206.22	-	-	180	4
Proglacial sediments, mostly fine grained, thin	10	282	253	118	127	220	5
Alluvial sediments, thin	0	-	-	-	-	220	6

Glaciofluvial ice-contact sediments, thick	1	250	250	-	-	250	7
Proglacial sediments, thick	1	329	329	-	-	250	8

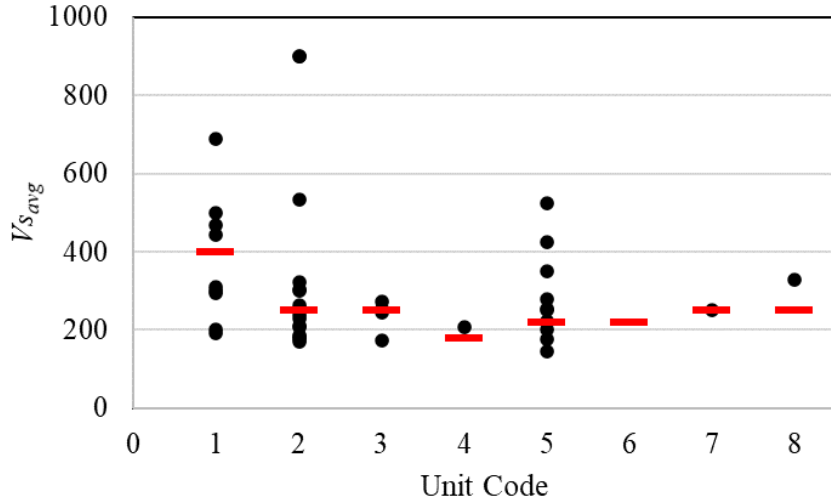


Figure 12. Vs_{avg} measurements of each of the 42 shear wave velocity profiles grouped by geologic unit. The red line in each grouping is the value for Vs_{avg} that we chose to use in this study. Unit codes are in Table 4.

With an f_0 map and simple estimates of Vs_{avg} for each of the surficial geologic units in the region, we develop curves relating for $Vs30$ to f_0 for each Vs_{avg} using Equation 7, as illustrated in Figure 13. This procedure is simply a way to approximate regional $Vs30$ distributions with the more abundant f_0 data. These curves reveal that $Vs30$ based site classes change at discrete f_0 values due to the assumption of a single-layer-over-halfspace model. The f_0 to $Vs30$ relationships use a basement velocity of 2500 m/s, similar to that commonly used for reference rock conditions in the central and eastern US (Stewart et al. 2020; Goulet et al., 2017, 2018; Pacific Earthquake Engineering Research Center (PEER), 2015a, 2015b). For example, a $Vs_{avg} = 220$ m/s geologic unit with an f_0 value below 3.2 Hz is a site class D and with an f_0 value above 3.2 Hz is a site class C. These relationships can be used to estimate $Vs30$ when the surficial geology of the profile (and therefore an estimate of Vs_{avg}), and f_0 are known. In the case of this work, where our estimates are broad, the relationship is used to convert a geologic unit distribution of f_0 to a distribution of $Vs30$.

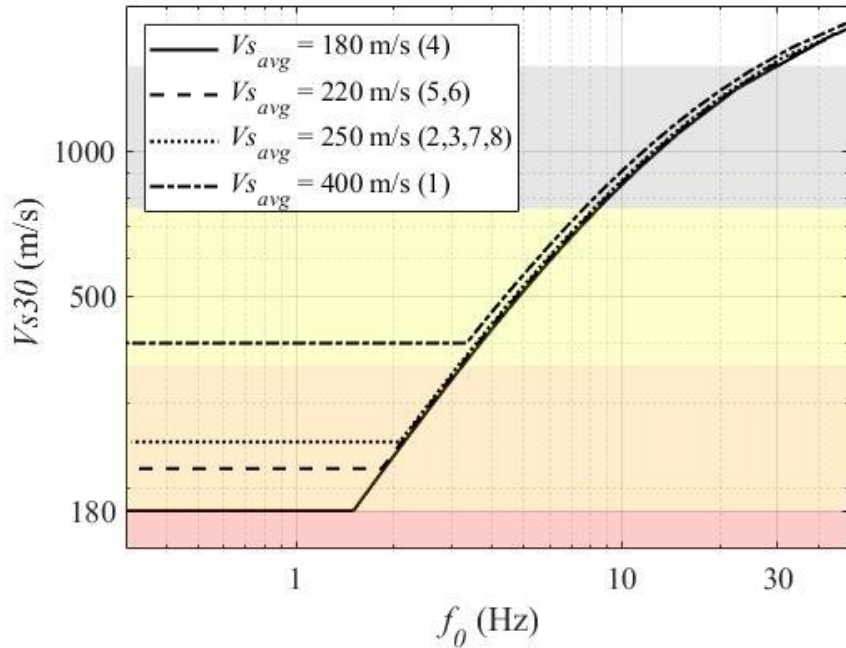


Figure 13. Relationship between f_0 and $Vs30$ for the 4 Vs_{avg} estimates of the 8 surficial units in the study. The unit codes are in parentheses in the figure legend. The flat line in the low frequency ranges represents the point at which the overburden layer exceeds 30 meters and thus the $Vs30$ value is equal to the Vs_{avg} of the overburden layer. A shear-wave velocity of 2500 m/s is used for the basement layer in this plot. The background colors represent site classes, red is site class E, orange is D, yellow is C, grey is B, and white is A.

4.4 Developing $Vs30$ distributions by applying Equation 7 to the f_0 distributions

Applying equation 7 to all the f_0 values within each geologic unit, we estimate distributions of $Vs30$ and $Vs30$ -based site class for each station (Figure 14, Table 5). For example, median $Vs30$ values in Proglacial sediments, mostly fine-grained, thin are typically $Vs30$ -base site class D (median $Vs30 = 311$ m/s) but have a large dispersion (IQR = 286 m/s) indicating that these deposits can be shallow and can thus have potentially higher $Vs30$ values. Both thick glaciofluvial ice contact sediments and thick proglacial sediments are consistently deep and therefore, have $Vs30$ spatial distributions with 0 m/s IQR reflecting little significant lateral change in $Vs30$ across the units since the bedrock depth is never below 30 meters and we are using a constant Vs_{avg} and therefore the f_0 distribution does not contribute to the $Vs30$ distribution.

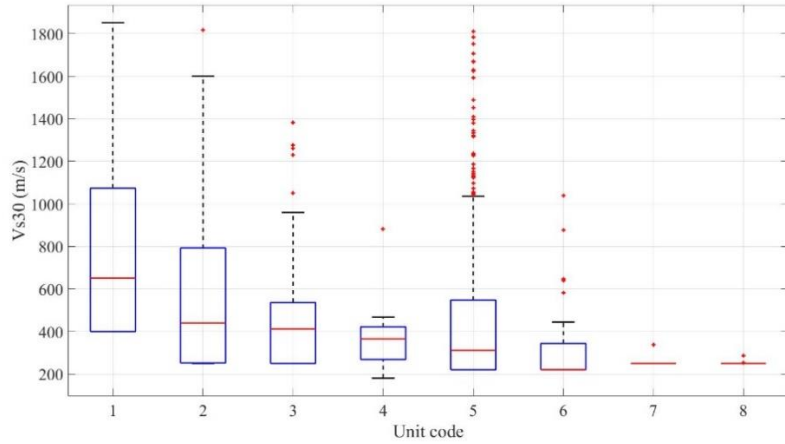


Figure 14. Distributions of $Vs30$ of each station within each surficial geologic unit in the database. This plot is the distribution that results from converting the f_0 distributions in Figure 9 to $Vs30$ using the relationships in Figure 13.

Table 5. Vs_{avg} for each surficial geologic unit as well as measures of central tendency and dispersion (median and IQR) for each $Vs30$ distribution computed from converting f_0 to $Vs30$ using the procedure In Equation 7 and the relationship plotted in Figure 14.

Surficial unit	Vs_{avg} (m/s) ^r	Vs_{30} median (m/s) ^r	Vs_{30} IQR (m/s) ^r	Unit code
Glacial till	400	651.14	673.84	1
Glaciofluvial ice-contact sediments, thin	250	439.56	542.07	2
Proglacial sediments, coarse-grained, thin	250	412.27	285.96	3
Coastal zone sediments, mostly fine-grained	180	365.07	153.15	4
Proglacial sediments, mostly fine grained, thin	220	311.33	327.34	5
Alluvial sediments, thin	220	220	123.35	6
Glaciofluvial ice-contact sediments, thick	250	250	0	7
Proglacial sediments, thick	250	250	0	8

Another way we interpret these estimates of $Vs30$ spatial distributions is to use pie charts of site classes of each unit as shown in Figure 15. All the glacial till stations, with the unit's higher Vs_{avg} value and typically higher f_0 values, are either site class A, B, or C (Figure 15). Thin glaciofluvial ice contact sediment stations are mostly classified as site class C or D with some high f_0 stations pushing the classification into B and A. Thin, coarse-grained proglacial sediments are similar to thin glaciofluvial ice-contact sediments but with greater proportion of the higher site classes resulting from the lower f_0 values in its distribution. Coastal zone sediments are majority site class C, indicating mostly higher f_0 values, but in the few stations of this geology with low f_0 values (deep profiles), the stations are site class E due to the low Vs_{avg} value. Like coastal zone sediments, thin fine-grained proglacial sediments have a range of site classes including a significant portion of site class D where f_0 values are low. Thin alluvial sediments are mostly site class D indicating f_0 consistently below 3.2 Hz. Both thick glaciofluvial and proglacial sediments are entirely site class D. These geologic classifications are located on Cape Cod and Long Island where frequencies are consistently around 1 Hz, and thus $Vs30 = Vs_{avg} = 250$ m/s = site class D at all the stations in the unit (Figure 15).

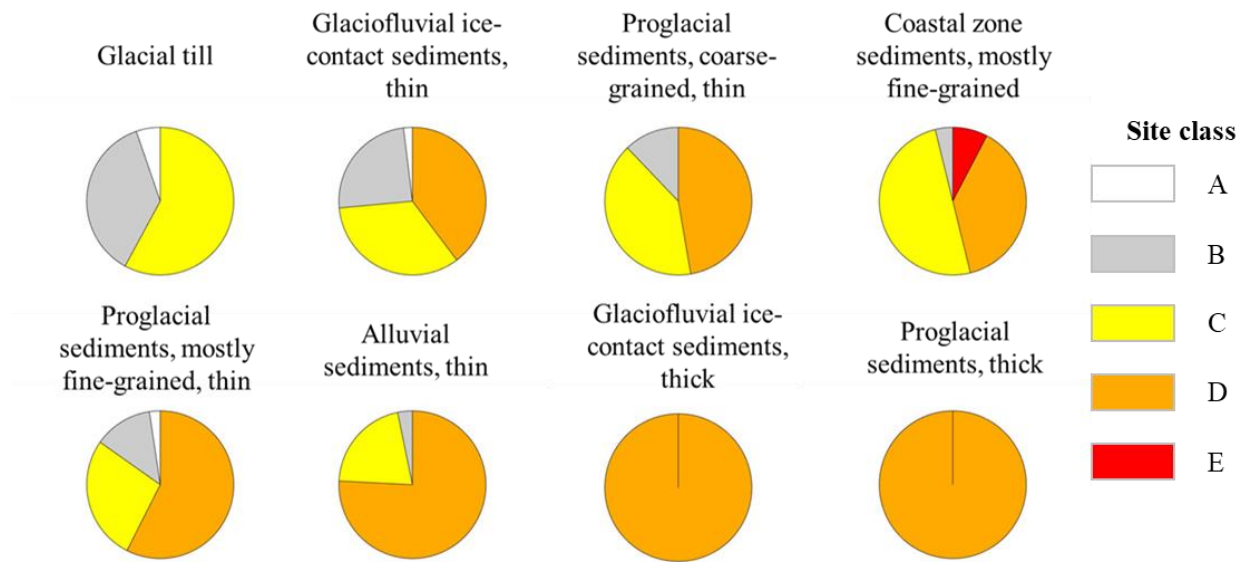


Figure 15. Pie charts showing the proportion of site classes derived from each geologic unit's f_0 values and the relationship in Equation 7. The colors represent site classes, red is site class E, orange is D, yellow is C, grey is B, and white is A.

5.0 Discussion

In this study, we outline the development of regional-scale f_0 distribution site susceptibility maps for New England. f_0 is inexpensive and rapid to deploy and can thus be collected at the regional scale. f_0 is a function of the depth to the impedance contrast and the average overburden velocity (Vs_{avg}) and is a known reliable site parameter in highly resonant site response regions. We apply the procedure to New England because the region is a high impedance environment and thus is reasonably approximated at a large scale by the single-layer-over-halfspace model. Two site susceptibility maps are currently available for use in the region: the global slope-based $Vs30$ model of Wald and Allen (2007) and the New England-specific geology-based $Vs30$ model of Becker et al. (2011). Our methodology incorporates local geophysical information in terms of f_0 and Vs_{avg} , groups it by surficial geologic unit classifications and yields a regional-scale site susceptibility map of f_0 distributions, first approximations of Vs_{avg} , and byproduct estimates of surficial unit $Vs30$ spatial distributions.

Though the primary purpose of this paper is to create a regional-scale site susceptibility map in terms of f_0 for New England, we also show how f_0 distributions can be converted into $Vs30$ distributions using the procedure described in Hassani an Atkinson (2016). Grouping the $Vs30$ pixel values from the Wald and Allen (2007) model by the same 8 surficial geologic polygons from the Soller et al. (2009) map and computing the $Vs30$ distributions by surficial geologic unit reveals interesting comparisons to our f_0 -based distribution estimates as shown in Figure 16. With the exception of “coastal zone sediments, mostly fine grained, thin” (unit code 4) each distribution that we estimated exhibits a lower central tendency than that of the Wald and Allen (2007) distribution. In particular, the thick glaciofluvial ice contact sediments and the thick proglacial sediments (unit codes 7 and 8) reveal the importance of using local data for site susceptibility mapping. The Wald and Allen (2007) model is not able to account for the depth-to-bedrock, it simply assigns $Vs30$ values by a slope value. In this geologic structure (Cape Cod and Long Island), the impedance contrast is deep and thus the near surface unconsolidated sediments are relatively low velocity for more than 30 meters. The $Vs30$ estimates of the Wald and Allen (2007) model are higher than our

estimates as summarized in Table 6. This result shows the importance of incorporating local data into regional site susceptibility maps.

We also compare the Becker et al. (2011) $Vs30$ ranges to those we developed in this paper. Becker et al. (2011) converts surficial geologic units directly into seismic site classes. This technique does not consider sediment thickness. Where these sediments are shallow, the $Vs30$ value is estimated to be higher than observed when sediment thickness is less than 30 meters. The Becker et al. (2011) $Vs30$ distribution ranges in Figure 16 consistently exhibit lower median values than those computed in this study except for on the Atlantic Coastal Plain sediments (Unit codes 7 and 8) which are always greater than 30 meters and thus have $Vs30$ values equal to the Vs_{svg} value. Percent differences are summarized in Table 6. For example, Proglacial sediments mostly fine-grained, thin (Unit code 5) have stations with f_o values that are often high, indicating a shallow depth to the impedance contrast and a higher $Vs30$ value. In general, our $Vs30$ spatial distribution estimates tend to be lower than those of Wald and Allen (2007) and higher than those of Becker et al. (2011) (Figure 16, Table 6). The Wald and Allen (2007) model is a broad global average and thus smooths over local fluctuations and Becker et al. (2011) model does not account for sediment thickness. Neither of the prior maps used any locally collected point data in the development of their $Vs30$ maps. Using distributions of local geophysical data (f_o), our study results in more local estimates of f_o and $Vs30$ while accounting for uncertainty and acknowledging the generalization inherent in developing distributions using surficial geology.

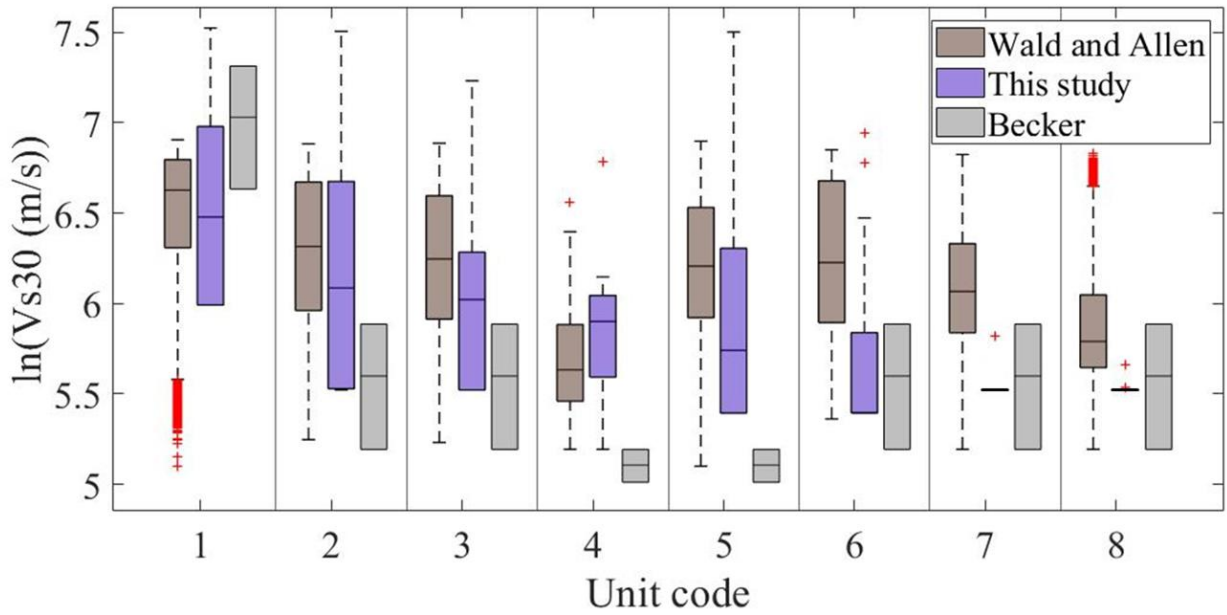


Figure 16. Comparison of the Wald and Allen (2007) and Becker et al. (2011) $Vs30$ spatial distributions and those estimated in this study using the procedure of Hassani and Atkinson (2016). The Wald and Allen (2007) distributions (brown) were computed by grouping the model pixel values by the surficial geologic unit map. The Becker et al. (2011) distributions (grey) are the range of $Vs30$ values within the site class that was assigned to the geologic unit.

Table 6. Percent median difference between Wald and Allen (2007), Becker et al. (2011) and our study's $Vs30$ distributions per geologic unit.

Unit Code	Wald and Allen (2007) to this study (%)	Becker et al. (2011) to this study (%)
1	102.32	108.65
2	103.95	92.08
3	103.82	93.00
4	95.42	86.54
5	108.19	88.95
6	115.58	103.87
7	109.96	101.42
8	104.89	101.42

Given the low resolution of the surficial geology map (Soller et al. 2009) that is the base map for this project, we investigate spatial variability of the local f_0 residuals by subtracting the median assigned to the surficial geologic unit. The residuals of each f_0 station value are plotted as shown in Figure 17a and are

observed to be spatially correlated. Since f_0 is a function of depth to the impedance contrast, this spatial correlation is likely a strong function of bedrock trend. The Maine Coast has a significant proportion of residuals greater than zero, meaning the local values are typically higher than the surficial geology distribution median. This implies that the Maine Coast proglacial, fine-grained, thin sediments are typically shallower than the other similarly classified sediments (Figure 17b). In the Boston Basin, the negative residuals are almost entirely contained within the center of the basin while the outer ring contains positive residuals. This is typical of a basin structure – the center of the basin is deeper and therefore has lower f_0 values than the shallower basin edge (Figure 17c). Cape Cod has positive residuals on the inside of the Peninsula and negative residuals towards the tip of the Peninsula. The residuals are much smaller, however, than those of the Maine Coast of the Boston Basin since this area has low f_0 variability.

A future improvement to this project would be to improve the geospatial modeling of f_0 to reduce the model residuals. These improvements could be accomplished using one of the following strategies: use higher resolution surficial geologic data; further subdivide the map into subregions in addition to geologic units; or perform geostatistical modeling (interpolation) of the important units and regions for which we have a significant amount of data like Boston and Cape Cod and then merge the higher resolution models back into the regional model.

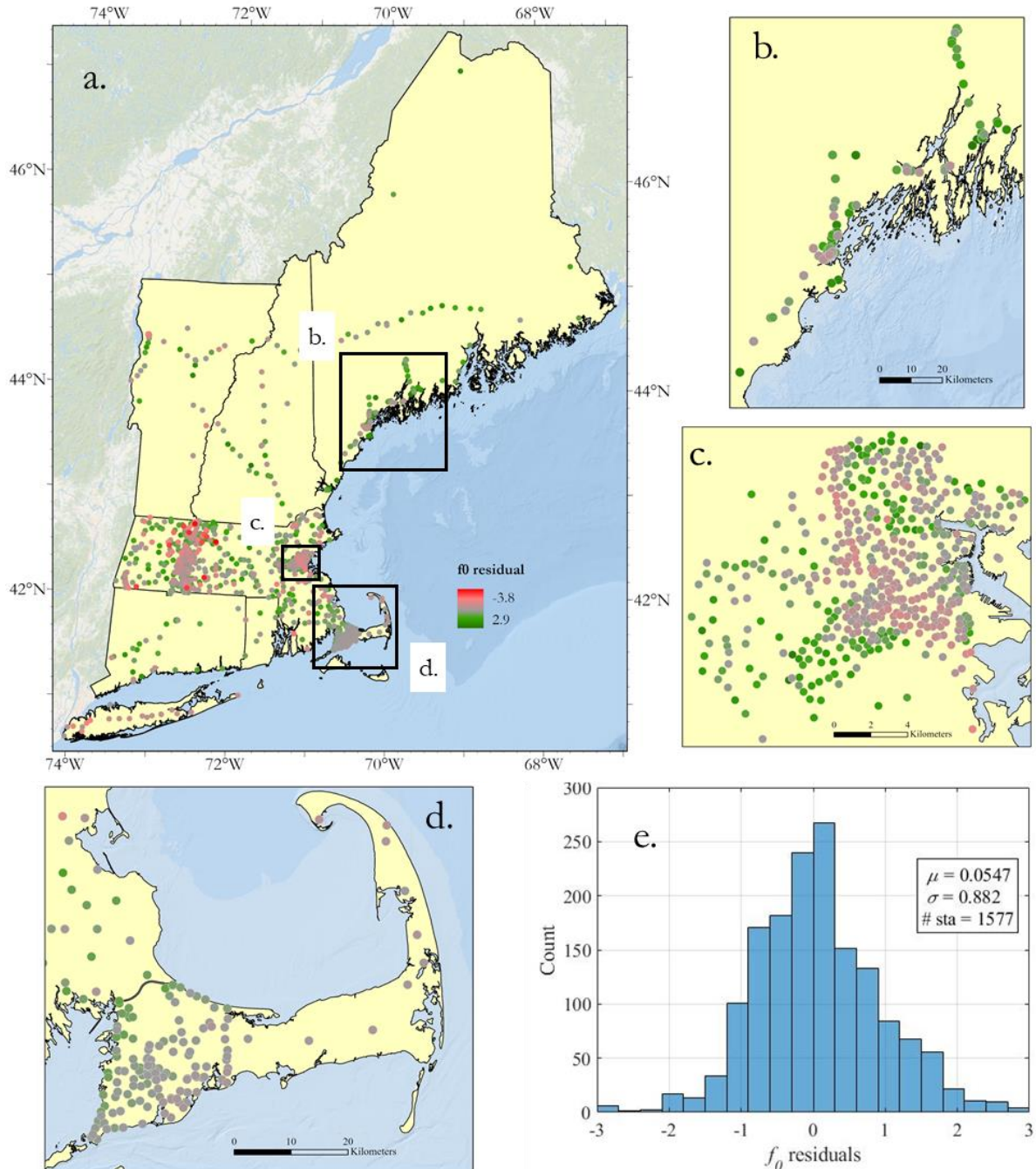


Figure 17. Spatial f_0 residuals computed by subtracting each surficial geologic grouping f_0 distribution natural logarithm median from each station $\ln(f_0)$ within that grouping. a) the entire f_0 dataset with boxes indicated the regions that are zoomed in on in the next three figures, b) the Maine Coast, c) the Boston Basin, d) Cape Cod and e) the distribution of all the residuals. A grey color indicates zero residual, a red color a negative residual and a green color a positive residual.

6.0 Conclusion

We develop a regional-scale site susceptibility map based on the major surficial geologic units in New England by developing f_0 distributions. We use f_0 is the primary site susceptibility mapping parameter as others have demonstrated its use in high impedance environments like New England. Using the surficial geologic units from the conterminous US surficial geology map of Soller et al. (2009) and the methodology that Wills and Clahan (2006) used to create surficial geology based $Vs30$ maps, we compute distributions of f_0 for each of eight combined surficial geologic units mapped in New England. We find that the thick glaciofluvial ice-contact sediments and thick proglacial sediments of Cape Cod and Long Island (The Atlantic Coastal Plain) are characterized by f_0 distributions with the lowest medians (1.06 and 1.03 Hz respectively) and narrowest interquartile ranges (0.23 and 0.28 Hz respectively) in New England, which we interpret as being the thickest sediments in the region. The f_0 distribution of the thin, proglacial sediments, mostly fine-grained in the Boston Basin, the coast of Lake Champlain and the Maine coast has a relatively low median (2.70 Hz), however it has high variability (3.65 Hz interquartile range) since the sediment thickness varies widely in this geologic unit. The f_0 distribution of the thin alluvial sediments of the Connecticut River Valley also has a low f_0 median (1.83 Hz) however, it has less variability than the proglacial sediments, mostly fine-grained thin (1.59 Hz). We present maps of the median and interquartile range of the f_0 spatial distributions and their corresponding $Vs30$ spatial distribution approximations.

We also develop estimates of Vs_{avg} for each surficial geologic unit in the New England subregion of the US conterminous surficial geologic map. We estimate distributions of $Vs30$ from the f_0 spatial distributions using the relationship of Hassani an Atkinson (2016). Our results yield $Vs30$ distributions with lower median values than the Wald and Allen (2007) global relationship model and generally higher median values than the Becker et al. (2011) geology driven model. The procedure we present can be applied to make regional site susceptibility maps in high impedance environments, using a regional geologic map, an f_0 database with decent spatial coverage of that region, and a way to estimate Vs_{avg} for each of the surficial units in that region.

Acknowledgements

This research was funded by USGS awards #G20AP00040 and #G20AP00041. The data provided and the consultation on velocity estimates for different geologic units by Dr. Steve Mabee of the Massachusetts Geological Survey and by Mike Howley of the New Hampshire Geological Survey were invaluable. We thank the two anonymous reviewers whose comments were essential for helping us clarify the paper's purpose.

Chapter 3

Mapping fundamental frequency (f_0) as a site response parameter using a multi-scale approach with state-level surficial geologic maps and local sedimentary deposit information

Pontrelli, M.A., Baise, L.G., Ebel, J.E. (2023b) Mapping fundamental frequency (f_0) as a site response parameter using a multi-scale approach with state-level surficial geologic maps and local sedimentary deposit information, *Engineering Geology*, in review

Abstract

Site characterization maps are essential for regional planning and seismic hazard analyses. In this research, we develop site characterization maps for New England, USA, a glaciated region with a high impedance contrast between sediments and bedrock. These maps are of distributional parameters of soil fundamental frequency (f_0), average overburden shear-wave velocity (Vs_{avg}), and $Vs30$. The maps are based on a variety of data sources across multiple scales including local site data (1619 f_0 measurements, 40 shear-wave velocity profiles), high resolution topographic data (SRTM DEM), 6 state-scale surficial geologic maps ranging in scales from 1:24,000 to 1:500,000, and one state mapped at the national scale (1:5,000,000). We identify six local sedimentary deposit subregions and define their extent using a digital elevation model. We group the geologic units across the state-scale maps into seven common units by depositional environment. The seven mapped surficial geologic units and the six local subregions are intersected creating 39 surficial geology classifications. We compute f_0 distributions in each classified unit and define them by their mean (μ_{ln}) and standard deviation (σ_{ln}). Vs_{avg} distributions are estimated for each of the seven mapped surficial geologic units using the 40 available shear-wave velocity profiles. With distributions of f_0 and Vs_{avg} in each classified unit, we assume a single-layer-over halfspace sediment model with vertically propagating SH-waves through horizontally layered media and use it to relate f_0 , Vs_{avg} , $Vs30$, and bedrock velocity (V_R). Using Monte Carlo sampling of the f_0 and Vs_{avg} distributions, we estimate $Vs30$ distributions in each classified unit and make regional maps of the distributional parameters μ_{ln} and σ_{ln} of f_0 , Vs_{avg} , and $Vs30$. Using high resolution state-scale maps, and high-resolution topography to map local sedimentary basins increases the accuracy of regional site characterization and reduces local bias as compared to maps developed using only national scale surficial geology.

Keywords: Site response, fundamental frequency, site characterization, impedance contrast, Shear-wave velocity

1.0 Introduction

Site characterization maps are essential for regional planning and seismic hazard analyses. Researchers have developed site characterization maps at regional, national, and global scales using a variety of data sources including surficial geology, geospatial topographic and geomorphologic data, and local geotechnical and geophysical data. The best-known global example is the Wald and Allen (2007) global maps of V_{s30} based on topographic slope from the Shuttle Radar Topography Mission (NASA, 2013) global digital elevation model. At a regional scale, Stewart et al. (2014) developed relationships between V_{s30} , terrain type, surficial geology and slope and verified these relationships against a dataset of shear-wave velocity profiles for Greece. Similarly, Parker et al. (2017) developed V_{s30} estimates in Central and Eastern North America using large-scale geologic maps, Wisconsin glaciation delineation, sedimentary basin structure and 30 arcsec topographic gradient and Mori et al. (2020b) developed a V_{s30} map of Italy using slope, concavity, and texture with boring logs and V_s profiles to calibrate the V_{s30} estimates.

The majority of site characterization maps use V_{s30} as the primary parameter. In this paper, we choose to focus on the f_0 parameter as prior work has provided clear evidence that f_0 is a strong predictor of site response in high impedance environments like those of the Central and Eastern US (Baise et al. 2016; Yilar et al. 2017; Schleicher and Pratt, 2021; Yassminh, 2019; Pontrelli et al. 2023a) and Eastern Canada (Hassani and Atkinson, 2016; Braganza et al. 2016). In addition to its applicability in the Central and Eastern United States, researchers are using f_0 as an additional site term in ground motion models (GMMs). Pinilla-Ramos et al. (2022) discuss how, in the absence of V_{s30} measurements at a site, f_0 has a high correlation to amplification for short periods. They show that using f_0 within the ASK14 GMM (Abrahamson et al. 2014) has a significant effect on the ground motion estimates changing median spectral acceleration factors by 0.6-1.6 for periods between 0.5 and 4 s. Hassani and Atkinson (2016) also show that f_0 can be a proxy for V_{s30} and when used as an explanatory variable in the NGA-east GMM reduces variability.

New England is a glaciated region and typically has soft glacial sediments overlying hard basement rock. During the Wisconsin glaciation, the Laurentide ice sheet covered the region, clearing most of the existing pre-glacial materials and depositing glacial sediments on the cleared bedrock surface. This unique high impedance contrast structure tends to have soft, low velocity sediment overlying hard, high velocity bedrock, a structure that is approximated in this study using the layer-over-halfspace model and the assumption of one-dimensional propagation of vertical SH-waves through horizontally layered media. Baise et al. (2016) demonstrated that the glacial and marine sediments of the Boston Basin result in large amplification at a fundamental frequency driven by the depth to the impedance contrast. Yilar et al. (2017) performed a microzonation analysis of the Boston Basin using the Horizontal-to-Vertical Spectral-Ratio (HVSR) technique of Nakamura (1989) to show how f_0 varies with depth to the impedance contrast across the basin. Similarly, Braganza et al. (2016) model site response in Eastern Canada using f_0 and overburden sediment type as a stiffness proxy to model site amplification for use in GMMs and ShakeMap applications – a similar framework to that used in this study. Therefore, New England is an ideal region to use f_0 as a site response parameter because it is a high impedance environment with abundant HVSR measurements.

The layer-over-halfspace model is a physics-based framework that assumes a single overburden velocity (Vs_{avg}), a bedrock velocity (V_R) and a depth to the impedance contrast (d_s). This model is applicable in high impedance environments and is useful to form a regional understanding of seismic site parameters. In this model, f_0 is equal to $Vs_{avg}/4d_s$ and thus, with surface measurements of f_0 and Vs_{avg} , d_s can be estimated – providing a simplified model of the overburden, from which an estimate of $Vs30$ can be computed. In this study we use this framework at the geologic unit scale, looking at geophysical measurements f_0 and Vs_{avg} across a unit to approximate a distribution of $Vs30$ within that unit. The site characterization maps presented in this work are driven by the f_0 parameter derived from HVSR curves collected in the field. All f_0 measurements within a geologic unit are used to develop an f_0 distribution within that unit. Vs profiles are used to define Vs_{avg} for each profile which are then grouped within geologic units to compute distributions of Vs_{avg} within each unit. With f_0 and Vs_{avg} distributions in each unit, $Vs30$ distributions are computed using

Monte Carlo sampling (10,000 samples) of the f_0 and Vs_{avg} distributions and using the assumption of one-dimensional propagation of vertical SH-waves through a single layer-over-halfspace model.

In Pontrelli et al. (2023a), the authors developed similar maps for f_0 , Vs_{avg} , and $Vs30$ by surficial geologic unit using the 1:5,000,000 scale Soller et al. (2009) conterminous surficial geology map of the US. This strategy yielded maps of f_0 distribution parameters for large, generalized geologic units in New England. This paper improves upon the Pontrelli (2023a) maps in three ways. Firstly, the Soller et al. (2009) conterminous US surficial geology map is a low-resolution map (1:5,000,000 scale) and therefore does not capture high-resolution deposits in terrain like tight river valleys that are relevant for city or site scale site characterization. This paper uses 6 state-scale surficial geologic maps with higher resolutions from 1:24,000 to and one nation-scale state map at 1:5,000,000 (Soller et al. 2009). Secondly, Pontrelli et al (2023a) did the site characterization based on seven simplified surficial geologic regions, not accounting for local differences within the same geologic classification. This study allows for differentiation of known deposits within a single geologic classification based on locally defined sedimentary deposits. For example, the “Proglacial sediments, mostly fine-grained, thin” unit from the Soller (2009) map used in Pontrelli et al. (2023) includes marine and lacustrine sedimentary deposits but has typical f_0 values that are significantly different in Maine, Vermont, and Boston. These differences are driven by differences in local geologic history which manifests as differences in thicknesses and sediment composition. This study addresses this issue by adding six subregions defined as local sedimentary deposit classifications resulting in 39 classified units. The six subregions provide more accurate classifications for important and known sedimentary deposits in the region. Finally, Pontrelli et al. (2023a) uses a single value of Vs_{avg} for each surficial geologic unit whereas this work assigns a distribution to Vs_{avg} and estimates the distribution of $Vs30$ using Monte Carlo sampling of both the f_0 and Vs_{avg} distributions.

2.0 Data

The site characterization maps in this study require 3 inputs: surficial geology classifications, a regional f_0 dataset, and a shear-wave velocity dataset. The surficial geology classifications for this project are derived from state scale surficial geology maps, local knowledge of specific sedimentary deposits, and a digital elevation model.

2.1 State-scale surficial geologic maps

To develop the high-resolution surficial geology classifications, a regional surficial geologic map is created from existing state surficial geologic maps. These state-scale maps are in general higher spatial resolution than the Soller et al. (2009) Conterminous US surficial geologic map, ranging in scale from 1:24,000 to 1:500,000 (Table 1) with the exception of the New Hampshire map which uses the Soller et al (2009) map. The Massachusetts and Connecticut maps are the highest resolution (1:24,000 scale). The Rhode Island map is 1:100,000 scale, New York and Vermont maps are 1:250,000 scale, and the Maine map is 1:500,000 scale all of which are significantly higher resolution than the Soller et al. (2009) map. The higher resolution maps can capture finer basin delineations in the region (as shown in Figure 1 for the greater Boston area) which is an advantage for site characterization. When aggregating the state-scale maps, there are a total of 106 unique units (Table 1). This number is reduced to 7 units using depositional environment: till (*t*), fines (*f*), alluvium/outwash (*al*), swamp (*s*), artificial fill (*af*), beach and dune deposits (*bd*), and moraine deposits (*m*). The final aggregated map (Figure 2a) shows the basic surficial geologic trends in the region. The fine deposits are located predominantly in the Boston Basin (*BB*, Figure 2b), the coast of Maine (*MC*), the coast of Lake Champlain (*CS*) and the Connecticut River Valley (*CRV*). The deposits of the Boston Basin are the “Boston Blue Clay”, those of the Maine coast are the “Presumpscot formation”, those of the coast of Lake Champlain are the “Champlain Sea sediments” and those of the Connecticut River Valley are the glaciolacustrine “Lake Hitchcock deposits”. The alluvium/outwash deposits are contained in river valleys, adjacent to moraines (on Cape Cod and Long Island (*ACP*) and in topographic depressions. The artificial fill makes up a small portion of the total area of the region and is

concentrated almost entirely in the Boston Basin. The till deposits are mapped in most of the region's land area - in the uplands and adjacent to the valleys and subregions with major low-velocity geologic deposits. This map is used as the primary surficial geology map for the region. Distributions for $V_{s\text{avg}}$ are developed using this map.

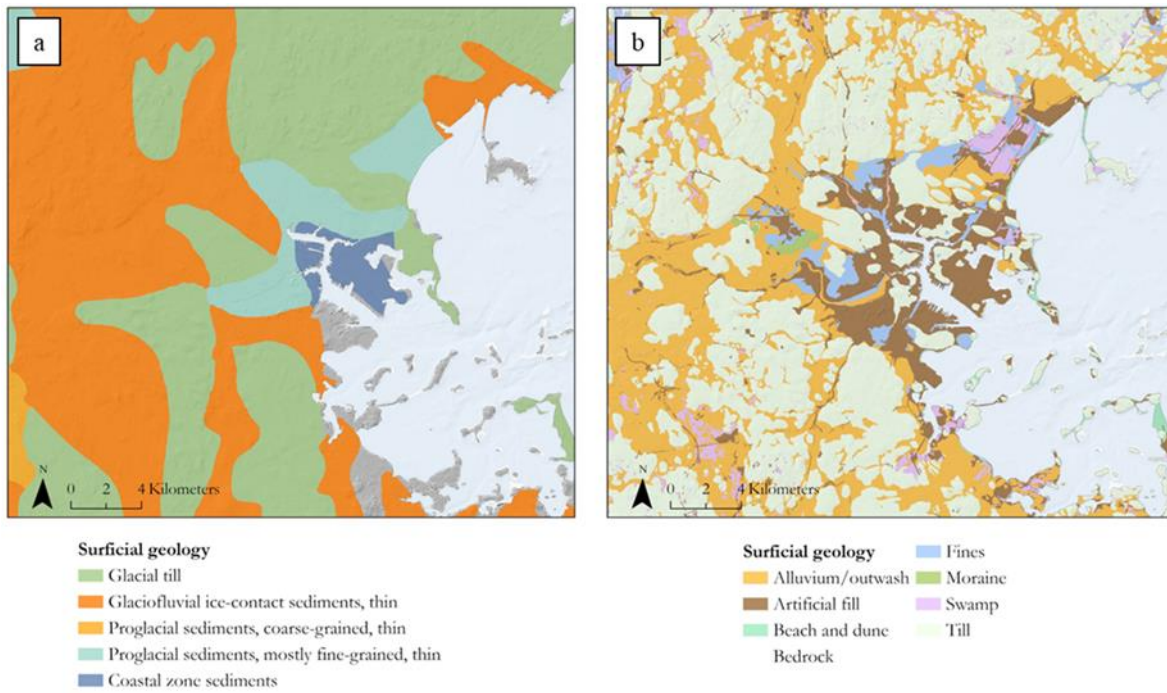


Figure 1. a) Surficial geology from the 1:5,000,000 scale Soller et al. (2009) map showing the Boston Basin. b) Surficial geology derived from the 1:24,000 scale surficial geology map of Massachusetts from Stone et al. (2018) showing the Boston Basin.

Table 1. Summary table of the state surficial geologic maps used in this study with their scales and number of units indicated.

State	Scale	# of units	Source
Massachusetts	1:24,000	23	Stone et al. (2018)
Connecticut	1:24,000	10	Stone et al. (1992)
Maine	1:500,000	17	Thompson (1985)
Vermont	1:250,000	32	Doll et al. (1970)
Rhode Island	1:100,000	5	RIGIS (1989)

New Hampshire	1:5,000,000	9	Soller et al. (2009)
New York	1:250,000	10	Cadwell (1986)
Total	-	106	-

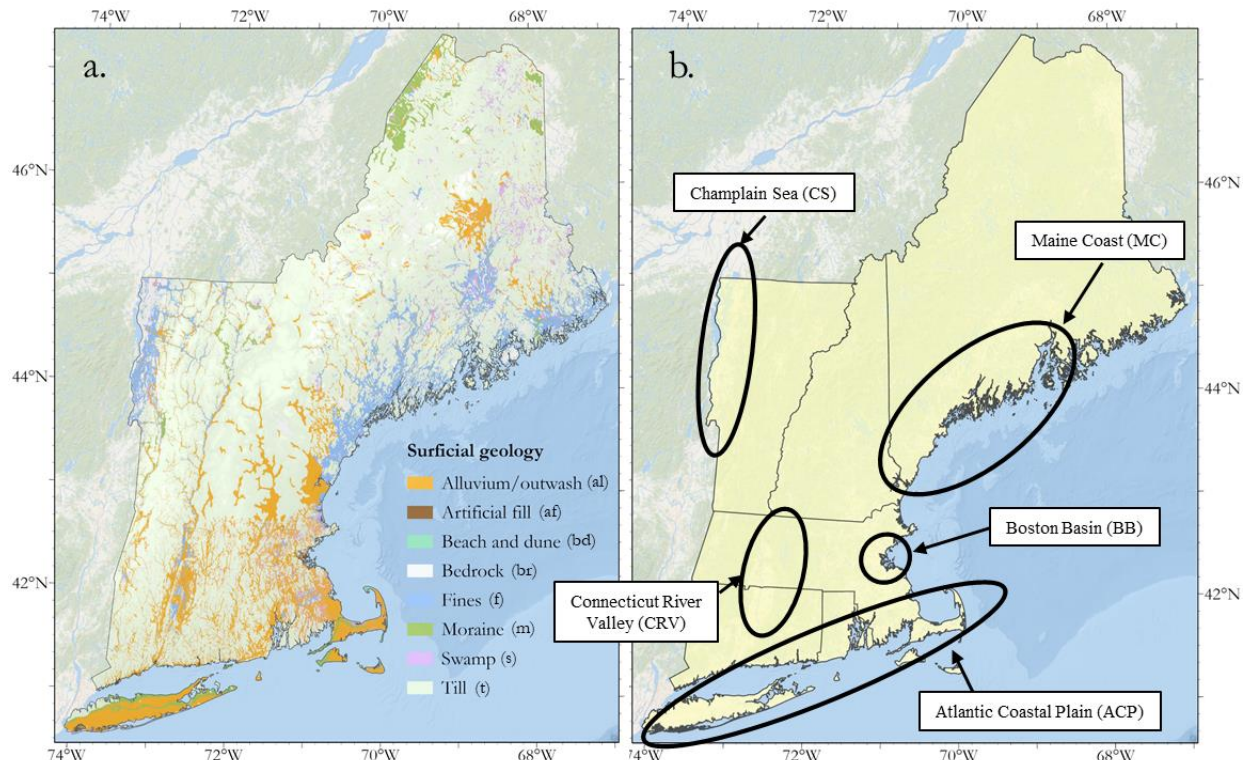


Figure 2. a) Final geology map created by aggregating the state-scale surficial geologic and reducing the number of units to 7. *b)* Map of the region showing the general locations of the subregions which are defined by local sedimentary deposits.

2.2 Local sedimentary deposit subregion map

As demonstrated in Pontrelli et al. (2023a), f_0 values grouped by surficial geologic unit from the Soller (2009) map exhibit spatially correlated deviations from the median of that unit's distribution. For example, the fine proglacial sediments have consistently higher f_0 values in the Boston Basin than in the Maine coast. This demonstrates that the Boston Basin fine, proglacial sediments deposits are consistently thicker and/or have lower average shear-wave velocities than those of the Maine deposits and thus have

consistently lower f_0 measurements. This study resolves this issue by using a subregion grouping layer to identify local sedimentary deposits that are known to have different characteristics such as differences in depth or shear-wave velocity.

The major local units in the region are identified in a literature review and are located on the state-scale maps after identification. Baise et al. (2016) and Yilar et al. (2017) discuss the Boston Blue Clay, artificial fill, and Charles River alluvial sediments in the Boston Basin all of which are mapped in the state surficial geology map (Stone et al. 2018). The Boston Blue Clay is a well-known marine clay unit underlying the greater Boston area (Johnson 1989). The Connecticut River flood plain alluvium and lacustrine sediments of Glacial Lake Hitchcock are identified as high site response hazard in Becker et al. (2011) and are mapped in the state geology map in the Connecticut River Valley. Cape Cod and Long Island are both terminal moraines from the Wisconsin glaciation composed of Atlantic Coastal Plain sediments which are mapped in Stone et al. (2018) and Cadwell (1986). They are also the only mapped “>100 ft” sediments in New England in the Soller (2009) map. The Presumpscot Formation on the Coast of Maine is identified as high seismic site response hazard in Marvinney and Glover (2015) and is mapped in Thompson (1985). The Champlain Sea sediments are studied using HVSR curves in Motazedian et al. (2020) and are mapped in Doll et al. (1970).

Several researchers have performed basin delineation using a variety of methods including using Digital Elevation Models (DEMs). All these strategies have merit and a variety of applicability, some general, some specific. Coleman and Cahan (2012) catalog 144 sedimentary basins in the US using geologic classifications: Intracratonic, Pericratonic, Intercratonic and Oceanic. They compile databases developed by geologists and aggregate them into a unified GIS of basins with these classifications. Nweke et al. (2020) map basins in Southern California to study site response using geomorphology. They use a digital elevation model to make four classifications: Basin, Basin edge, Valley, and Mountain-hill. They make the classifications by making a grid of regularly spaced points and labeling them with the four classifications. They then use four morphology characteristics elevation, slope, curvature, and texture and develop a logistic

regression model on the training dataset to apply to the rest of the region. Outside of the field of seismic site response, the hydrologic community has also mapped basins using digital elevation models (Dávila-Hernández et al. 2022; Alireza et al. 2020; Gilbert et al. 2016). The strategy employed in this study is to use surficial geology maps to find areas where the mapped non-till geologies, which are likely low velocity sediments, meet mapped tills, which are likely higher velocity and mapped in uplands. In New England, major geologic units often extend to a line of equal elevation either of maximum sea level in the case of glaciomarine clays or the maximum level of a glacial lake in the case of glaciolacustrine clays. Glaciomarine clays (Boston Blue Clay in the Boston Basin, the Champlain Sea sediments adjacent to Lake Champlain, the Presumpscot Formation along the Maine Coast) were deposited below the maximum relative sea level line and glaciolacustrine clays (Lake Hitchcock sediments of the Connecticut River Valley) were deposited below the maximum elevation of the glacial lake. This study identifies and maps local sedimentary units by finding the approximate elevation along which the non-till geology to till boundary is located.

The local sedimentary basin subregion map was developed first by identifying the major relevant amplifiable units in New England using the surficial geology maps and then using the Shuttle Radar Topography Mission (NASA, 2013) 1 Arc-second digital elevation model clipped to New England and Long Island. With these areas identified, a coarse polygon is drawn around the general area (Figure 3b) and the DEM is clipped to this polygon. Pixels are then selected from the clipped DEM below an elevation threshold (Figure 3c) and the threshold is changed until the shape of the selected pixels approximately matches the location of the map where the surficial geology map transitions from a non-till geology to tills (Figure 3d). Elevation thresholds are defined for the Boston Basin (BB), the Maine Coast (MC), the Connecticut River Valley (CRV), and the Champlain Sea (CS, Table 2). Two more subregions: the Atlantic Coastal Plain and New England General subregions, are created using different strategies. The Atlantic Coastal Plain subregion (ACP) is defined as all the land on Cape Cod and Long Island, specifically as that land east of the East River on Long Island and east of the Cape Cod Canal of Cape Cod. Cape Cod and

Long Island are grouped into one subregion in this study because they have similar geologic pasts and have similar fundamental frequency values and HVSR curve shapes. The New England General subregion (NEG) is defined as all the land outside of the other 5 subregions, which we call “New England General” (Figure 3e).

Table 2. Elevation thresholds that we defined for the subregions in the study.

Subregion	Elevation (m)
Boston Basin	18
Maine Coast	62
Connecticut River Valley	100
Champlain Sea	100

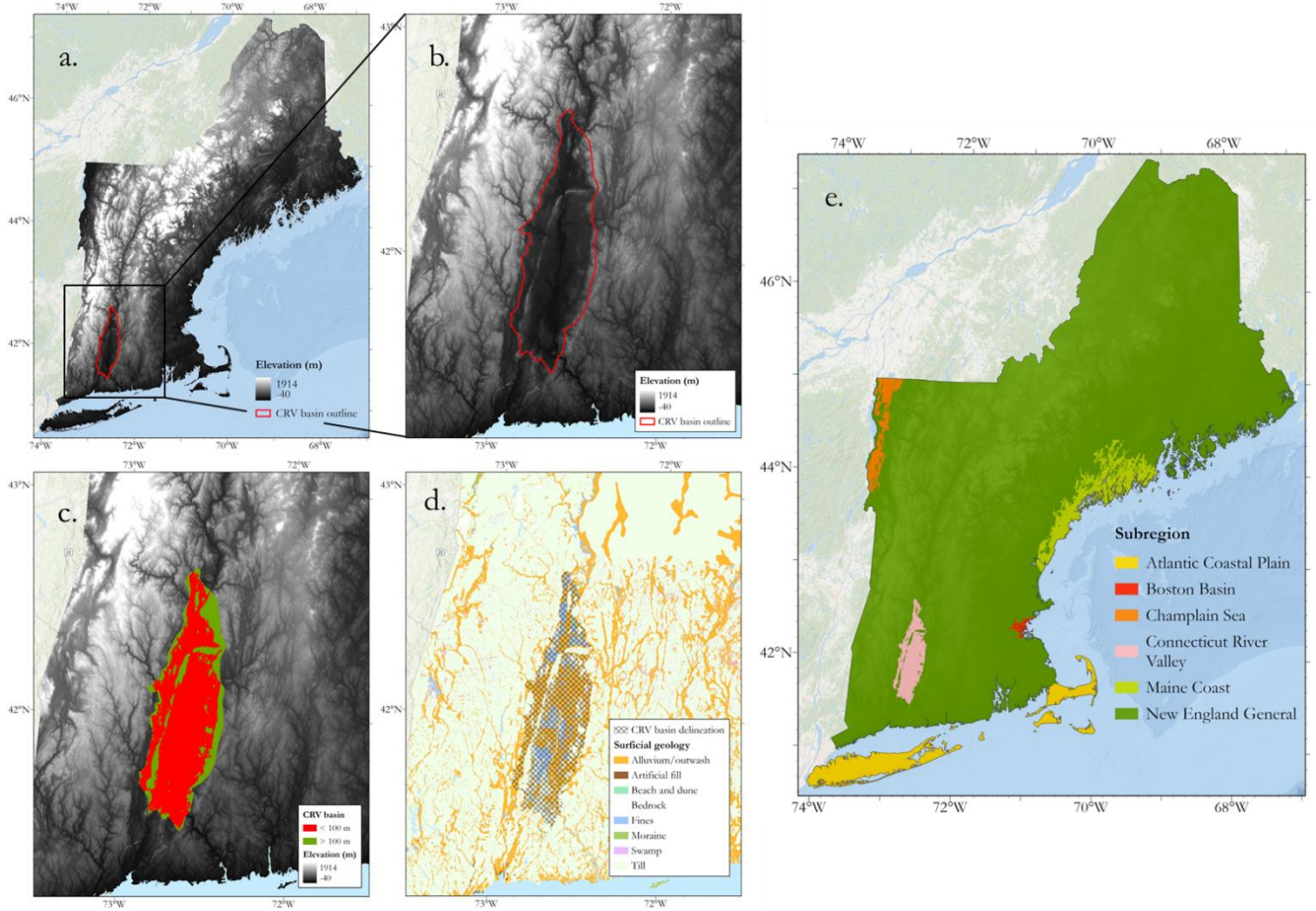


Figure 3. Example of creating the subregion polygon for the Connecticut River Valley. a) The location of the raster clip from within the entire raster, b) the raster clip, c) the raster clip with pixels colored green if they are over 100 m and pixels colored red if they are below 100 m, d) The overlay of the selection of pixels below 100 meters (cross-hatched symbology) with the surficial geology showing where the polygon outline meets the soft-hard surficial geology boundary and e) The final subregion map.

2.3 f_0 data

The f_0 dataset used in this study has 1619 stations, 487 of which come from a field campaign by the authors (Pontrelli et al. 2023a), 570 come from Yilar et al. (2017), 198 come from Fairchild et al. (2013) and 545 come from Mabee (2022). These four studies develop HVSR curves using the Nakamura (1989) method and follow the procedures of the SESAME project (SESAME, 2004 a and b). The spatial extent of the f_0 database is shown in Figure 4. The Pontrelli et al. (2023a) field campaign has coverage in the Champlain Sea, the Maine Coast, the Atlantic Coastal Plain (Figure 4a, Figure 2b) and in transects across New England

to sample non-major geologic deposits. The Yilar et al. (2017) dataset contains stations exclusively in the Boston Basin – it was a microzonation study of the basin. The Fairchild et al. (2013) dataset contains stations in eastern Cape Cod; it was performed to map bedrock depth in Cape Cod to inform groundwater modeling. The Mabee (2022) dataset has f_0 stations spatially distributed evenly throughout the state of Massachusetts; it was done to map depth-to-bedrock across the state. The east west transects of stations provide data from a variety of terrains in the region including stations across the Green Mountains, the northern Connecticut River Valley, the White Mountains and the mountains in central Maine (Figure 4a). Example HVSR curves from the 5 significant geologic units are shown in Figures 4b-f.

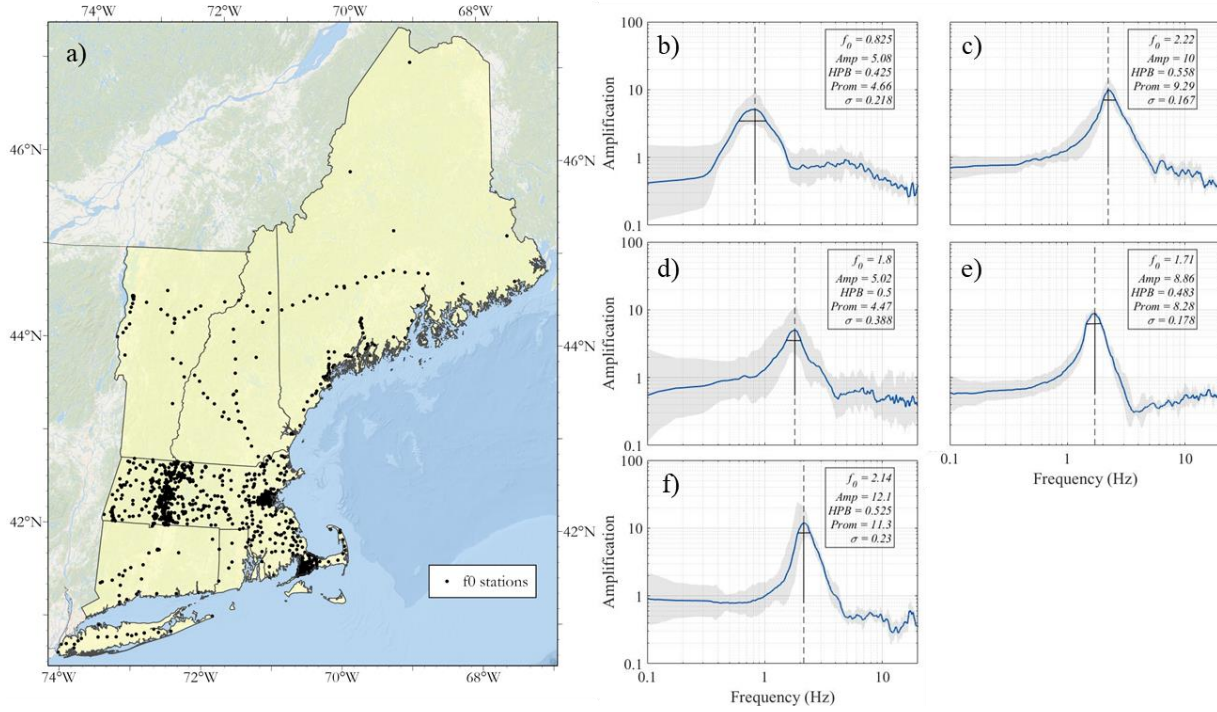


Figure 4. a) Locations of the f_0 stations used in this study. Example HVSR curves with the fundamental peak frequency (f_0), amplitude (Amp), Halfpower bandwidth (HPB), Prominence ($Prom$) and sigma (σ) values in b) Cape Cod, c) the Connecticut River Valley, d) the Champlain Sea, e) the Maine Coast, and f) the Boston Basin. These general region outlines are in Figure 2b. The values used to describe the peak are outlined in Pontrelli et al. (2023a).

2.4 Vs data

The Vs_{avg} dataset used in this study has 40 shear-wave velocity profiles with 5 collected in a field campaign by the authors and presented in Pontrelli et al. (2023a), 27 collected in Thompson et al. (2014), 5 collected in Hager geosciences (2016) which are presented in Mabee and Duncan (2017), and 3 collected in Lens and Springston (2013). The data of Pontrelli et al. (2023a), Hager geosciences (2016) and Lens and Springston (2013) were processed using multichannel analysis of surface waves (MASW, Park et al. 1999) and those of Thompson et al. (2014) were processed using spectral analysis of surface waves (SASW, Nazarian et al., 1983). The Vs dataset has good coverage in the Connecticut River Valley and Boston Basin. The Vs dataset does not have good coverage in the remaining subregions, so we only use the geologic map to make groupings for the Vs_{avg} distribution estimations. This assumes that Vs_{avg} values are similar within a geologic unit between different subregions, even though in reality there is likely some Vs_{avg} variability between subregions. The used μ_{ln} and σ_{ln} for the Vs_{avg} distributions are shown as vertical red and blue lines respectively in Figures 5b-g. The estimation of these values is presented in section 3.2 Vs_{avg} distributions.

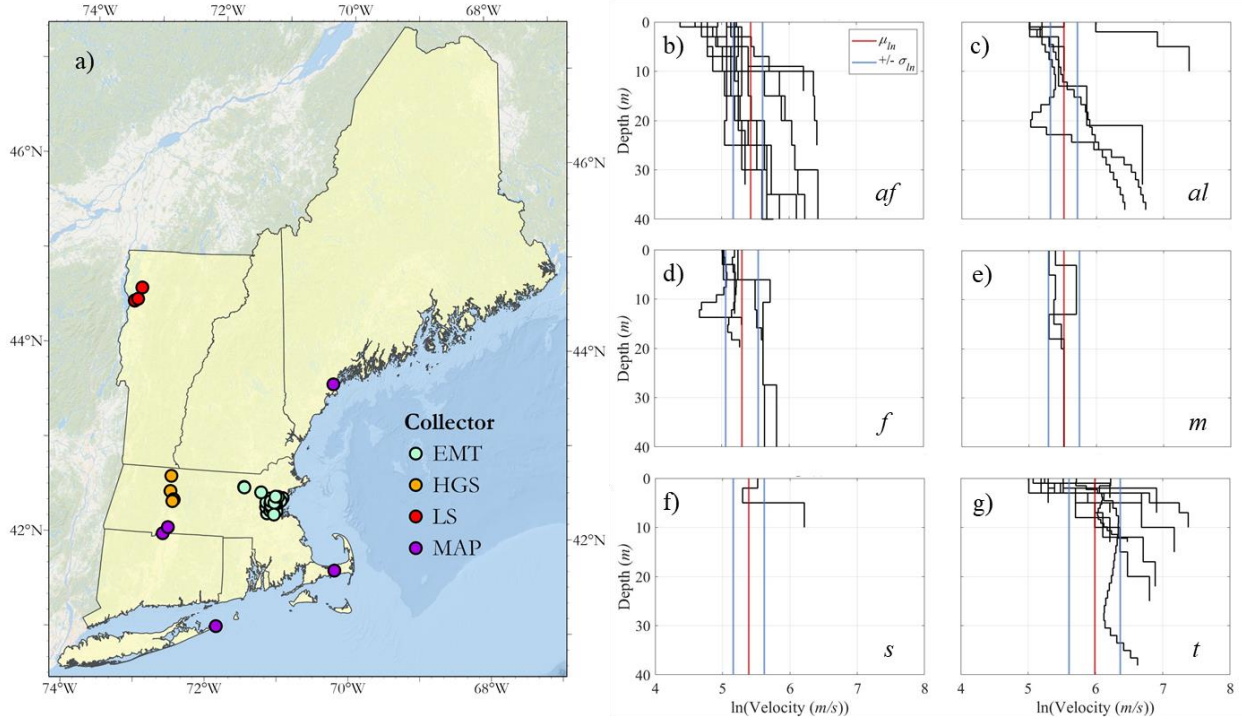


Figure 5. a) Locations of the V_s profiles used to compute $V_{s_{avg}}$ in this study. Collector EMT is Thompson et al. (2014), HGS is Hager Geoscience (2016) which is reported in Mabee and Duncan (2017), LS is Lens and Springston (2013), and MAP is the data collected in Pontrelli et al. (2023a). The V_s profiles grouped into their respective surficial geologic classification with their used $V_{s_{avg}}$ μ_{ln} value indicated in red +/ their used σ_{ln} value indicated in blue in units b) artificial fill (af), c) alluvium/outwash (al), d) fines (f), e) moraine (m), f) swamp (s), and g) till (t).

3.0 Methods

3.1 f_0 distributions

To create the final set of units for the f_0 and $V_{s_{avg}}$ points, the surficial geologic layer (Figure 2a) is intersected with the subregion layer (Figure 3e) yielding 39 units. To characterize the f_0 stations using the derived surficial geology map, the f_0 layer is intersected with the geologic map layer. From this dataset, f_0 distributions are computed for each of the 39 surficial geologic units. The lognormal distribution is used as it is a common distribution for geotechnical properties and fits the data well as seen in Figure 6. The mean and standard deviation of the distributions are computed by taking the natural logarithm of each measurement in the grouping and calculating the mean (μ_{ln}) and standard deviation (σ_{ln}) of the log-

transformed data. The median (Mdn) of the lognormal distribution is also calculated in natural units of Hz using the equation

$$Mdn = \exp(\mu_{ln}) \quad (1)$$

Figure 6 demonstrates the procedure within the Boston Basin. In Figure 6a, the f_0 stations are plotted over the Boston Basin surficial geology map. The values are grouped by the unit, histograms are plotted, and lognormal distribution parameters μ_{ln} , σ_{ln} , and Mdn are calculated (Figure 6b). Following this process, the distribution parameters, including the number of f_0 values in each unit is added to the geologic layer attribute table.

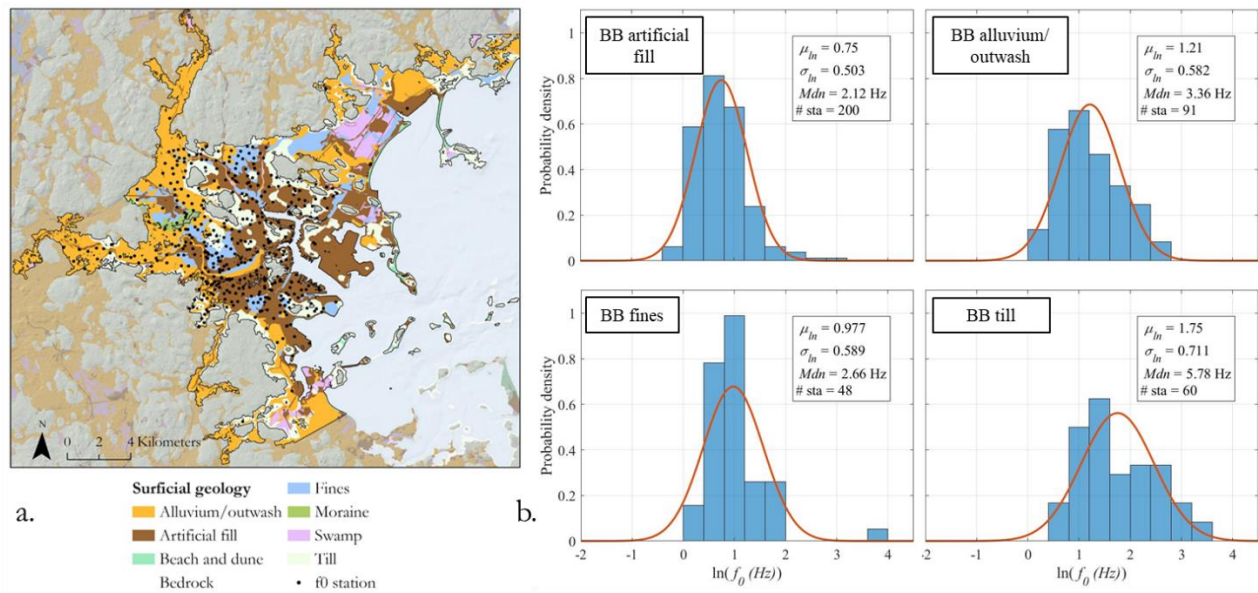


Figure 6. a) The Boston Basin subregion surficial geologic map with the f_0 stations plotted in black and b) the f_0 distributions within each of the Boston Basin surficial geologies with μ_{ln} , σ_{ln} , Mdn , and the number of f_0 stations in the distribution indicated on the plot.

Figure 6 shows four Boston Basin f_0 distributions. There are, however, seven surficial geologic units in the subregion (excluding bedrock). Beach and dune, moraine, and swamp deposits within the subregion have very few or no f_0 stations within them. To handle cases like this, we apply a rule where any geologic unit with fewer than 5 f_0 stations uses a distribution composed of all the f_0 stations in non-till units

in the subregion, that is the fines, alluvium/outwash, swamp, artificial fill, beach and dune, and moraine units. We refer to this distribution as the “soft geology” distribution for the rest of this paper. This generalization allows characterization of units that have little or no data while still using local information. For example, the “Boston Basin moraine” grouping has only 4 f_0 stations in it, and yet there are 343 f_0 stations within the Boston Basin soft geology distribution. For this unit, we assign the f_0 mean and standard deviation of the Boston Basin soft geology distribution (Figure 7a). In instances where fewer than 5 till stations in the subregion are available, such as the Champlain Sea (0 till stations), we use the New England General till distribution for the grouping’s f_0 distribution statistics which has an f_0 Mdn value of 8.6 Hz (Figure 7b).

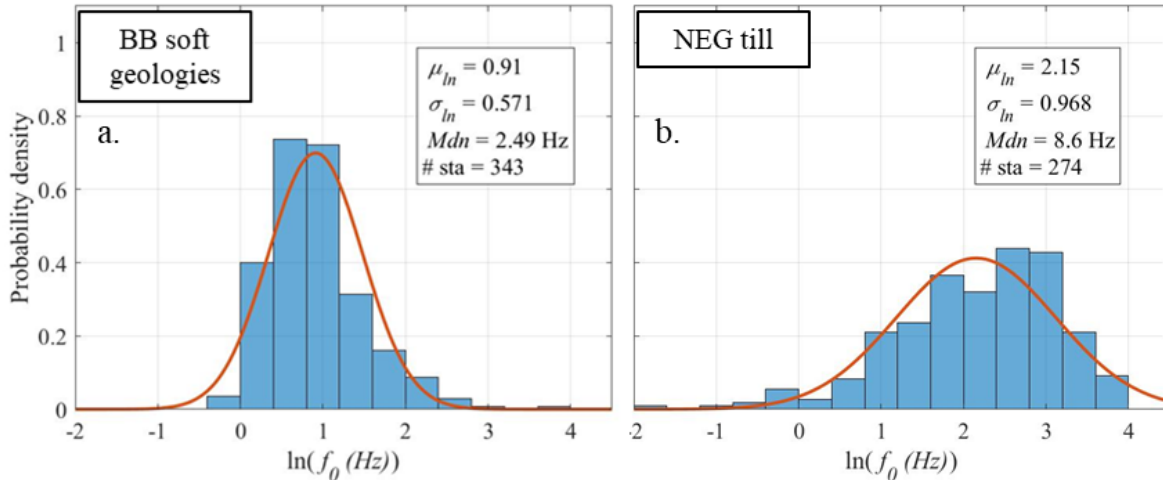


Figure 7. a) Soft geology distribution for the Boston Basin developed to be used when little or no data is available to compute an f_0 distribution within a grouping. μ_{ln} , σ_{ln} , Mdn and the number of f_0 stations in the distribution are indicated on the plot. This distribution is composed of all the f_0 stations in the fines, alluvium/outwash, swamp, artificial fill, beach and dune, and moraine units. b) The New England General till distribution that is used where subregion till units have fewer than 5 stations.

3.2 $V_{s_{avg}}$ distributions

This study only has 40 V_s profiles that are not well spatially distributed across the entire region and subregions; thus, $V_{s_{avg}}$ distributions are estimated using the merged surficial geology map (Figure 2a) instead of by subregion and geologic unit. $V_{s_{avg}}$ is computed on each shear-wave velocity profile using Equation 3 over the velocities until the sediment-bedrock interface. Figure 8 illustrates the distribution of

Vs_{avg} values in the shear-wave velocity database by surficial geologic units and Table 3 summarizes the estimated distributional parameters for each unit. Because there are not enough Vs_{avg} measurements to characterize all seven geologic units with a high degree of confidence, engineering judgements are made in the final determination of the distribution parameters of each unit. For these judgements, we round the mean of the distribution to two significant figures. In some cases, we increase or decrease the rounding for reasons described in the following paragraph. With enough Vs data, these estimations would not need to be made. The units with the most Vs_{avg} measurements in the study are till (13), artificial fill (12), fines (7) and alluvium/outwash (5). The units with the fewest measurements in the study are swamp (1), beach and dune (0), and moraine (2).

Till has measured till Mdn value is 373 m/s, though there are two clusters in the plot of till Vs_{avg} values (Figure 8a). The lower cluster decreases the measured Mdn value. Due to the observed clustering in the distribution, this study uses a higher-than-measured Mdn estimate of 400 m/s value for till Vs_{avg} value, which yields a μ_{ln} estimate of 5.99. In the till unit, the measured σ_{ln} of 0.38 is retained to capture the measured spread in the data for the till Vs_{avg} distribution. The alluvium/outwash unit has a measured Mdn value of 239 m/s. We round this measured Mdn value to 250 m/s and use it for the Vs_{avg} value for alluvium/outwash deposits, yielding a μ_{ln} estimate of 5.52. The measured σ_{ln} of 0.20 is used for the unit. For swamp, beach and dune and moraine deposits, there are 1, 0 and 2 stations respectively. For these units, a similar approach is taken to that of the f_0 distributions with little data – the non-till soft geology stations are pooled to create a soft geology distribution. This pooled distribution has a measured Mdn of 229 m/s. A rounded Mdn value of 220 m/s is used for swamp and beach and dune deposits, yielding a μ_{ln} value of 5.39 for both units. We alter the rounded Mdn value to 250 m/s for this unit since the two measured moraine deposit Vs_{avg} values are higher than the non-till distribution Mdn . This estimate of Mdn yields a μ_{ln} estimate of 5.52. The soft geology pooled distribution σ_{ln} of 0.23 is used for all three of these units. The artificial fill deposits have a measured Mdn Vs_{avg} value of 227 m/s. A rounded Mdn value of 220 m/s yielding a μ_{ln} of 5.39 and the measured σ_{ln} of 0.22 are used for this unit. The fine deposit Vs_{avg} distribution has a measured

Mdn of 204 m/s. A rounded 200 m/s is used for the unit's Mdn estimate, yielding a μ_{ln} estimate of 5.30, and the grouping's σ_{ln} estimate of 0.24 is used.

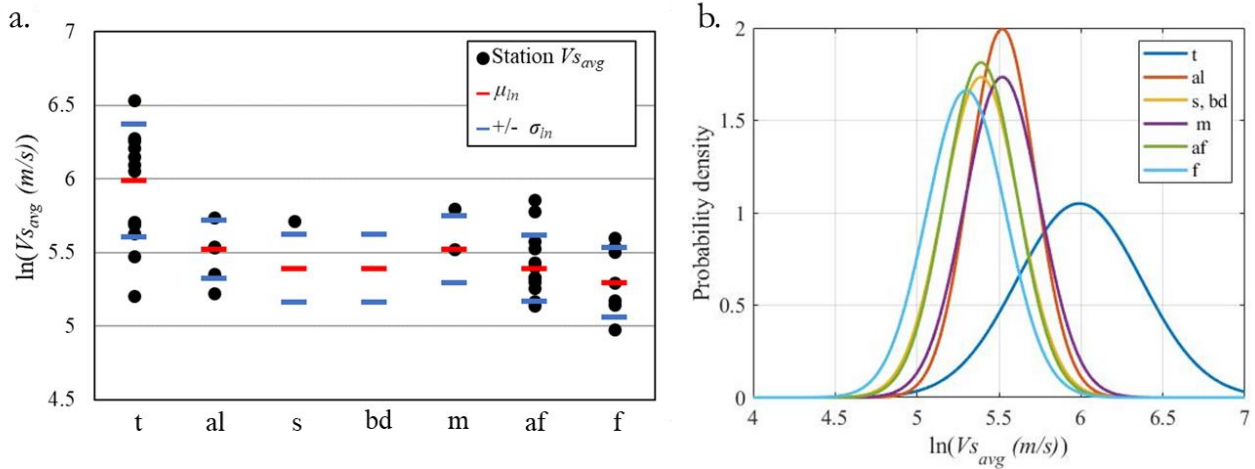


Figure 8. a) The 40 $V_{s_{avg}}$ values grouped by surficial geology with the μ_{ln} value selected for use to define the unit's $V_{s_{avg}}$ distribution and the σ_{ln} value $\pm \mu_{ln}$ shown in blue. b) Plot of the 6 $V_{s_{avg}}$ distributions (in natural-log space) used in this study for the seven surficial geologic units, till, alluvium/outwash, swamp, beach and dune, moraine, artificial fill, and fines. Values of μ_{ln} and σ_{ln} for the distributions are in the "Used values" section of Table 3 along with the Mdn value.

Table 3. The results from the $V_{s_{avg}}$ μ_{ln} and σ_{ln} estimation analysis. The general information of the geologic grouping is shown in the left third of the table. The values measured from the data are shown in the center of the table. The values used to define the $V_{s_{avg}}$ distributions for each geologic unit are shown in the right third of the table.

Surficial geology	Code	# stations	Measured μ_{ln}	Measured σ_{ln}	Measured Mdn	Used μ_{ln}	Used σ_{ln}	Used Mdn
Till	t	13	5.92	0.38	373.69	5.99	0.38	400
Alluvium/outwash	al	5	5.48	0.20	239.18	5.52	0.20	250
Swamp *	s	1	5.71	-	303.03	5.39	0.23	220
Beach and dune *	bd	0	-	-	-	5.39	0.23	220
Moraine *	m	2	5.66	0.20	287.18	5.52	0.23	250
Artificial fill	af	12	5.43	0.22	227.26	5.39	0.22	220
Fines	f	7	5.32	0.24	204.57	5.30	0.24	200

3.3 Vs30 distribution estimation

The methodology in this paper is driven by f_0 , which has abundant measurements in New England compared to $Vs30$ and which can be used to gain insight into $Vs30$ through the layer-over-halfspace approximation using surficial geology as a proxy of for overburden stiffness (Vs_{avg}). Vs_{avg} is estimated on a regional scale using geologic units from surficial geology maps and is related to f_0 in the layer-over-halfspace model through depth to the impedance contrast with the equation:

$$f_0 = \frac{Vs_{avg}}{4d_s} \quad (2)$$

where d_s is the depth of the overburden. Vs_{avg} is defined as the weighted average of the overburden layers until the impedance contrast using the equation:

$$Vs_{avg} = \sum_{i=1}^n \frac{h_i}{h_i/V_i} \quad (3)$$

where d_i is the thickness and V_i is the shear-wave velocity of the i^{th} geotechnical layer. $Vs30$ is calculated using Equation 3 where $\sum_{i=1}^n d_i = 30$ m. $Vs30$ is the most common site response measurement and is used in most ground motion prediction equations as a basis for seismic site classification in the International Building Code and as a HAZUS input. When using the average overburden velocity (Vs_{avg} , Equation 3) instead of a multi-velocity overburden, $Vs30$ is calculated using the equation

$$Vs30 = \frac{30}{\left(\frac{d_s}{Vs_{avg}} + \frac{d_R}{V_R} \right)} \quad (4)$$

where d_R is the thickness of the basement rock which is $30\text{m} - d_s$ and V_R is the velocity of the basement rock. Since f_0 is a function of d_s and Vs_{avg} , Equation 2 can be substituted into Equation 4 yielding the relationship between f_0 , Vs_{avg} and $Vs30$:

$$Vs30 = \frac{30}{\frac{1}{4f_0} \left(1 - \frac{Vs_{avg}}{V_R} \right) + \frac{30}{V_R}} \quad (5)$$

With each geologic unit classified by a distribution of f_0 and Vs_{avg} a single-layer-over half space sediment model with one-dimensional propagation of vertical SH-waves is assumed to relate f_0 , Vs_{avg} , $Vs30$, and bedrock velocity (V_R). Using Monte Carlo sampling of the f_0 and Vs_{avg} distributions, $Vs30$ distributions are estimated in each classified unit. Each of the 39 surficial geologic units have estimates of μ_{ln} and σ_{ln} for both f_0 and Vs_{avg} – these units are iterated through and in each unit 10,000 samples of f_0 , and Vs_{avg} are drawn from the lognormal distributions of the estimated f_0 and Vs_{avg} distributions and are run through Equation 5, computing $Vs30$ (Figure 9). A bedrock velocity (V_R) of 2500 m/s is assumed, which is similar to the shear-wave velocity used for bedrock in the Central and Eastern United States (Stewart et al., 2020; Goulet et al., 2017, 2018; Pacific Earthquake Engineering Research Center (PEER), 2015a, 2015b) and calculate d_R as $30m - d_s$. In Baise et al. (2016) the authors test V_R values of 2000 and 3000 m/s stating that measurements of V_R in the Boston Basin yield results around 2000 m/s but fits of theoretical to empirical transfer functions are improved using 3000 m/s. Since the layer-over-halfspace model that we use for the $Vs30$ estimate in this study doesn't account for more complex and likely increasing velocities with depth, we use 2500 m/s, lower than that used in the PEER work but higher than the measurements discussed in Baise et al. (2016). This process creates a distribution of $Vs30$ for each unit which can be characterized by a μ_{ln} and σ_{ln} .

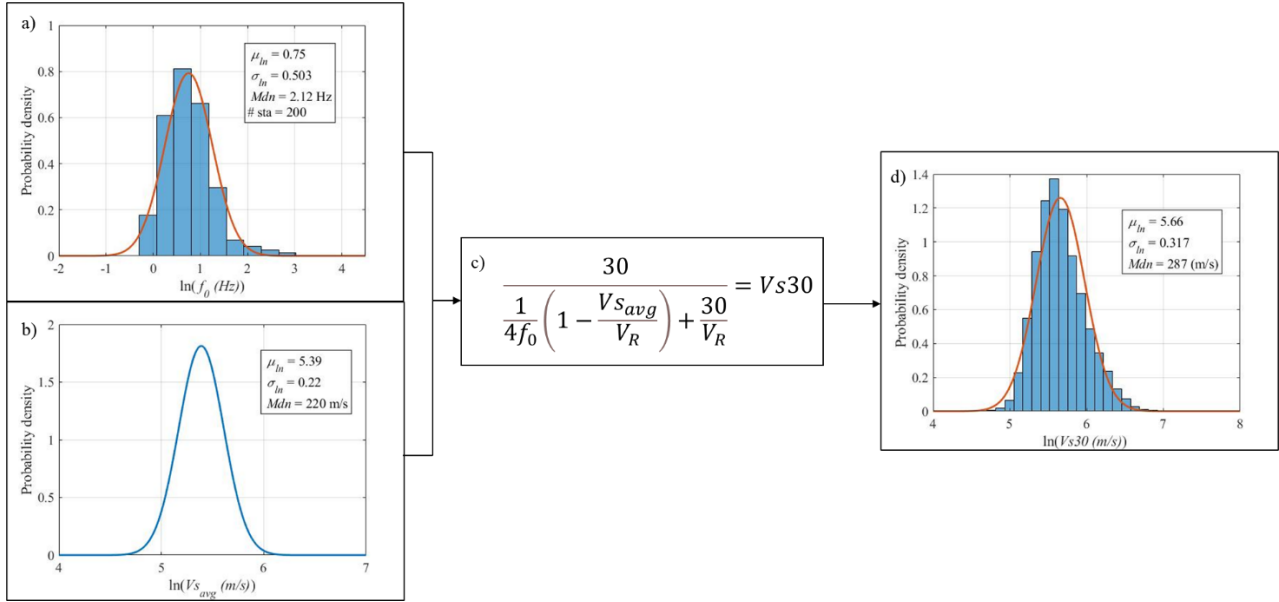


Figure 9. Propagating distributions of f_0 and Vs_{avg} through the layer-over-halfspace model to develop distributions of $Vs30$. This example uses data from the Boston Basin artificial fill. a) f_0 distribution from a subregion and geologic distribution with its fit distribution from estimates of the mean (μ_{ln}) and standard deviation (σ_{ln}) and its computed median (Mdn) computed from $\exp(\mu_{ln})$. b) Fit distribution of Vs_{avg} of artificial fill from an estimate of μ_{ln} and σ_{ln} from data. c) The layer-over-halfspace model (Equation 5). d) The output $Vs30$ distribution from the input distributions.

4.0 Results

4.1 f_0 distributions by surficial geologic unit

The f_0 distributions across the individual geologic units in each subregion are shown in Figure 10.

The New England General subregion tends to have geologic units with higher f_0 values than those units in other subregions. For example, it has the till f_0 distribution with the highest f_0 values, which means that the tills that are within other subregions (which are thick, low velocity deposits) have lower f_0 values. The subregion has the highest f_0 values in the swamp, artificial fill, and moraine units and the second highest fines and alluvium/outwash units, second to the Maine Coast subregion (Figure 10). The New England General subregion has the soft geology distribution with second highest f_0 μ_{ln} of 1.48 and Mdn of 4.39 Hz. This suggests that only the major surficial units in the region have significantly low (<3 Hz) f_0 values and that outside of these deposits, smaller deposits in the region are likely shallower and higher velocity, though

on occasion they can be thick (Figure 11). The Maine Coast subregion also tends to have geologic units with higher f_0 values than the same units in other subregions. Its fines unit has the highest f_0 distribution of any fines unit in another subregion, indicating that though much of the coast is mapped as the marine clay Presumpscot formation, much of this formation has eroded away and most of the Maine Coast overburden layer is thin. The Maine Coast also has the soft geology distribution with the highest μ_{ln} value of 1.86 and Mdn of 6.42 Hz. The Boston Basin and Connecticut River Valley tend to have geologic unit f_0 distributions with similar f_0 values. These basins have similar depths and shear-wave velocities. The fines unit of the Boston Basin is composed of the Boston Blue Clay and the fines unit of the Connecticut River Valley is composed of the Lake Hitchcock sediments and both have f_0 distributions with relatively low f_0 values with some variability mainly caused by higher values on the basin edges where the units pinch. The Connecticut River Valley alluvium/outwash sediments are made up of the Connecticut River flood plain alluvium, which has lower f_0 values than the Boston Basin alluvium/outwash that is made up of the Charles and Mystic River alluvium. The artificial fill unit in the Boston Basin has low f_0 values with some variability where the fill is shallow with higher f_0 values. The Connecticut River Valley and Boston basin have soft geology $f_0 \mu_{ln}$ values of 0.95 and 0.91, respectively, corresponding to Mdn values of 2.59 and 2.49 Hz, respectively (Figure 11). The Champlain Sea sediments are similar to those of the Boston Basin and Connecticut River Valley being large fine deposits. The unit's soft geology distribution is lower than the Boston Basin and Connecticut River Valley with an $f_0 \mu_{ln}$ of 0.75 and Mdn of 2.13 Hz, indicating a thicker deposit on average than the other two subregions. Finally, The Atlantic Coastal plain consistently has units with f_0 distributions with lower f_0 values than those of units in other subregions with little variability in the distributions between units within the subregion. The unit's soft geology distribution has the lowest $f_0 \mu_{ln}$ of any subregion at 0 and Mdn of 1 Hz. The final μ_{ln} and Mdn values of the f_0 distributions are mapped in Figure 12 and the σ_{ln} and station density are mapped in Figure 13.

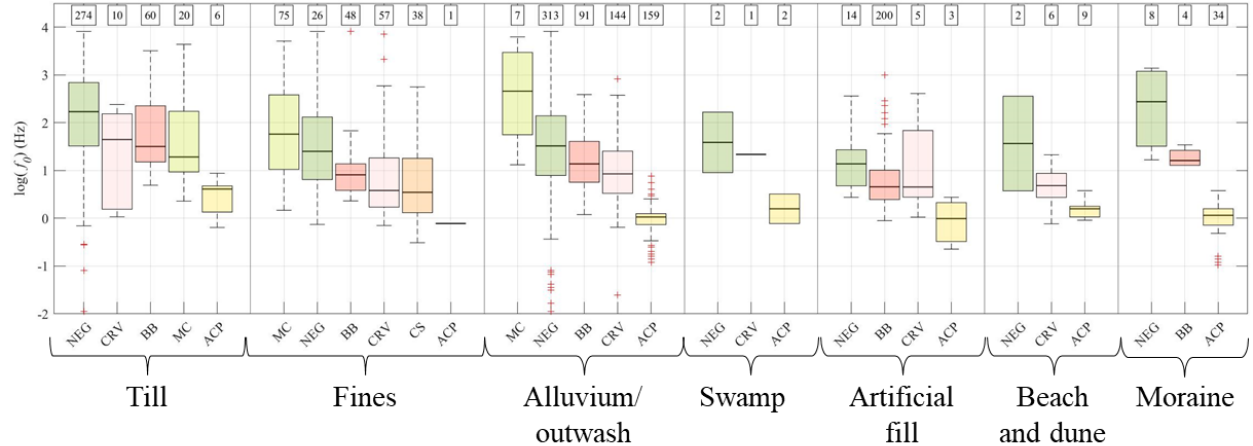


Figure 10. Box and whisker plots of the f_0 distributions of each subregion grouped by surficial geologic unit. This figure allows a comparison across the same geology between different subregions, (e.g. a Maine coast fine and a Boston Basin fine sediment). Boxes are color-coded by subregion and the number of stations in each unit is plotted above each box and whisker plot.

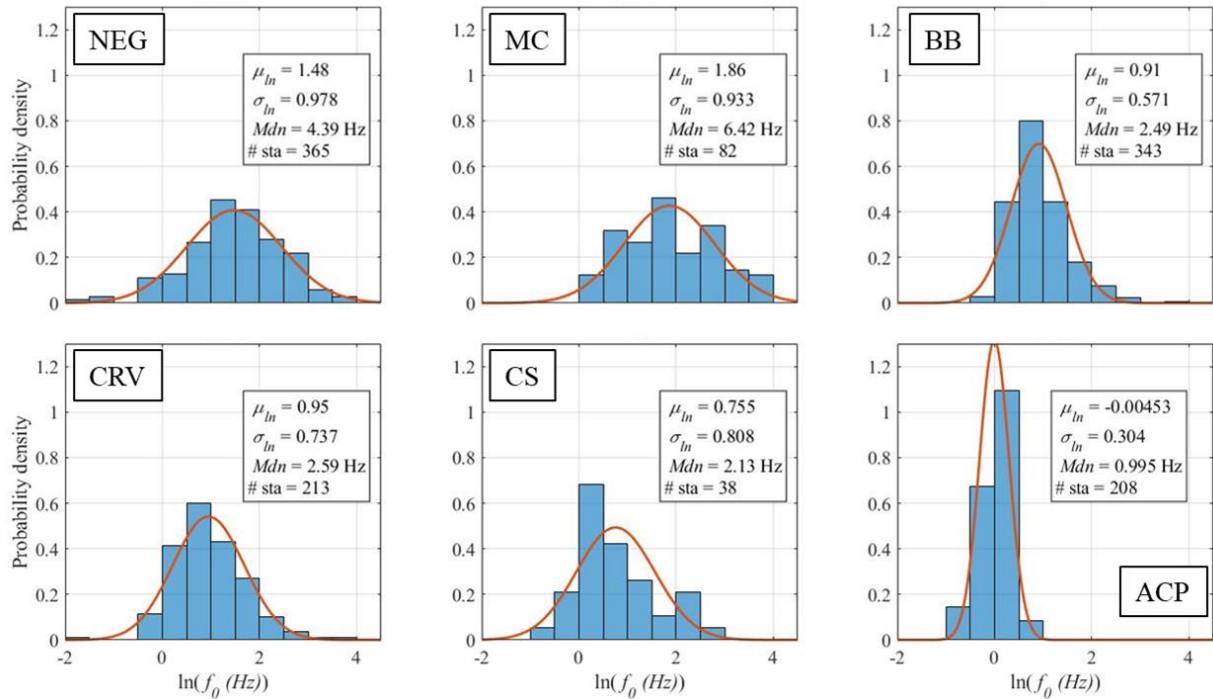


Figure 11. Soft geology distributions for each subregion developed to be used when little or no data is available to develop an f_0 distribution within a grouping. μ_{ln} , σ_{ln} , Mdn and the number of f_0 stations in the distribution are indicated on the plot.

The central tendencies of each of the f_0 distributions across the region reveal several important characteristics of site response in New England. First, the New England General till covers most of the map and has an $f_0 \mu_{ln}$ of 2.15 and Mdn of 8.6 Hz. This is a higher Mdn value than was found for till in Pontrelli

et al. (2023a) using the Soller (2009) geologic units (6.16 Hz) and is the result of creating the New England General subregion. The Maine Coast geologic units have much higher f_0 values than the other subregions with significant fine deposits. The region soft geology distribution has a Mdn value of 6.42 Hz and the Mdn of the distribution of the fines (the Presumpscot clays) is 6.01 Hz. This is in contrast to the fine proglacial sediment Mdn of 2.7 Hz estimated in Pontrelli et al. (2023a) using the Soller (2009) map. We interpret these results as the Maine Coast region having fine deposits that are generally thinner than the other sedimentary fine deposits, likely due to greater erosion in the unit since the isostatic rebound in the region began in the Holocene. The Boston Basin subregion has a soft geology distribution with a μ_{ln} of 0.91 and an Mdn of 2.49 Hz. The fines and the artificial fill within the subregion have distributions with f_0 μ_{ln} of 0.98 (Mdn = 2.66 Hz) and 0.75 (Mdn = 2.12 Hz) respectively. In addition to these two geologic deposits in the Boston Basin, the alluvium/outwash deposits that make up the Charles River and Mystic River basins also have low f_0 values, though with a higher f_0 μ_{ln} than those of the fine and artificial fill deposits with a μ_{ln} of 1.21 (Mdn = 3.36 Hz). Some stations in this unit are in the deeper parts of the basin (with lower f_0 values) and some are in alluvium/outwash deposits closer to the uplands where the basin pinches out (with higher f_0 values). The Connecticut River Valley has some variability between the geologies within the subregion, namely CRV fines have a μ_{ln} of 0.85 (Mdn = 2.33 Hz) and CRV alluvial sediments have a μ_{ln} of 1.0 (Mdn = 2.71 Hz) but in general, the unit is consistently low frequency with the subregion units having an overall Mdn value of 2.59 Hz. The Champlain Sea sediment fines make up most of the Champlain Sea subregion and have a μ_{ln} of 0.76 and an Mdn of 2.13 Hz. These sediments are deposited in large flat expanses adjacent to the Lake Champlain. Finally, the lowest f_0 values of a subregion in the study are in the Atlantic Coastal plain with f_0 μ_{ln} = 0 and Mdn = 1 Hz regardless of the geology and with low variability (μ_{ln} = 0.3) indicating little lateral change in f_0 across the subregion.

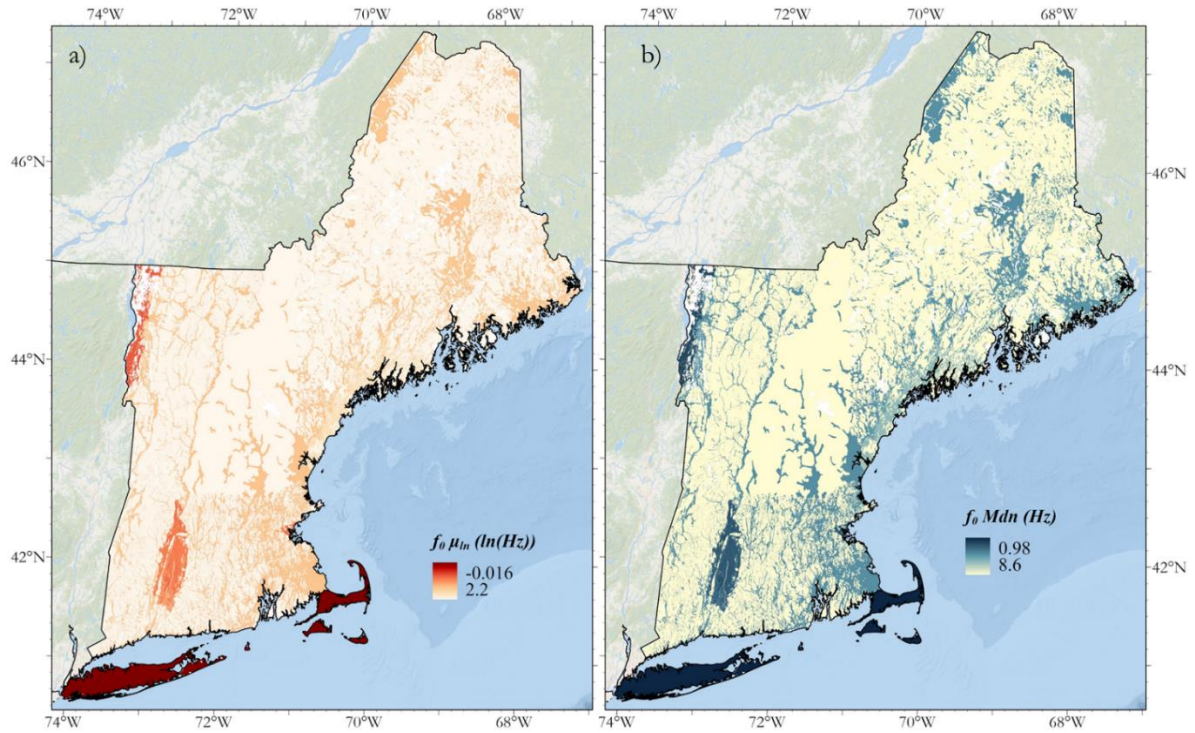


Figure 12. a) $f_0 \mu_{ln}$ map. b) $f_0 Mdn$ map

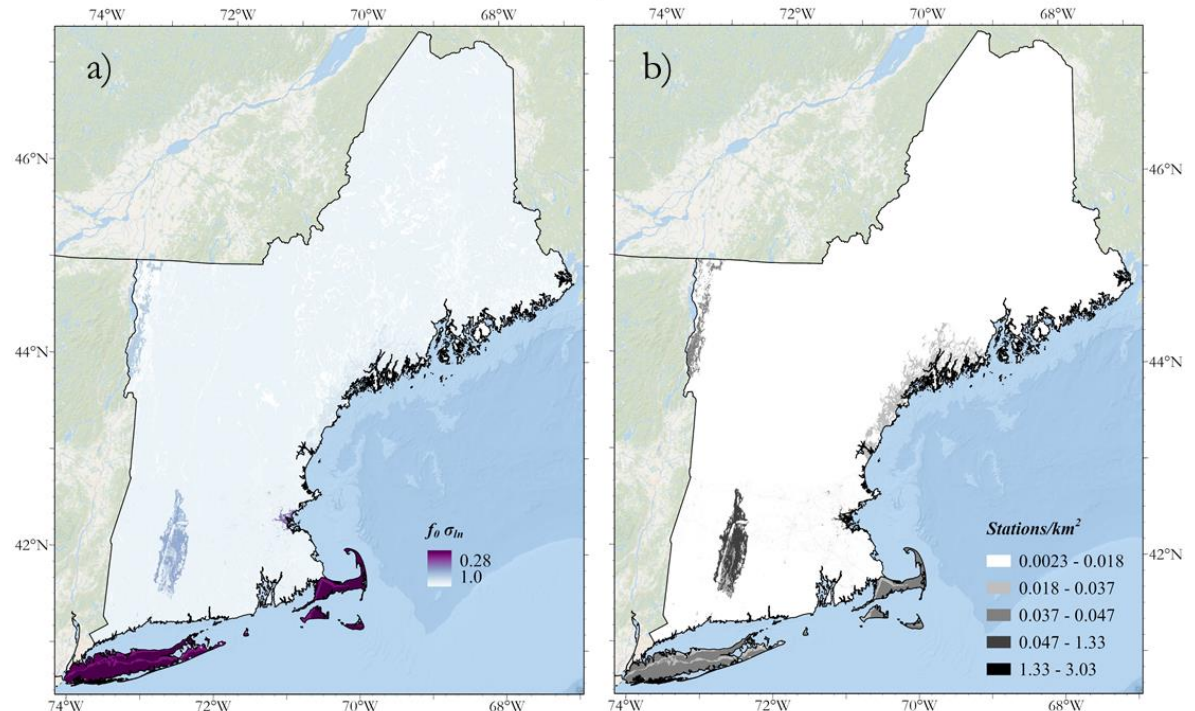


Figure 13. a) $f_0 \sigma_{ln}$ map. b) Map of the density of stations computed by dividing the number of stations in a unit by the area of the unit.

4.2 Vs_{avg} μ_{ln} and σ_{ln} and Mdn maps

The Vs_{avg} map closely corresponds to the surficial geology in the region. The lowest Vs_{avg} regions (“fines”, $\mu_{ln} = 5.3$, $Mdn = 200$ m/s) are within the areas with large fines deposits. These deposits are in the northwest in the Champlain Sea, in the northeast on the Maine Coast, in eastern Massachusetts in the Boston Basin, and in central Massachusetts and Connecticut in the Connecticut River Valley. Beach and dune deposits and swamp deposits ($\mu_{ln} = 5.39$, $Mdn = 220$ m/s) are found in small pockets around the region. Artificial fill ($\mu_{ln} = 5.39$, $Mdn = 220$ m/s) is also found in small pockets around the region, though most of it is deposited in the Boston Basin where it poses significant site response hazard. Both alluvium/outwash deposits and moraine deposits are classified by distributions with a $\mu_{ln} = 5.52$, $Mdn = 250$ m/s. Cape Cod and Long Island (the Atlantic Coastal Plain subregion) are almost entirely composed of these deposits. Alluvium/outwash deposits also compose the Connecticut River Valley flood plain and the smaller alluvial valleys in the state. Moraine deposits are less prominent outside of the Atlantic Coastal Plain, although they are mapped sporadically across the region. Finally, till deposits ($\mu_{ln} = 5.99$, $Mdn = 400$ m/s), are mapped throughout most of the region in uplands, primarily in the New England general subregion (Figure 14).

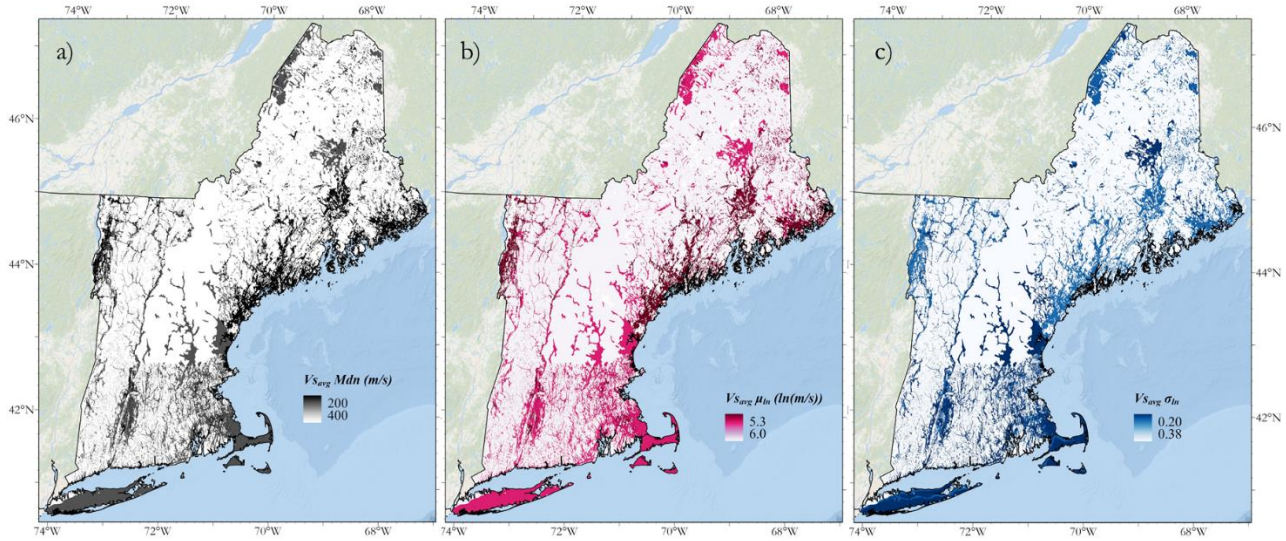


Figure 14. a) Vs_{avg} Mdn map. b) Vs_{avg} μ_{ln} map. c) Vs_{avg} σ_{ln} map.

4.3 $Vs30$ μ_{ln} and σ_{ln} and Mdn maps

Table 4 summarizes the distributional properties for $Vs30$ that result from propagating f_0 and Vs_{avg} distributions through the layer-over-halfspace model and the assumption of one-dimensional propagation of vertical SH-waves through horizontally layered media for the 39 surficial geologic units in New England (Table 4). In the New England General subregion, the till unit, which makes up most of the map, has an f_0 μ_{ln} of 2.15 ($Mdn = 8.6$ Hz) corresponding to a $Vs30$ μ_{ln} of 6.71 ($Mdn = 820$ m/s). Though most of the Maine Coast subregion is mapped as “fines” which are the Presumpscot Formation, the f_0 distribution of these fines has much higher values yielding a $Vs30$ $\mu_{ln} = 6.36$, $Mdn = 580$ m/s. In the Boston Basin the units typically have relatively low f_0 values. These yield $Vs30$ estimates slightly higher than the average velocities of the geologies in the basin (artificial fill $Vs30$ $\mu_{ln} = 5.66$, $Mdn = 286$ m/s, fines $Vs30$ $\mu_{ln} = 5.78$, $Mdn = 323$ m/s). Where the basin depth decreases at the edges, these $Vs30$ values decrease, but in most of the area of the basin, profiles are deep enough that $Vs30$ Mdn values corresponding to NEHRP site class D sites with f_0 Mdn values are between 2 and 3 Hz. The Connecticut River Valley has very similar properties to the Boston Basin with f_0 values slightly higher than for the Boston Basin, yielding a fine $Vs30$ with $\mu_{ln} = 5.76$, $Mdn = 318$ m/s and an alluvium/outwash $Vs30$ distribution with $\mu_{ln} = 5.89$, $Mdn = 361$ m/s. In the Champlain Sea subregion, the majority of the subregion is mapped as fines which are the Champlain Sea sediments, which have similar f_0 values to the fines Boston Basin and Connecticut River Valley yielding $Vs30$ values with $\mu_{ln} = 5.70$, $Mdn = 299$ m/s. Finally, the lowest f_0 values of a subregion in the study are in the Atlantic Coastal plain. With surficial geologies with Vs_{avg} values with μ_{ln} values of 5.39 ($Mdn = 220$ m/s) or 5.52 ($Mdn = 250$ m/s), this translates to $Vs30$ μ_{ln} values of approximately 5.39 ($Mdn = 220$ m/s) or 5.52 ($Mdn = 250$ m/s). These $Vs30$ μ_{ln} values are equal to the Vs_{avg} μ_{ln} values because the Atlantic Coastal Plain units are greater than 30 meters thick, and thus the $Vs30$ distributions are approximately equal to the Vs_{avg} distributions.

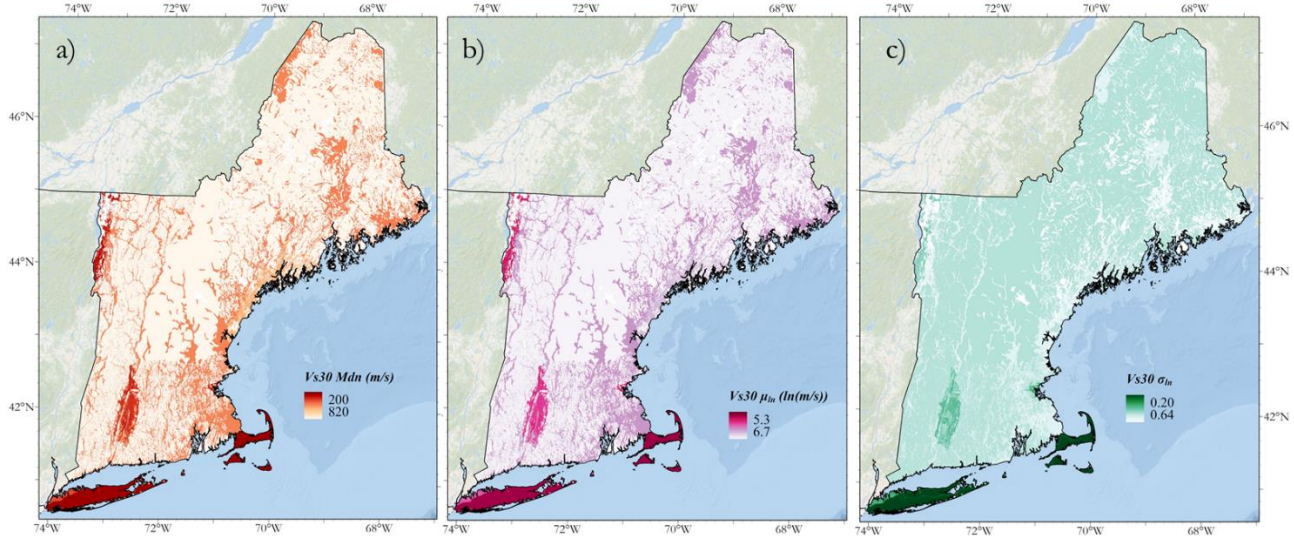


Figure 15. a) Regional map of Mdn $Vs30$ computed by propagating each f_0 and Vs_{avg} distribution of each grouping through the layer-over-halfspace model. b) The corresponding $Vs30 \mu_{ln}$ map. c) The corresponding $Vs30 \sigma_{ln}$ map.

Table 4. Final output table with the means, standard deviations, and medians for each subregion/geologic grouping for f_0 , Vs_{avg} and $Vs30$.

* indicates where a soft geology (Figure 11) distribution was used.

† indicates where the New England General till (Figure 7b) distribution was used.

Subregion	Geology	# stations	$f_0 \mu_{ln}$	$f_0 \sigma_{ln}$	$f_0 Mdn (Hz)$	Vs_{avg}	Vs_{avg}	$Vs_{avg} Mdn$	$Vs30$	$Vs30$	$Vs30 Mdn$
						μ_{ln}	σ_{ln}	(m/s)	μ_{ln}	σ_{ln}	(m/s)
MC	al	82*	1.86	0.93	6.42	5.52	0.20	250	6.43	0.59	620.07
MC	bd	82*	1.86	0.93	6.42	5.39	0.23	220	6.41	0.60	606.85
MC	f	75	1.79	0.90	6.01	5.30	0.24	200	6.36	0.60	579.98
MC	m	82*	1.86	0.93	6.42	5.52	0.23	250	6.44	0.57	624.94
MC	s	82*	1.86	0.93	6.42	5.39	0.23	220	6.43	0.60	617.70
MC	t	274†	2.15	0.97	8.60	5.99	0.38	400	6.71	0.51	822.36
NEG	t	274	2.15	0.97	8.60	5.99	0.38	400	6.71	0.51	820.52
NEG	af	14	1.26	0.65	3.54	5.39	0.22	220	6.01	0.45	405.72
NEG	al	313	1.46	0.99	4.32	5.52	0.20	250	6.20	0.58	494.59

NEG	bd	365*	1.48	0.98	4.39	5.39	0.23	220	6.17	0.60	478.60
NEG	f	26	1.52	1.01	4.58	5.30	0.24	200	6.19	0.64	485.60
NEG	m	365*	1.48	0.98	4.39	5.52	0.23	250	6.22	0.58	500.67
NEG	s	365*	1.48	0.98	4.39	5.39	0.23	220	6.19	0.61	486.33
CS	f	38	0.76	0.81	2.13	5.30	0.24	200	5.70	0.47	299.96
CS	m	38*	0.76	0.81	2.13	5.52	0.23	250	5.82	0.42	335.69
CS	s	38*	0.76	0.81	2.13	5.39	0.23	220	5.75	0.44	313.80
CS	bd	38*	0.76	0.81	2.13	5.39	0.23	220	5.74	0.45	311.86
CS	al	38*	0.76	0.81	2.13	5.52	0.20	250	5.81	0.40	334.29
CS	t	274 ^r	2.15	0.97	8.60	5.99	0.38	400	6.71	0.51	816.69
BB	t	60	1.75	0.71	5.78	5.99	0.38	400	6.50	0.42	665.28
BB	af	200	0.75	0.50	2.12	5.39	0.22	220	5.66	0.31	286.82
BB	al	91	1.21	0.58	3.36	5.52	0.20	250	5.99	0.39	398.09
BB	bd	343*	0.91	0.57	2.49	5.39	0.23	220	5.76	0.38	318.87
BB	f	48	0.98	0.59	2.66	5.30	0.24	200	5.78	0.41	323.37
BB	m	343*	0.91	0.57	2.49	5.52	0.23	250	5.82	0.35	336.16
BB	s	343*	0.91	0.57	2.49	5.39	0.23	220	5.76	0.37	318.73
CRV	f	57	0.85	0.83	2.33	5.30	0.24	200	5.76	0.50	318.48
CRV	s	213*	0.95	0.74	2.59	5.39	0.23	220	5.82	0.45	338.58
CRV	bd	213*	0.95	0.74	2.59	5.39	0.23	220	5.82	0.44	337.43
CRV	af	213*	0.95	0.74	2.59	5.39	0.22	220	5.82	0.45	338.35
CRV	al	144	1.00	0.70	2.71	5.52	0.20	250	5.89	0.41	361.18
CRV	t	10	1.29	0.96	3.63	5.99	0.38	400	6.33	0.47	562.96
ACP	t	214	0.01	0.32	1.01	5.99	0.38	400	5.99	0.37	400.99
ACP	al	159	-0.02	0.28	0.98	5.52	0.20	250	5.52	0.20	249.81
ACP	bd	208*	0.00	0.30	1.00	5.39	0.23	220	5.40	0.22	220.84

ACP	af	208*	0.00	0.30	1.00	5.39	0.22	220	5.39	0.21	220.27
ACP	f	208*	0.00	0.30	1.00	5.30	0.24	200	5.31	0.23	203.30
ACP	m	34	-0.01	0.39	0.99	5.52	0.23	250	5.53	0.23	251.05
ACP	s	208*	0.00	0.30	1.00	5.39	0.23	220	5.40	0.22	220.51

5.0 Discussion

In general, low f_0 measurements in a subregion are an indicator of a deep, resonant site with a high impedance contrast between sediments and bedrock. Using the f_0 maps developed in this study, there are some key interpretations that can be drawn about the behavior of major sediment deposits in the New England region. First, the New England General subregion tends to have high f_0 values indicative of shallow, higher shear-wave velocity deposits. Though some small areas of sediments with low f_0 values exist in this subregion, they are less significant than the larger deposits in other subregions. Second, the Maine Coast, though mapped as predominantly fine deposits, has f_0 distributions with high f_0 values, demonstrating that these fine deposits tend to be shallower and/or lower velocity than those mapped in other subregions, in particular, the Boston Basin, Connecticut River Valley and Champlain Sea. Third, the Boston Basin is a deep sedimentary basin composed of mainly artificial fill, fine and alluvium/outwash deposits, all of which have relatively low f_0 values corresponding to mostly site class D and E sediments. The f_0 values increase at the basin edge, but the majority of the area of the Basin have low f_0 values. Fourth, the Connecticut River Valley has similar f_0 values to the Boston Basin, though is composed of mainly alluvium/outwash and fine deposits. Like the Boston Basin, it has some higher f_0 values at the basin edge. Fifth, the Champlain Sea subregion is predominantly mapped as fine deposits and has low f_0 values, slightly lower than those of the Boston Basin and Connecticut River valley indicating that the unit is either deeper on average or lower velocity on average than these other two subregions. Finally, the Atlantic Coastal Plain has units that have the lowest f_0 values of any of the corresponding units in the other subregions. This is because the subregion has little f_0 variability and is consistently much deeper than the other subregions.

A simple framework for conceptualizing site classification in high impedance environments is to use two axes: a frequency axis and a stiffness axis. The frequency axis uses f_0 measurements which are proportional to the depth to the impedance contrast, and the stiffness axis uses shear-wave velocity estimates, which are measurements of stiffness and are correlated to mechanical properties of the overburden sediments. Incorporating the importance of depth-to-the impedance contrast is something that $Vs30$ does not do – $Vs30$ is a parameter that is computed using measured values above a predetermined depth of 30 meters. It is a proxy for the average stiffness of that 30-meter profile and can thus yield the same results in deep profiles providing no information of frequencies of resonance (Pinilla-Ramos et al. 2022). In a two-axis framework, a stiffness axis provides information of the amplitude of shaking (which is proportional to the impedance at the soil-bedrock interface) and a frequency axis provides information on the frequency of shaking at the surface. In Figure 16, we have plotted the $Mdn\ Vs_{avg}$, and $Mdn\ f_0$ for each geology in each subregion. The Atlantic Coastal Plain cluster has geologies with different Vs_{avg} values corresponding to different amplitudes of shaking (a function of the impedance value at the soil-bedrock interface) at the fundamental frequency but very similar frequencies because the fundamental frequency values are very constant across the subregion (a function of the depth to the impedance contrast). In the Boston Basin, Connecticut River Valley, and Champlain Sea, there is similar variability in amplitude at the fundamental frequency as the geology (and therefore stiffness) changes and variability in the fundamental frequency as the depth of the basins change. These subregion geologies have points with $Mdn\ f_0$ values clustered between 2 and 4 Hz with till values higher – around 4 Hz for Connecticut River Valley, 6 Hz for the Boston Basin and 9 Hz for Champlain Sea. The New England General and Maine Coast have points clustered at higher frequencies indicating they are consistently shallower than these other regions.

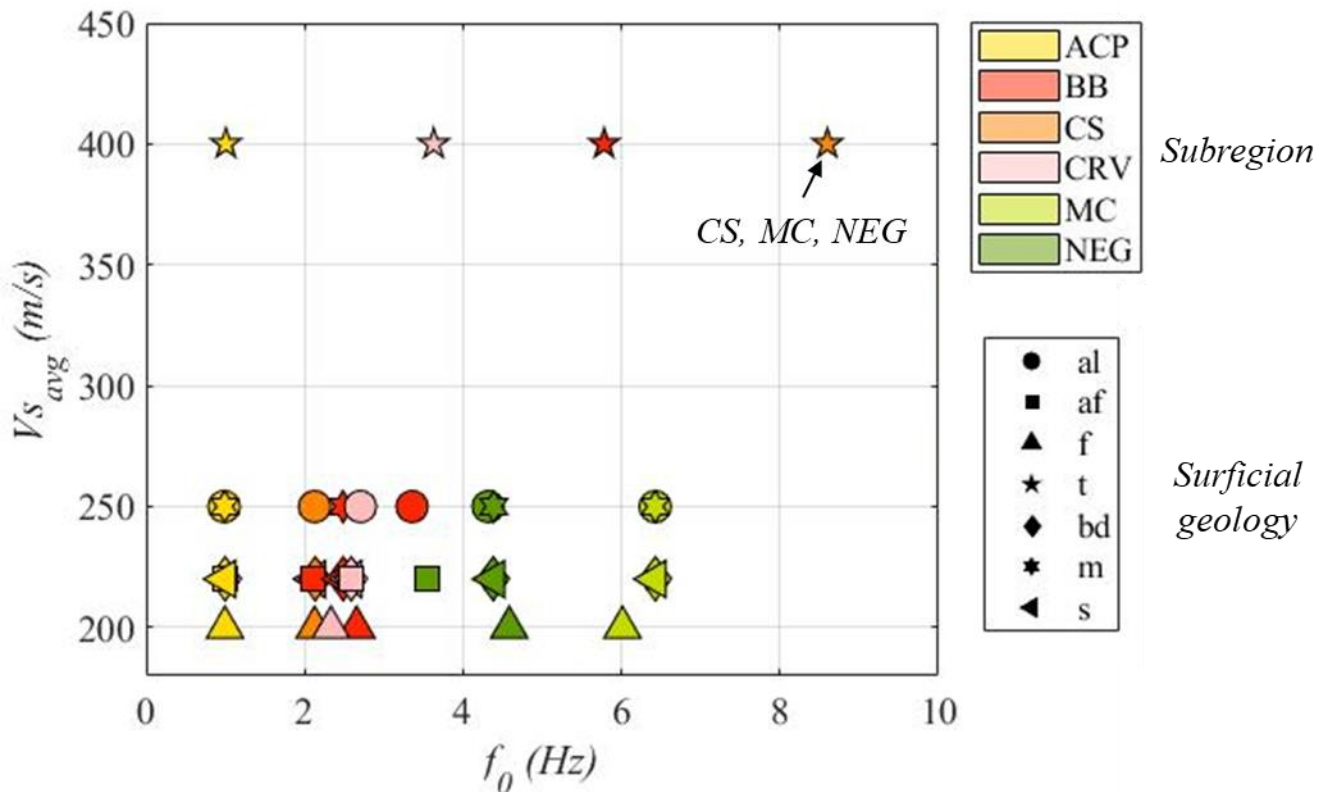


Figure 16. Demonstration of a two-axis approach to conceptualize site classification of high impedance environments. In this plot, the y-axis (the stiffness axis) is composed of $Mdn\ Vs_{avg}$ values of each geology in each subregion. The x-axis (the frequency axis) is composed of $Mdn\ f_0$ values within each of these geologic units of the subregion. The stiffness axis is related to the amplitude of the fundamental frequency and the frequency axis is related to the depth to the impedance contrast. The top right star contains till points for the CS, MC and NEG subregions because each of these units uses the general till distribution.

The site characterization maps developed in this study are an improvement on those made in Pontrelli et al. (2023a) because this study uses higher resolution geologic maps and a subregion grouping layer to create more refined f_0 distributions computed from more local measurements. These improvements result in an 8.7% reduction in the standard deviation of the residuals between the station f_0 value and the μ_{ln} of the f_0 distribution of the geologic unit of that station between the f_0 map of Pontrelli et al. (2023a) and that made in this paper. Most of this residual reduction comes from changes to distributions in subregions with f_0 values that deviate significantly from other regions with the same geologic classification. For example, the Maine Coast, though composed of fine clay deposits like the Boston Basin and the coast of Lake Champlain, has consistently high f_0 values. In this case, grouping by geologic unit is insufficient, since

f_0 values are higher in the Maine Coast fine deposits than other fine sediments in the region. In Figure 17, the Maine coast residual distribution from the Pontrelli et al. (2023a) map is higher than that of the residuals calculated from the f_0 map produced in this study and is biased (it is not centered around 0). The residual between the station $\ln(f_0)$ value and μ_{ln} of the distribution for the Maine Cost in Pontrelli et al. 2023a is 0.67. Using higher resolution geologic maps and only incorporating local data reduces this residual down to -0.05 in this study (Table 5). Additionally, both the Champlain Sea and Boston Basin have f_0 values much lower than the mean of the geologic distributions from Pontrelli et al. (2023a) which are -0.43 and -0.37 respectively (Table 5). By creating distributions using just data within these respective subregions, this mean residual is reduced to 0 in both subregions in this study. In each subregion, this study reduces the mean residual compared to that of Pontrelli et al. (2023a) (Table 5). Treating regions independently from other regions with the same geologic classification regions reduces the residuals between the measured f_0 and the mean of the f_0 distribution of the geologic unit.

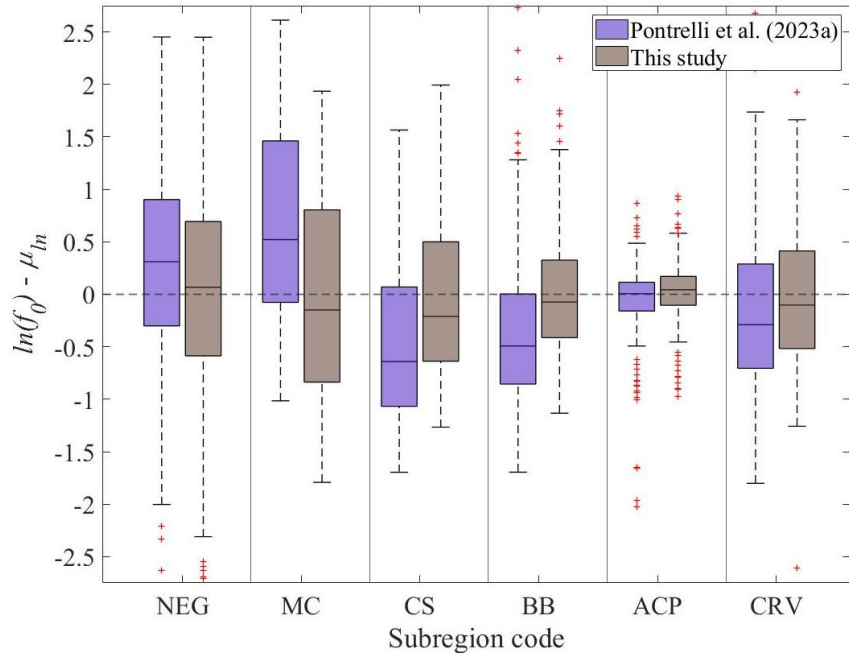


Figure 17. Histogram of the residuals between the station $\ln(f_0)$ value and μ_{ln} of the distribution of the geologic unit for each subregion for Pontrelli et al. 2023a (purple) which uses the Soller (2009) geologic map and no subregion grouping layers and this study (brown) which uses higher resolution geologic maps and a subregion grouping layer. The horizontal dotted line is at 0 where the station f_0 value and the median of the distribution of the unit are equal.

Table 5. Mean residuals between the station $\ln(f_0)$ value and μ_{ln} of the distribution of the geologic unit for each subregion for Pontrelli et al. 2023a and this study.

Subregion	Mean residual (Pontrelli et al. 2023a)	Mean residual (this study)
NEG	0.25	0.01
MC	0.67	-0.05
CS	-0.43	0.00
BB	-0.37	0.00
ACP	-0.06	0.02
CRV	-0.21	0.00

6.0 Conclusion

In this study we develop regional maps of the site characterization parameter f_0 for New England using estimates of mean (μ_{ln}) and standard deviation (σ_{ln}) in geologic units so that central tendency and uncertainty of each unit are characterized. The two key steps in the procedure are 1) developing a surficial geology map that includes high resolution state-level maps and local knowledge of sedimentary deposits and 2) creating a large f_0 dataset for the region. By using a surficial geology map that includes information on surficial geologic unit and local sedimentary deposit subregions, the units can be characterized using local f_0 data from each subregion, rather than aggregating data across all of the region. For example, in the Boston Basin, the f_0 distribution for artificial fill in the basin that we compute in this study is entirely made up of data from within the Boston Basin artificial fill polygon.

By increasing the resolution of the surficial geology maps and including subregions of local sedimentary deposits when developing f_0 distributions, we made an 8.7% reduction in the standard deviation of the residuals between the station f_0 value and the μ_{ln} of the f_0 distribution of the geologic unit of that station from the f_0 map of Pontrelli et al. (2023a). When not subdividing geologic units by local sedimentary deposits, each unit distribution is biased compared to the distribution of the unit subregion f_0 values. By considering only stations within a subregion in developing the f_0 distributions, this bias is reduced (Table 5). The main interpretations from applying this procedure are that 1) the Maine Coast tends to have high f_0

values compared to other large fine deposits, 2) the Atlantic Coastal Plain has low f_0 values and little variability regardless of the unit and 3) The Boston Basin, Connecticut River Valley and Champlain Sea have relatively low f_0 values with some higher values where the basin pinches out, increasing the variability of the unit f_0 distributions within each subregion.

In addition, we use the layer-over-halfspace model and the assumption of one-dimensional vertical propagation of SH-waves through horizontally layered media as a framework for developing estimates of $Vs30$ from f_0 and Vs_{avg} distributions by surficial geologic unit. We then create regional maps of f_0 , Vs_{avg} and $Vs30$ μ_{ln} and σ_{ln} . The layer-over-halfspace model uses f_0 measurements which are ideal to use in a high impedance environment like New England and for which there is a larger, better spatially distributed dataset than there is for shear-wave velocity measurements. The layer-over-halfspace model also uses estimates of average overburden velocity, Vs_{avg} , for which there are 40 measurements in the region, and which is expected to laterally vary less than f_0 . We use the estimated distributions of f_0 and Vs_{avg} to Monte Carlo sample 10,000 profiles in each geologic unit to compute estimate distributions of the common site amplification proxy $Vs30$. This Monte Carlo sampling provides more robust characterization of the uncertainty of $Vs30$ distribution estimates when computed from f_0 and Vs_{avg} .

Regional site characterization maps are important for understanding site response characteristics in major soil units. They can be used to guide city or site scale analyses and can be used as inputs into risk or hazard analyses that require a site response input layer. In this study, driven by the unique high impedance New England geologic environment, we provide maps of f_0 as a site characterization parameter for site response analysis, seismic hazard analyses, and use in Ground Motion Models.

Data Availability

All data used in this paper came from published sources listed in the references. Please see the supplementary material for links to the specific sites for data download, and descriptions of the supplementary data provided for this study. A table of f_0 data is provided with information about each station's geology and subregion that can be used to recreate Figures 4a (the f_0 station locations), 6b, 7, 10, 11, and all of Table 4. A shapefile with the f_0 distribution statistics is provided that can be used to recreate Figures 1b, 2a, 3e, 6a, 12, 13, 14, and 15, the attribute table of which can be used to recreate Figure 16.

Acknowledgements

This research was funded by USGS awards #G20AP00040 and #G20AP00041. The first author was also funded internally by the Edgerton Fellowship at Tufts University, for which he is grateful.

Chapter 4

Maps of distributional parameters of f_0 for Massachusetts, USA derived
from a high-resolution continuous depth-to-bedrock map

Abstract

Site characterization maps are essential for regional planning and seismic hazard analyses and are most often represented in terms of $Vs30$ or $Vs30$ -based National Earthquake Hazards Reduction Program (NEHRP) site classifications. Recent trends in engineering seismology indicate that site fundamental frequency (f_0) may be an additional (or alternative) site characterization parameter for seismic site response. In this work, we present high-resolution regional site characterization maps in terms of f_0 for Massachusetts, USA, using the state 100-m resolution depth-to-bedrock (z) map, a database of 1342 Horizontal-to-Vertical Spectral Ratio (HVSR) f_0 measurements, the state 1:24,000-scale surficial geologic map, and a regional sediment deposit classification map. The depth-to-bedrock map characterizes uncertainty by providing mean and standard deviation estimates for z . To characterize sediment velocities, we use the 1342 f_0 measurements and their corresponding z values sampled from the depth-to-bedrock map and model them by linearizing the power law relationship $f_0 = \alpha z^\beta$ and using linear regression to estimate the α and β coefficients. The α and β coefficients are estimated in the four major geologic groupings and the four local deposits in the state and define shear-wave velocity power laws for each classification. The uncertainty of the α coefficient (σ_{resid}) is also computed and used to represent the shear-wave velocity uncertainty which is propagated into the final f_0 distribution prediction. The mean and standard deviation values at each pixel of the depth-to-bedrock map are Monte Carlo sampled 1000 times creating a depth distribution which combined with the power law velocity model allows for the computation of distributions of f_0 at each 100m pixel in the state and their mean, μ_{ln} and standard deviation, σ_{ln} . Because f_0 is a parameter that describes sediment resonance, f_0 values are masked when depth-to-bedrock is shallow as these thin sediment over bedrock areas do not lead to significant resonance or sediment amplification at relevant frequencies of engineering interest. This procedure yields estimates of f_0 distributions that incorporate depth-to-bedrock uncertainty and shear-wave velocity uncertainty at locations where sediment resonance is important. Using spatially discontinuous f_0 data, paired with continuous depth-of-bedrock, surficial geology, and local sedimentary deposit information yields site characterization maps for Massachusetts that characterize site

response using the entire overburden profile, not just the top 30 meters. This approach is an advantageous framework, particularly in high impedance environments where resonance is the dominant characteristic and is strongly controlled by depth-to-bedrock. The resulting map provides continuous estimates of f_0 and can be used to derive continuous maps of $Vs30$.

Keywords: Site response; seismic site characterization maps; fundamental site frequency; uncertainty propagation; seismic hazard

1.0 Introduction

Seismic site response has historically been estimated using the $Vs30$ site parameter which is the time-averaged shear-wave velocity over the top 30 meters of the geotechnical profile (Borcherdt, 1994). $Vs30$ is typically used in Ground Motion Models (GMMS) as a site term (Chiou and Youngs, 2008; Zalachoris and Rathje, 2019; Wong et al. 2022), used in engineering design codes to define short and long period amplification (F_a and F_v), and serves as a common proxy for sediment stiffness in a wide range of geospatial models for secondary earthquake effects like liquefaction (Rashidian and Baise, 2020; Zhu et al. 2017; Zhu et al. 2015) and landslides (Sur et al. 2022). As a result of its widespread use, researchers have developed regional and global maps of $Vs30$ to be used as inputs to a variety of tools like geospatial models, GMMS, ShakeMap and HAZUS (Wills and Clahan, 2006; Yong, 2016; Wald and Allen, 2007; Foster, 2019; Thompson et al. 2014; Parker et al. 2017; Mori et al. 2020b; Stewart et al. 2014; Heath et al. 2020). $Vs30$ is a useful measurement and due to the widely used slope-based $Vs30$ map developed by Wald and Allen (2007) is broadly available. Unfortunately, $Vs30$ has two important limitations: 1) it does not incorporate information from layers deeper than 30 meters and 2) using $Vs30$ to assign site classes ignores the frequency of maximum site amplification of the sediment transfer function and therefore performs poorly for highly resonant sediments.

Several studies have incorporated f_0 (fundamental site frequency) as an alternate or additional site characterization term into GMMS and have discussed the value of the f_0 parameter in prediction of ground

motion parameters. Chao et al. (2020) show that including HVSR curves into GMMs significantly reduces the standard deviation of station residuals, in some cases up to 90% for a dataset in Taiwan. Kwak and Seyhan (2020) develop a site amplification model that first develops a relationship between total site effects and $Vs30$ and then fits the residuals based on the site fundamental frequency. The paper shows that including f_0 further reduces site term error from the initial reduction resulting from the use of $Vs30$. Kwak et al. (2017) use f_0 to supplement ergodic site amplification equations to account for frequency-specific amplifications in profiles with high impedance contrasts. Ghofrani and Atkinson (2014) compare the effectiveness of f_0 and the amplitude at f_0 to the effectiveness of $Vs30$ as parameters to describe site response. They conclude that f_0 contains as much information as $Vs30$, works better than $Vs30$ for deep soil sites, is directly related to the depth to the impedance contrast and in general has significant advantages over $Vs30$ as a site parameter. Pinilla-Ramos et al. (2022) show how f_0 is highly correlated to site amplification at short periods. They use f_0 in the ASK14 GMM (Abrahamson et al. 2014) as a substitute for $Vs30$ which reduces median spectral acceleration factors by 0.6-1.6 for periods between 0.5 and 4 s. Hassani and Atkinson (2016) use f_0 as a proxy for $Vs30$ in the NGA-east GMM reducing prediction variability. These studies show that f_0 provides useful site information that $Vs30$ in isolation cannot provide and thus that f_0 is worthy of study and development as a site characterization parameter for site response and ground motion studies in the earthquake engineering community.

A methodology for the inexpensive measurement of fundamental frequency (f_0) was proposed in Nakamura (1989) using the Horizontal-to-Vertical Spectral Ratio (HVSR) technique making its measurement available to the field of earthquake engineering. Under the Nakamura (1989) formulation, the fundamental peak of the HVSR curve is empirically similar to the fundamental peak of a soil transfer function which represents the amplitude difference at each frequency of free surface shaking to bedrock shaking of vertically propagating shear-waves through horizontally stratified media (Lermo and Chávez-García, 1993). The HVSR curve fundamental peak has been shown to be empirically similar to the fundamental peak of a soil transfer function and can therefore be related to velocity through wave

propagation. The quarter wave-length equation is commonly used to relate f_0 , overburden shear-wave velocity (V_s) and depth to the impedance contrast (z) ($f_0 = V_s/4z$; Thomson, 1950; Haskell, 1953 and 1960; Kramer, 1996). This relationship allows for the estimate of any one variable given the other two in the equation. f_0 is more generally a function of the shear-wave velocity profile and the depth to the impedance contrast allowing for its relationship to be computed using more complex shear-wave velocity profiles.

Ibs-von Seht and Wohlenberg (1999) formalizes an alternate technique for relating f_0 to z by assuming a power law depth dependent shear-wave velocity profile with two coefficients that can be fit to a plot of f_0 vs. z . This technique is a physically realistic model where the shear-wave velocity profile is characterized by power law coefficients (Delgado, 2000). The technique has been used in the literature to map depth-to-bedrock values from a large database of f_0 measurements with some paired z measurements (Parolai, 2002). In this study, we use a dense set of measured f_0 values and their corresponding z values from the depth-to-bedrock map to establish velocity power laws in terms of power law coefficients (α and β).

f_0 is particularly valuable as a site characterization parameter in regions where the overburden-bedrock interface results in a strong impedance contrast. In this case, the site response is strongly resonant, resulting in strong amplifications over narrow frequency bands. These conditions are common to glaciated terrain such as found in New England (Baise et al, 2016; Pontrelli et al. 2023a), Canada (Motazedian et al. 2020; Motazedian et al. 2010; Assaf et al. 2022) and Alaska (Thornley et al. 2021). Others have developed microzonation maps for cities such as Boston, Montreal, and Vancouver as well as regional geology-based maps (Pontrelli et al., 2023a). The state of Massachusetts presents a unique opportunity to develop a state-scale high-resolution site characterization map based on a newly published high resolution (100 m) depth-to-bedrock map derived from 71,890 borings, 1342 f_0 measurements, 1506 other geophysical measurements, and 602,777 depth estimates from geology and topography relationships in the state (mabee et al. 2023). Using spatially discontinuous measurements of f_0 , paired with continuous data on depth-to-

bedrock, surficial geology, and local sedimentary deposits, we develop high resolution site characterization maps for Massachusetts that characterize site response using the entire overburden profile, not just the top 30 meters and provide estimates of f_0 .

In this study, the depth-to-bedrock map (Mabee et al. 2023) is paired with 1342 f_0 measurements, a 1:24,000 scale surficial geology map of Massachusetts (Stone et al. 2018), and a map of four major local sedimentary deposits (Pontrelli et al. 2023b). The local sedimentary deposits are identified to differentiate sediment velocities across geologically similar, yet mechanically different sediments. Shear-wave velocity profiles are estimated for four geologic units and four local sedimentary deposits. Shear-wave velocity profiles are estimated assuming a power law velocity relation with depth and $f_0 - z$ data pairs at locations where measured f_0 values exist. For each geologic unit or sedimentary deposit, a shear-wave velocity profile is estimated as a power law with uncertainty represented by the uncertainty of the α coefficient. The power law coefficients are calculated using linear regression which allows for the estimate of a prediction interval for overburden velocity at a given depth. The depth-to-bedrock model also includes uncertainty at each pixel which is used to represent depth as a distribution at each pixel. Using distributions of depth and shear-wave velocity at each pixel, we use a Monte Carlo approach to sample 1000 f_0 values at each of the 1000 sampled depth values. This sampling yields an f_0 distribution of 1,000,000 samples from which the mean (μ_{ln}) and standard deviation (σ_{ln}) and median (Mdn) at each pixel in the depth-to-bedrock model are estimated. Finally, since much of the Massachusetts overburden is shallow (45% of the map area is less than 4m depth) resulting in high f_0 values that are not observed in the data, a frequency threshold is selected above which the map is masked. This threshold is selected as the point at which the median of the computed $Vs30$ distribution at the pixel transitions from site class C to site class B (above 760 m/s).

2.0 Data

Four datasets are used to develop the f_0 map in this study: a depth-to-bedrock map, a surficial geologic map, a map of major local sedimentary deposit subregions, and an f_0 dataset. As sources of datasets, this study uses the Massachusetts depth-to-bedrock map of Mabee et al. (2023), the state surficial geologic map of Stone et al. (2018), the subregion map of Pontrelli et al. (2023b), and the f_0 dataset compiled in Pontrelli et al. (2023a) subset to the state of Massachusetts.

2.1 Depth-to-bedrock map

The depth-to-bedrock map of Mabee et al. (2023) (Figure 2) was developed from a database of 663,671 depth-to-bedrock measurements composed of boring logs, HVSR measurements, seismic refraction surveys, and shallow depth-to-bedrock points derived from topography and geologic classifications (Figure 1) that were interpolated using ordinary Kriging and then modified using geologic mapping principals. The purpose of the model is to constrain depth-to-bedrock estimates in unknown areas in the state based on the interpolation of a large database of known depth-to-bedrock measurements with the goal of reducing uncertainty in highway projects, especially during the design and planning phases. The Mabee et al. (2023) study involved the careful compilation of all depth-to-bedrock measurements in the state, the assignment of uncertainty to those measurements, the interpolation between data points using ordinary Kriging, and the rigorous interpretation of the interpolation to identify and rectify errors and modeling artifacts. The process yielded a depth-to-bedrock prediction raster (Figure 2a) and an uncertainty raster (Figure 2b) both at 100m resolution. The uncertainty raster includes both the data uncertainty and the modeling uncertainty of the Kriging procedure. The prediction raster is interpreted in this study as the mean of a lognormal distribution of possible depth values at each pixel. The uncertainty raster is interpreted in this study as the standard deviation of the lognormal depth distribution.

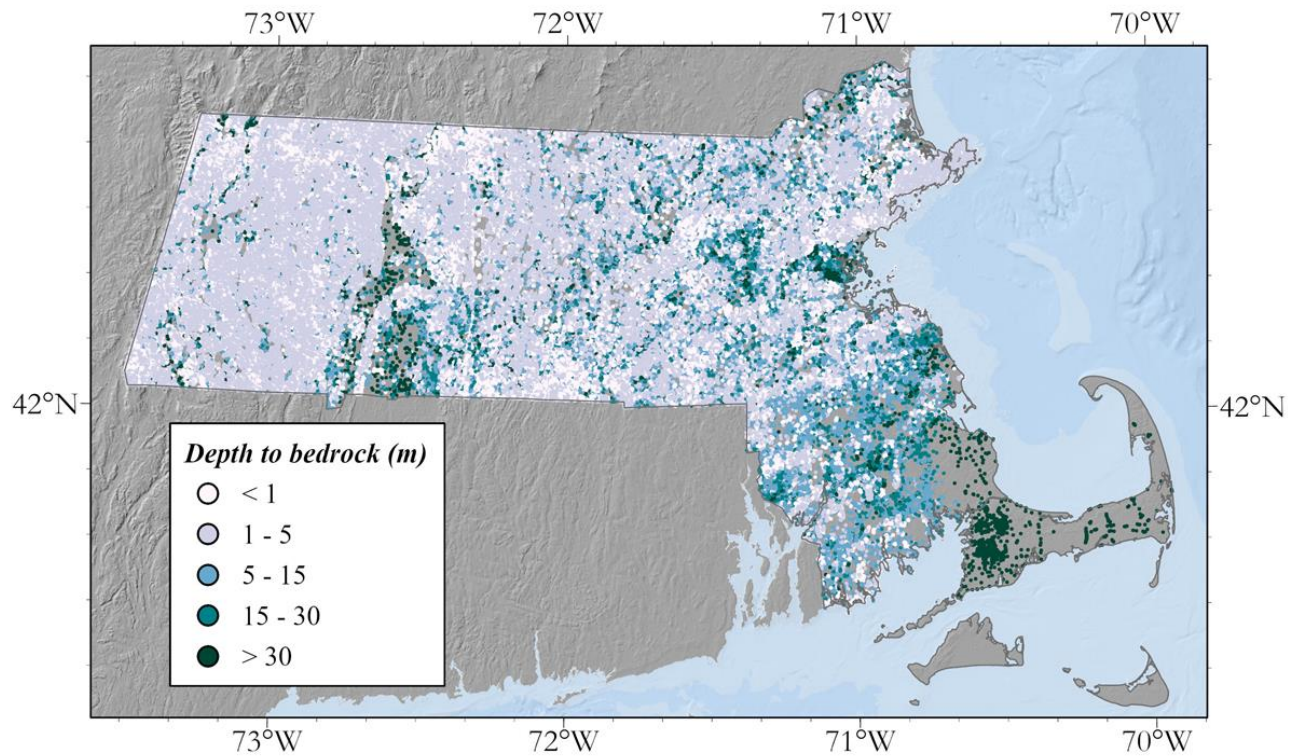


Figure 1. Depth-to-bedrock data used in Mabee et al. (2023) to create the interpolated depth-to-bedrock map used in this study. Much of this data (602,777 points) are shallow depth estimates in upland tills that were created in Mabee et al. (2023). These are very dense which gives the appearance of a continuous surface, but this map is entirely composed of point data.

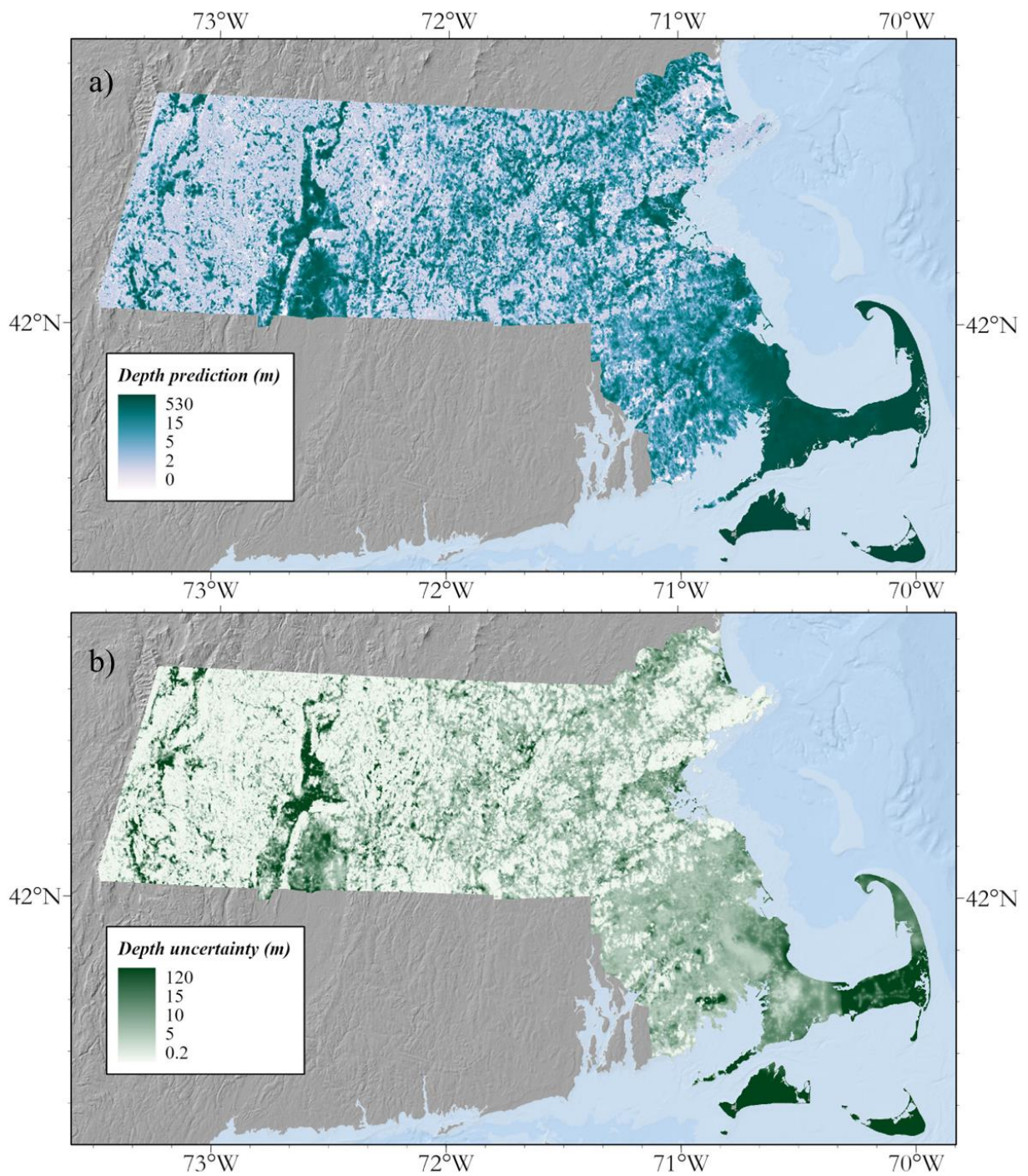


Figure 2. a) Massachusetts depth-to-bedrock map of Mabee et al. (2023) used as the mean depth-to-bedrock in this study. b) Depth-to-bedrock uncertainty used as the standard deviation of the distribution of possible depths at each pixel.

2.2 Surficial geologic map

The Massachusetts state surficial geologic map (Stone et al. 2018) is 1:24,000-scale and developed from the 189 7.5-minute quadrangles in Massachusetts. The unconsolidated surficial units are classified by grain-size, geomorphic features, stratigraphic relationships, and age. The map contains 23 units (Figure 3a). Since this study models the geologic overburden using power law shear-wave velocity profiles from f_0 and depth-to-bedrock information, it is necessary to group the geologic units into fewer groups, so more data are used for the estimates of α and β of each group. The 23 surficial geologic units are grouped into four groups based on their similar mechanical properties (Table 1; Figure 3b; Steve Mabee, Bill Clement, Chris Duncan, Byron Stone person. commun. 2022). The grouped map is shown in Figure 3b.

Table 1. Surficial geologic groupings of the Massachusetts units into 4 groups of similar mechanical properties. The group names are used in the text to give each grouping a general physical meaning in terms of their approximate shear-wave velocities relative to one another.

Group	Group Name	Units
Group 1	Low velocity	Artificial fill; Cranberry bog deposits; Salt-marsh and estuarine deposits; Swamp deposits
Group 2	Mid-low velocity	Glacial stratified deposits, fine; Glacial stratified deposits, glaciomarine fine
Group 3	Mid-high velocity	Floodplain alluvium; Alluvial-fan deposits; Beach and dune deposits; Inland-dune deposits; Valley-floor fluvial deposits; Stream-terrace deposits; Marine regressive deposits; Glacial stratified deposits, coarse; Stagnant-ice deposits; Talus deposits
Group 4	High velocity	Glacially-modified coastal plain hill deposits; End moraine deposits; Thrust-moraine deposits; Thick valley till and fine deposits; Thin till; Thick till
Bedrock	-	Bedrock outcrops

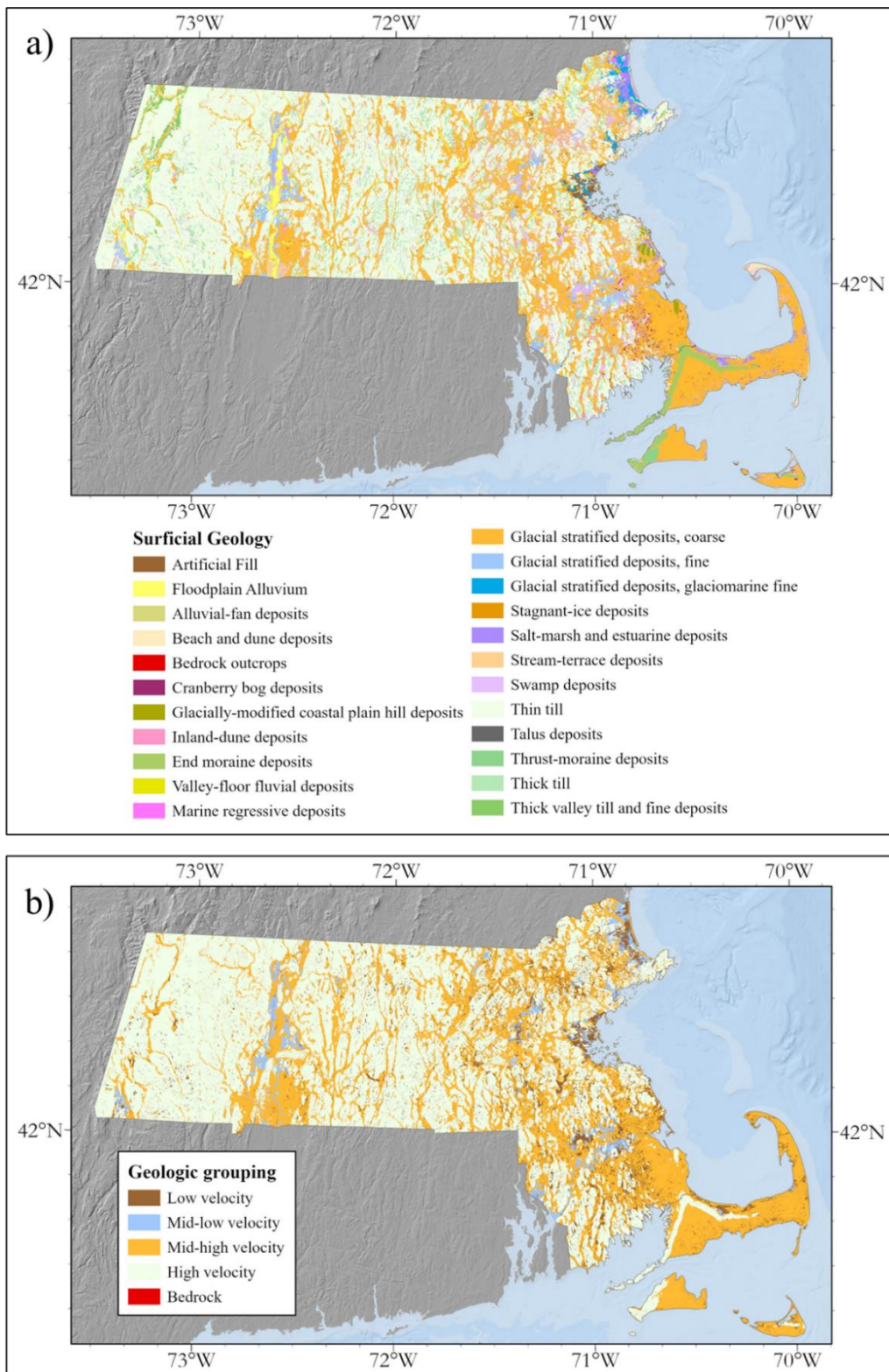


Figure 3. The Massachusetts state surficial geologic map of Stone et al. 2018.b) The Massachusetts surficial geologic map grouped into four groups with similar mechanical properties in Table 1.

2.3 Subregion map

The local deposit subregion map created in Pontrelli et al. (2023b) was developed to identify major local sedimentary deposits relevant for site response in the region (Figure 4). This subregion map defines four subregions in the state. The Boston Basin (*BB*) is composed of the marine clay deposit Boston Blue Clay, extensive artificial fill deposits of anthropogenic origin, and alluvial outwash sediments in the flood plain of the Charles and Mystic Rivers. The Connecticut River Valley (*CRV*) is composed of lacustrine clay deposit Glacial Lake Hitchcock sediments and alluvial/outwash sediments in the Connecticut River flood plain. Cape Cod (*CC*) is a terminal moraine composed of glacial outwash sediments and bands of till which make up the Sandwich moraine. Massachusetts General (*MG*) is defined as all the area outside of the first three subregions and is predominantly composed of till, though also contains some river valleys composed of outwash sediments that are smaller than the Connecticut River Valley. The subregions were created using a digital elevation model and state-scale geologic maps. Lines of equal elevation adjacent to each major geologic deposit were identified where till soil classifications meet soft surficial geologic classifications.

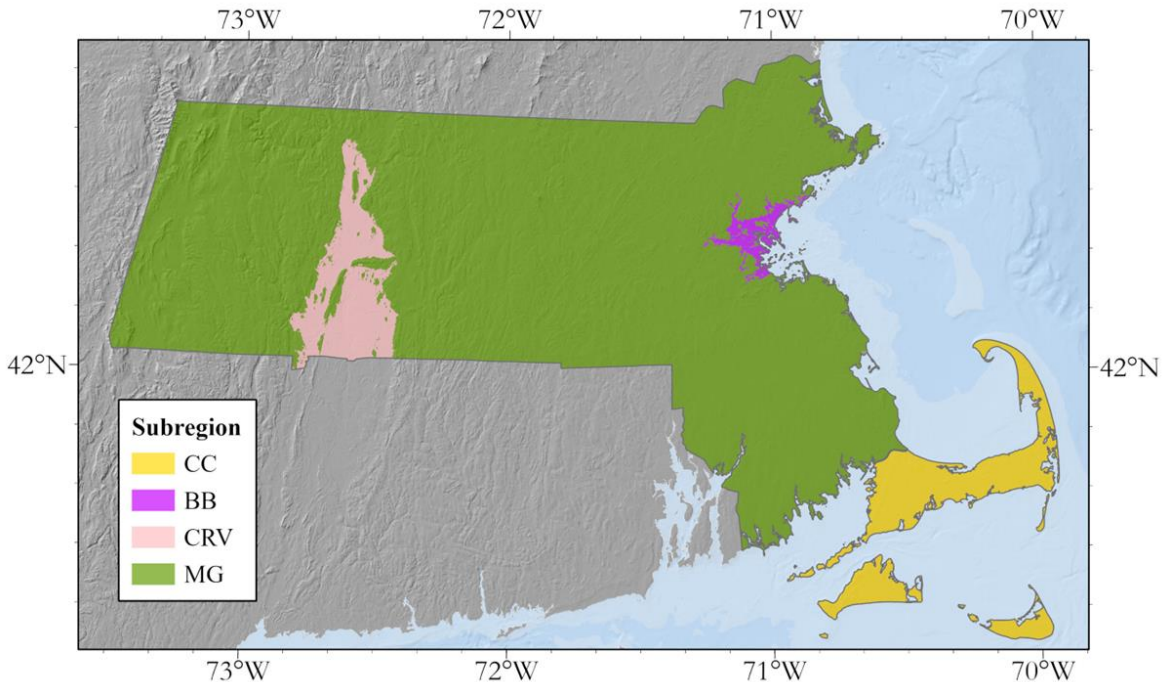


Figure 4. The local deposit subregion map developed in Pontrelli et al. 2023b. This is used to group the f_0 points by local geologic deposit and create $f_0 - z$ relationships for each of those deposits.

2.4 f_0 dataset

The f_0 dataset used in this study has 1342 f_0 measurements in Massachusetts. They are compiled from four studies: 570 are from Yilar et al. (2017), 198 are from Fairchild et al. (2013), 545 are from Mabee et al. (2022) and 29 are from Pontrelli et al. (2023a). The Yilar et al. (2017) study has f_0 stations concentrated in the Boston Basin where they were used to perform a microzonation study of the city. The Fairchild et al. (2013) study is on the eastern portion of Cape Cod where researchers mapped depth-to-bedrock to develop a groundwater model for the area. The Mabee (2022) study is evenly spread throughout the state and was used in the development of the dataset that turned into the depth-to-bedrock model in Figure 2. They collected f_0 data where the borehole dataset was lacking. Finally, the Pontrelli et al. 2023a stations were collected along the length of Cape Cod and in an east-west transect through the center of the state to estimate typical f_0 values in large geologic deposits in the New England region.

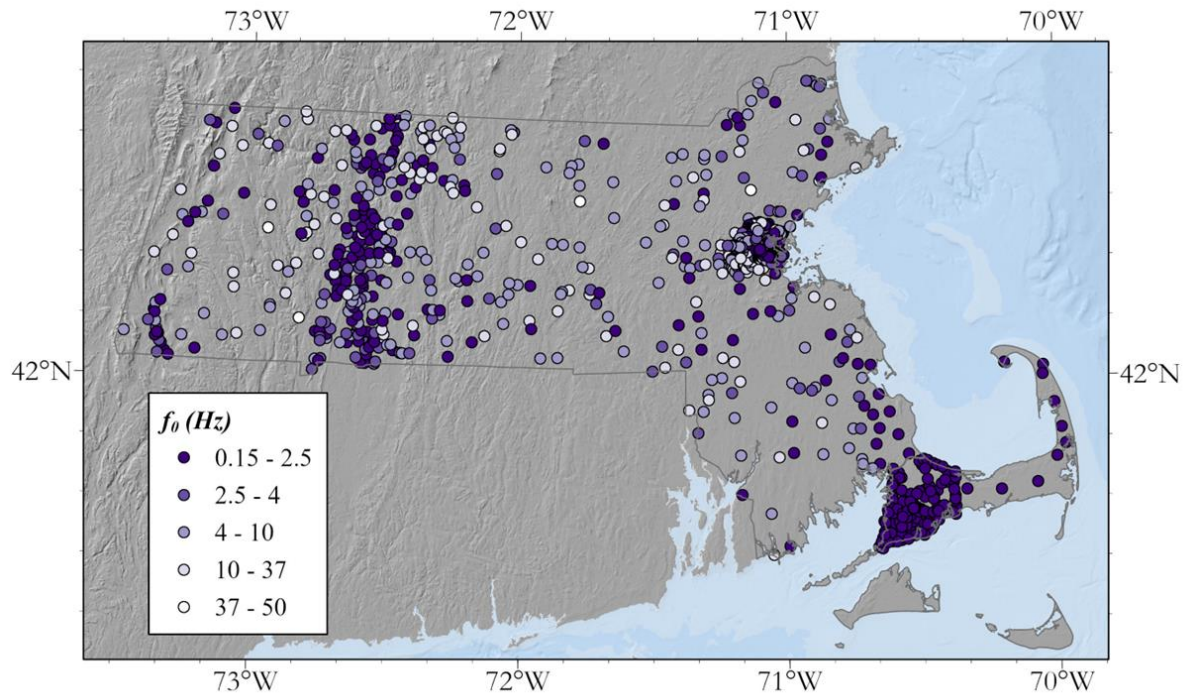


Figure 5. f_0 dataset used in the study and compiled from Fairchild et al. (2013), Yilar et al. (2017), Mabee et al. (2022) and Pontrelli et al. (2023a). These points are used to sample from the depth-to-bedrock model (Figure 2a) to create a dataset of paired $f_0 - z$ data from which the α and β coefficients to represent the power law shear-wave velocity profile are computed.

3.0 Methods

The methodological framework of this study is: to 1) develop power law shear-wave velocity profiles for each geologic unit and subregion using $f_0 - z$ pairs of data, 2) Monte Carlo sample each depth-to-bedrock map pixel distribution and propagate it through the shear-wave velocity profiles to compute f_0 distributions and calculate $f_0 \mu_{ln}$ and σ_{ln} and 3) mask the final f_0 map based on an f_0 threshold.

3.1 $f_0 - z$ relationships and the link to power-law velocity profiles

Ibs-von Seht and Wohlenberg (1999), describe the theoretical background for the relationship between f_0 and depth to the impedance contrast (z) and provide an example for a dataset in the western Lower Rhine Embayment in Germany. This approach is further discussed in Delgado et al. (2000) which provides the equation for converting the relationship coefficients α and β , into shear-wave velocity profiles. Both Ibs-von Seht and Wohlenberg (1999) and Delgado (2000) use a shear-wave velocity to depth relationship in which the shear-wave velocity increases in relation to depth as a power law (Equation 1). This relationship has theoretical background in both Seed et al. (1986), and Kramer, (1996).

$$Vs(z) = v_0 * ((1 + z)^x) \quad (1)$$

where v_0 is the surface shear-wave velocity, z is the depth and x is the depth dependence of the velocity. Given the assumption of a power law velocity relationship with depth, the relationship between f_0 and z is:

$$f_0 = \alpha z^\beta \quad (2)$$

$$z = a f_0^b \quad (3)$$

Equation 3 is commonly used in the literature with a and b being published coefficients. This is because it is common to estimate z with measured f_0 values at the free surface. In this study, a depth-to-bedrock model (Figure 2) is used for the z variable in the $f_0 - z$ relationship and f_0 is derived from HVSR curves collected across Massachusetts and the α and β coefficients are estimated using regression. The α and β coefficients derived from Equation 2 can be used to convert back to a shear-wave velocity profile using Equation 4.

$$V_s = 4\alpha z^{\beta+1} \quad (4)$$

Once the velocity profiles are established, since a detailed depth-to-bedrock model derived from tens of thousands of borings and other measurements is available, f_0 is estimated using Equation 2 continuously across Massachusetts.

3.2 Developing the shear-wave velocity profiles from f_0 and z

The goal of this work is to propagate both depth and shear-wave velocity uncertainty through the sediment overburden system to develop distributions of f_0 . The accounting of shear-wave velocity uncertainty comes from the scatter in the $f_0 - z$ relationship. Linear regression is used to estimate the α and β coefficients and allows for the estimation of a prediction interval for f_0 . The power law in Equation 2 is converted to a linear equation which allows for the application of linear regression. To linearize Equation 2, the natural logarithm of both sides of the equation is taken:

$$\ln f_0 = \ln(\alpha z^\beta) \quad (5)$$

Expanding the right side of the equation yields

$$\ln f_0 = \ln(\alpha) + \ln(z^\beta) \quad (6)$$

which simplifies to

$$\ln f_0 = \ln(\alpha) + \beta \ln(z) \quad (7)$$

Given a dataset of f_0 points and corresponding z points, Equation 7 allows for the transformation of both f_0 and z values to natural-log space and for linear regression to be performed to determine the α and β coefficients. The standard deviation of the residuals (σ_{resid}) around the linear regression for Equation 7 is used to create a normal distribution of possible f_0 values.

To develop the velocity profiles using the $f_0 - z$ data, the f_0 dataset (Figure 5) is sampled for the corresponding depth (z) value from depth-to-bedrock model (Figure 2a). Since the depth values used for the coupled $f_0 - z$ points, are the modeled data from the depth-to-bedrock model (Figure 2a), there are uncertainties in their values. Where there are modeling errors in the depth model, the f_0 and z values can have unphysical average overburden velocities. These datapoints are removed by computing the average

overburden velocity using $f_0 = Vs/4z$ and then removing datapoints with Vs_{avg} less than 120 m/s and greater than 700 m/s as shown in Figure 6.

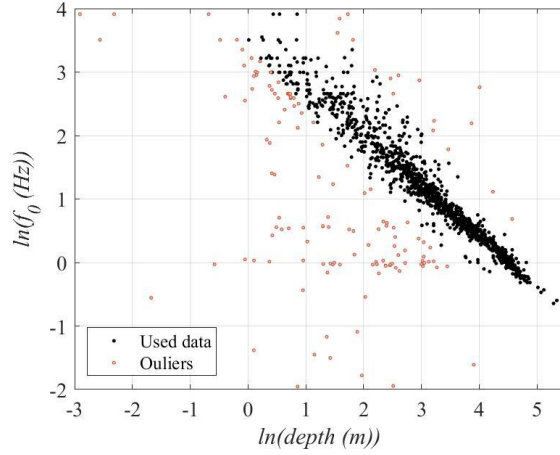


Figure 6. The f_0 and z data used to estimate shear-wave velocity profiles. The used data is plotted in black and the removed data (which have Vs_{avg} values less than 120 m/s or greater than 700 m/s) are plotted in orange.

The dataset is subdivided by geologic unit and subregion and models are developed. To compute the α and β coefficients from the $f_0 - z$ data for each geologic unit and subregion, the natural logarithm of both the f_0 and z datapoints are taken and plotted against one another. This allows for the linear fitting of the two variables using Equation 7 with intercept $\ln(\alpha)$ and slope β . Linear least squares regression is performed using the bisquare method and a linear model is fit to the data (Figure 7a). The bisquare method weights the point residual based on how far it is from the regression line; the further a data point is from the trendline, the less it is weighted. This minimizes the effect of the data far from the line on the estimation of the $\ln(\alpha)$ and β coefficients. After fitting the model, the model residuals are used to compute a σ_{resid} value which is used to estimate an f_0 distribution for each z value. This σ_{resid} value is the uncertainty of the $\ln(\alpha)$ term.

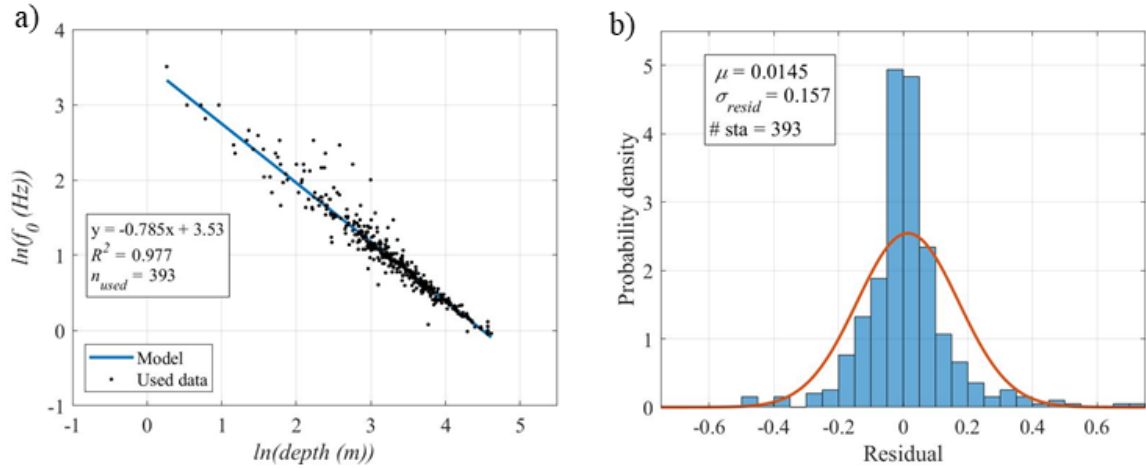


Figure 7. Linear model of the f_0 and z data of the Boston Basin subregion with fit with coefficients $\ln(\alpha)$ and β in Equation 7. The equation in the box in the left of the plot, y is equal $\ln(f_0)$, x is equal to $\ln(z)$, the slope (in this case -0.785) is equal to β and the intercept (in this case 3.53) is equal to $\ln(\alpha)$. b) The residuals of the model in Figure 7a. The σ_{resid} value is used as a prediction interval to estimate a distribution of f_0 values for each z value.

After developing the model using the procedure outlined above, two final steps are taken: α is computed by exponentiating the intercept of the linear regression line, and a shear-wave velocity profile is generated from Equation 4. For the model developed above the Boston Basin (Figure 7a), $\beta = -0.785$, $\ln(\alpha) = 3.53$, $\alpha = 34.2$ and the shear-wave velocity profile resulting from these values is plotted in Figure 8. To create uncertainty bounds around the shear-wave velocity profile, profiles with $\ln(\alpha) \pm 2\sigma_{\text{resid}}$ are plotted in addition to the fitted $\ln(\alpha)$ value.

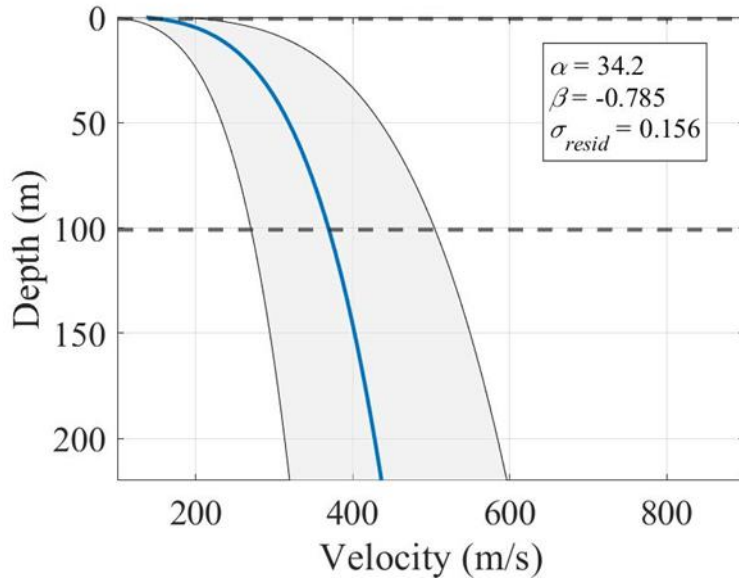


Figure 8. The mean shear-wave velocity profile for the α and β values computed from the linear regression analysis of the Boston Basin subregion in Figure 7a. Each f_0 point has a depth to the impedance contrast so for each individual point, this theoretical profile is truncated at the computed depth to the impedance contrast. The uncertainty bands (filled in grey) are computed using the σ_{resid} value (Figure 7b) and are equal to $\pm 2\sigma_{resid}$ which is a 95% confidence interval. The maximum and minimum depths of the data values used in the model are the dashed black lines.

3.3 Predicting f_0 distributions from the depth-to-bedrock model

The methodology for predicting distributions of f_0 begins with the depth-to-bedrock map which is sampled at each pixel for an estimate of the mean (μ) and standard deviation (σ) of a lognormal distribution of depth-to-bedrock at that pixel. The mean is assumed to be the value of the prediction (Figure 2a). The uncertainty map of the model (Figure 2b) is used to represent one standard deviation. To convert to the μ_{ln} and σ_{ln} parameters of the lognormal distribution from the natural unit mean and standard deviation, Equations 9 and 10 are used.

$$\mu_{ln} = \ln \left(\frac{\mu^2}{\sqrt{\mu^2 + \sigma^2}} \right) \quad (8)$$

$$\sigma_{ln} = \sqrt{\ln \left(1 + \frac{\sigma^2}{\mu^2} \right)} \quad (9)$$

From the mean and standard deviation values, 1000 depth samples are sampled from a lognormal distribution (Figure 9a). This procedure ensures that no depth values are less than one (since the distribution

is lognormal) and that when Equation 2 is linearized to Equation 7, the resulting natural-log transformed depth distribution is normally distributed ensuring that the f_0 distribution in natural-log space (Figure 9d) is normally distributed and the f_0 distribution in natural unit space (Figure 9e) is log-normally distributed.

For each z sample using the natural log of depth, $\ln(f_0)$ is estimated using the velocity model using the α and β coefficients (Figure 9b). 1000 samples of the velocity profile are drawn using the α and β coefficients and σ_{resid} (Figure 9b). This process is repeated resulting in 1,000,000 samples to define the distribution of f_0 for that pixel defined by μ_{\ln} and σ_{\ln} (Figure 9d). Finally, this distribution is exponentiated and the median (Mdn) f_0 value is computed in natural units (Figure 9e).

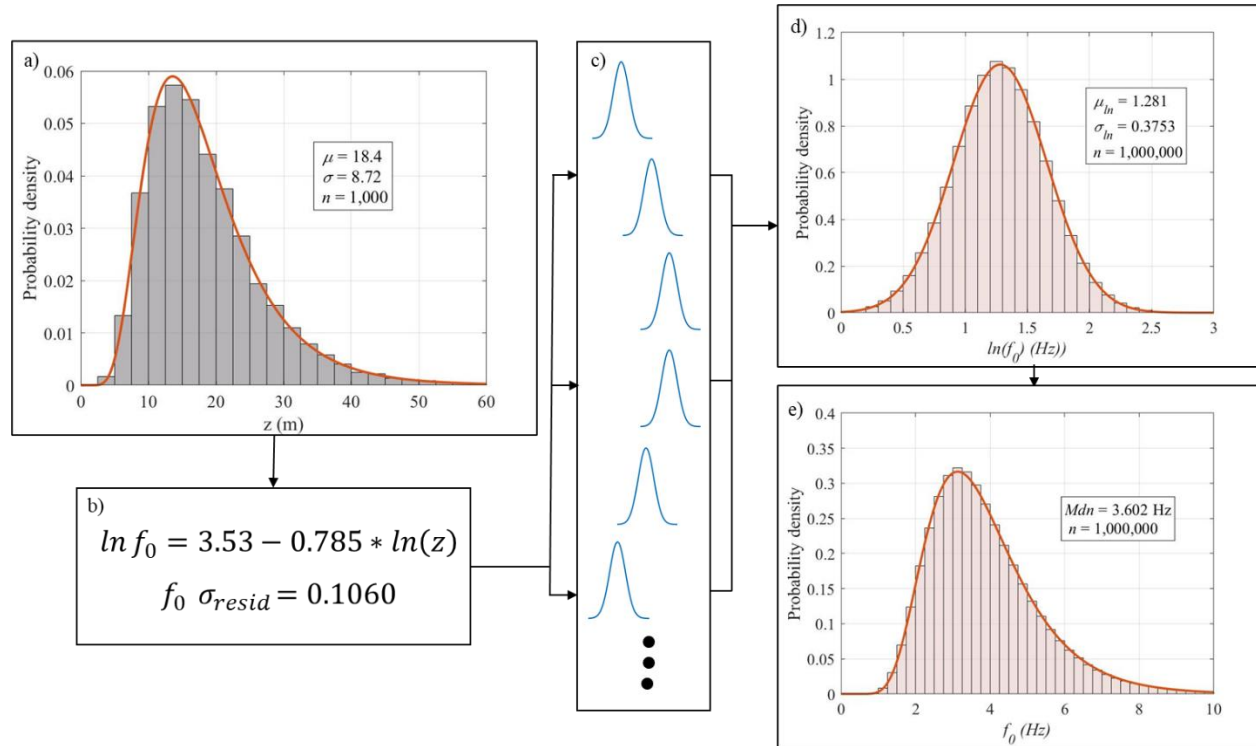


Figure 9. An example from a pixel in the Boston Basin of the steps for computing f_0 distributions from the depth-to-bedrock map and the $f_0 - z$ relationships. a) The lognormal distribution of possible pixel depths with a mean equal to the depth prediction value and a standard deviation equal to the uncertainty. These are converted to the μ_{\ln} and σ_{\ln} parameters of the lognormal distribution using Equations 9 and 10. b) The $f_0 - z$ relationship with the α and β coefficients and σ_{resid} value for the Boston Basin. c) Cartoons of the 1000 f_0 distributions for each depth sample. Each of these distributions has 1000 samples and there are 1000 of them (one for each depth value). d) The final f_0 distribution made from the 1000000 f_0 samples at each pixel. The distribution is used to compute μ_{\ln} and σ_{\ln} . e) The exponentiated distribution of Figure 9d in natural units of Hz from which the median (Mdn) is computed.

3.4 Selecting an f_0 threshold to mask the f_0 map

The majority of Massachusetts is composed of shallow, non-resonant tills and therefore poses little site response hazard. Additionally, many of these sites may not result in an HVSR curve with a fundamental peak. Dense glacial sediments and bedrock sites are expected to have flat HVSR curves. For thin sediment sites, the f_0 values are expected to be very high and not as relevant for engineering structures. Figure 10 demonstrates this phenomenon for selected sites in the Boston Basin. The left column of Figure 10 shows HVSR curves of deep resonant sites in the center of the Boston Basin, the middle column shows HVSR curves in shallower sites towards the basin edge and the right column shows shallow till sites on the edge of the Boston Basin. These HVSR curves demonstrate the phenomenon of less resonant soils toward basin edges. Therefore, an f_0 threshold is selected above which soil resonance is not expected. The final f_0 map is masked using this f_0 threshold.

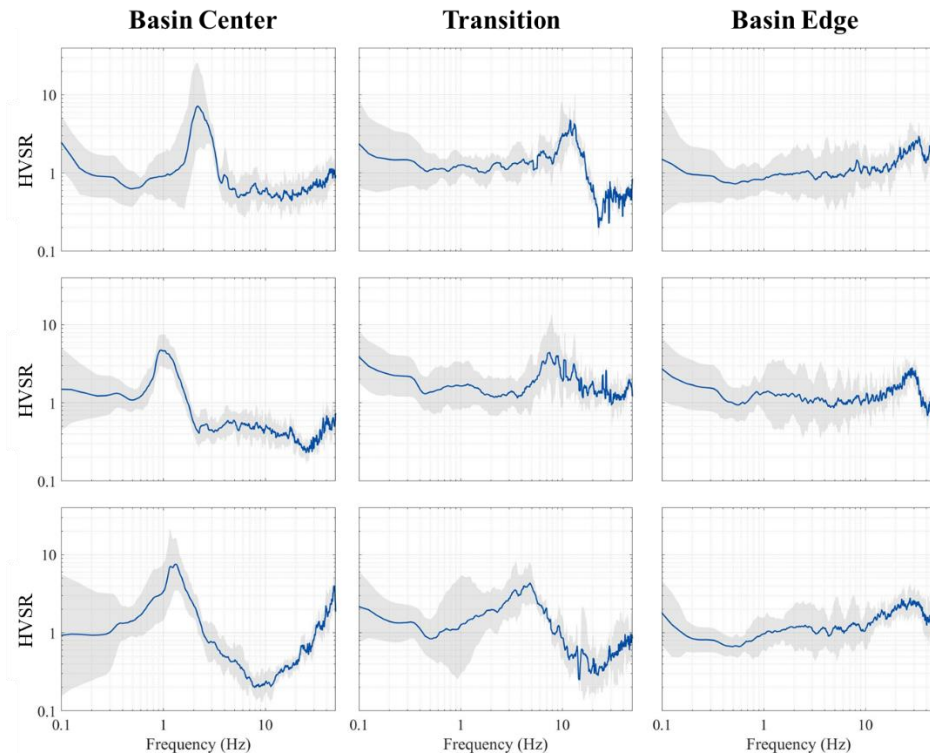


Figure 10. Selected HVSR curves demonstrating the transition from resonant soils in the center of the Boston Basin to less resonant soils on the basin edge. The plots in the left column are HVSR curves from the center of the basin, the middle column are curves approaching the basin edge, and the right column are curves on the basin edge.

The technique for selecting the f_0 threshold in this study contextualizes the observation of flattening HVSR curves as sediments thin within the existing $Vs30$ framework. The f_0 threshold is selected as the frequency at which the median shear-wave velocity profile transitions from a site class C to a site class B at a $Vs30$ value of 760 m/s. To find this frequency, the shear-wave velocity profile of the $f_0 - z$ relationship is used (Figure 11a). The f_0 value is computed based on the power law velocity profile for depths from 0 to 1000m. The $Vs30$ value is computed using the power-law shear-wave velocity profile until the designated depth-to-bedrock and by assuming a bedrock shear-wave velocity $Vs_{bedrock} = 2500$ m/s. This procedure yields relationships between depth and $Vs30$ (Figure 11c) and f_0 and $Vs30$ (Figure 11d) for each shear-wave velocity profile representing each subregion and geologic unit. As an example, using Figure 11d, the f_0 value at which the Boston Basin profile transitions from site class C to B is 10.84 Hz which corresponds to a depth of 4.32m. The final f_0 maps are masked where pixels in the Boston Basin have a Mdn value above this f_0 threshold. The f_0 and z thresholds for all the subregions and geologic units are in Table 3.

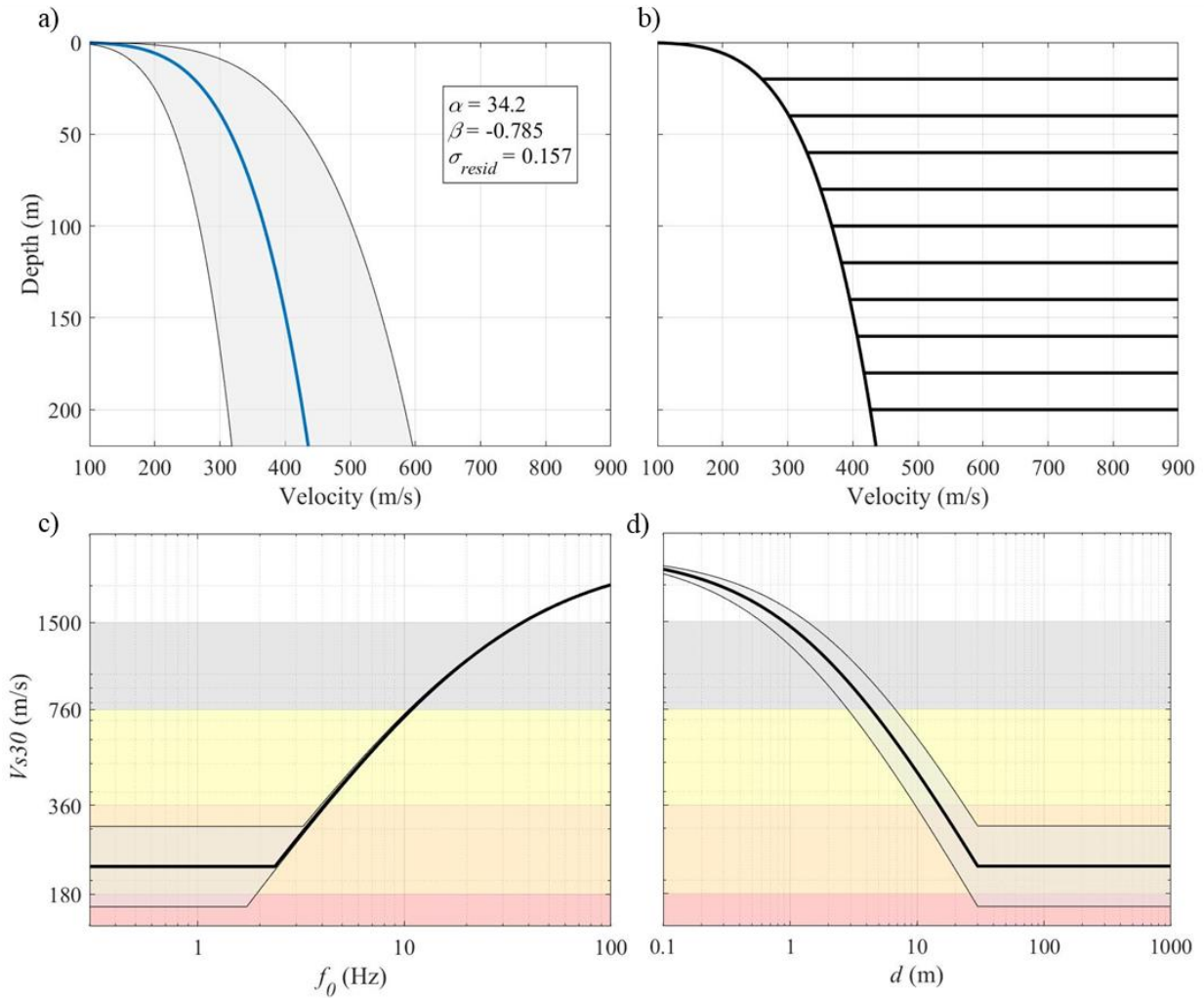


Figure 11. An example using the Boston Basin shear-wave velocity profile of the analysis performed to determine the f_0 threshold above which the final map is masked. a) The Boston Basin shear-wave velocity profile for the $f_0 - z$ relationship of all the data. b) Ten shear-wave velocity profiles based on the profile in Figure 11a where the profile is truncated at varying depths below which the profile is assigned a basement rock velocity of 2500 m/s. Each of these profiles has a depth, an f_0 value, and a V_{s30} value which allows for the relationships in Figures 11c and d. c) f_0 vs. V_{s30} with the seismic site classes shown. Red is site class E, orange is site class D, yellow is site class C, grey is site class B and white is site class A. The point where the line crosses from site class C to B (yellow to grey) is the f_0 value selected as the threshold above which the final map is masked. The grey fill is between the $\pm 2\sigma_{\text{resid}}$ uncertainty bands which are computed from the $\pm 2\sigma_{\text{resid}}$ shear-wave velocity profiles in Figure 11a. d) z vs. V_{s30} with the seismic site classes shown. The depth threshold value (which corresponds to the f_0 threshold value) is where the depth line crosses from seismic site class C to site class B.

4.0 Results

4.1 $f_0 - z$ relationships and corresponding α and β coefficients

$f_0 - z$ relationships are developed for each geologic grouping (Figure 3b) and each subregion (Figure 4) as shown in Figure 12 for each geologic grouping and in Figure 13 for each subregion. For each linear regression, the $\ln(\alpha)$, α , and β coefficients are tabulated as well as the residual σ value which is used to develop distributions of f_0 for each z value in the depth-to-bedrock distribution (Table 2). The R^2 value for each relationship is above 0.9. In general, the $\ln(\alpha)$, α , and β coefficients are very similar except for the Cape Cod (CC) subregion which has a much higher α value (93.14) and much lower β value (-1.00) than the other subregions of geology $f_0 - z$ relationships. The σ_{resid} value is highest in the G4 high velocity geologic grouping, which is composed of till geologic classifications and in the MG (Massachusetts General) subregion which is mainly composed of the upland tills across the state. The lowest σ_{resid} values are in the G1 geologic grouping, which is composed of low velocity deposits and the BB (Boston Basin) subregion which is the smallest subregion in the State and is composed of marine clays, artificial fills, and floodplain alluvium deposits.

Table 2. Model results for the $f_0 - z$ relationships for each geologic group and subregion. The $\ln(\alpha)$, α , and β coefficients are the intercept and slope respectively of the linear regression. The R^2 and n values are the coefficient of determination and the number of points used in the development of the $f_0 - z$ relationship. The μ_{resid} and σ_{resid} values are the mean and standard deviation of the residuals, respectively. The μ_{resid} value indicates the bias in the data from the trendline (of which there is little) and the σ_{resid} value indicates the amount of spread around the trendline which is manifested as the width of the distribution when the data are Monte Carlo sampled.

-	Grouping/ subregion	$\ln(\alpha)$	α	β	R^2	n	μ_{resid}	σ_{resid}
Geologic Group	G1	3.51	33.51	-0.780	0.977	221	0.0082	0.1371
	G2	3.57	35.40	-0.791	0.959	105	-0.0344	0.1880
	G3	3.64	38.03	-0.801	0.980	609	0.0202	0.1926
	G4	3.58	35.85	-0.777	0.944	266	0.0506	0.2769
Subregion group	BB	3.53	34.20	-0.785	0.977	393	0.0145	0.1568
	CRV	3.54	34.53	-0.772	0.959	192	-0.0056	0.2162
	CC	4.53	93.14	-1.002	0.946	194	0.0091	0.0744
	MG	3.62	37.32	-0.787	0.926	422	0.0405	0.2706

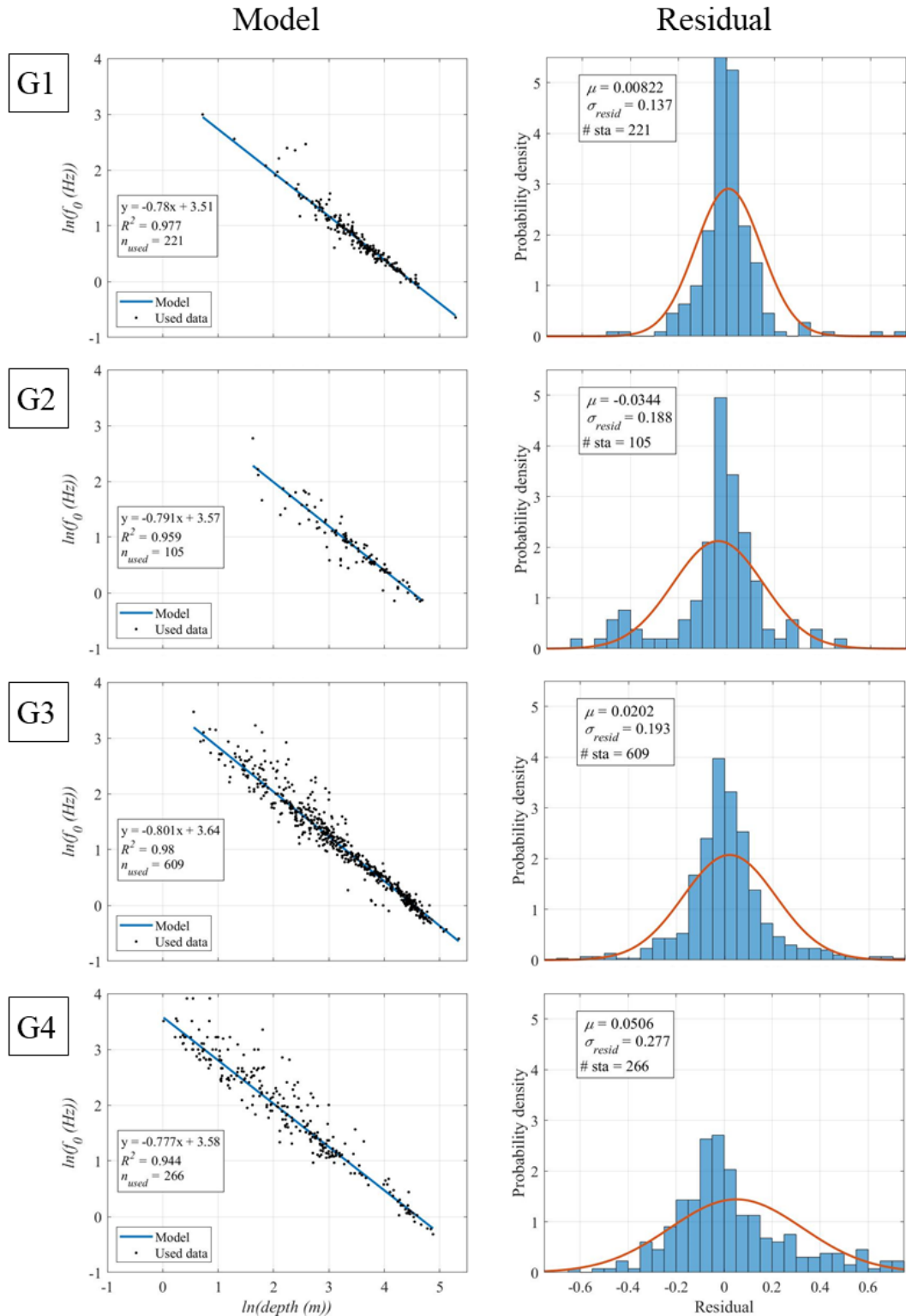


Figure 12. Results for the $f_0 - z$ relationships in each geology. The left column shows the $f_0 - z$ relationships and the right column shows the distribution of the residuals which is used as the prediction interval for the f_0 distribution at each depth value.

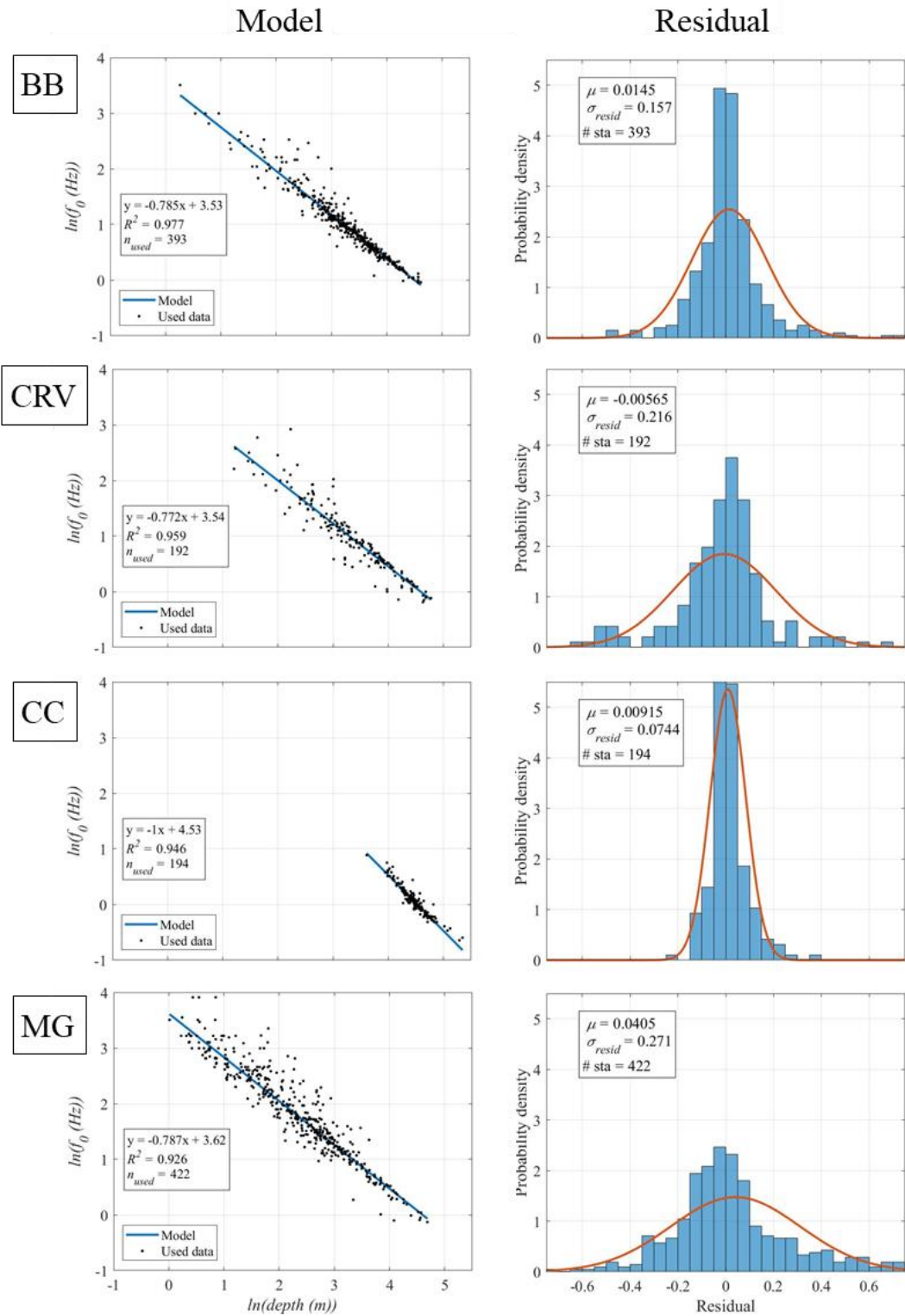


Figure 13. Results for the $f_0 - z$ relationships in each subregion.

4.2 Estimating shear-wave velocity profiles from the α and β coefficients using Equation 4

Using Equation 4, the α and β coefficients computed in the development of the $f_0 - z$ relationships are used to form shear-wave velocity profiles for each geologic unit (Figure 14) and subregion (Figure 15). These shear-wave velocity profiles are all similar in shape because they are modeled after a power law relationship between depth and velocity. The one exception is Cape Cod (CC, Figure 14). For the case of Cape Cod, this is a result of a modeling decision made in the development of the depth-to-bedrock model and the original f_0 data collection. The Cape Cod HVSR data, published in Fairchild et al. 2013 use an $f_0 - z$ relationship with a β value of -1, which corresponds to a layer-over-halfspace shear-wave velocity profile. These are the data that are used in the depth-to-bedrock map and the relationship therefore heavily influences the relationship that is developed in this study with depth values sampled from the depth-to-bedrock model. The shear-wave velocity profile with the highest values is the G4 high velocity geologic grouping consisting of tills and the Massachusetts General subregion consisting of areas outside of the major soft geological deposits.

Each $f_0 - z$ relationship is developed using ranges of f_0 and z data. The maximum and minimum used z values are shown in Figures 14 and 15 with dashed lines. With the geologic $f_0 - z$ relationships, every model is developed from some very shallow points (each relationship has a dashed line that is near zero). In the subregion relationships, however, three of the subregions (BB, CRV, and MG) have data ranging from approximately 0m depth to 100m depth. CC, however, only has data greater than 36m. This is an important detail. In a study focused on f_0 , z is a very important factor. z can vary widely across geologic units (a geologic unit classification does not depend on depth), but its range is relatively consistent in subregions. For example, the Boston Basin has a maximum and minimum depth-to-bedrock regardless of the geologic classification, whereas similar geologic classifications exist across the state of Massachusetts with widely varying depths depending on the local geologic deposit subregion. For this reason, we use the $f_0 - z$ relationships for the subregions (Figure 15) to develop the f_0 distribution maps.

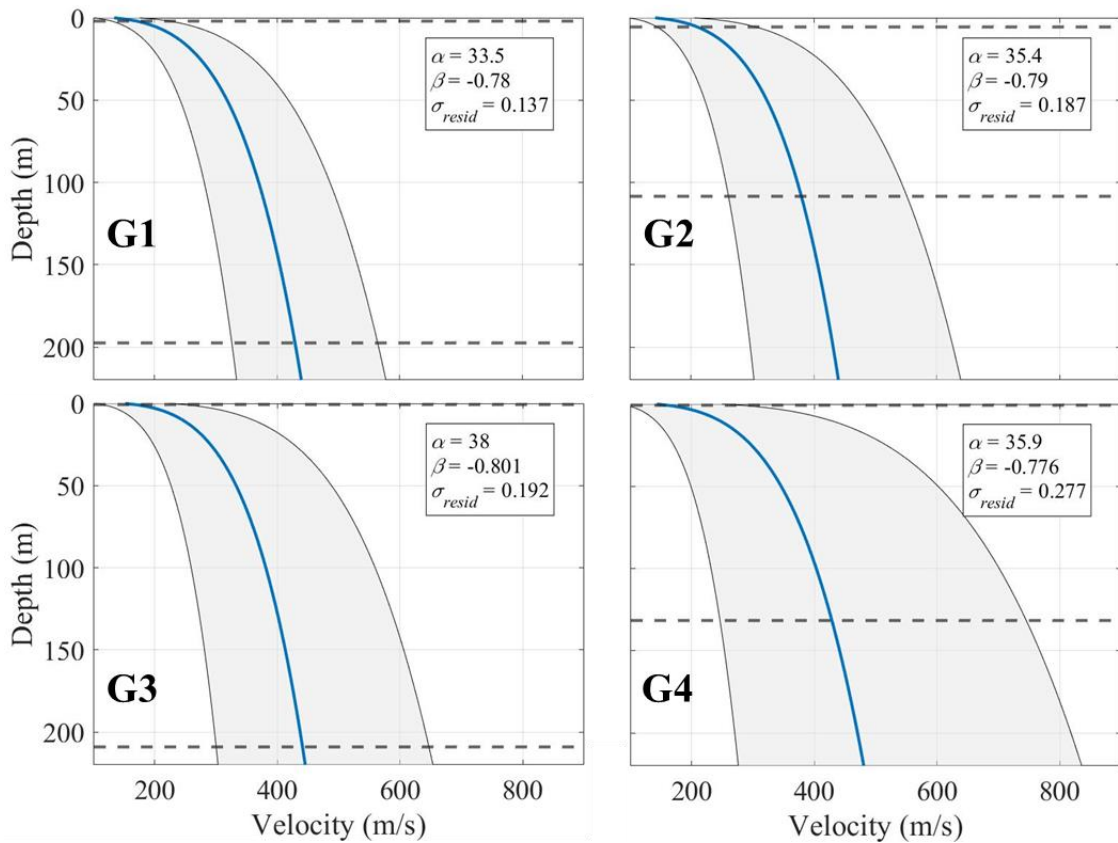


Figure 14. Shear-wave velocity profiles of corresponding to the α and β coefficients of each $f_0 - z$ relationship for each geologic grouping from Figure 12. The uncertainty is a 95% prediction interval using the σ_{resid} value from each model which is in the right column of Figure 12. The black dashed lines are the maximum and minimum depth values used in the data to create the relationship. This range can be seen as the range of points across the x-axis in the left column of Figures 12.

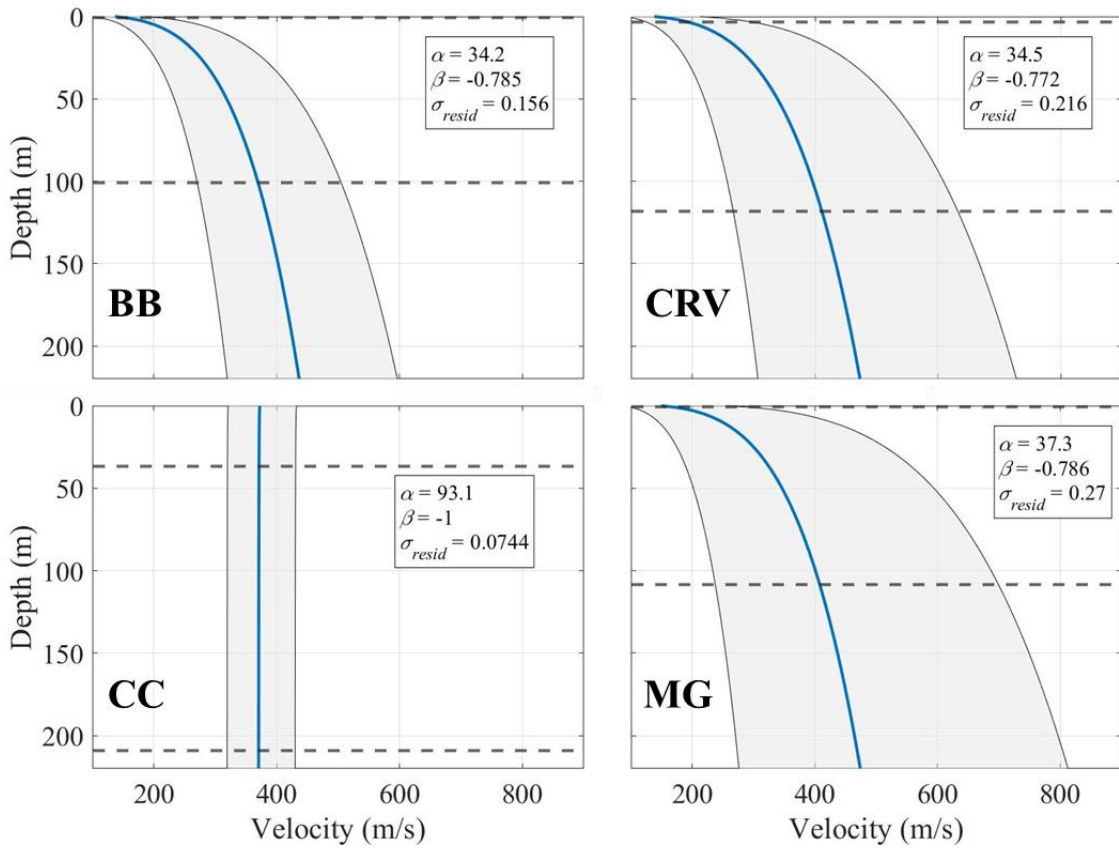


Figure 15. Shear-wave velocity profiles of corresponding to the α and β coefficients of each $f_0 - z$ relationship for each subregion from Figure 13. The uncertainty is a 95% prediction interval using the σ_{resid} value from each model which is in the right column of Figure 13. The black dashed lines are the maximum and minimum depth values used in the data to create the relationship. This range can be seen as the range of points across the x-axis in the left column of Figures 13.

Following the procedure outlined in section 3.4, f_0 thresholds are calculated to mask the final f_0 maps for each geologic unit and subregion. These are based on the *Mdn Vs30* value where the site transitions from a site class C to a site class B (Table 3)

Table 3. f_0 and z thresholds used to mask the final f_0 map for each geologic grouping and subregion.

-	Grouping/subregion	f_0 threshold	z threshold
Geologic group	G1	10.92	4.21
	G2	10.74	4.52
	G3	10.54	4.96
	G4	10.92	4.62
Subregion group	BB	10.84	4.32
	CRV	11.00	4.40
	CC	7.72	12.00
	MG	10.74	4.87

4.3 Maps of masked f_0 , μ_{ln} , and σ_{ln} and Mdn

Using the models developed for the subregions in Figure 13 (with coefficients in Table 2), the procedure outlined in section 3.3 is applied and maps of f_0 , μ_{ln} , σ_{ln} , and Mdn are computed. These maps can be used to develop an f_0 distribution at each 100m pixel. The μ_{ln} map is exponentiated to estimate the median of the lognormal distribution that represents each pixel.

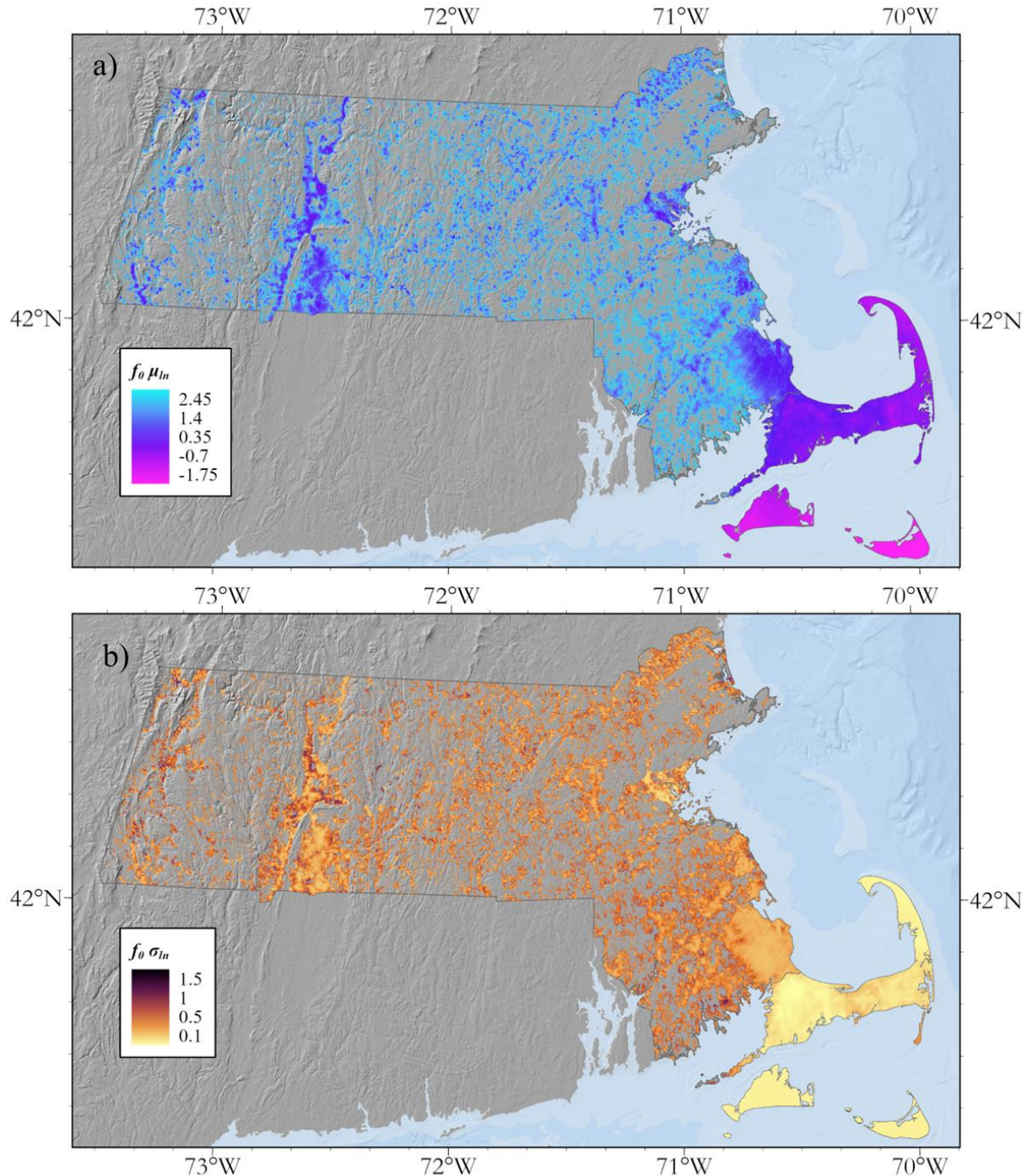


Figure 16. a) Map of $f_0 \mu_{ln}$ computed at each pixel of the depth-to-bedrock map (Figure 2a) using the $f_0 - z$ relationships in Figure 13 for the models developed for each subregion. b) Map of $f_0 \sigma_{ln}$. These maps together can be sampled to estimate a lognormal distribution of f_0 everywhere in the state. These maps have been masked using the procedure in section 3.6.

The pattern of f_0 values closely follows that of the depth-to-bedrock map in Figure 2a since the two variables are related through the $f_0 - z$ relationships and the $f_0 - z$ relationships have similar α and β coefficients (and thus similar shear-wave velocity profiles). The lowest f_0 values are located in Cape Cod, the Boston Basin and the Connecticut River Valley. These are where the overburden sediments are the deepest and, though the modeled shear-wave velocity profiles from the $f_0 - z$ relationships are different, they are not drastically different and thus predict f_0 values that vary consistently with the depth-to-bedrock map. The high frequency areas in the state are mainly in the upland till deposits where depth-to-bedrock values tend to be shallow. One important aspect of this study is to propagate uncertainty through the $f_0 - z$ relationships and estimate the final f_0 uncertainty. The low f_0 uncertainties tend to be where the f_0 values are also low (Figure 16). This is because the estimate of uncertainty (Figure 2b) is scaled by the mean value (Equation 10) in the estimate of σ_{ln} of the depth-to-bedrock distribution at each pixel. When exponentiated, the range of possible depths is greater in these areas than at shallower depths but, relative to the mean, they are lower. These products provide 1) a way to estimate a distribution of possible f_0 values at each 100m pixels in the state (Figure 16) and 2) an estimate of the median f_0 value at each pixel in the state in natural units of Hz (Figure 17). Figure 18 can be used for a rapid assessment of the potential central tendency f_0 value at a given location, but it is recommended that Figure 16a and b be used to estimate a robust prediction of the distribution of possible f_0 values, rather than a single number.

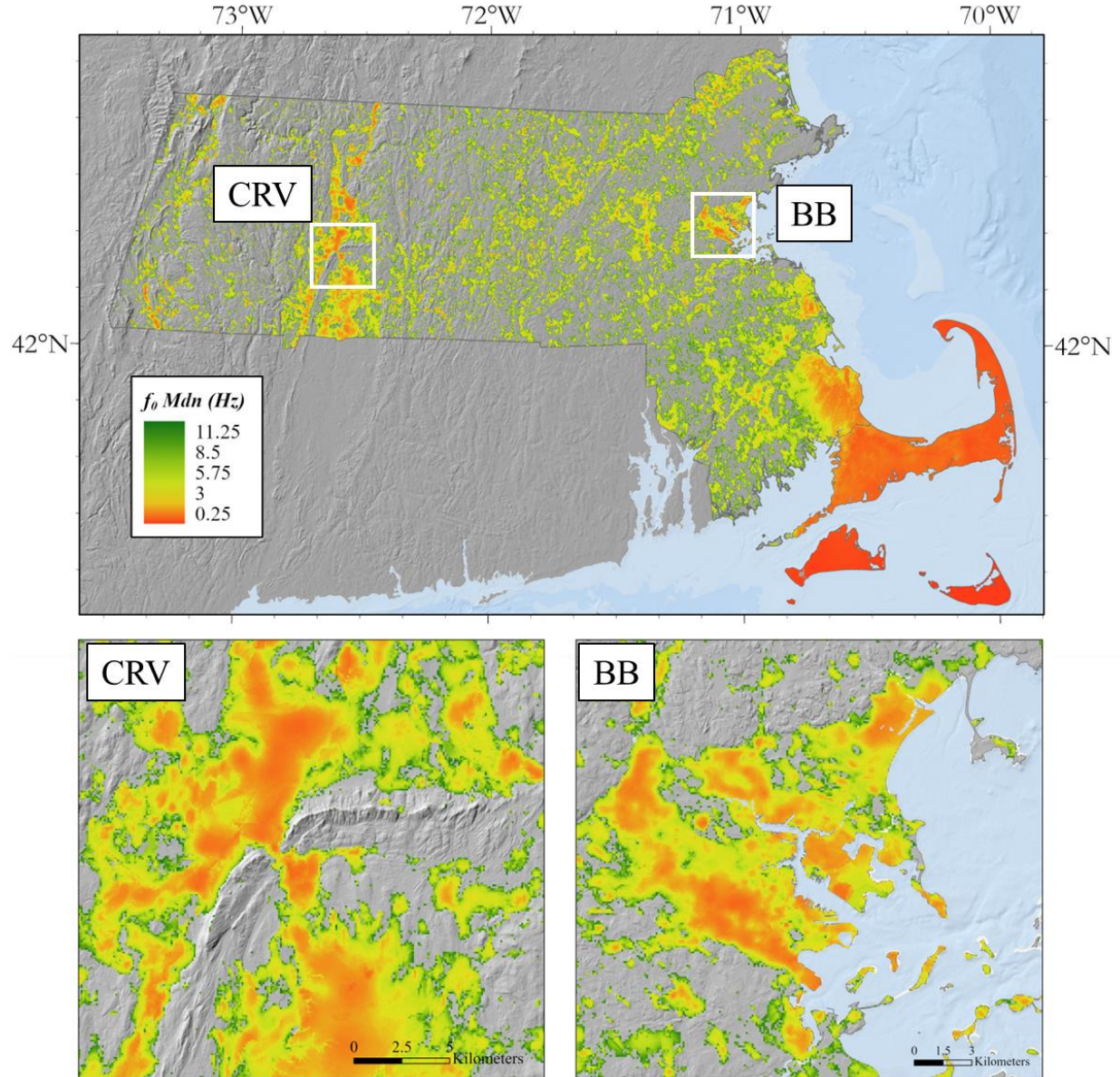


Figure 17. a) f_0 Mdn computed at each pixel. This map is Figure 16a exponentiated. The Connecticut River Valley and Boston Basin cutouts are the white squares. Below the main map, are the zoomed in f_0 Mdn maps of the Connecticut River Valley and the Boston Basin plotted over a hillshade map.

5.0 Discussion

This work maps distributions of f_0 across the state of Massachusetts. It is founded on the depth-to-bedrock map of Mabee et al. (2023) and converts the depth estimates to f_0 using $f_0 - z$ relationships developed using f_0 point data and depth values extracted from the depth-to-bedrock map. Uncertainty is accounted for in both the depth variable, which is modeled as a lognormal distribution with parameters

derived from the depth-to-bedrock map and accompanying uncertainty map, and in the power law velocity profiles resulting from the $f_0 - z$ relationships.

The $f_0 - z$ relationships developed in this study use a simplifying assumption that creates physically reasonable velocity gradients and increases the ease with which shear-wave velocity profile uncertainty estimation can be quantified. An alternative way to quantify shear-wave velocity profile is to take many shear-wave velocity profile measurements across a geologic unit or subregion and average them together to estimate a holistic model of the unit or subregion. Since so few published profiles exist in Massachusetts (35), this methodology makes it difficult to estimate both an average profile and to quantify that profile's uncertainty. By instead using coupled depth and f_0 measurements and assuming the shape of the shear-wave velocity profile (a power law with depth), a decent approximation of the average profile and uncertainty can be obtained without having thousands of shear-wave velocity profiles.

Figure 18 plots the power law velocity profiles for the Boston Basin, Connecticut River Valley, and Cape Cod with measured shear-wave velocity profiles for each of the subregions. In the Boston Basin, the power law profile does a qualitatively good job at modeling the data. The shallow high velocity profiles are located on tills at the basin edge with high or non-existent f_0 values. In the Connecticut River Valley, five of the profiles are modeled somewhat well by the power law. Two profiles which are located within the till in CRV have much higher velocities. This example demonstrates that further geologic subdivision within subregions is important as inter-subregion geologic units have varying velocities. Finally, the only Cape Cod shear-wave velocity profile is lower than the modeled velocity profile. As was discussed in section 4.2, Fairchild et al. (2013) chose to model the Cape Cod depths from f_0 data using a single-layer-over halfspace model rather than a power law with depth model. The one measured profile that we have for the region may indicate that a power-law velocity profile may be more realistic.

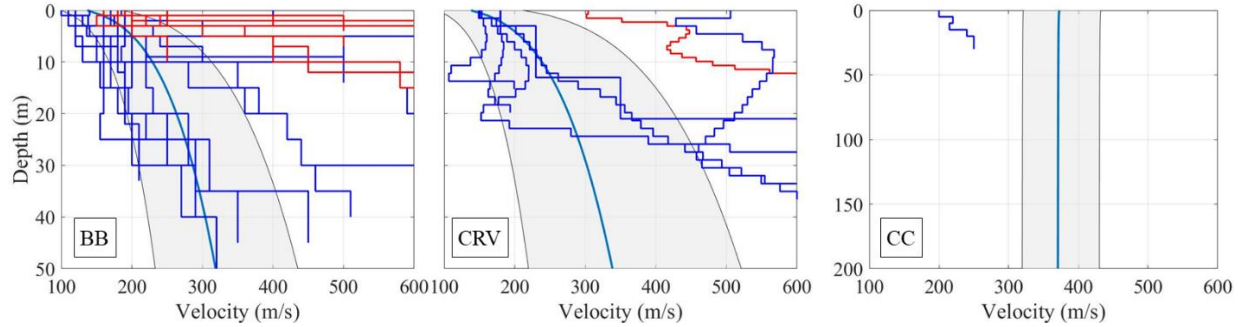


Figure 18. Power law shear-wave velocity profiles estimated in this study for three subregions with measured shear-wave velocity profiles in those subregions. Profiles classified as till are shown in red. Two high-velocity profiles in the Boston Basin and one high-velocity profile in the Connecticut River Valley are not classified as tills. These may be misclassified, or sample very shallow to bedrock. In general, the higher velocity profiles are classified as tills.

This paper shows that high-resolution depth information is essential for modeling of f_0 because f_0 is a function of depth and shear-wave velocity. Using the depth-to-bedrock model of Mabee et al. (2023) and estimates of overburden shear-wave velocity profiles allows for a relatively simple and repeatable way of creating estimates of f_0 distributions continuously across Massachusetts. In prior work by the authors, similar maps were created that used geologic polygons to group f_0 data and fit statistical distributions to those data in different geologic classifications (Pontrelli et al. 2023a and b). This technique provided ranges and probabilities of f_0 across a geologic unit, but within that unit, the technique cannot discriminate f_0 estimates. Since f_0 varies with basin geometry, a single distribution estimate per unit yielded spatially correlated residuals of the data to the median of the unit distribution. This issue is resolved with depth-to-bedrock information. With an estimate of a depth-to-bedrock surface across geologic units, variations in f_0 values in space are well modeled as a function of the varying depth estimates. Figure 19 illustrates how including depth information in the f_0 distribution modeling across Massachusetts significantly reduces the residuals between the data and the modeled μ_{ln} value. This result highlights how modeling site response using the overburden shear-wave velocity/depth-to-bedrock/fundamental frequency framework is the optimal approach for mapping of fundamental frequency if the data are available. These three values are measurable, relatable to one another and can have their uncertainty quantified allowing for the propagation of uncertainty.

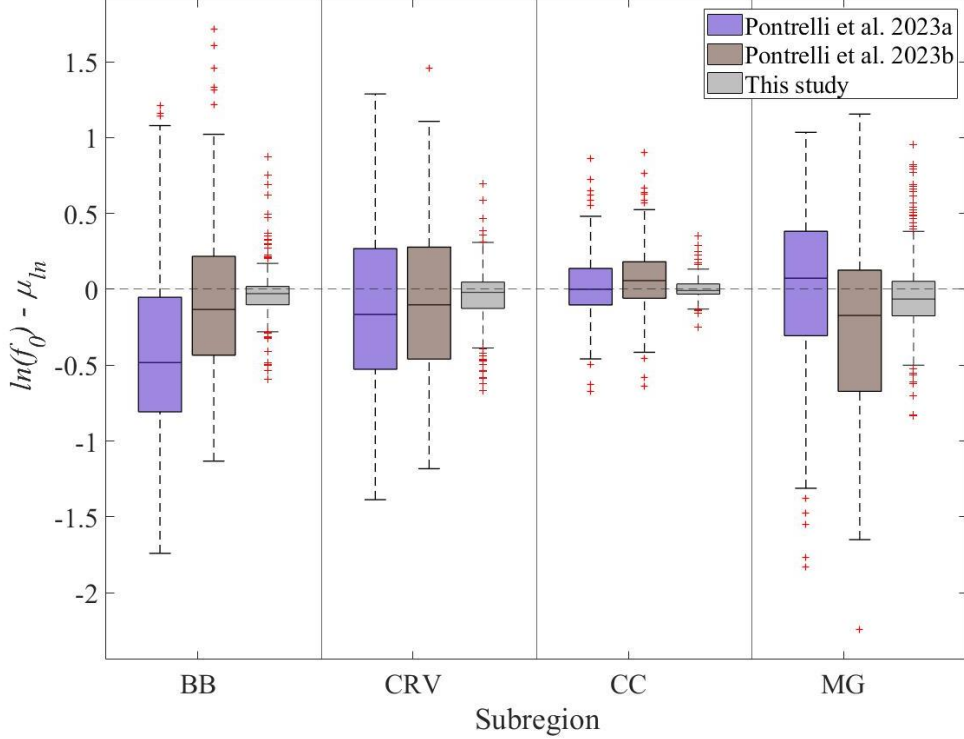


Figure 19. Comparison of residuals to the f_0 modeling of Pontrelli et al. 2023a and b. The dashed black line is the line where the measured f_0 value and the modeled f_0 value are equal.

This work was developed with a goal of mapping f_0 instead of $Vs30$ as a site characterization parameter. The method devised in this paper uses the technique of Ibs-von Seht and Wohlenberg (1999) to relate depth-to-bedrock, fundamental site frequency, and a shear-wave velocity profile. With such a large dataset of depth-to-bedrock information and a way to relate the depth data to f_0 data using $f_0 = \alpha z^\beta$ where α and β correspond to a power-law shear-wave velocity profile, it is possible to account for much of the f_0 prediction uncertainty in a relatively simple way using Monte Carlo sampling given that the uncertainties of the input parameters are well-understood and characterized.

In this study, at each pixel, it is relatively trivial to compute $Vs30$ at each of these profiles and tabulate μ_{ln} and σ_{ln} , of the distributions if one assumes a bedrock velocity. A commonly used reference rock condition in the Central and Eastern United States is 3000 m/s (Stewart et al. 2020; Goulet et al., 2017, 2018; Pacific Earthquake Engineering Research Center (PEER), 2015a, 2015b). In Baise et al. (2016), the authors test 2000 and 3000 m/s as bedrock shear-wave velocity values and find improvement in the fitting

of theoretical to empirical transfer functions using a bedrock shear-wave velocity of 2000 m/s over 3000 m/s. To create $Vs30$ distributions, this simple analysis assumes a bedrock shear-wave velocity of 2500 m/s. At each pixel and each sampled depth-to-bedrock value, (Figure 9a), the bedrock shear-wave velocity is assigned to all the layers below the depth-to-bedrock value. This extended shear-wave velocity profile is used to compute a $Vs30$ distribution at each pixel and μ_{ln} , σ_{ln} and Mdn values of that distribution are tabulated (Figure 20b).

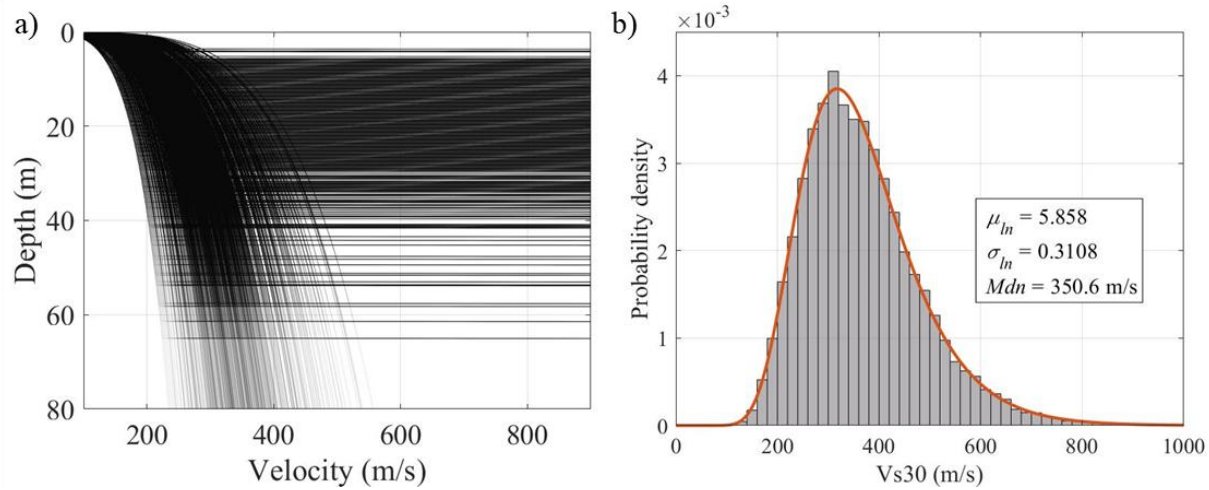


Figure 20. a) Simulated shear-wave velocity profiles for the same pixel in the Boston Basin used in the example in Figure 9. At each simulated shear-wave velocity profile, a $Vs30$ value is computed. b) the distribution of $Vs30$ values at this pixel with tabulated μ_{ln} , σ_{ln} and Mdn values.

The μ_{ln} , and σ_{ln} parameters of these distributions are shown in Figure 21 and the Mdn of these distributions is shown in Figure 22. Like with the f_0 distribution, it is recommended that the entire distribution be used to interpret the probable $Vs30$ value at each pixel, rather than the Mdn value as this incorporates uncertainty into the estimate.

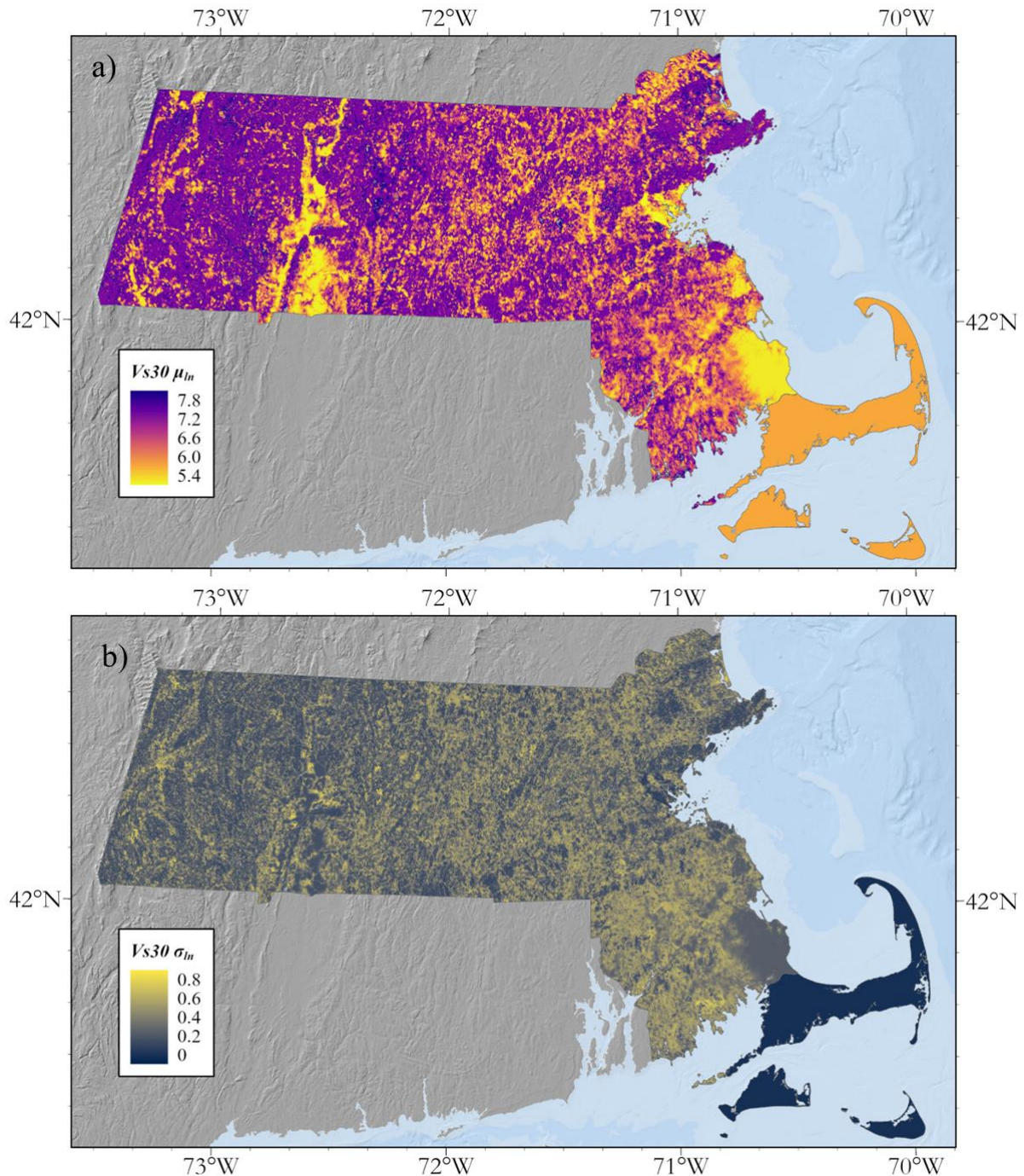


Figure 21. a) Map of $Vs30 \mu_{ln}$ computed at each pixel of the depth-to-bedrock map (Figure 2a) using the Power-law shear-wave velocity relationships in Figure 15 for the models developed for each subregion. b) Map of $Vs30 \sigma_{ln}$.

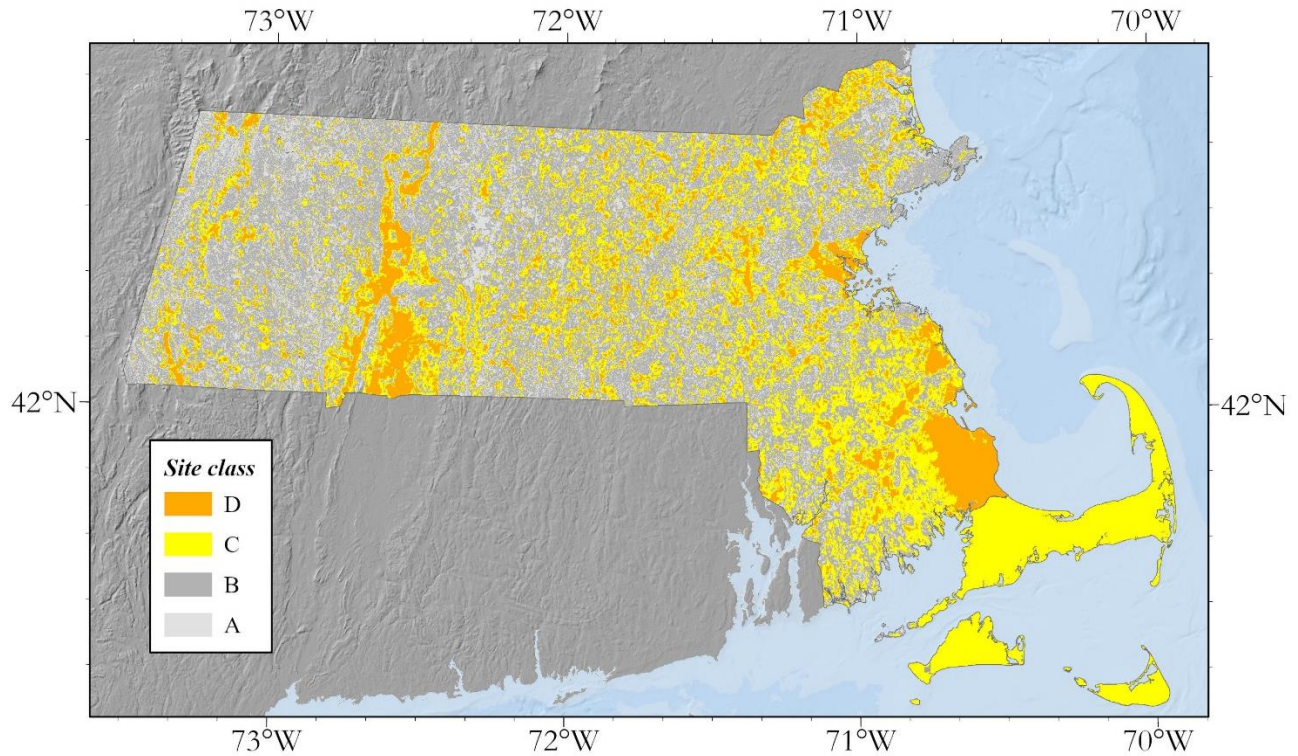


Figure 22. a) NEHRP site classification based on the Mdn of the $Vs30$ distribution of each pixel. A similar map could be made with any percentile in the $Vs30$ distribution.

These maps of $Vs30$ distribution parameters show that, in general, in Massachusetts greater depth-to-bedrock yields increased likelihood of low $Vs30$ values. Most of the area in the Boston Basin and the Connecticut River Valley have $Vs30$ distribution Mdn values that are site class D sites. Importantly, since $Vs30$ is represented as a distribution at each location and the uncertainty in that distribution is derived from depth-to-bedrock and shear-wave velocity uncertainty, a percentage of the realizations in each pixel in these basins are site class E. Thus, the true $Vs30$ value at each location still has a chance of being different than the Mdn value in Figure 22. On Cape Cod, the Mdn $Vs30$ value is 371 m/s which corresponds to a site class C. This value is constant across the entire Cape Cod region because the depth-to-bedrock values are all greater than 30 meters and the shear-wave velocity profile is modeled the same across the region. This $Vs30$ value of 371 m/s may be artificially high as it is a function of the layer-over-halfspace overburden velocity model used in Fairchild et al. (2011) (Figures 15, 18). Shallower layers in the geotechnical profile may be lower velocity than this model shows and thus typical $Vs30$ values on Cape Cod may have lower Mdn

values than this study's results indicate. The V_{s30} distributions generated in this study by assuming a bedrock velocity and using the depth and shear-wave velocity information to create a set of shear-wave velocity profiles provides a convenient methodology to obtain regional V_{s30} -based site classifications and their uncertainties.

6.0 Conclusions

The methodology applied in this study is a useful and repeatable way of estimating f_0 across a region. Importantly, it is founded on a high-resolution depth-to-bedrock model that is based on hundreds of thousands of depth-to-bedrock estimates. Given this high density of depth-to-bedrock information and an estimate of its uncertainty paired with power-law shear-wave velocity profiles (based on the $f_0 = az^\beta$ relationship), f_0 is predicted across the state.

In Massachusetts, depth-to-bedrock varies significantly across the region. The f_0 values in the state, therefore, also vary significantly with the depth-to-bedrock. We found that in the Boston Basin, f_0 values typically be as low as 1 Hz in the center of the basin where depth-to-bedrock values can be 60-90m deep and increase towards the basin edge and depth-to-bedrock decreases (Figure 17). This yields *Mdn* site class D sediments in the center of the Basin and site class C to B sediments towards the basin edge. These site classes in the center of the basin, however, may be as low as site class E due to the uncertainty in the shear-wave velocity profile. In the Connecticut River Valley, the maximum depth-to-bedrock values are slightly higher than in the Boston Basin, from 100-120 m, yielding minimum f_0 values below 1 Hz in the center of the Valley. Like in the Boston Basin, as the depth-to-bedrock decreases towards the edges, the f_0 values increase. The 3-dimensional geometries of these two basins, however, are different and therefore knowledge of the spatial distribution of sediments and depth-to-bedrock are essential to seismic hazard analysis. Cape Cod has consistently deep sediments with the deepest being over 500 m on the islands and shallowest being around 60 m at the beginning of the peninsula (Figure 2). These depths yield f_0 values ranging from 0.18 Hz at the lowest and 1.5 Hz at the highest. Unlike the Boston Basin and the Connecticut

River Valley, Cape Cod is not bounded by higher, non-resonant topography and therefore has no tapering of depth-to-bedrock with increasing f_0 values. This means that the $Vs30$ values computed in this study are uniform across the region because depth-to-bedrock never drops below 30 meters. The Boston Basin, Connecticut River Valley, and Cape Cod are the most important regions in Massachusetts in terms of site response and soil resonance, most of the rest of the state (57%) is composed of shallow, non-resonant soil with $Mdn\ Vs30$ values above 760 m/s.

The f_0 , depth-to-bedrock, overburden shear-wave velocity framework is a valuable physical model for understanding site response, particularly in high impedance environments. Given this framework, it is possible to quantify parameter uncertainty by propagating the uncertainty from the depth-to-bedrock model and the shear-wave velocity model into the f_0 map. Additionally, shear-wave velocity profiles can be simulated which allow for the estimate of $Vs30$ that incorporates uncertainty. Attempting to quantify the depth-dimension by aggregating geotechnical and geophysical point data is essential for future study and quantification of site response hazard, and ultimately the better design and construction of more earthquake resilient infrastructure.

CHAPTER 5

Conclusion

This dissertation maps f_0 as a site characterization parameter in New England. f_0 is a good site response parameter because it contains both velocity and depth information of the entire overburden until the impedance contrast. To compare it to the traditional $Vs30$ -based site response framework, each chapter of this dissertation computes suite of shear-wave velocity profiles using different overburden models (layer-over-halfspace and power law velocity profile) and computes $Vs30$, f_0 , and depth-to-bedrock for each profile. $Vs30$ is compared to both f_0 and depth-to-bedrock and it is shown that the three parameters are related to one another; in short, every shear-wave velocity profile with a high impedance contrast has an f_0 , a $Vs30$, and a depth to bedrock. f_0 is less expensive to collect than $Vs30$ and is a value that has a stronger physical basis than $Vs30$. Thus, this dissertation maps f_0 : it very useful and relatively simple to collect in large, spatially distributed datasets and, if one chooses, can be used to estimate $Vs30$ if needed. The same cannot be said for $Vs30$, f_0 cannot be predicted by $Vs30$ if the depth to the impedance contrast is greater than 30 meters. These three parameters are intimately related, but the understanding of the f_0 /depth-to-bedrock/overburden shear-wave velocity relationship is more useful in understanding the site response properties of the overburden than $Vs30$ alone, though $Vs30$ works very well in tandem with these three other parameters.

Chapter 1 of this dissertation establishes an f_0 and a shear-wave velocity dataset of New England. It then uses the Soller et al. (2009) conterminous US surficial geologic map to demonstrate that different geologic units have different f_0 distributions. Using the f_0 distributions in each unit, estimates of $Vs30$ are developed from estimates of Vs_{avg} and the f_0 distributions. This chapter contains the main dataset and fundamental ideas used in this dissertation including the use of f_0 distributions, the estimate of Vs_{avg} and the use of the f_0 distributions and Vs_{avg} to estimate $Vs30$ distributions.

In Chapter 1, it was observed that different local sedimentary deposits have different characteristics even if they have the same geologic classification. Chapter 2 addresses this observation and develops a local sedimentary deposit subregion map to subdivide the f_0 dataset further which significantly reduces the

residuals between the f_0 station measurements and the median of the f_0 distributions in each unit. Additionally, this chapter models Vs_{avg} as a random variable, improving estimates of $Vs30$.

Chapter 3 of this dissertation maps f_0 distributions in Massachusetts using a depth-to-bedrock model and $f_0 - z$ relationships to develop power-law velocity profiles. By Monte Carlo sampling depth as a random variable at each pixel in the depth-to-bedrock and then Monte Carlo sampling the power law velocity profiles to account for shear-wave velocity uncertainty, the methodology of this chapter generates 1,000,000 shear wave velocities at each 100m pixel from which f_0 distributions are computed. This chapter's product is founded on significantly more data than either of the first two chapters (from the 100,000 depth-to-bedrock points used to make the depth-to-bedrock map), making it a more significant fusion of data.

This dissertation makes site characterization maps of New England and Massachusetts using local geophysical and geotechnical data focusing of f_0 , depth to the impedance contrast and overburden shear wave velocity. In doing this, it maps fundamental frequency (f_0) on a regional scale as a site characterization parameter. The methodologies developed to map f_0 in New England quantify parameter uncertainty and can be applied to other areas with similar datasets. Each methodology used in this work characterizes uncertainty in the site response parameters it is using which are shear wave velocity profile uncertainty, depth to bedrock uncertainty and f_0 uncertainty. Using the frameworks developed in this work with larger f_0 and shear-wave velocity datasets, higher resolution geologic maps, and higher resolution depth-to-bedrock models will create increasingly better and better products. This is demonstrated in the sequence of the chapters each of which uses data that increase in mapping resolution and in density of geophysical and geotechnical point data resulting in higher resolution products with lower residuals between model and measurement. While more work needs to be done, the methodologies developed, and data compiled in this dissertation can be used as a foundation for better site characterization parameter mapping in New England that reduces residuals between the map estimate and point measurements and reduces uncertainty in the distribution estimates as point density increases with more data.

APPENDIX A

Supplementary material for Chapter 2

1.0 Attached Data Files

The supplementary material to this paper contains two files, an excel sheet titled “Final_table.xlsx” and a GIS polygon shapefile titled “Final_shapefile.shp”. “Final_table.xlsx” contains the 1577 HVSR stations with the following information:

Table 1. Information contained within the file “Final_table.xlsx”.

Column	Header	Information
A	Latitude	The latitude of the HVSR station
B	Longitude	The longitude of the HVSR station
C	f_0	The f_0 of the HVSR station
D	Unit Code	The unit code of the HVSR station
E	Surficial Geology	The surficial geology of the HVSR station
F	Vs_{avg}	The Vs_{avg} of the HVSR station based on the surficial geology
G	Vs_{30}	The Vs_{30} of the HVSR station
H	Site class	The site class of the HVSR station based on the Vs_{30}

“Final_shapefile.shp” contains a shapefile of the results of the analyses performed on “Final_table.xlsx”. The shapefile itself is composed of the polygons of the surficial geologic units used in this study and the added columns are properties of the distributions of f_0 within each unit. The projected coordinate system is UTM zone 19N. The columns contain the following information:

Table 2. Information contained within the file “Final_shapefile.shp”.

Header	Information
Surf_geo	The surficial geologic unit
Unit_code	The unit code corresponding to the surficial geologic unit used in several figures in the paper
Thickness	The thickness classification from the Soller et al. (2009) map.
Count	The number of HVSR stations in the unit
ln_median	The median of the log-transformed f_0 distribution within the unit.
ln_IQR	The IQR of the log-transformed f_0 distribution within the unit.
ln_per25	The 25th percentile of the log-transformed f_0 distribution within the unit.
ln_per75	The 75th percentile of the log-transformed f_0 distribution within the unit.

ln_mean	The mean of the log-transformed f_0 distribution within the unit.
ln_std	The standard deviation of the log-transformed f_0 distribution within the unit.
nat_median	The median value used in the study, calculated by exponentiating the column "ln_mean".
nat_IQR	The IQR used in the study calculate from nat_75per - nat_25per
nat_25per	Calculated by exponentiating the column "ln_per25"
nat_75per	Calculated by exponentiating the column "ln_per75"
nat_mean	Calculated by exponentiating the column "ln_mean"
nat_std	Calculated by exponentiating the column "ln_std"
Vsavg	The Vs_{avg} value used in the study. See discussion in paper for a discussion on how this value was obtained
Vs30_median	The median of the $Vs30$ distribution within the unit.
Vs30_IQR	The IQR of the $Vs30$ distribution within the unit.

To look at or recreate the HVSR curves or use the raw data, contact the primary author at Marshall.Pontrelli@tufts.edu who will share it with you, and download this [GitHub software package](#). The software package must be placed on the desktop for the programs within the data folder to run. The HVSR curves from the study are copied below with their peak picks in the following general groups:

2.0 The Conterminous US surficial geology map

When the conterminous map of Soller et al. (2009), is clipped to the New England region the resulting map contains 20 surficial geologic units representing 3 different thicknesses, 8 depositional environments and 8 grain sizes (Table 3). Site susceptibility also depends on sediment composition (density, stiffness: Vs) and sediment thickness. In terms of sediment composition which influences soil amplification because of impedance contrasts, most of the New England region is covered by some form of glacial till which we expect to be high velocity and shallow and to exhibit the least site response hazard of the typical surficial geologic units. There are extensive marine clay deposits (classified as “proglacial sediments, fine-grained”) on the coast of Maine down to Boston and along the coast of Lake Champlain in Vermont which we expect to exhibit significant site response hazard. These marine clay deposits on the Maine coast are the “Presumpscot formation”, in the Boston basin they are the “Boston Blue Clay” and on the Lake Champlain coast they are the “Champlain Sea Sediments”. On Cape Cod and Long Island there are extensive “thick

proglacial sediments” that are large, deep terminal moraines that represent the southernmost extent of the Wisconsin glaciation and form the northern edge of the Atlantic Coastal Plain. Finally, a large band of alluvial sediments are in central Massachusetts and Connecticut, bounded by thin proglacial sediments (clay). These are the Connecticut River valley flood-plain alluvial deposits sitting within the Glacial Lake Hitchcock lacustrine clay sediments. These sedimentary units (Presumpscot, Boston Blue Clay, Champlain Sea Sediments, Atlantic Coastal Plain, and Connecticut River sediments) are identified in this study as units with amplification potential and are therefore the focus of our field work.

In terms of sediment thickness, which is another important aspect of site characterization especially as it relates to resonance, the majority of New England consists of “Thin” deposits (less than 100 feet). These thin areas are mostly composed of glacial till. The areas of “Discontinuous deposits” (very shallow or non-existent overburden) are in mountainous areas. The only “Thick” classification (greater than 100 feet) in New England based on the Soller et al. (2009) maps is located on Cape Cod and Long Island (Figure 1b).

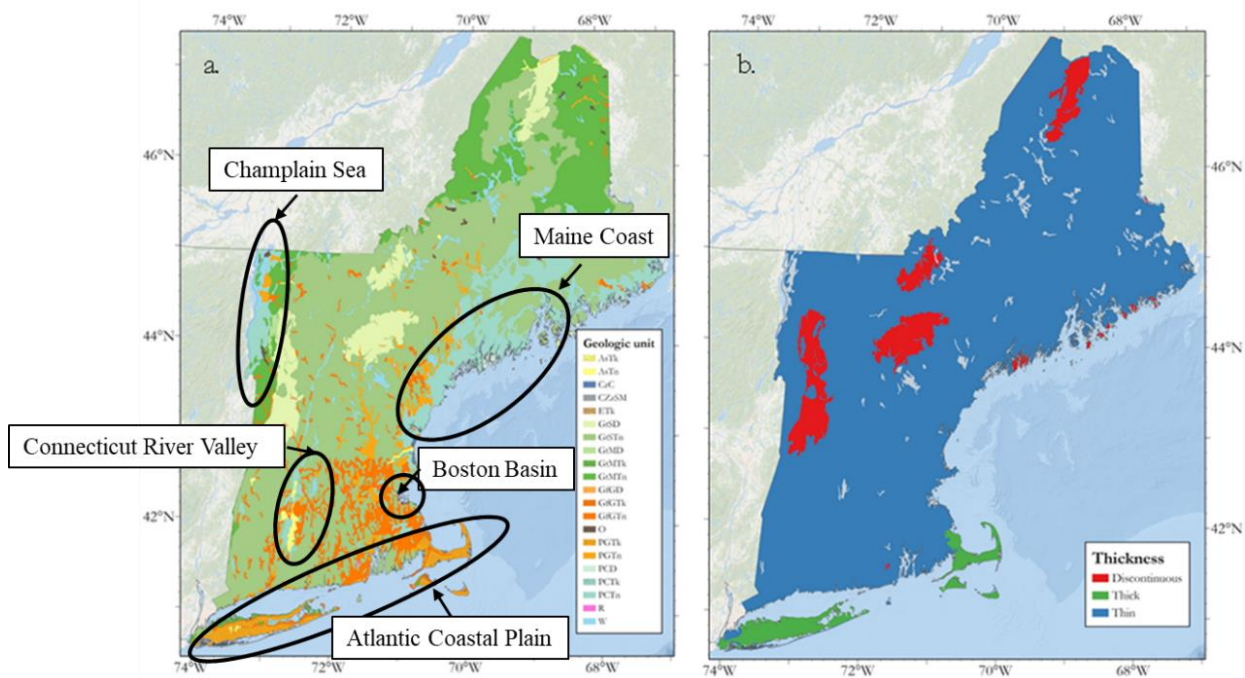


Figure 1. a) Conterminous map of the surficial geology in New England (Soller et al. 2009). The label descriptions are in Table 3. The major regions with amplifiable sedimentary units identified in this study

are labeled. b) Conterminous map overburden thicknesses. The thick overburden classification is entirely on Cape Cod and Long Island, the discontinuous classification is concentrated in the mountainous areas (the Green and White Mountains) as well as on rocky coastlines (Maine coast) and the thin classification covers the rest of New England.

Table 3. Surficial geologic units and their respective labels, thickness, depositional environment, and grain size from the conterminous map (Soller et al. 2009).

Surficial unit	Label	Thickness	Depositional environment	Grain size
Alluvial sediments, thick	AsTk	Thick	Alluvial	-
Alluvial sediments, thin	AsTn	Thin	Alluvial	-
Coastal zone sediments, mostly fine-grained	CzC	Thin	Coastal	Mostly fine-grained
Coastal zone sediments, mostly medium-grained	CzSM	Thin	Coastal	Mostly medium-grained
Eolian sediments, mostly dune sand, thick	ETk	Thick	Eolian	Mostly dune sand
Glacial till sediments, mostly sandy, discontinuous	GtSD	Discontinuous	Glacial till	Mostly sandy
Glacial till sediments, mostly sandy, thin	GtSTn	Thin	Glacial till	Mostly sandy
Glacial till sediments, mostly silty, discontinuous	GtMD	Discontinuous	Glacial till	Mostly silty
Glacial till sediments, mostly silty, thick	GtMTk	Thick	Glacial till	Mostly silty
Glacial till sediments, mostly silty, thin	GtMTn	Thin	Glacial till	Mostly silty
Glaciofluvial ice-contact sediments, mostly sand and gravel, discontinuous	GfGD	Discontinuous	Glaciofluvial	Mostly sand and gravel
Glaciofluvial ice-contact sediments, mostly sand and gravel, thick	GfGTk	Thick	Glaciofluvial	Mostly sand and gravel
Glaciofluvial ice-contact sediments, mostly sand and gravel, thin	GfGTn	Thin	Glaciofluvial	Mostly sand and gravel
Organic-rich muck and peat, thin	O	Thin	Organic-rich muck and peat	Peat
Proglacial sediments, mostly coarse-grained, thick	PGTk	Thick	Proglacial	Mostly coarse-grained
Proglacial sediments, mostly coarse-grained, thin	PGTn	Thin	Proglacial	Mostly coarse-grained
Proglacial sediments, mostly fine grained, discontinuous	PCD	Discontinuous	Proglacial	Mostly fine-grained
Proglacial sediments, mostly fine grained, thick	PCTk	Thick	Proglacial	Mostly fine-grained
Proglacial sediments, mostly fine grained, thin	PCTn	Thin	Proglacial	Mostly fine-grained
Residual materials developed in igneous and metamorphic rocks	R	Discontinuous	Residual materials	-
Water	W	-	-	-

2.1 Grouping the US Conterminous surficial geology map

Beginning with the conterminous US map (Soller et al., 2009) clipped to the New England region including Long Island (Figure 1a), we perform a spatial join with the HVSR database, count the number of f_0 stations in each surficial unit, and develop a distribution of f_0 within each unit (Table 4). Only the top 8 units from the spatial join have enough f_0 stations from which a distribution can be confidently developed. To account for the surficial units without many f_0 stations (the bottom 12 units in Table 4), all of which have relatively small area, we combined them into the categories of the top 8 units which have enough f_0 stations. Table 5 shows how we group and rename the units in Table 3. All the “thick” surficial geologic units without many points are located on Cape Cod or Long Island. These thick units likely have similar amplifying characteristics (depth and shear-wave velocities) to the rest of the units on Cape Cod and Long Island. Thus, we combine “proglacial sediments, mostly fine-grained, thick”, “Alluvial sediments, thick”, “Glacial till sediments, mostly silty, thick”, “Eolian sediments, mostly dune sand, thick” and “Proglacial sediments, mostly coarse grained, thick” into one category. We categorize both the thin and discontinuous glacial till with “glacial till sediments, mostly sandy, thin” because all the thin glacial till units likely have high velocities and are thin deposits. We categorize “coastal zone sediments, mostly medium-grained” and “coastal zone sediments mostly fine-grained” together since both are coastal zone sediments and are likely to have similar ground amplification characteristics. We also keep “residual materials, developed in igneous and metamorphic rock” and “organic-rich muck and peat” (Soller et al. 2009) as their own categories even though there are no f_0 stations within their areas, because they cover a very small area on the map and have interpretable site response characteristics from their geology and leave these units unmapped in the electronic supplement (Final_shapefile.shp). With these new geologic classifications (Figure 2), we perform another spatial join and calculate the number of stations, and the f_0 distributions of each new grouped unit.

Table 4. Surficial geologic units spatial joined to the f_0 stations with f_0 medians and IQR values calculated describing the central tendency and dispersion of the distribution of f_0 points within each unit.

Surficial unit	Thickness	Depositional environment	Grain size	# Stations	Median (Hz)	IQR (Hz)
Glaciofluvial ice-contact sediments, mostly sand and gravel, thin	Thin	Glaciofluvial	Mostly sand and gravel	461	4.00	6.60
Proglacial sediments, mostly fine grained, thin	Thin	Proglacial	Mostly fine-grained	381	2.70	3.65
Glacial till sediments, mostly sandy, thin	Thin	Glacial till	Mostly sandy	353	6.25	10.30
Proglacial sediments, mostly coarse-grained, thick	Thick	Proglacial	Mostly coarse-grained	174	1.03	0.32
Proglacial sediments, mostly coarse-grained, thin	Thin	Proglacial	Mostly coarse-grained	74	3.70	3.47
Alluvial sediments, thin	Thin	Alluvial	-	62	1.83	1.59
Glaciofluvial ice-contact sediments, mostly sand and gravel, thick	Thick	Glaciofluvial	Mostly sand and gravel	32	1.06	0.23
Coastal zone sediments, mostly fine-grained	Thin	Coastal	Mostly fine-grained	26	3.31	1.60
Glacial till sediments, mostly sandy, discontinuous	Discontinuous	Glacial till	Mostly sandy	4	2.75	2.01
Proglacial sediments, mostly fine grained, thick	Thick	Proglacial	Mostly fine-grained	3	0.48	0.04
Alluvial sediments, thick	Thick	Alluvial	-	2	0.46	0.08
Glacial till sediments, mostly silty, thick	Thick	Glacial till	Mostly silty	2	0.89	0.16
Glacial till sediments, mostly silty, thin	Thin	Glacial till	Mostly silty	2	3.17	0.25
Eolian sediments, mostly dune sand, thick	Thick	Eolian	Mostly dune sand	1	0.53	0.00
Coastal zone sediments, mostly medium-grained	Thin	Coastal	Mostly medium-grained	0	-	-
Glacial till sediments, mostly silty, discontinuous	Discontinuous	Glacial till	Mostly silty	0	-	-

Glaciofluvial ice-contact sediments, mostly sand and gravel, discontinuous	Discontinuous	Glaciofluvial	Mostly sand and gravel	0	-	-
Organic-rich muck and peat, thin	Thin	Organic-rich muck and peat	Peat	0	-	-
Proglacial sediments, mostly fine grained, discontinuous	Discontinuous	Proglacial	Mostly fine-grained	0	-	-
Residual materials developed in igneous and metamorphic rocks	Discontinuous	Residual materials		0	-	-

Table 5. Surficial geologic unit grouping based on the number of f_0 stations in the different units and the unit's location and geology. Each of these new names is represented by its "Unit Code" in the rest of the figures and tables.

New surficial name	Surficial unit groups	Thickness
Glaciofluvial ice-contact sediments, thin	Glaciofluvial ice-contact sediments, mostly sand and gravel, thin; Glaciofluvial ice-contact sediments, mostly sand and gravel, discontinuous	Thin
Proglacial sediments, fine grained, thin	Proglacial sediments, mostly fine grained, thin; Proglacial sediments, mostly fine grained, discontinuous	Thin
Glacial till	Glacial till sediments, mostly sandy, thin; Glacial till sediments, mostly sandy, discontinuous; Glacial till sediments, mostly silty, thin; Glacial till sediments, mostly silty, discontinuous	Thin
Proglacial sediments, thick	Proglacial sediments, mostly coarse-grained, thick; Proglacial sediments, mostly fine grained, thick; Alluvial sediments, thick; Glacial till sediments, mostly silty, thick; Eolian sediments, mostly dune sand, thick	Thick
Proglacial sediments, coarse grained, thin	Proglacial sediments, mostly coarse-grained, thin	Thin
Alluvial sediments, thin	Alluvial sediments, thin	Thin
Glaciofluvial ice-contact sediments, thick	Glaciofluvial ice-contact sediments, mostly sand and gravel, thick	Thick
Coastal zone sediments	Coastal zone sediments, mostly fine-grained; Coastal zone sediments, mostly medium-grained	Thin
Organic-rich muck and peat, thin	Organic-rich muck and peat, thin	Thin
Residual materials	Residual materials developed in igneous and metamorphic rocks	Thin

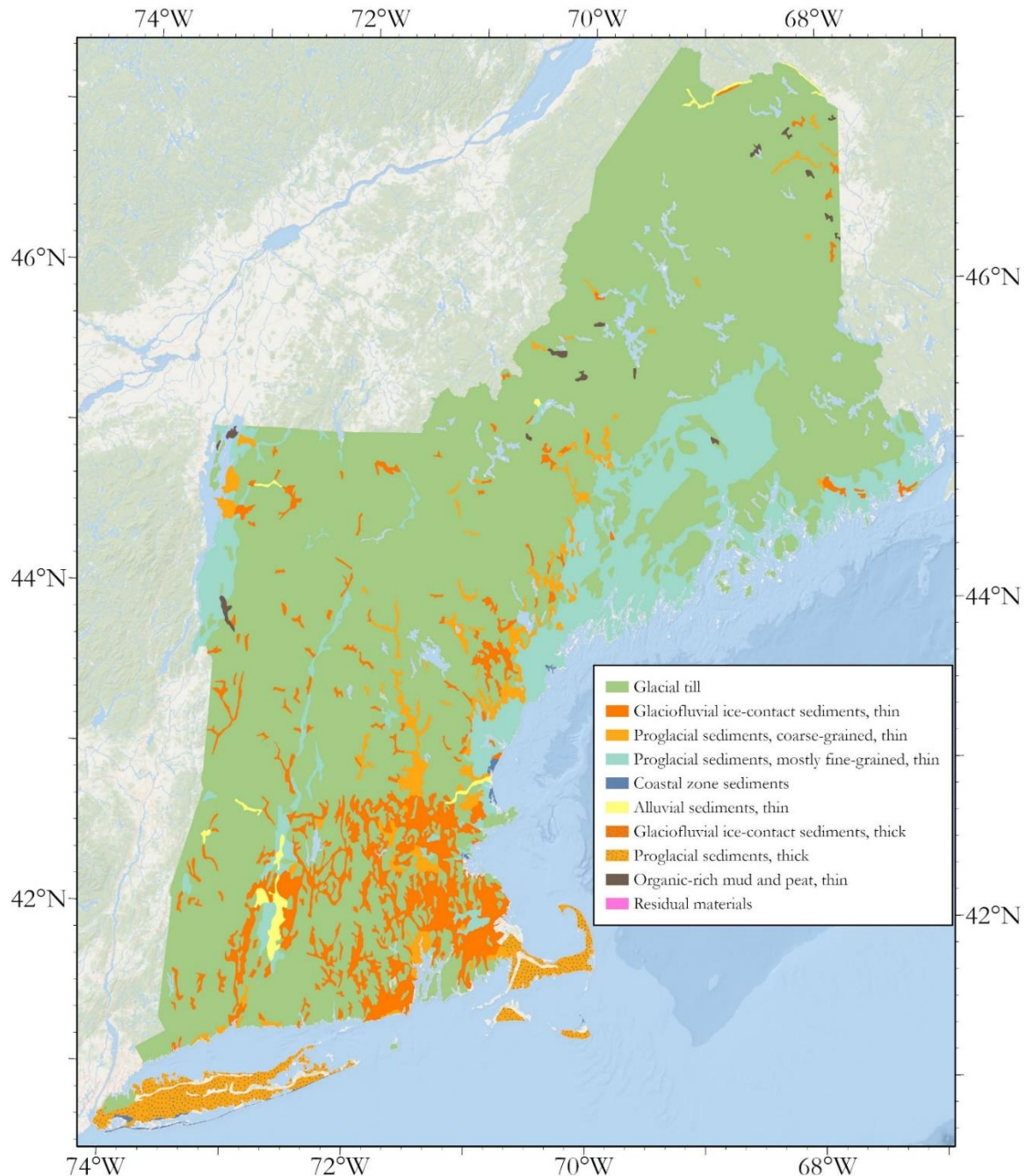


Figure 2. Merged geologies based on Table 5.

APPENDIX B

Supplementary material for Chapter 3

1.0 Data sources

Beginning with the geologic maps, the Soller et al. (2009) shapefile (which is used for the state of New Hampshire in this study) can be downloaded [here](#). The Massachusetts state geologic map (Stone et al. 2018) can be downloaded [here](#). The Maine state geologic map (Thompson, 1985) can be downloaded [here](#). The Vermont state geologic map (Doll, 1970) can be downloaded [here](#). The Connecticut state geologic map (Stone et al. 1992) can be downloaded [here](#). The Rhode Island state geologic map (RIGIS) can be downloaded [here](#). The New York state geologic map (Cadwell, 1986) can be downloaded [here](#). The SRTM Digital Elevation Model used in this study can be downloaded from the USGS earth explorer page [here](#).

The shear wave velocity profiles in this study were digitized from Lens and Springston (2013), Thompson et al. (2014), and Hager Geosciences (2016) (which was published in Mabee et al. (2018)), and were collected in Pontrelli et al. (2023a). You may request the digital profiles from the first author. See his contact information below.

The f_0 data for this study comes from Pontrelli et al. 2023a, Yilar et al. (2017), Fairchild et al. (2013) and Mabee (2022). All the f_0 points and their latitude and longitude are in the attached table “Final_Table.xlsx” which is described below. The raw microtremor data for the f_0 points from Pontrelli et al. (2023a) can be obtained upon request from the first author along with the tools needed to compute the HVSR curves and select the fundamental peak. The f_0 data from Fairchild (2013) can be downloaded [here](#). It is in “Final_Table.xlsx”. The f_0 data from Mabee (2022) is in review but will be published as a companion to a depth-to-bedrock model being developed in the state. These data are in “Final_Table.xlsx”. The f_0 data from Yilar et al. (2017) is available in “Final_Table.xlsx”.

To request more specific data (such as raw microtremor data, MASW data, HVSR curves, S-wave profiles, the clipped digital elevation model etc.), contact the primary author at Marshall.Pontrelli@tufts.edu who will share with you what you would like to see.

1.1 Attached Data Files

The supplementary material to this paper contains two files, an excel sheet titled “Final_Table.xlsx” and a GIS polygon shapefile titled “Final_shapefile.shp”. “Final_Table.xlsx” contains the 1619 HVSR stations with the following information:

Table 1. Information contained within the file “Final_table.xlsx”.

Column	Header	Information
A	Station_de	Description of the station
B	Latitude	The latitude of the HVSR station
C	Longitude	The longitude of the HVSR station
D	Frequency_Hz	The f_0 of the HVSR station in Hz
E	Geo_code	The geo code of the HVSR station
F	Geo_unit	The surficial geologic unit of the HVSR station
G	Subregion_code	The subregion code of the HVSR station
H	Subregion	The Subregion of the HVSR station

“Final_table.xlsx” contains all the information necessary to recreate Figures 4a (the f_0 station locations), 6b, 7, 10, 11, and all of Table 4.

“Final_shapefile.shp” contains a shapefile of the results of the analyses performed on “Final_table.xlsx”. The shapefile itself is composed of the polygons of the surficial geologic units and subregion units used in this study and the added columns are properties of the distributions of f_0 , $V_{S_{avg}}$, and V_{S30} within each unit. The projected coordinate system is UTM zone 19N. The columns contain the following information:

Table 2. Information contained within the file “Final_shapefile.shp”. “Final_shapefile.shp” contains all of the information in Table 4 of the paper.

Header	Information
Geo_Code	The surficial geologic unit code
Geo	The surficial geologic unit
Subregion	The subregion
Subregion_code	The subregion code
# sta	The number of stations used in the distribution parameter estimation. Note, that many of these are soft geology groupings (indicated with a “*” in Table 4) or NEG till distributions (indicated with a “†” in Table 4) and thus have the same number of stations and the same distribution characteristics.

f0_mu	The μ_{ln} value of the f_0 distribution for the unit
f0_sig	The σ_{ln} value of the f_0 distribution for the unit
f0_Mdn	The Mdn value of the f_0 distribution for the unit. This is equal to $\exp(\mu_{ln})$.
Vs_avg_mu	The μ_{ln} value of the Vs_{avg} distribution for the unit
Vs_avg_sig	The σ_{ln} value of the Vs_{avg} distribution for the unit
Vs_avg_Mdn	The Mdn value of the Vs_{avg} distribution for the unit. This is equal to $\exp(\mu_{ln})$.
Vs30_mu	The μ_{ln} value of the $Vs30$ distribution for the unit
Vs30_sig	The σ_{ln} value of the $Vs30$ distribution for the unit
Vs30_Mdn	The Mdn value of the $Vs30$ distribution for the unit. This is equal to $\exp(\mu_{ln})$.
Area	The area (in km^2) of the unit. For grouped units, this value is the sum of the areas of the units making up the grouping.
sta_per_area	The station density (# stations/Area) for the unit. This is used to make Figure 13b

“Final_shapefile.shp” contains all the information necessary to recreate Figures 1b, 2a, 3e, 6a, 12, 13, 14, 15, and the attribute table can be used to recreate Figure 16.

APPENDIX C

Supplementary material for Chapter 4

1.0 Data sources

The Mabee et al. 2023 depth-to-bedrock data on which this paper is primarily based can be downloaded [here](#) and the summary of the project on the Massachusetts Geological Survey website can be found [here](#). The dataset contains both the output depth-to bedrock and uncertainty rasters and the raw point depths used to make those rasters.

To request more specific data contact the author at Marshall.Pontrelli@tufts.edu who will share with you what you would like to see.

1.1 Attached Data Files

The supplementary material to this paper contains 15 files, 7 raster datasets and MATLAB files containing matrices that can be converted to the raster datasets. The data and the information they contain are described in Table 1

Table 1. Information contained within the data folder.

Filename	Data type	Information
f0_Mdn	Raster (.tif)	$f_0 Mdn$ output in Figure 17 (Hz)
f0_Mdn_mat	MATLAB file (.mat)	MATLAB matrix of the $f_0 Mdn$ output
f0_mean	Raster (.tif)	$f_0 \mu_{ln}$ output in Figure 16a
f0_mean_mat	MATLAB file (.mat)	MATLAB matrix of the $f_0 \mu_{ln}$ output
f0_std	Raster (.tif)	$f_0 \sigma_{ln}$ output in Figure 16b
f0_std_mat	MATLAB file (.mat)	MATLAB matrix of the $f_0 \sigma_{ln}$ output
mask	Raster (.tif)	Mask of f_0 maps using the criteria in section 3.4 and Table 3. A value of 1 means likely resonant area, a value of 0 means likely not a resonant area
mask	MATLAB file (.mat)	MATLAB matrix of the resonant sediment mask.
R_mat	MATLAB file (.mat)	Coordinate system MATLAB matrix
Vs30_Mdn	Raster (.tif)	$f_0 Mdn$ output in Figure 22 (m/s)
Vs30_Mdn_mat	MATLAB file (.mat)	MATLAB matrix of the $Vs30 Mdn$ output
Vs30_mean	Raster (.tif)	$Vs30 \mu_{ln}$ output in Figure 21a
Vs30_mean_mat	MATLAB file (.mat)	MATLAB matrix of the $Vs30 \mu_{ln}$ output
Vs30_std	Raster (.tif)	$Vs30 \sigma_{ln}$ output in Figure 21b
Vs30_std_mat	MATLAB file (.mat)	MATLAB matrix of the $Vs30 \sigma_{ln}$ output

References

Alireza, A., Tiefenbacher, J.P., Blaschke, T., Pradhan, B., Bui, D.T. (2020) Morphometric Analysis for Soil Erosion Susceptibility Mapping Using Novel GIS-Based Ensemble Model. *Remote Sensing* (Basel, Switzerland), vol. 12, no. 5, 2020, p. 874–, <https://doi.org/10.3390/rs12050874>.

Abrahamson, N.A., Silva, W.J., Kamai, R. (2014) Summary of the ASK14 Ground Motion Relation for Active Crustal Regions. *Earthquake Spectra* 2014; 30 (3): 1025–1055. doi: <https://doi.org/10.1193/070913EQS198M>

Assaf, J., Molnar, S., El Naggar, M. H., Sirohey, A. (2022) Seismic site characterization in Fraser River Delta in Metropolitan Vancouver. *Soil Dynamics and Earthquake Engineering*. Volume 161 doi: <https://doi.org/10.1016/j.soildyn.2022.107384>

Baise, L. G., Kaklamanos, J., Berry, B.M., Thompson, E.M. (2016). Soil Amplification with a strong impedance contrast: Boston Massachusetts. *Engineering Geology* 202 (2016) 1-13.

Becker, L.R., Fratto, E.S., Patriarco, S.P., Marvinney, R.G., Mabee, S.B., Thomas, M.A. (2011) Utilizing the Surficial Geology of the Northeast United States to Improve NEHRP Site Effect Classifications in HAZUS-MH: Collaborative Research with NESEC and the NESEC State Geologists. U.S Geological Survey National Earthquake Hazard Reduction Program Award No. G10AP00014.

Boore, D. M. (2005). SMSIM-Fortran Programs for Simulating Ground Motion from Earthquakes: Version 2.3-A of OFR 96-80-A. United States Department of the Interior. U. S Geological Survey.

Borcherdt, R.D., (1970). Effects of Local Geology on Ground Motion Near San Francisco Bay. *Bulletin of the Seismological Society of America*. Vol. 60, No. 1, pp. 29-61.

Borcherdt, R. D. (1991a). On the observation, characterization, and predictive GIS mapping of strong ground shaking for seismic zonation - A case study for San Francisco Bay region, *Bull. New Zealand Nat'l. Soc. Earthquake Engineering*, 24,287-305

Borcherdt, R.D. (1992). Simplified site classes and empirical amplification factors for site-dependent code provisions. NCEER, SEAOC, BSSC workshop on site response during earthquakes and seismic code provisions, Univ. Southern California, Los Angeles, California, Nov. 1992.

Borcherdt, R.D. (1994). Estimates of Site-Dependent Response Spectra for Design (Methodology and Justification). *Earthquake Spectra*, Vol 10, No. 4, 1994.

Braganza, S., Atkinson, G.M., Ghofrani, H., Hassani, B., Chouinard, L., Rosset, P., Motazedian, D., Hunter, J; Modeling Site Amplification in Eastern Canada on a Regional Scale. *Seismological Research Letters* 2016;; 87 (4): 1008–1021. doi: <https://doi.org/10.1785/0220160009>

Building Seismic Safety Council, 1995, NEHRP recommended provisions for seismic regulations for new buildings, 1994 edition: Federal Emergency Management Agency, FEMA 222A Report.

Cadwell, D.H. (1986) Surficial Geologic Map of New York. New York State Museum Map and Chart Series.

Cadwell, D.H., 2003, Generalized NEHRP Soil Site Classifications – 2003 Preliminary Recommendations to New York State Emergency Management Office, NYSGsurficialNEHRP.txt.

Carpenter, N.S., Wang, Z., Woolery, E.W., Rong, M (2018) Estimating Site Response with Recordings from Deep Boreholes and HVSR: Examples from the Mississippi Embayment of the Central United

States. *Bulletin of the Seismological Society of America* 2018; 108 (3A): 1199–1209. doi: <https://doi.org/10.1785/0120170156>

Chiou, B.J., Youngs, R.R. (2008) An NGA Model for the Average Horizontal Component of Peak Ground Motion and Response Spectra. *Earthquake Spectra*. 2008;24(1):173–215. doi:10.1193/1.2894832

Chao, S.H., Lin, C.M., Kuo C.H., Huang J.Y., Wen K.L., Chen Y.H. (2020) Implementing horizontal-to-vertical Fourier spectral ratios and spatial correlation in a ground-motion prediction equation to predict site effects. *Earthquake Spectra*. 2021;37(2):827–856. doi:10.1177/8755293020952449

Coleman, J. L., Jr., Cahan, S. M. (2012). Preliminary catalog of the sedimentary basins of the United States, USGS Open-File Report 2012–1111, U.S. Geological Survey.

Dávila-Hernández, S.; González-Trinidad, J.; Júnez-Ferreira, H.E.; Bautista-Capetillo, C.F.; Morales de Ávila, H.; Cázares Escareño, J.; Ortiz-Letechipia, J.; Robles Rovelo, C.O.; López-Baltazar, E.A. (2022) Effects of the Digital Elevation Model and Hydrological Processing Algorithms on the Geomorphological Parameterization. *Water* 2022, 14, 2363. <https://doi.org/10.3390/w14152363>

Delgado, J., López Casado, C., Giner, J., Estévez, A., Cuenca, A., Molina, S. (2000) Microtremors as a geophysical exploration tool: Applications and limitations. *Pure and Applied Geophysics*, 157: 1445–1462, 2000.

Doll, C.G., Stewart, D.P., MacClintock, P. (1970) Surficial Geologic Map of Vermont. Vermont Geological Survey.

Fairchild, G.M., Lane, J.W., Jr., Voytek, E.B., and LeBlanc, D.R., 2013, Bedrock topography of western Cape Cod, Massachusetts, based on bedrock altitudes from geologic borings and analysis of ambient seismic noise by the horizontal-to-vertical spectral-ratio method: U.S. Geological Survey Scientific Investigations Map 3233.

Farr, T.G., and Kobrick, M., 2000, Shuttle Radar Topography Mission produces a wealth of data: *EOS Trans.*, v. 81, p. 583–585.

Foster, K.M., Bradley, B.A., McGann, C.R., Wotherspoon, L.M. (2019) A VS30 Map for New Zealand Based on Geologic and Terrain Proxy Variables and Field Measurements. *Earthquake Spectra*. 2019;35(4):1865–1897. doi:10.1193/121118EQS281M

Gallipoli, M.R., Mucciarelli, M (2009) Comparison of Site Classification from VS₃₀, VS₁₀, and HVSR in Italy. *Bulletin of the Seismological Society of America* 2009; 99 (1): 340–351. doi: <https://doi.org/10.1785/0120080083>

Ghofrani, H., Atkinson, G.M. (2014) Site condition evaluation using horizontal-to-vertical response spectral ratios of earthquake in the NGA-West 2 and Japanese databases. *Soil Dynamics and Earthquake Engineering* Volume 67, pp. 30-43 doi. <https://doi.org/10.1016/j.soildyn.2014.08.015>

Gilbert, J.T., MacFarlane, W.W., Wheaton, J.M. (2016) The Valley Bottom Extraction Tool (V-BET): A GIS Tool for Delineating Valley Bottoms Across Entire Drainage Networks.” *Computers & Geosciences*, vol. 97, 2016, pp. 1–14, <https://doi.org/10.1016/j.cageo.2016.07.014>.

Goulet CA, Bozorgnia Y, Abrahamson NA, et al. (2018) Central and eastern North America ground-motion characterization—NGA-East final report. PEER report 2018/08. Berkeley, CA: Pacific Earthquake Engineering Research Center.

Goulet CA, Bozorgnia Y, Kuehn N, et al. (2017) NGA-East ground-motion models for the U.S. Geological Survey National Seismic Hazard Maps. PEER report no. 2017/03. Berkeley, CA: Pacific Earthquake Engineering Research Center.

Hager Geosciences (2016) Shear wave velocity data and analyses, Appendix B.

Haskell N. A. (1953) The dispersion of surface waves on multilayered media. *Bulletin of the Seismological Society of America*; 72:17–34.

Haskell, N. A. (1960). Crustal Reflection of Plane SH Waves. *Geophysical Research* 65(12): 4147-4150.

Hassani, B., Atkinson, G.M. (2016) Applicability of the Site Fundamental Frequency as a VS_{30} Proxy for Central and Eastern North America. *Bulletin of the Seismological Society of America* 2016; 106 (2): 653–664. doi: <https://doi.org/10.1785/0120150259>

Heath DC, Wald DJ, Worden CB, Thompson EM, Smoczyk GM. A global hybrid VS_{30} map with a topographic slope-based default and regional map insets. *Earthquake Spectra*. 2020;36(3):1570-1584. doi:10.1177/8755293020911137

Ibs-von Seht, M., Wohlenberg, J. (1999) Microtremor measurements used to map thickness of soft sediments. *Bulletin of the Seismological Society of America*, 88(1):250–259, 1999

Johnson, E.G. (1989) Geotechnical Characteristic of the Boston Area. Civil Engineering Practice. Vol 4 No 1-06.

Kramer, S.L. (1996). *Geotechnical Earthquake Engineering*, Prentice Hall, Upper Saddle River, N.J.

Kwak, D.Y., Seyhan, E. (2020) Two-stage nonlinear site amplification modeling for Japan with VS_{30} and fundamental frequency dependency. *Earthquake Spectra*. 2020;36(3):1359-1385. doi:10.1177/8755293020907920

Kwak, D.Y., Stewart, J.P., Mandokhail, S.J., Park, D. (2017) Supplementing VS_{30} with H/V Spectral Ratios for Predicting Site Effects. *Bulletin of the Seismological Society of America* 2017;; 107 (5): 2028–2042. doi: <https://doi.org/10.1785/0120160353>

Lawson, A.C., chairman, (1908) The California Earthquake of April 18, 1906: Report of the State Earthquake Investigation Commission: Carnegie Institution of Washington Publication 87, 2 vols.

Lens, J.E., Springston, G.E. (2013) Report on the Comparison of Shear Wave Velocity Measurements with Multispectral Analysis of Surface Waves (MASW) along with the Microtremor Array Method (MAM), Seismic Cone Penetration Tests (SCPT), and Standard Penetration Tests (SPT) for the Burlington and Colchester, Vermont USGS 7-1/2 Minute Quadrangles. Vermont Geological Survey.

Le Pense, S., Gatmiri, B., Maghoul, P. (2011) Influence of soil properties and geometrical characteristics of sediment-filled valleys on earthquake response spectra. *Proceedings of the 8th International Conference on Structural Dynamics*. ISBN 978-90-760-1931-4

Lermo J. Chávez-Garcia F. J. (1993). Site effects evaluation using spectral ratios with only one station, *Bull. Seismol. Soc. Am.* 84, 1350–1364

Mabee, S.B., Duncan, C.C. (2017), Preliminary NEHRP soil classification map of Massachusetts – Appendix B Hager Geoscience Shear Wave Velocity Data and Analyses. Prepared for the Massachusetts Emergency Management Agency and Federal Emergency Management Agency, 232 p.

Mabee, S.B., C.C. Duncan, W.P. Clement, and M. Pontrelli, 2023, Massachusetts depth to bedrock project: Massachusetts Geological Survey Technical Report TR 23-01, 172 p.

Mabee, S.B., Clement, W.P., Duncan, C., Pope, M., Moynahan, K., Miller, R., Davis, H., Low, A. (2022). A Data Set of Depth to Bedrock Describers in Drill Holes and Geophysical Surveys for Massachusetts – Release 1. *In review*.

Marvinney, R.G., Glover, H. (2015) The influence of the Presumpscot Formation on seismic hazard in southern coastal Maine. Maine Geological Survey.

MathWorks, (2022). Signal Processing Toolbox: User's Guide (R2021b). <https://www.mathworks.com/help/signal/ref/findpeaks.html>

Mori, F., Mendicelli, A., Moscatelli, M., Romagnoli, G., Peronace, E., Naso, G. (2020b). A new Vs30 map for Italy based on the seismic microzonation dataset. *Engineering Geology* 275 (2020) 105745 <https://doi.org/10.1016/j.enggeo.2020.105745>

Motazedian, D., Hunter, J.A., Belvau, M., Rosset, P. (2010) Seismic Microzonation of Montreal and Ottawa, Canada (2010) 9th US National and 10th Canadian Conference on Earthquake Engineering 2010: Paper No 1594.

Motazedian D., Torabi H., Hunter, J.A., Crow, H., Pyne, M. (2020) Seismic site period studies for nonlinear soil in the city of Ottawa, Canada. *Soil Dynamics and Earthquake Engineering* 136(2):106205. <http://dx.doi.org/10.1016/j.soildyn.2020.106205>

Nakamura, Y. (1989) A Method for Dynamic Characteristics Estimation of Subsurface using Microtremor on the Ground Surface. *Railway Technical Research Institute* 30(1): 25-33.

NASA Shuttle Radar Topography Mission (SRTM) (2013). Shuttle Radar Topography Mission (SRTM) Global. Distributed by OpenTopography. <https://doi.org/10.5069/G9445JDF>. Accessed: 2022-09-18

Nazarian, S., Stokoe, K. H. II and Hudson, W. R. 1983. Use of spectral analysis of surface waves method for determination of moduli and thicknesses of pavement systems, *Transp. Res.*, 930, 38–45.

Nweke, C. C., Stewart, J. P., Brandenberg, S. J. (2020). Site response of southern California sedimentary basins and other geomorphic provinces. Report GIRS-2020-12202012. Los Angeles, CA: B. John Garrick Risk Institute, Natural Hazards Risk and Resiliency Research Center, UCLA. DOI: 10.34948/N3159F

Olafsdóttir, E.A., Erlingsson, S., & Bessason, B. (2017). Tool for analysis of MASW field data and evaluation of shear wave velocity profiles of soils. *Canadian Geotechnical Journal*. Published on the web 11 July 2017, <https://doi.org/10.1139/cgj-2016-0302>

Pacific Earthquake Engineering Research Center (PEER) (2015a) NGA-East: Median ground-motion models for central and eastern North America. PEER report no. 2015/04. Berkeley, CA: PEER, University of California.

Pacific Earthquake Engineering Research Center (PEER) (2015b) NGA-East: Adjustments to median ground-motion models for central and eastern North America. PEER report 2015/08. Berkeley, CA: PEER.

Park, C.B., Miller, R.D., and Xia, J., 1999, Multichannel analysis of surface waves (MASW); *Geophysics*, 64, 800-808.

Parker, G.A., Harmon, J.A., Stewart, J.P., Hashash, Y.M.A., Kottke, A.R., Rathje, E.M., Silva, W.J., Campbell K.W. (2017) Proxy-Based VS30 Estimation in Central and Eastern North America. *Bulletin of the Seismological Society of America* 2017;; 107 (1): 117–131. doi: <https://doi.org/10.1785/0120160101>

Parolai, S., Bormann, P., Milkereit, C., (2002). New Relationships between Vs, Thickness of Sediments, and Resonance Frequency Calculated by the H/V Ratio of Seismic Noise for the Cologne Area (Germany). *Bulletin of the Seismological Society of America*, Vol. 92, No. 6, pp. 2521–2527, August 2002.

Pinilla-Ramos, C., Abrahamson, N., Kayen, R (2022) Estimation of Site Terms in Ground-Motion Models for California Using Horizontal-to-Vertical Spectral Ratios from Microtremor. *Bulletin of the Seismological Society of America* 2022; 112 (6): 3016–3036. doi: <https://doi.org/10.1785/0120220033>

Pitilakis, K., Riga, E., Anastasiadis, A., Fotopoulou, S., Karafagka, S. (2019) Towards the revision of EC8: Proposal for an alternative site classification scheme and associated intensity dependent spectral amplification factors. *Soil Dynamics and Earthquake Engineering*. 126(2019): <https://doi.org/10.1016/j.soildyn.2018.03.030>

Pontrelli, M.A., Baise, L.G., Ebel, J.E. (2023a) Regional-Scale Site Characterization Mapping in High Impedance Environments Using Soil Fundamental Resonance (f_0): New England, USA. *Engineering Geology* Volume 315. doi: <https://doi.org/10.1016/j.enggeo.2023.107043>

Pontrelli, M.A., Basie, L.G., Ebel, J.E. (2023b) Mapping Fundamental Frequency (f_0) as a Site Response Parameter Using a Multi-Scale Approach with State-Level Surficial Geologic Maps and Local Sedimentary Deposit Information. Available at SSRN: <https://ssrn.com/abstract=4435102> or <http://dx.doi.org/10.2139/ssrn.4435102>

Rashidian, V., Baise, L.G., (2020), Regional Efficacy of a global geospatial liquefaction model. *Engineering Geology* Volume 272 doi. <https://doi.org/10.1016/j.enggeo.2020.105644>

RIGIS, (1989) Rhode Island Glacial Deposits; Rhode Island Geographic Information System (RIGIS) Data Distribution System, URL: <http://www.rigis.org>, Environmental Data Center, University of Rhode Island, Kingston, Rhode Island (last date accessed: 30 September 2014)

Schleicher, L.S., Pratt, T.L. (2021) Characterizing Fundamental Resonance Peaks on Flat-Lying Sediments Using Multiple Spectral Ratio Methods: An Example from the Atlantic Coastal Plain, Eastern United States. *Bulletin of the Seismological Society of America* 2021;; 111 (4): 1824–1848. doi: <https://doi.org/10.1785/0120210017>

Seed, H. B., Wong, R. T., Idriss, I. M., Tokimatsu, K. (1986), Moduli and Damping Factors for Dynamic Analyses of Cohesionless Soils, *J. Geotech. Eng.* 112, 1016–1032.

SESAME (2004a). Guidelines for the implementation of the H/V spectral ratio technique on ambient vibrations. European Commission - Research General Directorate.

SESAME (2004b). Site Effects Assessment Using Ambient Excitations. European Commission - Research General Directorate. Project No. EVG1-CT-2000-00026 SESAME.

Sheriff, R.E., Geldart, L.P. (1995). *Exploration Seismology*, Second Edition. Cambridge University Press.

Soller, D.R., Reheis, M.C., Garrity, C.P., and Van Sistine, D.R., 2009, Map database for surficial materials in the conterminous United States: U.S. Geological Survey Data Series 425, scale 1:5,000,000 [<https://pubs.usgs.gov/ds/425/>].

Stewart JP, Parker GA, Atkinson GM, Boore DM, Hashash YMA, Silva WJ. Ergodic site amplification model for central and eastern North America. *Earthquake Spectra*. 2020;36(1):42-68. doi:10.1177/8755293019878185

Stewart, J.P., Klimis, N., Savvaidis, A., Theodoulidis, N., Zargli, E., Athanasopoulos, G., Pelekis, P., Mylonakis, G., Margaris, B (2014). Compilation of a Local VS Profile Database and Its Application for Inference of VS30 from Geologic- and Terrain-Based Proxies. *Bulletin of the Seismological Society of America* 2014; 104 (6): 2827–2841. doi: <https://doi.org/10.1785/0120130331>

Stambouli, B. A., Zendagui, D., Bard, PY. et al. Deriving amplification factors from simple site parameters using generalized regression neural networks: implications for relevant site proxies. *Earth Planets Space* 69, 99 (2017). <https://doi.org/10.1186/s40623-017-0686-3>

Stone, J.R., Schafer, J.P., London, E.H. and Thompson, W.B., 1992, U.S. Geological Survey special map, 2 sheets, scale 1:125,000

Stone, J.R., Stone, B.D., DiGiacomo-Cohen, M.L., and Mabee, S.B., comps., 2018, Surficial materials of Massachusetts—A 1:24,000-scale geologic map database: U.S. Geological Survey Scientific Investigations Map 3402, 189 sheets, scale 1:24,000; index map, scale 1:250,000; 58-p. pamphlet; and geodatabase files, <https://doi.org/10.3133/sim3402>.

Sur, U., Singh, P., Meena, S.R., Singh, T.N. (2022) Predicting Landslides Susceptible Zones in the Lesser Himalayas by Ensemble of Per Pixel and Object-Based Models. *Remote Sens.* 2022, 14, 1953. <https://doi.org/10.3390/rs14081953>

Thompson, E.M., Baise, L.G., Tanaka, K., Kayen, R.E. (2012) A taxonomy of site response complexity. *Soil Dynamics and Earthquake Engineering*. 41(2012): 32-43.

Thompson, E.M., Carkin, B., Baise, L.G., Kayen R. E., 2014. Surface Wave Site Characterization at 27 Locations Near Boston, Massachusetts, Including 2 Strong-Motion Stations. U. S. Geological Survey OFR 2014-1232

Thompson, E. M., Wald, D. J., Worden, C. B. (2014) A Vs30 map for California with geologic and topographic constraints, *Bulletin of the Seismological Society of America* 104, 2313–2321.

Thompson, E.M., 2018, An Updated Vs30 Map for California with Geologic and Topographic Constraints (ver. 2.0, July 2022): U.S. Geological Survey data release, <https://doi.org/10.5066/F7JQ108S>.

Thompson, W.B., Borns Jr., H.W, (1985). Surficial Geologic Map of Maine. Maine Geological Survey

Thomson WT. (1950). Transmission of elastic waves through a stratified solid. *Journal of Applied Physics*: 21:89–93.

Thornley, J.D., Dutta, U., Douglas, J., Yang, Z. (2021) Evaluation of horizontal to vertical spectral ratio and standard spectral ratio methods for mapping shear wave velocity across Anchorage, Alaska. *Soil Dynamics and Earthquake Engineering*. Volume 150 doi: <https://doi.org/10.1016/j.soildyn.2021.106918>

Wald, D. J., and Allen, T. I., 2007, Topographic slope as a proxy for seismic site conditions and amplification, *Bulletin of the Seismological Society of America*, 97, no. 5, 1379-1395.

Wills, C. J., and K. B. Clahan (2006). Developing a map of geologically defined site-conditions categories for California, *Bull. Seism. Soc. Am.* 96, 1483–1501.

Wong I., Darragh, R., Smith, S., Wu, Q., Silva, W., Kishida, T. (2022) Ground motion models for shallow crustal and deep earthquakes in Hawaii and analyses of the 2018 M 6.9 Kalapana sequence. *Earthquake Spectra*. 2022;38(1):579-614. doi:10.1177/87552930211044521

Yassminh, R., Gallegos, A., Sandvol, E., Ni, J. (2019) Investigation of the Regional Site Response in the Central and Eastern United States. *Bulletin of the Seismological Society of America* 2019; 109 (3): 1005–1024. doi: <https://doi.org/10.1785/0120180230>

Yilar, E., Baise, L.G., Ebel, J.E. (2017) Using H/V measurements to determine depth to bedrock and Vs30 in Boston, Massachusetts. *Engineering Geology* 217, 12-22

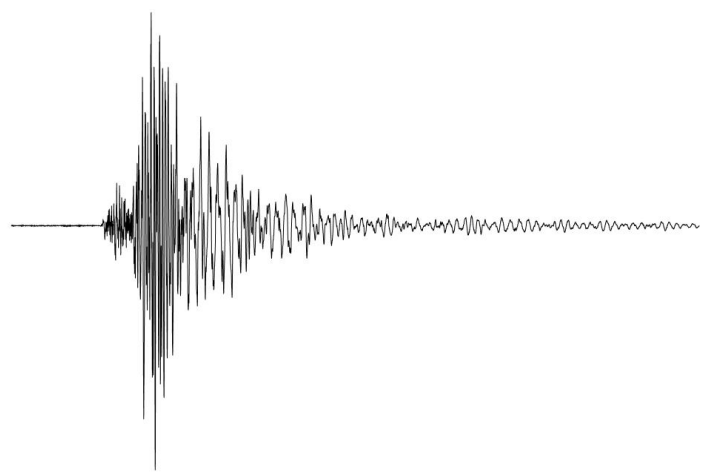
Yong, A. (2016) Comparison of Measured and Proxy-Based VS30 Values in California. *Earthquake Spectra*. 2016;32(1):171-192. doi:10.1193/013114EQS025M

Zalachoris, G., Rathje, E.M. (2019) Ground Motion Model for Small-to-Moderate Earthquakes in Texas, Oklahoma, and Kansas. *Earthquake Spectra*. 2019;35(1):1-20. doi:10.1193/022618EQS047M

Zhu, C., Pilz, M., Cotton, F. (2020) Evaluation of a novel application of earthquake HVSR in site-specific amplification estimation. *Soil Dynamics and Earthquake Engineering*. 139(2020): <https://doi.org/10.1016/j.soildyn.2020.106301>.

Zhu, J., Baise, L.G., Thompson, E.M. (2017) An Updated Geospatial Liquefaction Model for Global Application. *Bulletin of the Seismological Society of America* 2017;; 107 (3): 1365–1385. doi: <https://doi.org/10.1785/0120160198>

Zhu, J., Daley, D., Baise, L.G., Thompson, E.M., Wald, D.J., Knudsen, K.L. (2015) A Geospatial Liquefaction Model for Rapid Response and Loss Estimation. *Earthquake Spectra*. 2015;31(3):1813-1837. doi:10.1193/121912EQS353M



ProQuest Number: 30633146

INFORMATION TO ALL USERS

The quality and completeness of this reproduction is dependent on the quality and completeness of the copy made available to ProQuest.



Distributed by ProQuest LLC (2023).

Copyright of the Dissertation is held by the Author unless otherwise noted.

This work may be used in accordance with the terms of the Creative Commons license or other rights statement, as indicated in the copyright statement or in the metadata associated with this work. Unless otherwise specified in the copyright statement or the metadata, all rights are reserved by the copyright holder.

This work is protected against unauthorized copying under Title 17, United States Code and other applicable copyright laws.

Microform Edition where available © ProQuest LLC. No reproduction or digitization of the Microform Edition is authorized without permission of ProQuest LLC.

ProQuest LLC
789 East Eisenhower Parkway
P.O. Box 1346
Ann Arbor, MI 48106 - 1346 USA